

Helena Teague

## LUBAC is required for the RIG-I mediated antiviral response

### Summary

RNA viruses are responsible for many of the most recent threats to human health by emerging infectious diseases, including epidemics caused by Influenza, Zika, Dengue and novel Coronaviruses. The body's first line of defence against viruses is the innate immune system. Pattern recognition receptors (PRR) detect pattern associated molecular patterns (PAMPs), such as incoming viral genomes. The RIG-I like receptor family sense viral RNA in the host cell cytoplasm, with RIG-I sensing double stranded regions of RNA with an exposed 5' triphosphate group, present in viruses such as Influenza and Zika. The resulting signalling platform activates both IRF3 and NF- $\kappa$ B, resulting in induction of an antiviral response. Early sensing of infection is essential for effective clearance of virus infection with minimal damage to the host.

In this study we set out to understand the contribution of the linear ubiquitin chain assembly complex (LUBAC) to the sensing of RNA and RNA viruses by RIG-I. By using synthetic RNAs, 3p-hpRNA and Poly(I:C), and RNA viruses to specifically stimulate RIG-I, we confirmed the requirement of signalling proteins MAVS and NEMO for activation of IRF3 and NF- $\kappa$ B in this context. TBK1 and IKK $\epsilon$  were shown to function redundantly to activate IRF3 but not NF- $\kappa$ B. Linear ubiquitin chains are produced exclusively by the tripartite E3 ligase LUBAC, made up of HOIP, HOIL and SHARPIN, and are required for NF- $\kappa$ B activation by PRR such as TLR3 and MDA5 signalling. Here we show that the catalytic component HOIP, and HOIL-1, are required for activation of both IRF3 and NF- $\kappa$ B-dependent antiviral signalling during RIG-I activation. Conversely, SHARPIN is not required for either IRF3 or NF- $\kappa$ B-driven responses, an observation that helps rectify previous inconsistencies in the literature. Expression of a catalytic dead mutant of HOIP, and the resultant loss of M1 chains, only partially abrogated activation of IRF3 and NF- $\kappa$ B, suggesting LUBAC has an additional mechanism for regulating RIG-I signalling. HOIP and SHARPIN were shown interact with both NEMO and TBK1 after stimulation of RIG-I, suggesting LUBAC acts as a scaffold to recruit proteins to the signalling complex. We have therefore defined the different roles of individual LUBAC components in RIG-I signalling and established that this complex is essential for innate immune sensing of multiple RNA viruses.



UNIVERSITY OF  
CAMBRIDGE

**LUBAC is required for the RIG-I mediated  
antiviral response**

By

Helena Claire Teague

Clare College

Thesis submitted for the degree of

Doctor of Philosophy

August 2021

# Declaration

---

I declare here that this thesis is the result of my own work and includes nothing which is the outcome of work done in collaboration, except where it is specified in the text and declared here. Work done in collaboration includes all Zika virus infections and the subsequent RNA extraction, Western blotting analysis and growth curve experiments, which was done in collaboration with Nerea Irigoyen and Charlotte Lefevre.

This thesis is also not substantially the same as any work that has already been submitted before for any degree or other qualification, either at the University of Cambridge or at any other University or similar institution.

Finally, this thesis does not exceed the prescribed word limit for the Biology Degree Committee.

# Acknowledgements

---

*"In academia we are all smart, distinguish yourself by being kind"*

*"In this world, you must be oh so smart, or oh so pleasant. Well, for years I was smart. I recommend pleasant." - Elwood P Dowd*

I hope that I have been kind to everyone whose path I have crossed here, I definitely won't miss the opportunity to be so now.

My first and biggest thanks must go to Dr. Brian J Ferguson. Your ideas, supervision and support for all aspects of my PhD have been invaluable, and I thank you for giving me a lot of autonomy and forcing me to think about things before coming to my aid. Your relaxed leadership and lab environment has allowed me to take responsibility for my work and forced me to stretch myself and become a better scientist and critical thinker. Your expertise outside of the project and even the lab has also been of great value to me. I extend this thank you to Professor Henning Walczak and his group at University of Cologne and University College London, especially Dr. Diego de Miguel Samaniego and Dr. Eva Rieser, as well as Dr. Rune Damgaard at the Technical University of Denmark. Without your immense generosity with both resources and knowledge, my project would have very different.

To the members of the labs of Dr. Brian Ferguson, Dr. Geoffrey Smith and the rest of the Division of Immunology, thank you so much for everything: the scientific advice, the boundless support, the incredible friendships I have made and all of the food and drinks we have shared together, you made (almost) every day working here an unbridled joy. I also specifically thank Rahul Singh and Diane Xu, for teaching me that there is so much more to working in the lab than research, that my way is not the only way that things get done, and that I get just as much reward out of teaching as I do from doing my own work.

To my family, your enthusiasm and concern for my attempts in a subject you don't know anything about is incredible. Thank you for simultaneously having my back and calling me out when I'm wrong, and for championing and supporting me for my entire academic career. To my friends, thank you for being my counter-point through all of this. Your blind faith in my abilities is beyond comforting on days when I have absolutely no idea what I am doing, or when I absent-mindedly throw my most important samples in the bin. A special mention to my Humphries Wayers team-

mates, who provided the highlight of many of my most difficult weeks when I needed it the most, as well as lots of the answers to quiz questions I was left raising my eyebrows to.

Finally, Adam. Thank you for not being a scientist, because there have been many days where I just couldn't talk to another scientist when I got home. Thank you for cooking so many dinners when I have been late home from the lab, and for not asking me why I was bothering when I made it all look like a lot of hard work with very little reward. You have been my centre-point through all this, making me realise what was important and giving me 1000 reasons to have a proper work-life balance every day, which benefited my PhD and my life more than I can know.

# Abstract

---

RNA viruses are responsible for many of the most recent threats to human health by emerging infectious diseases, including epidemics caused by Influenza, Zika, Dengue and novel Coronaviruses. The body's first line of defence against viruses is the innate immune system. Pattern recognition receptors (PRR) detect pattern associated molecular patterns (PAMPs), such as incoming viral genomes. The RIG-I like receptor family sense viral RNA in the host cell cytoplasm, with RIG-I sensing double stranded regions of RNA with an exposed 5' triphosphate group, present in viruses such as Influenza and Zika. The resulting signalling platform activates both IRF3 and NF- $\kappa$ B, resulting in induction of an antiviral response. Early sensing of infection is essential for effective clearance of virus infection with minimal damage to the host.

In this study we set out to understand the contribution of the linear (M1-linked) ubiquitin chain assembly complex (LUBAC) to the sensing of RNA and RNA viruses by RIG-I. By using synthetic RNAs, 3p-hpRNA and Poly(I:C), and RNA viruses to specifically stimulate RIG-I, we confirmed the requirement of signalling proteins MAVS and NEMO for activation of IRF3 and NF- $\kappa$ B in this context. TBK1 and IKK $\epsilon$  were shown to function redundantly to activate IRF3 but not NF- $\kappa$ B. M1-linked ubiquitin (M1-Ub) chains are produced exclusively by the tripartite E3 ligase LUBAC, made up of HOIP, HOIL and SHARPIN, and are required for NF- $\kappa$ B activation by PRR such as TLR3 and MDA5 signalling. Here we show that the catalytic component HOIP, and HOIL-1, are required for activation of both IRF3 and NF- $\kappa$ B-dependent antiviral signalling during RIG-I activation. Conversely, SHARPIN is not required for either IRF3 or NF- $\kappa$ B-driven responses, an observation that helps rectify previous inconsistencies in the literature. Expression of a catalytic dead mutant of HOIP, and the resultant loss of M1 chains, only partially abrogated activation of IRF3 and NF- $\kappa$ B, suggesting LUBAC has an additional mechanism for regulating RIG-I signalling. HOIP and SHARPIN were shown interact with both NEMO and TBK1 after stimulation of RIG-I, suggesting LUBAC acts as a scaffold to recruit proteins to the signalling complex. We have therefore defined the different roles of individual LUBAC components in RIG-I signalling and established that this complex is essential for innate immune sensing of multiple RNA viruses.

# Contents

Declaration.....	ii
Acknowledgements.....	iii
Abstract.....	v
List of Figures .....	xiii
List of Tables .....	xv
Abbreviations.....	xvi
Chapter One: Introduction.....	1
1.1 Sensing of viruses by the innate immune system.....	1
1.1.1 Overview of the innate immune system.....	1
1.1.2 Importance of the innate immune system .....	2
1.1.3 Sensing of pathogens by pattern recognition receptors .....	4
1.2 Sensing of RNA viruses.....	6
1.2.1 Toll like receptors.....	7
1.2.2 RIG-I-like receptors .....	7
1.3 RIG-I.....	9
1.3.1 Activation of RIG-I and MDA5 by distinct RNAs.....	9
1.3.2 Activation of RIG-I.....	10
1.3.3 The RIG-I signalling pathway.....	11
1.3.4 Outcomes of RIG-I signalling.....	14
1.3.5 Regulation of RIG-I signalling .....	17
1.4 Viruses.....	19
1.4.1 Viruses as infectious agents.....	19
1.4.2 The impact of viruses on humanity.....	20
1.4.3 RNA viruses known to activate RIG-I .....	21
1.4.3.1 Sendai virus.....	21
1.4.3.2 Influenza A virus.....	21
1.4.3.3 Zika virus .....	22
1.5 LUBAC and M1-ubiquitin chains .....	23
1.5.1 Ubiquitin.....	23
1.5.2 LUBAC.....	26
1.5.3 Regulation of LUBAC .....	27
1.5.4 The importance of LUBAC in humans .....	28

1.5.5	LUBAC-mediated regulation of immune signalling pathways .....	30
1.5.6	LUBAC and RNA sensing.....	31
1.5.7	LUBAC and RIG-I signalling.....	32
1.5.8	M1-ubiquitin chain-independent functions of LUBAC.....	32
1.5.9	LUBAC-independent functions of HOIL-1 and SHARPIN .....	33
1.6	Thesis aims and objectives.....	34
Chapter Two: Materials and Methods .....		35
2.1	Maintenance of cell lines .....	35
2.1.1	Wild-type cell lines.....	35
2.1.2	Edited cell lines .....	35
2.1.3	Maintenance conditions .....	36
2.1.4	Passaging cells.....	36
2.1.5	Seeding cells for experiments .....	36
2.2	Generation of cell lines by CRISPR/Cas9 .....	36
2.2.1	CRISPR Guide Design.....	37
2.2.2	Cloning of constructs .....	37
2.2.3	Transfection of CRISPR constructs .....	38
2.2.4	Cell Sorting and Cloning .....	38
2.2.5	Confirmation of successful knock-out .....	38
2.3	Stimulation of cells.....	39
2.3.1	Transfection of synthetic RNAs.....	39
2.3.2	IFN $\alpha$ stimulation.....	39
2.3.3	TNF $\alpha$ stimulation.....	39
2.4	Virus infection .....	39
2.4.1	Sendai virus .....	39
2.4.2	IAV .....	40
2.4.2.1	Generation and titration of virus stocks .....	40
2.4.2.2	Infection of cells .....	40
2.4.2.3	Virus growth curve analysis .....	40
2.4.3	Zika virus .....	41
2.4.3.1	Generation of and titration of virus stocks .....	41
2.4.3.2	Infection of cells .....	41
2.4.3.3	Virus growth curve analysis .....	41

2.5 RT-qPCR.....	42
2.5.1 Cell Lysis and RNA Extraction.....	42
2.5.2 cDNA synthesis.....	42
2.5.3 qPCR.....	43
2.5.3.1 Targets .....	43
2.5.3.2 qPCR protocol .....	44
2.5.3.3 $\Delta\Delta C_t$ calculations .....	45
2.6 Western blotting.....	45
2.6.1 Harvesting cell lysates.....	45
2.6.1.1 Harvesting whole cell lysate .....	45
2.6.1.2 Harvesting lysates during infection or stimulation .....	45
2.6.1.3 Harvesting lysates from ZIKV infection .....	46
2.6.2 Sodium dodecyl sulphate polyacrylamide gel electrophoresis (SDS-PAGE) .....	46
2.6.3 Transfer .....	47
2.6.4 Immunoblotting.....	47
2.6.5 Detection.....	48
2.7 Enzyme-linked immunosorbent assay (ELISA) .....	48
2.7.1 Sample preparation .....	48
2.7.2 ELISA.....	48
2.7.3 Analysis .....	49
2.8 Phos-flow .....	49
2.8.1 Fixing cells .....	49
2.8.2 Staining cells.....	49
2.8.3 Analysis of samples .....	50
2.9 LUBAC overexpression in HEK cells.....	50
2.9.1 Constructs .....	50
2.9.2 Transfection of overexpression constructs.....	50
2.10 Cell death analysis.....	51
2.10.1 Methods of inducing cell death .....	51
2.10.1.1 Staurosporine.....	51
2.10.2 Methods of measuring cell death.....	51
2.10.2.1 Imaging CPE.....	51
2.10.2.2 Measuring active caspase 3-expressing cells.....	51

2.10.3 Vitality Assay .....	51
2.11 Co-immunoprecipitation.....	52
2.11.1 TNF $\alpha$ stimulation and harvesting for Flag-IP .....	52
2.11.2 SeV infection and harvesting for Flag-IP .....	53
2.11.3 Flag-IP and washing .....	53
2.12 Statistical analysis .....	54
Chapter Three: Developing tools to study RIG-I signalling in A549 cells .....	55
3.1 Introduction .....	55
3.2 RNA sensing in A549 cells .....	55
3.2.1 A549 cells as a model for studying RIG-I signalling.....	55
3.2.2 A549 cells generate an immune response to stimulation with synthetic RNAs .....	56
3.2.3. A549 cells generate an immune response when infected with respiratory RNA viruses, SeV and IAV .....	58
3.2.4 A549 cells as a model to study ZIKV infection .....	60
3.3 Characterising the signalling response of A549 cells to synthetic RNAs and RNA viruses .....	62
3.3.1 Stimulation of RIG-I by synthetic RNAs activates Type I IFN, chemokines and ISGs .....	63
3.3.2. Infection of A549 cells with SeV activates IRF3 and NF- $\kappa$ B, driving expression of IFN, chemokines and NF- $\kappa$ B stimulated genes .....	65
3.3.3. Infection of A549 cells with IAV R+K results in potent IRF3 activation, resulting in IFN, chemokine and ISG expression .....	68
3.3.4. Infection of A549 cells with ZIKV PE243 drives transcription of Type I and III IFN, ISGs and NF- $\kappa$ B dependent genes.....	69
3.4. RIG-I is required for immune activation of A549 cells by synthetic RNAs and RNA viruses.....	70
3.4.1 RIG-I is an ISG, upregulated during immune stimulation .....	70
3.4.2 Generation of RIG-I deficient A549 cells.....	71
3.4.3. A549 RIG-I $-/-$ cells respond to various receptor stimuli.....	72
3.4.4. Stimulation of A549 cells by synthetic RNAs is dependent on RIG-I .....	73
3.4.5. Stimulation of A549 cells by SeV and IAV R+K is dependent on RIG-I .....	74
3.4.6. Stimulation of A549 cells by ZIKV is dependent on RIG-I.....	77
3.5. Discussion.....	78
3.5.1 A549 as a model system to study RIG-I signalling .....	79
3.5.2 There is variation between the immune gene expression profile in response to different RIG-I ligands .....	79
3.5.3 The response to synthetic RNAs and RNA viruses in A549 cells was entirely dependent on RIG-I.....	82

3.6 Conclusion.....	85
Chapter Four: Characterising the RIG-I signalling pathway.....	87
4.1 Introduction.....	87
4.2 MAVS is the central adaptor protein of the RIG-I signalling pathway.....	87
4.2.1 MAVS is required for transcription downstream of RIG-I activation by SeV and 3p-hpRNA, but not Poly(I:C).....	88
4.3 NEMO is required for activation of both IRF3 and NF- $\kappa$ B during RIG-I signalling.....	89
4.3.1 NEMO is required for transcription of IFN-I-dependent genes during stimulation of RIG-I with synthetic RNAs.....	89
4.3.2 NEMO is required for activation of both IRF3- and NF- $\kappa$ B-dependent responses to SeV infection.....	90
4.4 TBK1 and IKK $\epsilon$ function redundantly to activate IRF3 during RIG-I signalling in A549 cells.....	92
4.4.1 TBK1 and IKK $\epsilon$ function redundantly in the RIG-I response to synthetic RNAs.....	93
4.4.2 TBK1 and IKK $\epsilon$ function redundantly in the IRF3-dependent response to SeV infection, but are not required for the NF- $\kappa$ B dependent response.....	94
4.5 How are TBK1 and IKK $\epsilon$ recruited to the RIG-I signalling pathway.....	96
4.5.1 TANK/NAP1/SINTBAD are not essential for recruitment of TBK1 and IKK $\epsilon$ to the RIG-I signalling complex during stimulation with synthetic RNAs.....	97
4.5.2 TANK/NAP1/SINTBAD are not essential for recruitment of TBK1 and IKK $\epsilon$ to the RIG-I signalling complex during SeV infection.....	98
4.5.3 The role of RIP1 in the RIG-I signalling pathway is unclear.....	100
4.5.4 Optineurin appears not to be required in the RIG-I response to SeV infection.....	102
4.6 Discussion.....	102
4.6.1 Limitations of experimental system.....	103
4.6.2 Requirement for MAVS and NEMO in RIG-I signalling.....	105
4.6.3 The role of TBK1 and IKK $\epsilon$ in IRF3 activation in non-immune cells.....	106
4.6.4 The mechanism of recruitment and activation of TBK1 and IKK $\epsilon$ at the RIG-I signalling complex in A549 cells remains unclear.....	106
4.6.5 How a better insight into the RIG-I signalling complex helps us study the contribution of LUBAC to RIG-I signalling.....	109
4.7 Conclusion.....	109
Chapter Five: HOIP is required for RIG-I-driven immune responses.....	113
5.1 Introduction.....	113
5.2 Determining the best system to study the role of HOIP in RIG-I signalling.....	114

5.2.1 Overexpression of LUBAC components in HEK does not affect the immune response to SeV .....	114
5.2.2 Use of HOIP-deficient A549 cells to study the role of LUBAC in RIG-I signalling .....	115
5.3 HOIP is required for RIG-I-driven transcription of antiviral genes.....	116
5.3.1 HOIP is required for efficient transcription of IFN-I, ISGs and chemokines in response to 3p-hpRNA and Poly(I:C) stimulation.....	116
5.3.2 HOIP is required for efficient transcription of IFN-I, IFN-III, NF- $\kappa$ B-dependent genes and chemokines in response to SeV infection .....	118
5.3.3 HOIP is required for efficient transcription of IFN-I, ISGs and chemokines in response to IAV R+K infection .....	119
5.3.4 HOIP is required for efficient transcription of IFN-I, IFN-III, ISGs and chemokines during to ZIKV infection .....	120
5.4 HOIP is required for activation of RIG-I signalling pathway components.....	123
5.4.1 Western blotting analysis and phos-flow are not sensitive enough to provide insight into the role of HOIP in signalling pathway activation during stimulation with synthetic RNAs .....	123
5.4.2 HOIP increases activation of TBK1, IRF3 and I $\kappa$ B $\alpha$ in response to SeV infection .....	124
5.5 HOIP is required for RIG-I-driven chemokine secretion in response to synthetic RNA ligands and SeV infection .....	126
5.6 HOIP is also required for a RIG-I-driven antiviral immune response in HaCaT cells.....	127
5.6.1 HOIP is required for RIG-I driven transcription in HaCaT cells in response to synthetic RNAs and RNA viruses .....	127
5.7 Catalytic activity of HOIP is only partially required for its role in RIG-I signalling .....	128
5.7.1 Mutation of residue C885 inactivates the catalytic activity of HOIP .....	129
5.7.2 Expression of immune genes is only partially dependent on the catalytic activity of HOIP .....	131
5.7.3 Phosphorylation of IRF3, TBK1 and I $\kappa$ B $\alpha$ is not dependent on the catalytic activity of HOIP .....	133
5.7.4 Chemokine expression is only partially dependent on the catalytic activity of HOIP .....	134
5.8 The LUBAC complex functions as a scaffold during RIG-I signalling .....	134
5.8.1 LUBAC components co-IP with NEMO and SHARPIN during SeV infection .....	134
5.9 HOIP does not play a role in preventing RIG-I-driven cell death in A549 cells .....	136
5.9.1 RIG-I-driven cell death is not activated in A549 cells lacking HOIP .....	137
5.10 Discussion.....	140
5.10.1 Addressing previously conflicting studies showing opposing roles for HOIP in the regulation of RNA sensing. ....	140
5.10.2 A suggested two-step mechanism for the regulation of RIG-I signalling by LUBAC and M1-ubiquitin chains.....	142
5.10.3 HOIP does not act to restrict virus replication in our system .....	144

5.10.4 Involvement of LUBAC in RIG-I-driven cell death .....	145
5.11 Conclusion.....	146
Chapter Six: The role of accessory proteins HOIL-1 and SHARPIN in RIG-I signalling.....	147
6.1 Introduction .....	147
6.2 HOIL-1 is required for a RIG-I-driven immune response to synthetic RNAs and RNA viruses.....	147
6.2.1 Characterisation of the immune response in MEF TNF $-/-$ HOIL-1 $+/-$ and HOIL-1 $-/-$ cells...	148
6.2.2 The synthetic RNA-driven immune response is dependent on HOIL-1 .....	151
6.2.3 The antiviral transcriptional response to SeV infection is dependent on HOIL-1.....	151
6.2.4 HOIL-1 is required for activation of RIG-I signalling proteins during SeV infection.....	153
6.3 SHARPIN is not required for a RIG-I driven immune response to synthetic RNAs or RNA virus infection .....	154
6.3.1 Generation of A549 SHARPIN $-/-$ cells .....	154
6.3.2 Mixed requirement of SHARPIN for a synthetic RNA-driven immune response in A549 cells .....	155
6.3.3 SHARPIN is not required for the SeV-driven immune response in A549 cells.....	156
6.3.4. SHARPIN is not required for a RIG-I-driven immune response in MEF cells.....	157
6.4 Discussion.....	159
6.4.1 HOIL-1, like HOIP, is required for RIG-I-driven immune responses .....	160
6.4.2 SHARPIN is not required for gene transcription following RIG-I activation.....	161
6.4.3 In addition to their function in LUBAC, HOIP, HOIL-1 and SHARPIN all have independent functions in signalling pathways.....	162
6.5 Conclusion.....	166
Bibliography .....	171

# List of Figures

---

<b>Figure</b>	<b>Title</b>	<b>Page no.</b>
<b>1.1.1</b>	PRR sensing in non-specialist immune cells	5
<b>1.2.2</b>	Domain structure and function of RLR family and MAVS adaptor protein	8
<b>1.3.3</b>	Schematic of the RIG-I signalling pathway	14
<b>1.3.4</b>	A simplified pathway of activation of the IFN response by RIG-I	16
<b>1.3.5</b>	Regulation of RIG-I by post-translational modifications and binding proteins	18
<b>1.5.1</b>	The ubiquitination system	24
<b>1.5.2</b>	Schematic representation of the domain structure and interactions between the LUBAC components	26
<b>1.5.5</b>	LUBAC-mediated regulation of the signalling outcomes of the TNF-RSC	30
<b>2.8.3</b>	Gating strategy for phos-flow analysis in FlowJo	50
<b>2.10.2</b>	NC-250 vitality assay parameters	52
<b>3.2.1</b>	A549 cells express many of the components of the RIG-I signalling machinery	56
<b>3.2.2</b>	A549 cells generate an immune response when stimulated by synthetic RNAs	58
<b>3.2.3</b>	A549 cells generate an immune response when stimulated by RNA viruses	60
<b>3.2.4</b>	A549 cells are a suitable model to study innate immune sensing of ZIKV	62
<b>3.3.1</b>	Synthetic RNAs activate IRF3-dependent pathways, but not NF- $\kappa$ B dependent	65
<b>3.3.2</b>	SeV infection drives activation of IRF3- and NF- $\kappa$ B-dependent pathways	67
<b>3.3.3</b>	IAV R+K infection drives activation of IRF3-, but not NF- $\kappa$ B-dependent pathways	69
<b>3.3.4</b>	ZIKV PE243 infection drives transcription of IRF3- and NF- $\kappa$ B-dependent genes	70
<b>3.4.1</b>	RIG-I is an ISG that is upregulated by Type I IFN and SeV infection	71
<b>3.4.2</b>	Generation and characterisation of a RIG-I $-/-$ cell line	72
<b>3.4.3</b>	A549 RIG-I $-/-$ cells have immune signalling capacity	73
<b>3.4.4</b>	Stimulation of A549 cells by synthetic RNAs is dependent on RIG-I	74
<b>3.4.5</b>	Stimulation of A549 cells by SeV and IAV R+K is dependent on RIG-I	76
<b>3.4.6</b>	Stimulation of A549 cells by ZIKV is dependent on RIG-I at early time points	78
<b>4.2.1</b>	MAVS is required for RIG-I-driven immune signalling following stimulation with synthetic RNAs and RNA viruses	89
<b>4.3.1</b>	NEMO is required for synthetic RNA-driven activation of IRF3- and NF- $\kappa$ B-dependent pathways	90
<b>4.3.2</b>	NEMO is required for SeV-driven activation of IRF3- and NF- $\kappa$ B-dependent pathways	92
<b>4.4.1</b>	TBK1 and IKK $\epsilon$ act redundantly during RIG-I stimulation by synthetic RNAs	94
<b>4.4.2</b>	TBK1 and IKK $\epsilon$ act redundantly during stimulation of RIG-I by SeV	96
<b>4.5.1</b>	TANK/NAP1/SINTBAD are not essential for RIG-I-driven pathways downstream of activation by synthetic RNAs	98

<b>4.5.2</b>	TANK/NAP1/SINTBAD are not essential for RIG-I-driven pathways downstream of activation by SeV	99
<b>4.5.3</b>	RIP1 may play a role in RIG-I-driven IRF3 activation by SeV	101
<b>4.5.4</b>	Optineurin is not essential for RIG-I-driven pathways downstream of activation by SeV	102
<b>4.7.1</b>	Schematic of the mechanism of IRF3 activation by RIG-I	109
<b>4.7.2</b>	Schematic of the mechanism of NF- $\kappa$ B activation by RIG-I	110
<b>5.2.1</b>	Reproducing previous LUBAC-overexpression experiments in HEK293T cells	115
<b>5.2.2</b>	Characterisation of A549 HOIP $-/-$ and +TAP-HOIP-WT cells	116
<b>5.3.1</b>	RIG-I-driven expression of immune genes in response to synthetic RNAs is dependent on HOIP	117
<b>5.3.2</b>	RIG-I-driven expression of immune genes in response to SeV infection is dependent on HOIP	118
<b>5.3.3</b>	HOIP may contribute to innate immune sensing of IAV	120
<b>5.3.4</b>	RIG-I-driven expression of immune genes in response to IAV R+K infection is dependent on HOIP	122
<b>5.4.1</b>	Stimulation with synthetic RNAs is too weak to quantify using Western blotting	124
<b>5.4.2</b>	HOIP is required for activation of signalling pathway components in response to Sendai virus	125
<b>5.5.1</b>	HOIP is required for CXCL10 secretion during stimulation with synthetic RNAs and SeV	127
<b>5.6.1</b>	HOIP is required for RIG-I signalling in HaCaT cells after stimulation with Poly(I:C) and SeV infection	128
<b>5.7.1</b>	Characterisation of TAP-HOIP-WT and TAP-HOIP-C885S cells	131
<b>5.7.2</b>	Expression of immune genes in response to synthetic RNAs and SeV infection is only partially dependent on the catalytic activity of HOIP	132
<b>5.7.3</b>	Phosphorylation of signalling proteins during SeV infection appears not to be dependent on the catalytic activity of HOIP	133
<b>5.7.4</b>	CXCL10 secretion in response to SeV infection is only partially dependent on the catalytic activity of HOIP	134
<b>5.8.1</b>	LUBAC co-IPs with NEMO and TBK1 during SeV infection	136
<b>5.9.1</b>	RIG-I does not drive cell death in A549 cells, even in the absence of HOIP	140
<b>6.2.1</b>	Characterising the MEF TNF $-/-$ HOIL-1 $+/-$ cell line	150
<b>6.2.2</b>	Synthetic RNA-driven expression of immune genes is dependent on HOIL-1	151
<b>6.2.3</b>	HOIL-1 is required for RNA virus-driven immune gene expression	153
<b>6.2.4</b>	HOIL-1 is required for SeV-driven activation of signalling pathway components	154
<b>6.3.1</b>	Characterisation of SHARPIN $-/-$ A549 cells	155
<b>6.3.2</b>	SHARPIN is not required for synthetic RNA-driven immune gene transcription in A549 cells	155
<b>6.3.3</b>	SHARPIN is not required for the SeV-driven response in A549 cells	157
<b>6.3.4</b>	SHARPIN is not required for RIG-I driven immune gene transcription in MEF cells	159
<b>6.5.1</b>	Schematic of the proposed mechanism of LUBACs involvement in RIG-I signalling complex formation	167
<b>6.5.2</b>	Schematic of the proposed mechanism of LUBACs involvement in RIG-I signalling complex enhancement	169

# List of Tables

---

<b>Table</b>	<b>Title</b>	<b>Page no.</b>
1.2.	Expression, cellular localisation, agonists and viruses detected by RNA sensing PRR	6
2.1.1	Wild-type cell lines used in this study	36
2.1.2	Genetically edited cell lines used in this study	36
2.2.1	sgRNAs used for CRISPR/Cas9 knockout generation	38
2.5.3.1A	Primers used to detect mRNA transcription in human cell lines	44
2.5.3.1B	Primers used to detect mRNA transcription in murine cell lines	45
2.5.3.2	qPCR thermocycling conditions	45
2.6.4A	Primary antibodies used for Western blotting	48-49
2.6.4B	Secondary antibodies used for Western blotting	49
2.8.2	Antibodies used for phos-flow analysis	50

# Abbreviations

---

<b>-/-</b>	Homozygous knockout
<b>2-ME</b>	2 mercaptoethanol
<b>3p-hpRNA</b>	3' triphosphate hairpin RNA
<b>5'ppp-dsRNA</b>	5' triphosphate double stranded RNA
<b>7AAD</b>	7-Aminoactinomycin D
<b>A</b>	Alanine
<b>A549</b>	Adenocarcinomic human alveolar basal epithelial cells
<b>ABC-DLBCL</b>	Activated B-cell-diffuse large B-cell lymphoma
<b>ADAR-1</b>	RNA-specific adenosine deaminase 1
<b>AGS</b>	Aicardi-Goutieres syndrome
<b>AIDS</b>	Acquired immune deficiency syndrome
<b>AIM2</b>	Absent in melanoma 2
<b>APS</b>	Ammonium persulphate
<b>ASC</b>	Apoptosis-associated speck-like protein containing a CARD domain
<b>βTrCP</b>	β transducin repeat-containing protein
<b>BACH</b>	BTB Domain and CNC Homolog
<b>BCA</b>	Bicinchoninic acid
<b>Bcl</b>	B-cell lymphoma
<b>BHK</b>	Baby hamster kidney (cells)
<b>BMDC</b>	Bone marrow-derived cells
<b>BSA</b>	Bovine serum albumin
<b>C</b>	Cysteine
<b>CARD</b>	Caspase recruitment domain
<b>Cas9</b>	CRISPR-associated 9
<b>Cbl</b>	Casitas B-lineage lymphoma proto-oncogene
<b>CCL</b>	CC-chemokine ligand
<b>CD40</b>	Cluster of differentiation 40
<b>cDNA</b>	Complimentary DNA
<b>cGAS</b>	cyclic GMP-AMP (cGAMP) synthase
<b>CHAK</b>	CC-Chemokine-activated killer
<b>ciAP</b>	Cytoplasmic Inhibitor of apoptosis protein
<b>CKII</b>	Casein kinase II
<b>CLR</b>	C-type lectin receptors
<b>CoV</b>	Coronavirus
<b>COVID-19</b>	Coronavirus disease 2019
<b><i>Cpdm</i></b>	Chronic proliferative dermatitis
<b>CPE</b>	Cytopathic effect
<b>CRISPR</b>	Clustered Regularly Interspaced Short Palindromic Repeats
<b>cRNA</b>	Complementary RNA
<b>Ct</b>	Threshold cycle
<b>CTD</b>	C-terminal domain
<b>CVB</b>	Coxsackievirus B
<b>CXCL</b>	CXC-chemokine ligand
<b>CYLD</b>	Cylindromatosis
<b>Da</b>	Dalton
<b>DAMP</b>	Damage-associated molecular patterns
<b>DDX</b>	DExD/H-box helicase

<b>DENV</b>	Dengue virus
<b>DHX</b>	DEAD-box helicase
<b>DI</b>	Defective interfering
<b>DISC</b>	Death-inducing signalling complex
<b>DMEM</b>	Dulbecco's Modified Eagle Medium
<b>DNA</b>	Deoxyribonucleic acid
<b>dNTP</b>	Deoxynucleotide
<b>dsRNA</b>	double-stranded RNA
<b>DMEM</b>	Dulbecco's Modified Eagle's Medium
<b>DMSO</b>	Dimethylsulfoxide
<b>dNTP</b>	Deoxynucleotide
<b>ds</b>	Double-stranded
<b>DTT</b>	Dithiothreitol
<b>DUB</b>	Deubiquitinase
<b>EBV</b>	Epstein Barr virus
<b>EDTA</b>	Ethylenediaminetetraacetic acid
<b>ELISA</b>	Enzyme-linked immunosorbent assay
<b>EMCV</b>	Encephalomyocarditis virus
<b>ERK</b>	Extracellular signal-regulated kinase
<b>EV</b>	Empty vector
<b>EYA</b>	Eyes absent
<b>FACS</b>	Fluorescence-activated cell sorting
<b>FADD</b>	Fas-associated protein with death domain
<b>FAF1</b>	Fas-associated factor 1
<b>FCS</b>	Foetal calf serum
<b>FMDV</b>	Foot and mouth disease virus
<b>g</b>	Gravitational force
<b>GAPDH</b>	Glyceraldehyde 3-phosphate dehydrogenase
<b>GFP</b>	Green fluorescent protein
<b>gRNA</b>	Genomic RNA
<b>GSH</b>	Reduced glutathione
<b>H1N1</b>	Hemagglutinin 1 Neuraminidase 1
<b>HA</b>	Haemagglutinin
<b>HaCaT</b>	Cultured Human Keratinocyte cells
<b>HBV</b>	Hepatitis B virus
<b>HCV</b>	Hepatitis C virus
<b>HECT</b>	Homologous to E6AP C-Terminus
<b>HEK293</b>	Human embryonic kidney 293
<b>HEPES</b>	4-(2-hydroxyethyl)-1-piperazineethanesulfonic acid
<b>His</b>	Histidine
<b>HMW</b>	High molecular weight
<b>HO-1</b>	Haem oxygenase
<b>HOIL-1</b>	Heme-oxidized IRP2 ubiquitin ligase-1
<b>HOIP</b>	HOIL-1-interacting protein
<b>HOIPIN</b>	Small-molecule inhibitors of LUBAC
<b>HPRT</b>	Hypoxanthine phosphoribosyltransferase 1
<b>HPV</b>	Human papilloma virus
<b>IAV</b>	Influenza A virus
<b>IBR</b>	In between RING
<b>IFI16</b>	IFN-gamma inducible protein 16

<b>IFIT</b>	Interferon induced protein with tetratricopeptide repeats
<b>IFITM</b>	Interferon-inducible transmembrane
<b>IFN</b>	Interferon
<b>IFNLR</b>	IFN lambda receptor
<b>IFNAR</b>	IFN alpha receptor
<b>IκBα</b>	nuclear factor of kappa light polypeptide gene enhancer in B-cells inhibitor, alpha
<b>IKK</b>	IκB kinase
<b>IL</b>	Interleukin
<b>ILC</b>	Innate lymphoid cell
<b>IP</b>	Immunoprecipitation
<b>IRAK</b>	Interleukin-1 receptor (IL-1R) associated kinase
<b>IRES</b>	Interferon response element sequence
<b>IRF</b>	Interferon regulatory factor
<b>IRP2</b>	Iron regulatory protein 2
<b>IRS-1</b>	Insulin receptor substrate-1
<b>ISG</b>	Interferon stimulated gene
<b>ISGF3</b>	IFN-stimulated gene factor 3
<b>ISRE</b>	interferon sensitive response element
<b>ITC</b>	isothermal titration calorimetry
<b>JAK</b>	Janus kinase
<b>JNK</b>	c-Jun N-terminal kinases
<b>K</b>	Lysine
<b>KO</b>	Knock out
<b>LB</b>	Lysogeny Broth
<b>LGP2</b>	Laboratory of genetics and physiology 2
<b>LMP</b>	Low melting point
<b>lncRNA</b>	Long non-coding RNA
<b>LPS</b>	Lipopolysaccharide
<b>LTM</b>	LUBAC-tethering motif
<b>LUBAC</b>	Linear Ubiquitination Chain Assembly Complex
<b>M1</b>	Methionine 1-linked ubiquitin chain
<b>MAM</b>	Mitochondrial-associated endoplasmic reticulum membranes
<b>MAPK</b>	Mitogen assisted protein kinase
<b>MARCH</b>	membrane-associated RING-CH-type finger
<b>MAVS</b>	Mitochondrial antiviral-signalling protein
<b>MDA5</b>	Melanoma differentiation antigen 5
<b>MDCK</b>	Madin-Darby Canine Kidney cells
<b>MDSC</b>	Myeloid-derived suppressor cells
<b>MEF</b>	Murine embryonic fibroblast
<b>MEM</b>	Minimum essential media
<b>MEX3C</b>	Mex-3 RNA binding family member C
<b>MG-132</b>	Proteasome inhibitor (carbobenzoxy-Leu-Leu-leucinal)
<b>miRNA</b>	Micro-RNA
<b>MLKL</b>	Mixed Lineage Kinase Domain Like Pseudokinase
<b>MNoV</b>	Murine Norovirus
<b>MOM</b>	Mitochondrial outer membrane
<b>MOI</b>	Multiplicity of infection
<b>MPV</b>	Metapneumovirus
<b>MyD88</b>	Myeloid differentiation primary response 88

<b>MX1</b>	MX Dynamin Like GTPase 1
<b>n</b>	Number of repeats
<b>NA</b>	Neuramidase
<b>NAP1</b>	Nucleosome assembly protein 1
<b>NDFP</b>	Nedd4 interacting protein
<b>NDP</b>	Nuclear Domain 10 Protein
<b>NDV</b>	Newcastle Disease Virus
<b>NEMO</b>	NF-kappa-B essential modulator
<b>NET</b>	Neutrophil extracellular trap
<b>NF-H2O</b>	Nuclease free water
<b>NF-kB</b>	Nuclear factor kappa-light-chain-enhancer of activated B cells
<b>NFkBIA</b>	NF-kB inhibitor alpha
<b>NK</b>	Natural killer (cells)
<b>NLR</b>	NOD-like receptor
<b>NLRP3</b>	Nucleotide-binding oligomerization-like receptor family, pyrin domain-containing protein 3
<b>NOD</b>	Nucleotide-binding oligomerization domain-containing protein
<b>NPL4</b>	Nuclear protein localisation 4
<b>NS1</b>	Non-structural protein 1
<b>NZF</b>	NPL4 zinc finger 2
<b>OAS</b>	2'-5' oligoadenylate synthase
<b>OPTN</b>	Optineurin
<b>OTUD1</b>	OTU Deubiquitinase 1
<b>OTULIN</b>	OTU Deubiquitinase With Linear Linkage Specificity
<b>ORF</b>	Open reading frame
<b>p</b>	Phospho-/phosphate
<b>PAGE</b>	Polyacrylamide gel electrophoresis
<b>PAMP</b>	Pathogen-associated molecular patterns
<b>PARP</b>	Poly ADP ribose polymerase
<b>PBS</b>	Phosphate buffered saline
<b>PCBP</b>	Poly(RC) Binding Protein
<b>PCD</b>	Programmed cell death
<b>PCR</b>	Polymerase chain reaction
<b>PE</b>	phycoerythrin
<b>PEI</b>	Polyethylenimine
<b>PFA</b>	Paraformaldehyde
<b>PFU</b>	Plaque forming units
<b>PGN</b>	Peptidoglycan
<b>pH</b>	Potential Hydrogen
<b>PI</b>	Propidium iodide
<b>PI3K</b>	Phosphatidyl-Inositol 3-Kinase
<b>PKR</b>	Protein kinase R
<b>PMK</b>	Primary murine keratinocytes
<b>Poly(I:C)</b>	Polyinosinic:polycytidylic acid
<b>PPM1A</b>	Protein phosphatase 1A
<b>PR8</b>	A/Puerto Rico/8/34 (Influenza A virus strain)
<b>PRMT5</b>	Protein arginine methyltransferase 5
<b>PRR</b>	Pattern recognition receptors
<b>PRRSV</b>	Porcine reproductive and respiratory syndrome virus
<b>P/S</b>	Penicillin/Streptomycin

<b>PUB</b>	Peptide:N-glycanase/UBA- or UBX-containing proteins
<b>PXR</b>	Pregane X receptor
<b>qPCR</b>	Quantitative real-time PCR
<b>R</b>	Arginine
<b>RBCK1 (HOIL-1)</b>	RANBP2-Type and C3HC4-Type Zinc Finger Containing 1
<b>RBR</b>	RING-Between-RING
<b>RdRp</b>	RNA-dependent RNA polymerase
<b>RIG-I</b>	Retinoic acid-inducible gene I
<b>RING</b>	Really Interesting New Gene
<b>RIP1</b>	Receptor-interacting protein kinase 1
<b>RIPA (buffer)</b>	Radioimmunoprecipitation assay buffer
<b>RIPA</b>	RLR-induced IRF3-mediated pathway of apoptosis
<b>RLR</b>	RIG-I-like receptor
<b>RNF</b>	Ring finger protein
<b>RNA</b>	Ribonucleic acid
<b>RSC</b>	Receptor signalling complex
<b>RSV</b>	Respiratory Syncytial Virus
<b>RT</b>	Reverse transcriptase
<b>S/Ser</b>	Serine
<b>SAFA</b>	Scaffold attachment factor A
<b>SARS</b>	Severe acute respiratory syndrome
<b>SCF</b>	Skp1, Cdc53/Cullin1, F-box protein
<b>SD</b>	Standard deviation
<b>SDS</b>	Sodium dodecyl sulphate
<b>SeV</b>	Sendai virus
<b>sgRNA</b>	Small guide RNA
<b>SHARPIN</b>	SHANK-associated RH-domain-interacting protein
<b>shRNA</b>	Short hairpin RNA
<b>SINTBAD</b>	Similar to NAP1 TBK1 adaptor
<b>siRNA</b>	Small interfering RNA
<b>SLS</b>	Systemic lupus erythematosus
<b>SMS</b>	Singleton-Merten syndromes
<b>SMURF</b>	SMAD Specific E3 Ubiquitin Protein Ligase
<b>SPATA2</b>	Spermatogenesis associated 2
<b>STAT</b>	Signal Transducer and Activator of Transcription
<b>STING</b>	Stimulator of interferon genes
<b>STS</b>	Staurosporine
<b>SUMO</b>	Small ubiquitin-like modifier
<b>TAB</b>	TAK1-binding protein
<b>TAK</b>	TGF $\beta$ -activated kinase 1
<b>TANK</b>	TRAF family member associated NF- $\kappa$ B activator
<b>TAP</b>	Tandem affinity purification (tag)
<b>TAX1BP</b>	Tax1-binding protein 1
<b>TBK1</b>	TANK Binding Kinase 1
<b>TBST</b>	Tris buffered saline 0.1% Tween-20
<b>TEMED</b>	Tetramethylethylenediamine
<b>TF</b>	Transcription factors
<b>TICAM-1</b>	Toll Like Receptor Adaptor Molecule 1
<b>TIR</b>	Toll/IL-1R domains
<b>TKO</b>	Triple knock-out (TANK/NAP1/SINTBAD)

<b>TLR</b>	Toll-like receptor
<b>TMEV</b>	Theiler's murine encephalomyelitis virus
<b>TNF</b>	Tumour necrosis factor
<b>TPCK</b>	N-tosyl-phenylalanine-chloromethyl-ketone
<b>TRADD</b>	Tumour necrosis factor receptor type 1-associated DEATH domain protein
<b>TRAF</b>	TNF receptor associated factor
<b>TRIF</b>	TIR-domain-containing adapter-inducing interferon- $\beta$
<b>TRIM</b>	Tripartite motif-containing protein
<b>TYK</b>	Tyrosine kinase
<b>U251</b>	Glioblastoma-derived human cell line
<b>UBA</b>	Ubiquitin associated
<b>UBC</b>	Ubiquitin-conjugating enzyme
<b>UBE2L3L</b>	Ubiquitin-conjugating enzyme E2L 3
<b>UBL</b>	Ubiquitin-like
<b>USP</b>	Ubiquitin-specific peptidase
<b>UTR</b>	Untranslated region
<b>VB-48</b>	VitaBright-48 dye
<b>vRNA</b>	Viral RNA
<b>VSV</b>	Vesicular Stomatitis Virus
<b>WSN</b>	A/WSN/1933
<b>WT</b>	Wild-type
<b>YAP</b>	Yes-associated protein
<b>ZAP</b>	Zinc-finger antiviral proteins
<b>ZBP1</b>	Z-DNA binding protein 1
<b>ZIKV</b>	Zika virus

# Chapter One: Introduction

---

## 1.1 Sensing of viruses by the innate immune system

### 1.1.1 Overview of the innate immune system

The environment in which we live contains vast numbers of pathogens and toxic substances that threaten our health. Because of this, our immune system has evolved to protect us, based at least in part on its ability to recognise 'non-self' molecules and to differentiate them from 'self' molecules, a conceptual framework first described by Janeway<sup>1</sup>, as well as its ability to recognise 'self' damage signals to protect against danger<sup>2</sup>. Our immune system can be divided into two parts: the innate immune system, which forms the first line of defence against pathogen infection, tissue injury and genotoxic stress; and the adaptive immune system, which consists of co-ordinated receptor-antigen interaction-specific responses against known pathogens and is generally activated by the innate immune system, with some exceptions<sup>3</sup>. Activation of the adaptive immune system occurs through the clonal expansion of cells expressing the correct antigen-specific receptor corresponding to the invading pathogen<sup>4</sup>. Thus, the immediate activation of innate immune system, possible due to expression of its components in almost all cells of the body, is crucial for prevention of infection and maintenance of homeostasis<sup>5</sup>.

Almost all cells and tissues in the body contribute to the innate immune system, which is made up of three main components: physical barriers, which shield our cells from external substances and pathogens, predominantly comprised of the skin in humans<sup>6</sup>; secreted defence mechanisms<sup>7</sup>; and general immune responses in specialist and non-specialist cells<sup>8</sup>.

Non-specialist epithelial cells form the majority of our physical barrier to infection meaning that they are generally the cells first infected by pathogens and the first line of defence of innate immune system. Because of this, cellular systems like the mucosal surface of the lung epithelium are a critical innate immune interface<sup>9</sup>. The crux of the role of epithelial cells is their ability to detect pathogens, generally occurring through recognition of pattern associated molecular patterns (PAMPs) by pattern recognition receptors (PRR). Recognition activates a variety of intracellular signalling cascades, resulting in expression of many genes and synthesis and secretion of many molecules, including chemokines, cytokines, pro-inflammatory lipids and complement<sup>10,11</sup>. Together, these genes and secreted molecules orchestrate the early immune response by enabling the recruitment of multiple specialist immune cell populations.

There are a broad range of specialist innate immune cells, which although specialist, differ from adaptive immune cells as they do not express antigen-receptors and do not have the capacity for immunological memory<sup>12</sup>. The best known of these are neutrophils, macrophages, myeloid-derived suppressor cells (MDSC), innate lymphoid cells (ILCs), dendritic cells (DCs) and natural killer (NK) cells, all of which have unique responses to infection or damage<sup>13</sup>. Macrophages are the primary phagocytic component of the immune system, capable of engulfing pathogens and dead cells and producing both pro- or anti-inflammatory mediators, dependent on subset and environmental cues<sup>14,15</sup>. Neutrophils are also capable of phagocytosing bacteria and fungi<sup>13</sup>, as well as releasing granules to degrade proteins from larger pathogens<sup>16</sup>. Additionally, neutrophils undergo NETosis, where they release extrusions of their own nuclear and mitochondrial DNA as a neutrophil extracellular trap (NET) to kill or immobilise microbes<sup>17</sup>. The subset of MDSCs is comprised of neutrophils and monocytes, and is activated during pathological immune activation, acting to prevent dangerous persistent stimulation of myeloid cells through suppression of NK and T cell activation<sup>18</sup>. ILCs are made up of three subtypes of cells with wide-ranging effector functions, contributing to immunity by secreting effector cytokines and regulating the function of other innate and adaptive specialist immune cells, complementing the function of T cells in adaptive immunity<sup>19</sup>. DCs have many functions that both directly influence innate immunity and are critical for the induction of adaptive immunity. Innate functions include the production of IL-12 and Type I IFN and induction of innate lymphocyte expansion, whereas adaptive functions consist of antigen capture and processing and migration to T cell areas in lymphoid organs<sup>20</sup>. Finally, NK cells, often considered ILCs, are one of the main effector lymphocytes of the innate immune system. They are capable of cytokine production and cytolytic functions, as well as regulatory functions through their interaction with other immune cell subsets<sup>21</sup>.

### **1.1.2 Importance of the innate immune system**

The importance of the innate immune system is highlighted by its conservation through evolution. First appearing 750 million years ago, its key features that allow the generation of a response to invading pathogens are found in every species in the tree of life, conserved between kingdoms as disparate as plants, invertebrates and mammals<sup>22,23</sup>. In prokaryotic organisms, this is based around the ability to degrade invading pathogens, but this has become more complex in eukaryotic organisms, which generated additional mechanisms to maintain cellular integrity and survival, generally based around the binding of foreign elements and differentiation from 'non-self'<sup>22</sup>. Conserved through evolution, the more complex the organism, the more complex and sophisticated

the immune system it possesses became, illustrating the competitive 'struggle for existence' between species.

This importance is further highlighted by the phenotypes seen in individuals who have dysregulated innate immune systems. Immunodeficiency disorders resulting from impairment of the immune system are split into two groups: primary immunodeficiency, caused by genetic defects, and secondary immunodeficiency, resulting from environmental factors. Together, these are a heterogeneous group of around 150 diseases, each with differing phenotypes. Primary immunodeficiencies affecting the innate immune system include disorders in phagocytes, preventing pathogen phagocytosis and resulting in recurrent and severe bacterial and fungal infection; or in complement, causing development of autoimmune conditions like rheumatoid arthritis and systemic lupus erythematosus<sup>24</sup>. They also include deficiencies caused by mutations in PRRs or PRR signalling components. Secondary immunodeficiencies are most regularly caused by malnutrition-induced protein deficiency or drug treatments, both of which lead to suppression of immunity, or chronic infection, as in the case of HIV-induced acquired immune deficiency syndrome (AIDS)<sup>25</sup>.

Conversely, persistent stimulation of the innate immune system can be equally as damaging. Chronic inflammation is a result of a breakdown of self-tolerance, resulting in higher and persistent production of cytokines. This is often induced by pathogen infection, but also by things like bystander activation and superantigen-crosslinking<sup>26</sup>. Persistent activation can result in oxidative stress and tissue damage, causing wide-ranging injury including neurodegeneration, cancer and multi-organ failure<sup>27,28</sup>. Specific examples include Type I diabetes, where the immune system targets insulin producing cells<sup>29</sup>; arthritis, where the immune system attacks the joints<sup>30</sup>; and multiple sclerosis, where immune-mediated damage to the myelin sheaths surrounding neurones slows nerve transmission<sup>31</sup>. A group of autoimmune diseases, type I interferonopathies, are associated with the constitutive overproduction of type I interferon (IFN-I), a central component of the innate immune response. This results in systemic auto-inflammation, combined with varying levels of auto-immunity or immunodeficiency<sup>32</sup>. This includes AGS which is caused by mutations in one or more of seven genes, encoding primarily DNA and RNA binding proteins that normally protect cellular RNAs from detection by PRRs, resulting in constitutive activation<sup>32</sup>. Aicardi Goutières Syndrome (AGS) presents as a severe mental and physical handicap in infants. Mutations in PRRs RIG-I and MDA5 cause hypersensitivity or spontaneous activation of receptor signalling and are linked with AGS and Singleton-Merten syndrome and systemic lupus erythematosus (SLE)<sup>33,34</sup>, whilst TLR3 mutations have been associated with IAV-driven pathologies including encephalopathy and pneumonia<sup>35,36</sup>. RIG-I and MDA5 are also be implicated in auto-immunity when mutations cause dysregulated RNA

metabolism, with excess or mis-localised immunostimulatory RNAs resulting in their constitutive activation.

### 1.1.3 Sensing of pathogens by pattern recognition receptors

The majority of pathogens are first detected by germline encoded receptors called pattern recognition receptors (PRR), occurring in the first infected cells, which are often not specialist immune cells. Different families of these receptors sense a wide range of PAMPs not encoded in host cells, such as DNA and RNA species with 'non-self' characteristics and bacterial- and fungal-specific components, which then signal to activate immune responses, as shown in Figure 1.1.

One family of PRRs is the Toll like receptors (TLRs). They are membrane bound and predominantly detect bacteria, through the recognition of lipoproteins in Gram-positive bacteria (TLR2 and either 1 or 6), peptidoglycans (TLR2), lipopolysaccharide (LPS) (TLR4) and flagellin (TLR5). Most TLRs can also reside in endosomes, enabling them to function in this compartment. Here TLRs 3, 7, 8, and 9 sense endosomal DNA and RNA of bacterial and viral origin<sup>37-39</sup>. Like TLRs, a second family of PRRs, the C-type Lectin Receptors (CLRs), also function at the cell surface. Predominantly, they sense fungal carbohydrates like  $\beta$ -glucan and Mannans to activate signalling, however they can also function to modulate TLR signalling<sup>40,41</sup>. Like some TLRs, NOD-like receptors (NLRs) also respond to intracellular pathogens, recognising various ligands like peptidoglycan, flagellin, viral RNA and fungal hyphae, as well as detecting damage associated molecular patterns (DAMPs) from host cells<sup>42</sup>. Both CLRs and NLRs can also sense viruses through the detection of viral-specific lipids and proteins present in the viral envelope<sup>40</sup>. However, viral detection predominantly occurs through receptors that detect their nucleic acid genomes<sup>43</sup>. Both TLRs and RLRs sense viral RNA, with TLRs sensing RNA in the endosome<sup>44,45</sup> and RLRs in the cytoplasm of cells<sup>46</sup>. Viral DNA is sensed by TLR9<sup>47</sup>, as well as other cytosolic DNA sensors like DNA-PK, IFI16, RNA Pol III, ZBP1, AIM2 and cGAS<sup>48-53</sup>. The rapid and highly efficient response generated by activation of PRRs is possible because all pathogens can be sensed by multiple PRRs, and most if not all PRRs sense multiple pathogens.

The outcomes of PRR signalling are determined by the adaptor proteins through which each receptor signals. Many receptors contain specific protein/protein interaction domains such as caspase-recruitment domains (CARDs) or Toll/interleukin-1 receptor (TIR) domains, through which they initiate downstream signalling following ligation. TLRs signal through the TIR domain-containing adaptor proteins MyD88 and TRIF, activating both IRF3 and NF- $\kappa$ B resulting in transcription of IFN-I and pro-inflammatory cytokines<sup>38</sup>. CLRs generally function to activate or modulate NF- $\kappa$ B, via the Ras/Raf pathway, but can also internalise pathogens for degradation and antigen presentation

through Syk, dependent on cell-type and their ability to cross-talk with other PRRs<sup>41</sup>. NLRs also activate NF- $\kappa$ B, but additionally can induce the formation of distinct inflammasomes with ASC and pro-caspase 1, resulting in secretion of potent pro-inflammatory cytokines and activation of a cell death mechanism called pyroptosis<sup>54,55</sup>. NOD1 and 2 also activate autophagy to digest intracellular bacteria or viruses through the formation of autolysosomes<sup>56</sup>. Nucleic acid sensors predominantly signal to activate both IRF3 and NF- $\kappa$ B, albeit through different adaptor proteins, with DNA sensors signalling through the adaptor protein STING, TLRs through MyD88/TRIF and RLRs through MAVS. DNA sensors AIM2 and IFI16 can also activate non-canonical inflammasome formation<sup>57</sup>.

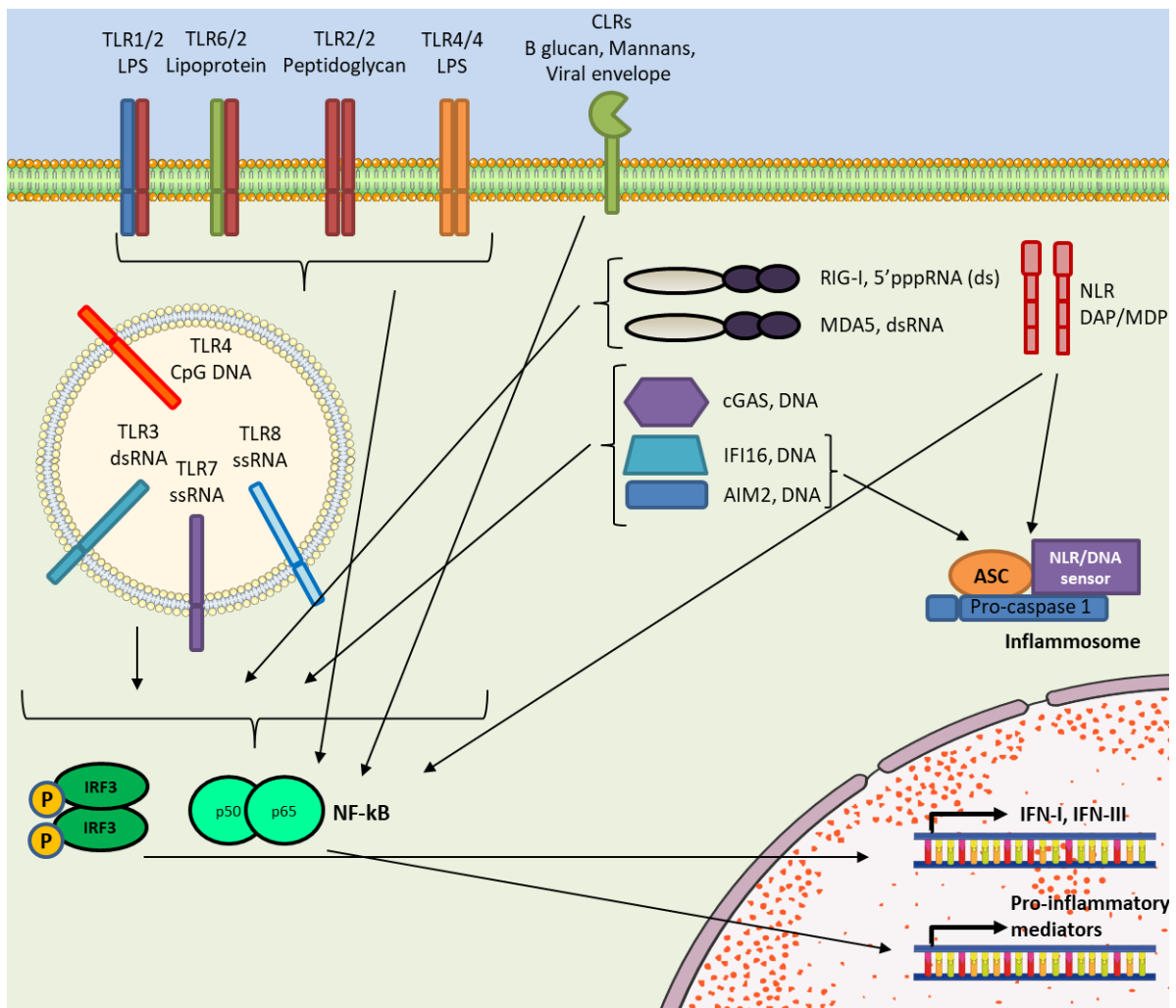


**Figure 1.1 PRR sensing in non-specialist immune cells**

PRRs sense distinct PAMPs and activate signal transduction pathways, including activation of IRF3, NF- $\kappa$ B and inflammasomes. Transcription factors IRF3 and NF- $\kappa$ B enter the nucleus and activate the transcription of Type I IFN (IFN-I) and pro-inflammatory mediators such as chemokines and cytokines.

## 1.2 Sensing of RNA viruses

As previously described, intracellular sensing of RNA viruses occurs by two PRR families: TLRs and RLRs. Despite sensing similar or overlapping RNA species often from the same viruses, their functions are not redundant, as they are expressed in distinct cell populations or cellular compartments (see Table 1.2.1).

PRR	Expression	Location	Agonist	Human-infecting viruses detected
<b>RIG-I</b>	Ubiquitous	Cytoplasm	5' ppp dsRNA short dsRNA 5' ppp ssRNA AU-rich 3' UTR RNase L cleavage products Circular viral RNA pU/UC HCV genomic RNA	Flaviviruses (including DENV, ZIKV, WNV, HCV), Coronaviruses (including SARS, MERS, SARS-CoV-2), Paramyxoviruses (SeV, MV), Adenoviruses, Rotaviruses, Picornaviruses, Rheoviruses, NDV, RSV, VSV, IAV/IBV, EBOV, JEV, Vaccinia virus, RVFV, Lassa virus, Nipah virus, Rabies virus, HIV, HepB
<b>MDA5</b>	Ubiquitous	Cytoplasm	Long dsRNA (>1kb) RNase L cleavage products AU-rich motifs	Picornaviruses (including EMCV, CBV, Rhinovirus), Flaviviruses (including DENV, WNV, HCV), Coronaviruses (SARS, SARS-CoV-2), Rotaviruses, Enteroviruses, MV, HBV, Saffold virus, Vaccinia virus, EBOV and HIV
<b>LGP2</b>	Ubiquitous	Cytoplasm	dsRNA	Picornaviruses (including EMCV), VSV, HCV, Poliovirus
<b>TLR3</b>	DC Macrophages NK cells Neural cells Fibroblast cells Epithelial cells	Endosome	Longer dsRNA (>40 bp) Structured RNA	Picornaviruses (including EMCV, Poliovirus), Flaviviruses (DENV, WNV, HCV), Coronaviruses, Herpesviruses (HSV-2, EBV), Rotaviruses, Coxsackievirus, HBV, Hantaan virus, HIV and IAV
<b>TLR7</b>	pDC B cells	Endosome	ssRNA, R848, CL097	Flaviviruses (HCV, DENV, WNV), Coronaviruses (SARS), Herpesviruses (HSV-1, KSHV) IAV, HIV-1, HBV
<b>TLR8</b>	Monocytes Macrophages mDC	Endosome	ssRNA, R848, CL095, CL097	Flaviviruses (HCV, DENV, WNV), Coronaviruses (SARS), Herpesviruses (HSV-1, KSHV) IAV, HIV-1, HBV

**Table 1.2.1: Expression, cellular localisation, agonists and viruses detected by RNA sensing PRR**

Adapted from 66,71,72.

This table contains a non-exhaustive list of families of viruses detected by the various receptors, as well as individual viruses of interest for their importance in either human disease or previous scientific studies. Abbreviations: Sendai virus (SeV), Newcastle Disease Virus (NDV), Respiratory Syncytial Virus (RSV), Measles virus (MV), Vesicular Stomatitis Virus (VSV), Influenza A virus (IAV), Ebola virus (EBOV), Japanese Encephalitis virus (JEV), Hepatitis C Virus (HCV), West Nile virus (WNV), Rift Valley fever virus (RVFV), Murine Norovirus (MNoV), Encephalomyocarditis virus (EMCV), Kaposi's sarcoma-associated herpesvirus (KSHV),

### 1.2.1 Toll like receptors

TLRs are type I transmembrane proteins and those that sense RNA reside in the endosomal membrane with the ligand binding domain projecting into the endosomal interior. Because of this, in order for naked viral RNA to be detected by TLRs, viruses must first be internalised by either autophagy or receptor-mediated endocytosis<sup>61-63</sup>. TLR3 senses both long dsRNA and branched RNA structures, which occur due to complementary regions in ssRNA stems<sup>44,64-66</sup>. TLR7 and 8 are very closely related and both sense ssRNA, but their expression profiles differ. TLR7 is predominantly expressed in plasmacytoid DCs and B cells, with inducible expression also detected in non-immune cells, and TLR8 is more strongly expressed in myeloid cells<sup>67</sup>.

Once activated, TLR7 and TLR8 recruit MyD88<sup>68</sup>, and signal to activate NF- $\kappa$ B and Mitogen-Activated Protein Kinases (MAPK) through recruitment of IL-1 receptor-associated kinases (IRAKs), TRAF6 and IRF7, as well as IFN-I through IRF5 and 7<sup>67</sup>. TLR3 signals through the alternative adaptor protein TRIF/TICAM-1<sup>58</sup>, resulting in the recruitment of TRAF proteins and RIP1. IFN-I is then activated by IRF3, requiring TRAF3 and TBK167 and NF- $\kappa$ B is activated through TRAF6 and RIP1<sup>70</sup>. TRIF-dependent signalling can also induce apoptosis, via caspase 8<sup>71,72</sup>.

### 1.2.2 RIG-I-like receptors

The RIG-I-like family of receptors (RLRs) sense RNA in the cytoplasm of infected cells and consist of three proteins: retinoic acid-inducible gene I (RIG-I), melanoma differentiation-associated protein 5 (MDA5) and laboratory of genetics and physiology 2 (LGP2). The proteins share a similar domain structure with two domains that allow for detection of RNA (Figure 1.2.2), the C terminal domain (CTD) that binds RNA, and a central helicase domain, which works with the CTD to detect immunostimulatory RNAs. As RIG-I and MDA5 also have two N-terminal caspase activation and recruitment domains (CARDs), they are capable of inducing downstream signalling through MAVS<sup>73</sup>. Because LGP2 lacks this CARD domain, it is incapable of activating downstream signalling. Instead, it is thought to regulate the activation of RIG-I and MDA5<sup>74</sup>.

LGP2 negatively regulates RIG-I signalling by various methods, such as competitively binding to and sequestering the 5' ends of immunostimulatory RNA<sup>75</sup>, preventing K63-linked ubiquitination of RIG-I by TRIM25<sup>75</sup> and preventing binding of RIG-I to MAVS to initiate downstream signalling<sup>76</sup>, all of which

occur independently of LGP2's catalytic activity<sup>77</sup>. Conversely, LGP2 promotes MDA5-mediated signalling outcomes, previously seen in response to EMCV and Poliovirus infection<sup>78,79</sup>, likely due to its ability to bind RNA ends and promote the internal binding of MDA5 to the RNA duplex and nucleation<sup>80</sup>. This process may occur through synergistic activation with RIG-I, requiring the helicase activity of both proteins<sup>81</sup>.

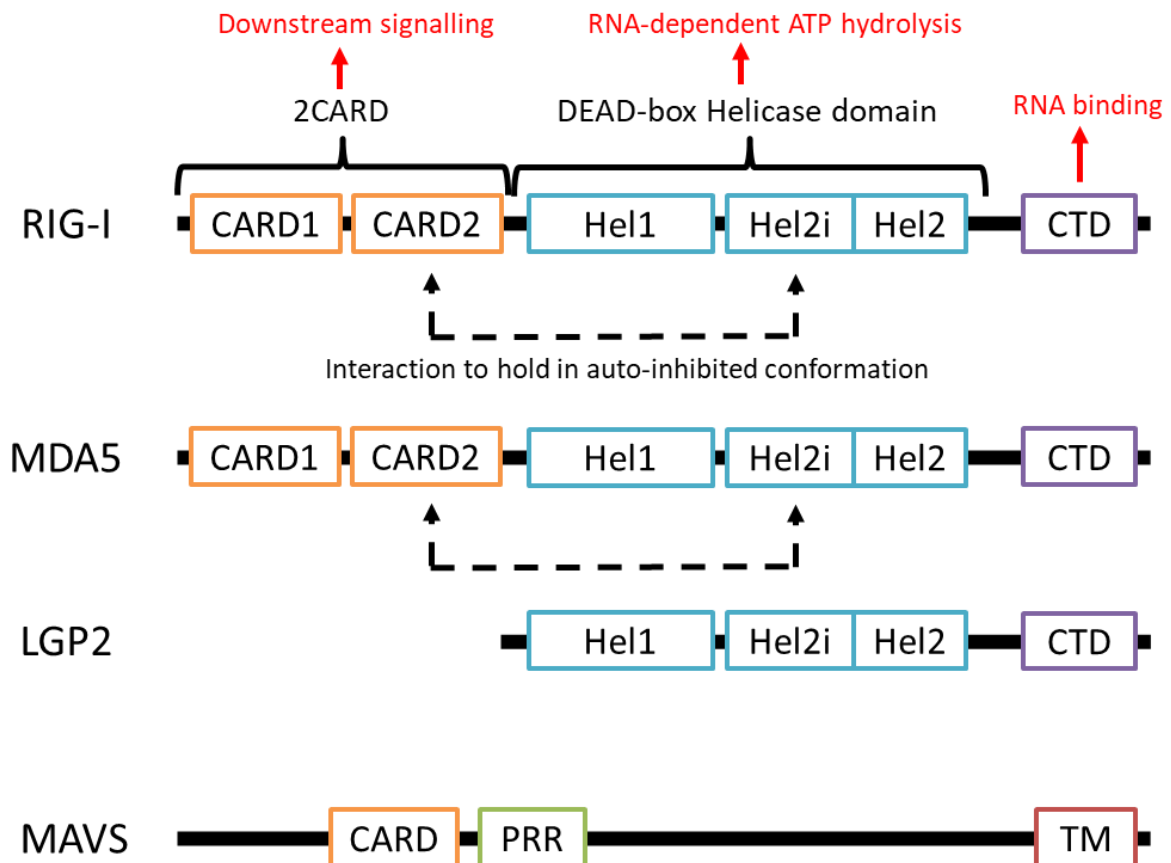


**Figure 1.2.2 Domain structure and function of RLR family and MAVS adaptor protein.** Adapted from: <sup>46</sup>. RIG-I and MDA5 are comprised of three major domain types: tandem caspase activation and recruitment domains (CARD), responsible for downstream signal transduction; a central DEAD box RNA helicase domains made of three subdomains (Hel1, Hel2i and Hel2), responsible for RNA-mediated ATP-hydrolysis; and a C-terminal domain (CTD) that binds RNA. In resting cells, an interaction between the CARD2 and Hel2i domains hold both RIG-I and MDA5 in an auto-inhibited state, released by RNA binding. LGP2 also contains a helicase and CTD, but no CARD domains. MAVS consists of a single CARD domain, a proline-rich region (PRR) and a transmembrane domain (TM).

## 1.3 RIG-I

### 1.3.1 Activation of RIG-I and MDA5 by distinct RNAs

Despite being localised in the same cellular compartment and signalling through the common adaptor protein MAVS, RIG-I and MDA5 are activated by distinct RNA species, determined by the Helicase-CTD motifs of the two proteins, which adopt different orientations relative to dsRNA<sup>82</sup>. The requirements for RIG-I activating RNAs are better characterised, with no concrete molecular structure of a MDA5 ligand yet determined.

The first identified requirement for a RIG-I-activating RNA was a 5' triphosphate group<sup>83,84</sup>, which induces activation due to the shape and orientation of the RIG-I CTD RNA binding pocket that interacts with the modified 5' end of the RNA<sup>85,86</sup>. Since then, it has been discovered that RNAs with a 5' diphosphate can also be accommodated by the CTD binding pocket<sup>87,88</sup>, such as those found in Reoviruses. In addition to phosphorylation of the 5' end of RNA, the structure of the nucleic acid itself also determines its RIG-I activating nature, as the 5' terminal nucleotide must be unmethylated at its 2'-O position in order to be accommodated by the RIG-I CTD<sup>87</sup>. Additionally, the nucleotide bound by the 5' triphosphate also needs to be base paired to a complementary strand of RNA<sup>89,90</sup>, required so the double-stranded region of RNA can be bound by the helicase domain, as it is this stable interaction with the RNA that displaces the CARD domains to activate signalling. Initially, it was thought that the preferred RNA conformation for potent RIG-I activation was blunt ended dsRNA structures<sup>89,90</sup>, but subsequent studies have suggested that a stem loop formed from a single-stranded region of RNA with complementarity to itself is in fact a better RIG-I ligand, again due to the shape of the RNA binding pocket of RIG-I<sup>91</sup>.

From these observations, it is currently believed that RIG-I binds to RNAs with regions of complementarity that drive secondary structure and a 5' multi-phosphate modification. However, due to discrepancies between the properties of various RIG-I-activating RNAs, such as those with sub-optimal 5' or 3' ends or ssRNA with internal poly-U/A-rich motifs, it has been proposed that some preferential features of RIG-I ligands may compensate for lack of another<sup>92,93</sup>.

The ability of RIG-I to recognise these specific features found only on viral RNAs is what allows it to differentiate 'self' from 'non-self'<sup>94-96</sup>. The presence of 5' phosphate groups and lack of 2'-O-methylation in viral RNAs is caused by the ribonucleoside triphosphate used by viral polymerases<sup>97,98</sup>, and the common formation of the pan-handle structure by viral RNAs occurs due to the complementarity of 5' and 3' regions of negative-sense RNA viral genomes<sup>89,99</sup>. Cellular RNAs are capped at the 5' end, with the cap shielding the phosphate groups and containing ribose 2'-O-

methylation. This feature is exploited by some viruses such as Flaviviruses, which mimic cellular RNAs by encoding a viral 2'-O-methyltransferase to add to 2'-O-methyl group to the 5' end of its RNAs to evade recognition<sup>100</sup>. Mammalian rRNAs and tRNAs are not capped but evade recognition as their 5' end is only monophosphorylated, which has been shown to be discriminated against by RIG-I<sup>101</sup>.

The activating properties of MDA5 ligands are less well characterised, although it is thought to sense predominantly long double-stranded RNA, originating from early studies showed that MDA5 was essential for the IFN-I response to Poly(I:C)<sup>102,103</sup>. Stimulation is sequence-independent but length-specific, with MDA5 able to discriminate between RNAs based on their length and regions of secondary structure<sup>104-106</sup>. This property is enabled by the ability of MDA5 to form filaments along RNA, which are more stable on longer RNAs, resulting in a stronger immune response<sup>94,95</sup>. MDA5 may also be preferentially activated by more complex, branched RNA structures, as it is more strongly activated by Poly(I:C) than other dsRNA analogues that cannot form branched structures<sup>107</sup>. MDA5 is essential for activation of the immune response to the Picornavirus family, including Encephalomyocarditis virus (EMCV), Rhinovirus and Coxsackie B virus, due to their positive-strand ssRNA genome. However, unlike RIG-I, which is the sole sensor of many viruses, MDA5 only plays a partial role in detection of the majority of viruses it senses<sup>104</sup>.

### 1.3.2 Activation of RIG-I

Upon binding to RNA, RIG-I surrounds the RNA, with three separate protein domains interacting with it<sup>108</sup>. The HEL1 domain interacts with the RNA backbone of both strands of RNA, HEL2i binds to the minor groove of the RNA backbone, important for the specific recognition of RNA, and the CTD forms a cavity with a positively charged centre to accommodate dsRNA<sup>109</sup>. As the CARDs of RIG-I domain compete with RNA for the same binding site in the helicase domain, binding of RNA by RIG-I results in the release of the CARD domains of RIG-I from the auto-inhibited conformation<sup>110</sup>.

However, the binding of activating RNA by RIG-I alone is not sufficient to activate downstream signalling, which also requires its ATPase activity<sup>111-113</sup>. The active ATPase domain in RIG-I is formed by the two helicase domains following the conformational change induced when RIG-I binds RNA<sup>114</sup>. This structural change enables catalysis of ATP by the ATPase domain, allowing RIG-I to release the bound RNA<sup>105,106,110</sup>. It also allows RIG-I to discriminate against host RNAs, as ATP catalysis quickly displaces RIG-I from self-RNAs but not from 5' triphosphate dsRNA<sup>115,116</sup>. Secondly, and more importantly, ATP hydrolysis by the ATPase domain drives oligomerisation of RIG-I by allowing RIG-I translocation from the 5' end of RNA towards the stem region, giving space for the binding of

another RIG-I monomer<sup>116</sup>. The 5'ppp end of the RNA throttles the translocation of RIG-I, delaying its unbinding from RNA and enabling a second RIG-I monomer to bind and form a stable dimer<sup>116</sup>. This oligomeric confirmation of RIG-I on immunostimulatory RNA allows the tetramerization of the CARD domains that is required for interaction with a single MAVS CARD domain and subsequent downstream signalling activation<sup>113,117-119</sup>.

RIG-I must also transition from the cytoplasm to the mitochondrial associated membranes (MAMs) to interact with MAVS. This requires formation of a complex between RIG-I, TRIM25 and the mitochondrial-targeting chaperone 14-3-3 $\epsilon$ <sup>120</sup>. RIG-I can then bind the MAVS CARD domain to stimulate self-perpetuating MAVS oligomerisation on the outside of the mitochondria, propagating the signal from RIG-I and enabling its downstream signalling activity<sup>113,117</sup>. The exact mechanism by which MAVS oligomerisation is triggered remains controversial, although all proposed mechanisms suggest the requirement for post-translational modifications of RIG-I.

The best characterised RIG-I-activating post-translational modifications are anchored and un-anchored K63-linked ubiquitin chains<sup>117,119,121</sup>. Anchored K63-ubiquitin chains are first conjugated to lysine 164 or 172 of RIG-I, allowing ubiquitination of 8 additional sites<sup>122</sup>. These ubiquitin chains, as well the non-covalent interaction of RIG-I with unanchored K63-ubiquitin chains, act to stabilise the oligomerised RIG-I CARD domains by binding along the outer rim of the tetramer, holding it in a signalling-competent "lock-washer" conformation<sup>117,123</sup>. Initially, ubiquitination of RIG-I CARD was thought to be the sole responsibility of TRIM25<sup>124,125</sup>, enabled by removal of phosphorylation modifications on the RIG-I CARD and CTD by protein phosphatase 1 (PP1)<sup>126</sup>. However, more recently it was shown to function redundantly with, or probably even secondarily to Riplet<sup>127</sup>, an E3 ligase that modifies both the CARD and the CTD of RIG-I<sup>128-130</sup>. Additional E3 ligases Mex-3 RNA binding family member C (MEX3C) and TRIM4 have been shown to conjugate K63-ubiquitin chains to the RIG-I-CARD<sup>131,132</sup>, although the role of this in downstream signalling is unknown<sup>133</sup>.

### 1.3.3 The RIG-I signalling pathway

RIG-I activation induces signalling outcomes through a downstream signalling cascade, shown in Figure 1.3.3. Oligomerisation of MAVS, which may form highly ordered filaments, occurs through a helical extension model, where the helical assembly of RIG-I-CARDs is extended by the binding of a MAVS CARD to form a larger filament<sup>117,118</sup>. This filamentous 'active' state MAVS activates downstream signalling<sup>134</sup>, resulting in activation of both IRF3 and NF- $\kappa$ B, however the exact mechanism by which this occurs is contested.

Upon oligomerisation, the increased proximity of multiple tumour necrosis factor receptor-associated factor (TRAF) binding sites in enables recruitment of TRAF proteins to the PRR domain of MAVS<sup>73</sup>, with TRAF2, 3 and 5 binding to the PVQET motif<sup>135–138</sup> and TRAF6 binds to the PGENSE and PEENEY motifs<sup>139</sup>. Recruitment activates the E3 ligase activity of TRAF proteins, leading to synthesis of K63-linked ubiquitin chains that serve as a scaffold for the recruitment and activation of many downstream signalling proteins<sup>135,137,138,140,141</sup>. Although there is some level of redundancy between the TRAF proteins and M1-ubiquitin chain-specific E3 ligase Linear Ubiquitin Chain Assembly Complex (LUBAC) for this function<sup>135,142,143</sup>, the generation of K63-linked ubiquitin chains is required<sup>144–147</sup>.

One of the proteins recruited to the K63-ubiquitin chains synthesised by TRAF proteins is NF- $\kappa$ B essential modulator (NEMO), also known as IKK gamma<sup>148</sup>. NEMO is thought to be one of the key players in the activation of both branches of the RIG-I signalling pathway and is required for activation of IRF3, 7 and NF- $\kappa$ B<sup>143,149</sup>. NEMO-mediated NF- $\kappa$ B activation occurs through recruitment of the canonical IKK complex proteins IKK $\alpha$  and  $\beta$ , which phosphorylate I $\kappa$ B $\alpha$  to induce its K48-linked ubiquitination and subsequent degradation. This releases active NF- $\kappa$ B subunits to allow dimerization and translocation into the nucleus<sup>150</sup>. NEMO-mediated IRF3 activation occurs through recruitment of the non-canonical IKK complex Serine/Threonine kinases TBK1 and IKK $\epsilon$ , which directly activate IRF3<sup>143,149</sup>. Their recruitment has been suggested to be mediated both through the IKK complex in a NEMO-dependent manner, and in a NEMO-independent manner through pre-association with the TRAF proteins<sup>143</sup>, although multiple additional adaptor proteins have also been suggested to facilitate this.

The first discovered of these was the TANK/NAP1/SINTBAD complex, which was suggested to recruit TBK1 to the RIG-I signalling complex using the TBK1-binding domains found in all three proteins<sup>151–153</sup>, a finding supported by the fact that proper function of NEMO has been suggested to rely on its TANK binding capacity<sup>154</sup>. However, their involvement has since been disputed as cells lacking all three proteins show no defect in RIG-I signalling outcomes<sup>143</sup>. Optineurin, a NEMO-related protein localised to the Golgi apparatus, also shares the TBK1-interaction domain present in TANK, NAP1 and SINTBAD, leading to its implication in TBK1 binding and activation<sup>155,156</sup>. However, it has also been shown to act as a negative regulator of RIG-I-mediated IRF3 and NF- $\kappa$ B activation<sup>157,158</sup>, disputing its previously suggested role in TBK1 recruitment. It is not known whether TBK1 and IKK $\epsilon$  are recruited to the RIG-I signalling complex by the same mechanism, although the direct recruitment of IKK $\epsilon$ , but not TBK1, to ubiquitinated MAVS has demonstrated<sup>159</sup>. Because of this, and the differing cytoplasmic

localisation of TBK1 and IKK $\epsilon$ , it is highly likely that they are recruited differently, despite their redundant functions.

In addition to their recruitment, TBK1 and IKK $\epsilon$  also need to be activated to drive activation of IRF3. This is mediated by auto-phosphorylation on Serine 172<sup>160</sup>, resulting in the reorganisation of its activation segment to enable phosphorylation of substrate proteins<sup>161</sup>. This generally occurs by the auto-catalytic mechanism of trans-autophosphorylation, induced at a high local concentration of TBK1<sup>134,161</sup>, such as when TBK1 is brought into signalling complexes via pre-association with adaptor proteins. However, proximity-induced trans-autophosphorylation is also reported to be induced by optineurin, which binds ubiquitinated TBK1 to form complexes at the Golgi<sup>162-164</sup>. In addition to phosphorylation, K63-linked polyubiquitination of both TBK1 and IKK $\epsilon$  is also required for activation of TBK1<sup>165,166</sup>.

TBK1 and IKK $\epsilon$  activate IRF3 via phosphorylation of Serine 386<sup>167-169</sup>. Despite being functionally redundant, their differential expression determines their respective roles in immunity, with TBK1 ubiquitously expressed but IKK $\epsilon$  only basally expressed in pancreas, thymus, spleen and specialist immune cells<sup>170</sup>, but upregulated during immune signalling<sup>171,172</sup>. In addition to activating IRF3, IKK $\epsilon$  has also been suggested to directly activate the ISGF3 complex through phosphorylation of STAT proteins, triggering transcription of an IKK $\epsilon$ -specific gene-set that includes ADAR-1 and IFIT3<sup>173</sup>.

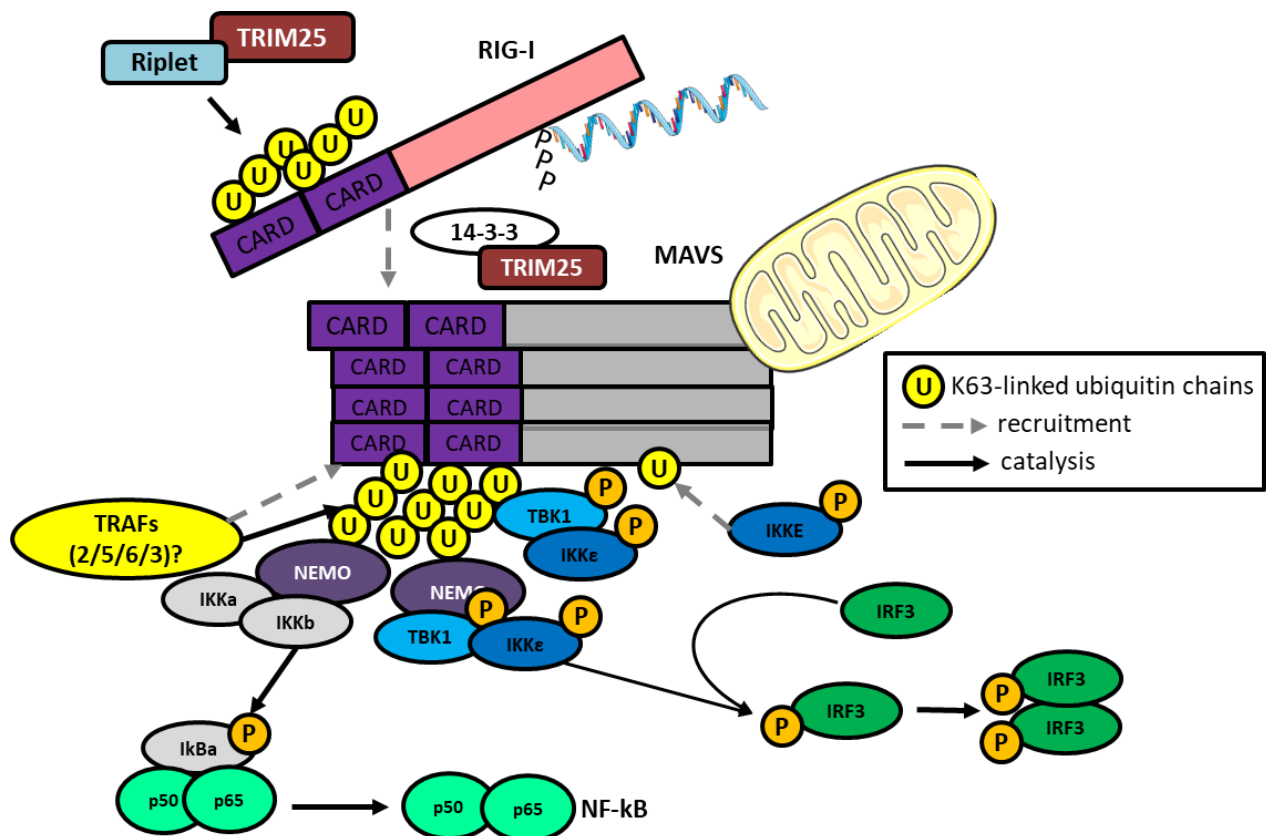


**Figure 1.3.3: A schematic of the RIG-I signalling pathway**

RIG-I binds to activating RNA species and is post-translationally modified, including the addition of K63-linked ubiquitin chains by both TRIM25 and Riplet. In a complex with TRIM25 and 14-3-3, RIG-I translocates to MAVS-containing mitochondrial membranes where the CARD domains interact and induce oligomerisation of MAVS. TRAF proteins are recruited to oligomerised CARD domains and conjugate K63-linked ubiquitin chains, which recruit NEMO, TBK1 and/or IKK $\epsilon$ . TBK1 and IKK $\epsilon$  are also recruited to NEMO and IKK $\epsilon$  to ubiquitinated MAVS. NEMO then activates NF- $\kappa$ B through recruitment of the IKK complex and TBK1/IKK $\epsilon$  activate IRF3.

### 1.3.4 Outcomes of RIG-I signalling

As previously described, RIG-I signalling results in the activation of IRF3 and NF- $\kappa$ B. Once activated, these transcription factors translocate to the nucleus, where they bind to specific sites in the promoter regions of many genes, inducing their transcription.

The interferon regulatory factor (IRF) family of transcription factors are an important feature of anti-viral immunity, regulating both innate and adaptive responses<sup>174</sup>. Once activated by phosphorylation, they form either homo- or hetero-dimers to become transcriptionally active<sup>175</sup>. IRF3 and 7 are the principal activators of IFN-I transcription after stimulation of cytosolic nucleic acid receptors. IRF3's ubiquitous expression allows it to initiate early IFN-I induction and IRF7 is upregulated in response to IFN, sustaining IFN-I activation in a feed-forward regulation loop<sup>176,177</sup>. In addition to IFN-I, IRF3 can also activate transcription of genes including *CXCL10*, *CCL5*, *ISG56* and interleukins like *IL-12*, *-15* and *-23*<sup>178-183</sup>.

The IFN-I family consists of a single IFN $\beta$  and 13 sub-types of IFN $\alpha$ , as well as some other less well characterised proteins IFN $\epsilon$ , IFN $\kappa$  and IFN $\omega$ <sup>184</sup>. IFN $\beta$  is produced by most cell types in response to IRF activation and IFN $\alpha$  is predominantly activated by IRF7 in specialised immune cells<sup>176,177</sup>. IFN $\alpha$  and  $\beta$  are secreted from cells and both bind to the IFN $\alpha$  receptor (IFNAR), activating the canonical IFN-I-induced signalling pathway shown in Figure 1.3.4. This includes the JAK/STAT pathway, where kinases Janus kinase 1 (JAK1) and tyrosine kinase 2 (TYK2) are activated by IFNAR, and in turn phosphorylate the transcription factors signal transducer and activator of transcription (STAT) 1 and 2<sup>185</sup>. Once activated, STAT1 and 2 form homo- and hetero-dimers, of which hetero-dimers bind to IRF9, and in some cases IKK $\epsilon$ , to form the IFN-stimulated gene factor 3 (ISGF3) complex. This complex binds to ISRE promoter elements, activating transcription of hundreds of interferon-stimulated genes (ISGs), which constitutes an antiviral immune response<sup>186,187</sup>. Homodimers of STAT1 or 2 bind the GAS promoter, which activates an inflammatory response through transcription of genes like IRF1 and CXCL9.

The Type III IFN (IFN-III) family, consisting of IFN $\lambda$ 1-4, is also frequently activated by virus infection<sup>188</sup>. IFN-III $\lambda$ s signal through an independent receptor, interferon lambda receptor 1 (IFNLR1). IFNLR1 is predominantly expressed in epithelial cells and some immune cell subsets, suggesting a function for IFN-III predominantly at mucosal surfaces<sup>189</sup>. Like IFNAR, IFNLR1 also activates ISGs through the canonical JAK-STAT pathway.

ISG transcription is activated predominantly by IFN-I-mediated IFNAR activation, however expression of some ISGs like ISG56 occurs directly through IRF3<sup>190</sup>, which binds to their promoter independently of IFN-I activation. Generally, ISGs function is to control virus levels in infected cells and to protect neighbouring cells from infection. This is managed by proteins like MX1, which inhibits viral replication<sup>191</sup> and IFITM proteins, which inhibit viral entry into cells<sup>192</sup>. Other ISGs, such as protein kinase R (PKR), zinc-finger antiviral proteins (ZAPs), tripartite motif (TRIM) family proteins and viperin also act synergistically as a positive feedback mechanism to enhance the antiviral response by further activating PRR signalling pathways<sup>193</sup>. One of the most highly induced ISGs is ISG15, which is a ubiquitin-like modifier protein that is covalently attached to other proteins, giving rise to many effects, such as sustained transcription of IRF3 through increased stability<sup>194</sup>, and inhibition of cell cycle progress through destabilisation of cyclin D1<sup>195</sup>. IFN further mediates the production of certain ISGs through activation of Phosphatidylinositol 3-Kinase (PI3K) signalling<sup>196</sup>, as IFN-I binds to insulin receptor substrate-1 (IRS-1), which in turn binds PI3K to activate its regulatory subunit<sup>197</sup>. IFN can also modulate the function of ISGs through inducing alternative splicing, which in the case of ADAR1 alters its cellular localisation<sup>198</sup>.

Activation of other signalling kinases like Janus-activated kinase (JNK), Extracellular signal-regulated kinase (ERK) and p38 mitogen-activated protein kinase (MAPK) by IFN-I and IFN-III is also essential for full immune activation and IFN-mediated control of certain viruses<sup>199,200</sup>. Activation of p38 MAPK is required for optimal ISG expression, as well as IFN-mediated control of certain viruses<sup>201–203</sup>. Erk mediates both IFN $\alpha$ -driven apoptosis and IFN-I induced inhibition of T-reg cell suppression of T and NK cells<sup>201,204</sup>, but also is essential for the transcription of *Isg15* and *Isg54* in mice<sup>205</sup>. In comparison, JNK signalling appears only to be weakly activated, but can promote pro-apoptotic and anti-viral signalling<sup>204,206</sup>. Finally, IFN activation also controls virus infection and immune gene transcription through affecting the expression of cellular miRNAs and lncRNAs<sup>207,208</sup>.

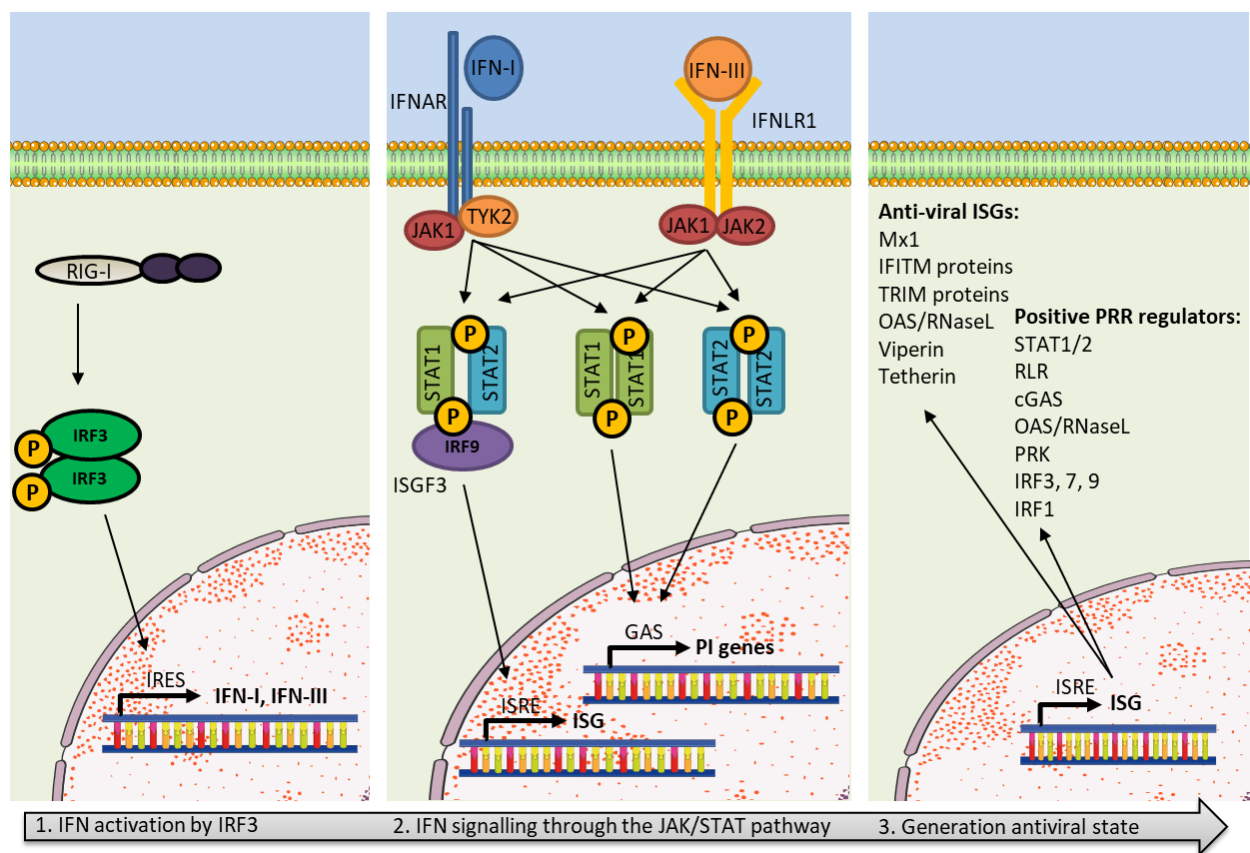


**Figure 1.3.4: A simplified pathway of activation of the IFN response by RIG-I**

Adapted from: <sup>189,209</sup>

IRF3 produced during RIG-I signalling binds to the IRES element in the promoter of both IFN-I and IFN-III genes, initiating their expression. Once expressed, they are secreted and bind to either IFNAR or IFNLR1 on the surface of nearby cells, activating the Jak-STAT signalling cascade. Formation of the ISGF3 complex activates ISG transcription through binding to the ISRE element in their promoter, whilst STAT1 and STAT2 homodimers bind to the GAS element and activate pro-inflammatory genes.

The other major transcription factor activated by RIG-I signalling is NF- $\kappa$ B. The NF- $\kappa$ B family of transcription factors consists of 5 structurally-related proteins: p50, p52, p65 (RelA), RelB and c-Rel. Once activated by degradation of I $\kappa$ B $\alpha$ , both homo- and hetero-dimers of these proteins mediate

transcription by binding to the  $\kappa$ B enhancer elements in the promoters of target genes<sup>150</sup>. The primary function of NF- $\kappa$ B is to activate the transcription of pro-inflammatory genes, but the exact inflammatory response varies between cell types. In innate immune cells like macrophages, NF- $\kappa$ B induces transcription of cytokines (tumour necrosis factor alpha) TNF- $\alpha$ , interleukins IL-1 $\beta$ , IL-6 and IL-12p40 and cyclooxygenase-2<sup>210</sup>, whereas in T cells, NF- $\kappa$ B activation regulates T cell receptor (TCR) signalling<sup>211,212</sup>. NF- $\kappa$ B also regulates inflammasome activation, as the transcription inflammasome proteins NLRP3, pro-IL-1 $\beta$  and pro-IL-18 are dependent on NF- $\kappa$ B-activation, occurring predominantly through the post-translational modification of signalling pathway proteins or by binding proteins.

### 1.3.5 Regulation of RIG-I signalling

As described earlier, RIG-I is subjected to both activating and inhibitory post-translational modifications to control its RNA binding ability and ATPase activity, as well as to regulate activation of downstream signalling, shown in Figure 1.3.5. The ubiquitination of RIG-I by TRIM25 and Riplet is opposed by several de-ubiquitylating enzymes (DUBs), including ubiquitin specific peptidases (USP) 3 and 21 and Cyldromatosis (CYLD), both of which specifically cleave K63-linked ubiquitin chains. M1-linked ubiquitination of TRIM25 by LUBAC also prevents RIG-I ubiquitination as it destabilises the TRIM25-RIG-I interaction<sup>213</sup>. Conjugation of differently linked ubiquitin chains, K48-linked ubiquitin, to the CARD and CTD of RIG-I by the E3 ligases Casitas B-lineage lymphoma proto-oncogene (Cbl) and ring finger proteins (RNF) 122 and 125, targets it for degradation<sup>214,215</sup>. This K48-ubiquitination is prevented by SUMOylation of RIG-I by TRIM38. Premature activation of RIG-I is prevented by phosphorylation of its CARDS by protein kinase C (PKC) isoenzymes PKC $\alpha$  and PKC $\beta$  and the CTD by casein kinase II (CKII)<sup>216,217</sup>, modifications that prevent TRIM25 binding and K63-linked ubiquitination<sup>218,219</sup>. The ATPase activity of RIG-I can also be positively regulated by PACT, which binds to the CTD of RIG-I to stimulate its ATPase activity<sup>220,221</sup>, and RNA binding protein DEAH-box helicase 15 (DHX15)<sup>222</sup>.

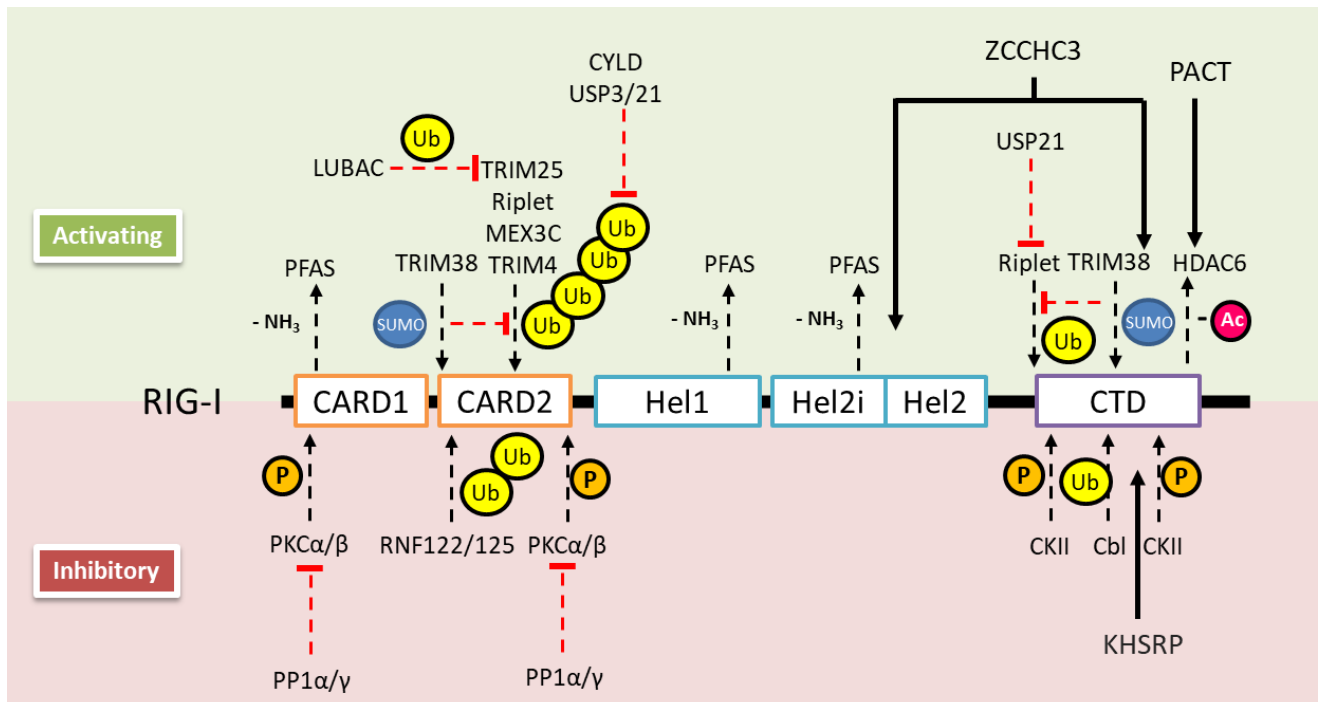


**Figure 1.3.5: Regulation of RIG-I by post-translational modifications and binding proteins**

Adapted from <sup>46</sup>.

RIG-I signalling is regulated by deamidation (-NH<sub>3</sub>), phosphorylation (P), SUMOylation (SUMO), ubiquitination (U), deacetylation (-Ac) and binding proteins. Activating modifications are found in the green section above the RIG-I schematic and inhibitory modifications in the red section below. Modifications are indicated by a dashed black arrow, with inhibition of these modifications indicated by a red dashed arrow with a flat head. Binding is indicated by a solid black arrow. Proteins responsible for modifying/binding are named for each modification.

Signalling is also regulated by post-translational modification of MAVS. Oligomerisation of MAVS requires K63-linked ubiquitination, catalysed by TRIM31<sup>223</sup>. This is promoted by O-GlcNAcylation at Ser366 of MAVS<sup>224</sup>, and phosphorylation by IKKε, which prevents the interaction of Fas-associated factor 1 (FAF1) with MAVS<sup>225</sup>. Recruitment of both TBK1 and IKKε to MAVS is promoted by TRIM-21 mediated K27-linked ubiquitination and K63-linked ubiquitination of MAVS<sup>138,226</sup>, although K27-linked ubiquitination by MARCH8 can also promote lysosomal autophagy of MAVS by NDP52<sup>227</sup>. MAVS is also modified by K48-linked ubiquitin chains at multiple sites by multiple E3 ligases: TRIM25<sup>228</sup>, AIP4<sup>229</sup>, PCBP1<sup>230</sup>, TAX1BP<sup>231</sup>, Smurf1, 2 and Ndfp1<sup>232,233</sup>, OTUD1<sup>234</sup>, MARCH5<sup>235</sup> and RNF5<sup>236</sup>, all of which mediate degradation of MAVS by various mechanisms. These ubiquitin chains are removed by OTUD4 to stabilise MAVS<sup>230</sup>, and their formation is inhibited by various proteins like cyclophilin A, which competes with TRIM25 for MAVS binding<sup>237</sup>. Phosphorylation of MAVS by TBK1 and IKKβ also positively regulates MAVS signalling by mediating recruitment of IRF3<sup>238</sup>, a mechanism blocked by PPM1A<sup>239</sup>.

In addition to regulation by host proteins, RIG-I signalling is also negatively regulated by many RNA viruses to subvert their detection. Firstly, many viruses disguise their RNA, for example by encoding

a 2'-O-methyltransferase or covalently bonding either viral or host proteins to the 5' end of their RNAs<sup>240–242</sup>. Additionally, viral proteins bind and sequester their own RNA to prevent detection<sup>243</sup>. After detection of viral RNA, subversion of signalling generally occurs through the prevention of ubiquitination of RIG-I by TRIM25, whose activity is directly inhibited by the NS1 protein of Influenza A virus (IAV) and Respiratory Syncytial virus (RSV)<sup>244,245</sup>, as well as proteins encoded by human papilloma virus (HPV), Epstein Barr virus (EBV), multiple Paramyxoviruses<sup>246,247</sup> and Dengue virus (DENV) sub-genomic RNA<sup>248</sup>. The E3 ligase Riplet is also targeted by multiple viral proteins to inhibit ubiquitination of RIG-I<sup>249,250</sup>, and multiple viral-encoded DUBs function to remove ubiquitin modifications<sup>251</sup>. Downstream signalling is blocked by many viral proteins that inhibit RIG-I's binding to MAVS<sup>252–254</sup>, or sequester it to a cellular location from which it cannot signal<sup>255</sup>.

MAVS is itself also inhibited by many by viral proteins that either cleave or degrade it. Cleavage occurs through viral proteases encoded by Hepatitis C virus (HCV)<sup>256</sup>, Seneca Valley virus<sup>257</sup>, human rhinovirus C<sup>258</sup>, and coxsackievirus B3 (CVB3)<sup>259</sup> and Hepatitis A<sup>260</sup>. Degradation of MAVS is mediated by viruses that promote the conjugation of K48-linked ubiquitin chains, such as Hepatitis B virus (HBV), HCV, Severe Acute Respiratory Syndrome (SARS) coronaviruses and rotaviruses<sup>261–264</sup>. Downstream signalling is inhibited by viral proteins that block the interaction of TRAF proteins with MAVS, such as human metapneumovirus (hMPV) M2-2, IAV NS1, HCV NS5A and the Nipah virus V protein<sup>265–268</sup>. Downstream signalling proteins are also targeted by viruses, mediated by direct interaction, prevention of signalling complex formation as is the case with SARS-CoV-2 Membrane protein<sup>269</sup>, or through mediating degradation, like the FMDV protein Lpro that targets TBK1<sup>270</sup>. As these signalling proteins are often common to many signalling pathways, their inhibition can block viral detection and downstream signalling from multiple receptors.

## 1.4 Viruses

### 1.4.1 Viruses as infectious agents

Viruses are one of the five major categories of infectious agents and are obligate intracellular parasites. Previously described as “entities hovering on the threshold of life”<sup>271</sup>, they are simply made up of a nucleic acid genome encapsulated in a shell of proteins and sometimes lipids, meaning that they are dormant until they have entered a host organism. Viruses are a simple but incredibly diverse class of pathogen, ranging in size from only 20 nm for Parovirus particles to approximately 1 µm for Ebola, and encoding anywhere between four and multiple-hundred proteins.

Viruses infect all known cellular organisms, including bacteria, fungi, metazoans and archaea, as well as all classes of animal and plant. For humans, virus entry into the body occurs predominantly through the mucous membranes in the nose, mouth, eyes, or breaches in the skin barrier. Infection arises through direct contact with contaminated objects, airborne droplet transmission, or via vectors such as mosquitos. Generally, the life cycle of a virus in a host cell has three main stages: entry, genome replication and exit<sup>272</sup>. Viruses enter cells by attachment to the cell membrane, penetration into the host cell cytoplasm, and uncoating of the protein shell to release its nucleic acid material. The viral genome is then used for replication and expression of viral proteins, which are assembled into new virus particles that are released from the cell. Viral infection often results in disease, caused by the disruption of normal cellular processes by the virus, often due to the hijacking of the cellular machinery to enable viral replication, production of viral proteins and release of new virus particles<sup>272</sup>.

Since their discovery, viruses have been classified by many methods including shared morphology and genome type, with standard taxonomy determined by evolutionary relationships. The most commonly used classification today is the Baltimore classification, which is based on how messenger RNA is synthesised by the virus during its replication cycle<sup>273</sup>. Within this framework, there are four classes of RNA viruses: those with a double-stranded genome (Group III), those with either a positive (Group IV) or negative sense (Group V) single-stranded genome, and single stranded RNA viruses with a DNA intermediate in their life cycle (Group VI).

### **1.4.2 The impact of viruses on humanity**

Humanity has felt the impact of viruses for long before their existence was discovered, most markedly by their ability to cause epidemic disease, a feature that began with the agricultural revolution, which put humans into contact with many new viruses, and has been further progressed by human migration, domestication of livestock and, most importantly to modern day society, the fact that most people now live in large, densely-populated communities<sup>271</sup>. Despite the invention of vaccines within this period, viruses have been the cause of the deadliest infectious events of the last 100 years, including the 1918 Spanish Influenza outbreak, which is estimated to have killed 21 million people<sup>274</sup>, the HIV/AIDS pandemic that has resulted in over 30 million people living with AIDS worldwide<sup>275</sup>, and the recent COVID-19 pandemic, which is likely to exceed the mortality of any novel virus since then. Virus infection is also the cause of a huge socio-economic burden<sup>276</sup>, as evidenced by COVID-19, which is estimated to have caused a 7% relative reduction of the global economy<sup>277</sup>.

### 1.4.3 RNA viruses known to activate RIG-I

In this study we are focused on the composition and outcomes of the RIG-I signalling complex, as well as how it is regulated. To enable our study of this, we employed multiple RNA viruses known to stimulate RIG-I, including respiratory viruses Sendai virus and IAV and arbovirus ZIKV.

#### 1.4.3.1 Sendai virus

Sendai virus (SeV) is a Paramyxovirus with a single-stranded negative sense RNA genome and a lipid envelope containing glycoproteins as well as haemagglutinin (HA) and neuramidase (NA) proteins<sup>278</sup>. Despite its ability to infect humans, natural infection with SeV only appears to occur in the upper respiratory tract of rodents<sup>279,280</sup>. SeV is a potent and specific activator of RIG-I, producing one of the best characterised natural RIG-I agonists, a 546 nucleotide copyback genome RNA species<sup>281,282</sup>. This is especially true for the Cantell strain of the virus, which potently activates RIG-I due to the production of large amounts of defective interfering (DI) RNA genomes, produced when the polymerase leaves the cRNA template and back-copies the 5' end of the viral RNA product during replication<sup>283</sup>. This results in short RNAs with perfect 5' and 3' complementarity that are preferentially bound by RIG-I over full-length viral. RIG-I's specificity for SeV is also conferred by the SeV V protein, which inhibits the helicase activity of MDA5 to prevent MDA5-mediated signalling<sup>284</sup>. Additionally, the expression of the SeV C protein is absent from many DI-producing strains of SeV, preventing its well described inhibition of RIG-I<sup>285,286</sup>.

Due to its ability to potently activate RIG-I, inducing a strong IFN-I response, SeV is used in basic and applied biology as a tool for delivering molecules into cells and for commercial generation of IFN<sup>287,288</sup>. More recently, SeV has been optimised for use in gene therapy techniques and as a virus vaccine adjuvant<sup>289,290</sup>.

#### 1.4.3.2 Influenza A virus

Influenza A virus (IAV) is one of three strains of Influenza, all of which belong to the *Orthomyxoviridae* family of RNA viruses. IAV has a segmented single-stranded negative-sense RNA genome and is an enveloped virus. Like with SeV, the viral envelope contains the surface proteins hemagglutinin (HA), which allows it to bind to receptors on the surface of cells to facilitate viral entry, and neuraminidase (NA), which enables viral replication and release<sup>291</sup>. Influenza A viruses are further classified by their antigenic variation, determined by the combination of HA and NA variants expressed on the viral envelope, with 16 variants of HA and 9 variants of NA identified<sup>292</sup>.

IAV is one of the major causes of respiratory infections in humans and animals<sup>293</sup>, infecting between 9 and 45 million Americans every year and generally causing constitutional and upper respiratory tract symptoms like fever, headache, cough and sore throat. However, cardiac, musculoskeletal and neurologic complications can result in severe disease highly pathogenic to humans<sup>294</sup>, with annual outbreaks resulting in approximately half a million deaths, mostly in the very young and old<sup>295–297</sup>. Much of the impact of IAV is enabled by its ability to undergo changes in the antigens present in its surface glycoproteins. This occurs both by antigenic drift, which makes small changes to the virus year on year; and antigenic shift, where reassortment of the viral genome with pre-existing strains, often from other species like pigs and chickens, results in a major change in the viral genome, often the cause of emergent pandemic strains of the virus<sup>298</sup>.

IAV is predominantly sensed by detection of its RNA genome or host RNA present in dying IAV infected cells by PRR at the mucosal surface and in respiratory epithelial cells. This is generally mediated through RIG-I and NLRP3 in the cytoplasm, and TLR3, 7 and 8 in the endosome<sup>299</sup>. Detection by TLRs results in the production of pro-inflammatory cytokines and chemokines, restriction of virus replication and recruitment of innate and adaptive immune cells. Detection of IAV by RIG-I, which occurs both in the cytoplasm and nucleus of infected cells<sup>300</sup>, depends heavily on the production of both defective interfering panhandle genomes and short aberrant mini-viral RNAs during natural IAV infection<sup>301,302</sup>, resulting in activation of pro-inflammatory cytokines through NF- $\kappa$ B and IFN-I by IRF3<sup>299</sup>.

To help avoid detection by the majority of PRRs, IAV replicates in the nucleus of cells, like Bornaviruses and Orthomyxoviruses. Whilst in the nucleus, these viruses 'steal' mRNA cap structures from host RNAs to avoid detection by nuclear RIG-I<sup>303</sup>. Antagonism of innate immune signalling by IAV infection is predominantly mediated by NS1, which has functions as wide-ranging as binding and sequestering RNA, shielding RNA from detection by RIG-I, inhibiting the ubiquitination of RIG-I by TRIM25, blocking host gene expression and interfering with the function of ISGs like PKR and OAS<sup>304</sup>.

### **1.4.3.3 Zika virus**

Zika virus (ZIKV) is a Flavivirus, closely related to Dengue (DENV) and Chikungunya (CHIKV). It has a positive-sense single-stranded RNA genome encoding a polyprotein that is cleaved into three structural and seven non-structural proteins including a protease, helicase and RNA-dependent RNA polymerase (RdRp)<sup>305</sup>. Unlike both SeV and IAV, ZIKV is spread by a vector: the *Aedes* mosquito, although it can also be vertically transmitted during pregnancy<sup>306</sup>. First discovered in rhesus macaques in Uganda in 1947, ZIKV-mediated human disease was identified in 1952. After over 50

years of almost no identified cases of natural infection, ZIKV outbreaks began in 2007. Generally, symptoms were mild: fever, headaches, rashes, joint pain and conjunctivitis. However, more recent outbreaks have linked ZIKV infection with congenital microcephaly in new-borns and Guillian-Barre syndrome in adults<sup>307,308</sup>.

ZIKV is detected by TLRs 3 and 7, initiating signalling cascades that activate an IFN-I and ISG response, as well as triggering apoptosis<sup>309</sup>. RIG-I also recognises the 5' non-coding region of viral genomes and signals through MAVS to activate a pro-inflammatory and IFN-I response through NF- $\kappa$ B and IRFs 3 and 7<sup>310</sup>. ZIKV infection also activates the cGAS-STING signalling axis<sup>311</sup>. The induction of both IFN-I and ISGs like IFIT1-3, Viperin and OAS1 by TLRs and RLRs restricts ZIKV replication<sup>312,313</sup>.

ZIKV, like other flaviviruses, encodes many proteins to antagonise PRR signalling pathways. The ZIKV NS3 proteins binds the molecular chaperone 14-3-3 to inhibit translocation of RIG-I<sup>314</sup>; the NS4A protein binds to the CARD domain of MAVS, preventing its interaction with RIG-I<sup>252,315</sup>; and NS1, NS2a, 2b and 4b proteins reduce RIG-I-mediated TBK1 phosphorylation<sup>316</sup>. ZIKV NS5 binds both TBK1 and TRAF6, preventing their interaction<sup>317</sup>, and also binds endogenous IRF3 to prevent IFN-I promoter activation 316. ZIKV can also inhibit the cGAS-STING pathway through cleavage of STING by NS2b3<sup>318</sup>, as well as Jak-STAT signalling<sup>319</sup>.

## 1.5 LUBAC and M1-ubiquitin chains

### 1.5.1 Ubiquitin

Ubiquitin is a small, highly conserved and highly stable globular protein, expressed almost invariantly in every organism from yeast to humans<sup>320</sup>. In a process called ubiquitination, ubiquitin is conjugated to many proteins as a post-translational modification to regulate many cellular processes, from protein degradation and DNA damage responses to intracellular signalling and protein trafficking<sup>320</sup>.

Ubiquitination of a target protein requires catalysis by an enzymatic cascade shown in Figure 1.5.1, consisting of three proteins: the E1 ubiquitin activating enzyme, the E2 conjugating enzyme and the E3 ubiquitin ligase. In order to conjugate ubiquitin to its substrate protein, the E1 enzyme activates ubiquitin by binding to its C terminus, a reaction which requires ATP. Activated ubiquitin is then transferred to the E2 conjugating enzyme, which forms a complex with the E3 ligase that binds the target substrate protein. This results in transfer of the ubiquitin moiety from the E3 to a lysine residue on the substrate protein<sup>321</sup>. To form ubiquitin chains, the E3 then unbinds the used E2 and binds to a new E2-ubiquitin complex and repeats the transfer of ubiquitin onto a residue on the

already-conjugated ubiquitin monomer. There are only two known E1 enzymes, about 40 E2 enzymes, but over 600 known E3 ubiquitin ligases<sup>322</sup>. Such diversity in E3 ligase enzymes is required, as they confer substrate specificity, determined by protein and non-protein interaction domains, recruitment motifs, and sometimes ubiquitin chain-type specificity<sup>323</sup>. E3 ligases are classified into three types: RING (Really Interesting New Gene), HECT (Homologous to E6AP C-Terminus) and RBR (RING-between-RING), based on the structure and mechanism of action of their ligase domain. RING E3 ligases catalyse direct transfer of ubiquitin from the E2 to the substrate protein, whereas HECT and RBR ligases use a two-step process to catalyse this, via a cysteine residue in the E3<sup>323</sup>.

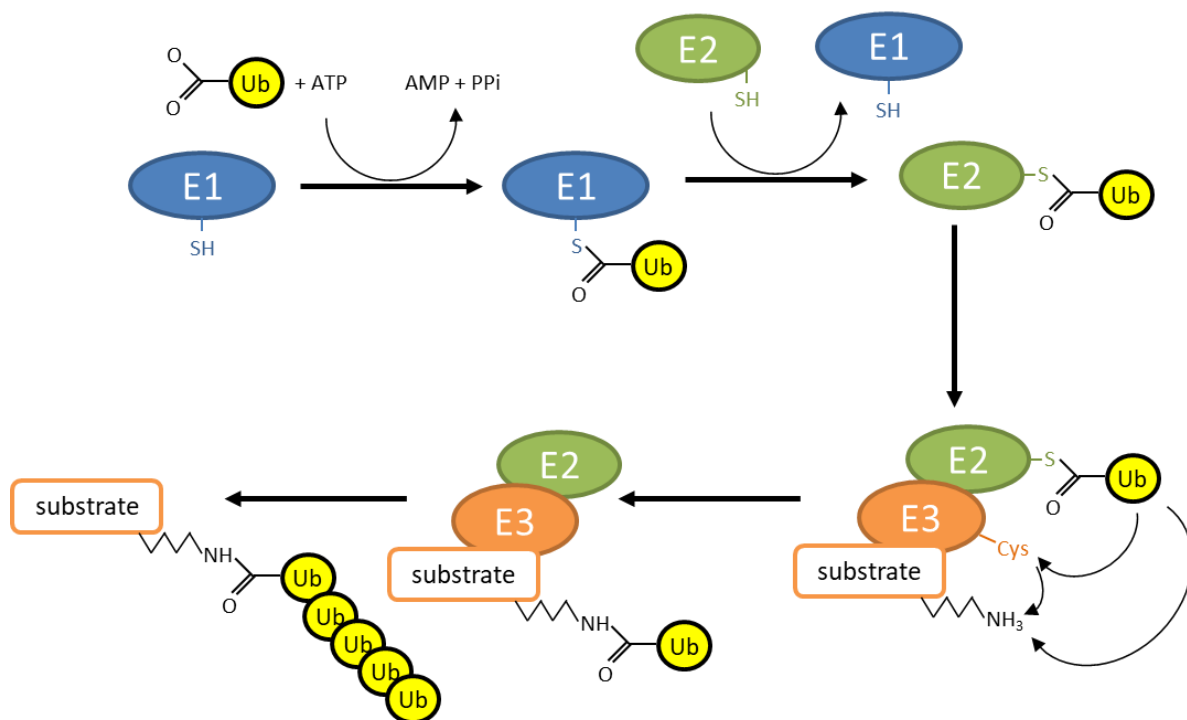


**Figure 1.5.1: The ubiquitination system**

Adapted from <sup>321,324</sup>

The E1 activating enzyme binds and activates ubiquitin, requiring ATP. It then transfers ubiquitin to the E2 conjugating enzyme, which binds the E3 ligase, forming a complex that can bind the substrate protein. Ubiquitin is then transferred from the E2 to a lysine on the surface of the substrate protein, either directly, for RING ligases, or via a catalytic cysteine on the E3, for HECT and RBR ligases.

The ability of ubiquitin to modulate such a broad range of processes is determined by its ability to form very diverse modifications, referred to as the ubiquitin code<sup>320</sup>. Substrate proteins can be modified by a single ubiquitin molecule at a single lysine residue, termed mono-ubiquitination; or at multiple lysine residues, multi-mono-ubiquitination. Once a substrate is modified by a single

ubiquitin, polyubiquitination occurs through the binding of additional ubiquitin moieties to the initial ubiquitin<sup>325</sup>.

Polyubiquitination results in the formation of 8 different types of homotypic chains, due to the binding of additional ubiquitin moieties onto one of seven lysine residues on the previous ubiquitin, or its N-terminal methionine. M1-linked, otherwise known as linear, ubiquitin chains are joined in a head-to-tail fashion via the C-terminal carboxyl group and the N-terminal methionine. These different linkage types (M1, K6, K11, K27, K29, K33, K48 and K63-linked) have different functional significances. K48-linked ubiquitin chains are the most common modification, marking proteins for proteolytic degradation to regulate many cellular processes like cell division and development, the stress response and immune signalling pathways<sup>326</sup>. Both K11- and K29-linked chains have been established as secondary proteasomal degradation signals, with K11-linked chains used generally in cell cycle regulation<sup>326,327</sup>. Other ubiquitin chain-linkage types are non-degradative, with K6-linked chains possibly involved in mitochondrial homeostasis<sup>328</sup> and K33-linked chains predominantly involved in protein trafficking and signalling regulation<sup>329</sup>. The remaining chain types, K63-, K27- and M1-linked ubiquitin chains are involved in the regulation of diverse signalling pathways. The most common of these are K63-linked chains<sup>321</sup>, which have a similar structure and function to M1-linked chains<sup>331</sup>. K27-linked chains are the least well understood but are thought to serve as scaffolds in the DNA damage response, recruiting downstream signalling proteins<sup>327</sup>.

Heterotypic ubiquitin chains, characterised by the modification of multiple residues of a single ubiquitin moiety in the ubiquitin chain, are more recently discovered<sup>332</sup>. Their function can differ from or improve the function of either of chain linkage-types it is comprised of, thought to occur due to an increased concentration of ubiquitin close to the substrate protein. For example, K11/K48-linked heterotypic chains result in more efficient proteasomal degradation than seen with K11 or K48-linked chains alone, by improving recognition of the substrate protein by the proteasome<sup>333</sup>. Similarly, K29/K48- and K48/K63-linked ubiquitin chains reveal novel pathways to proteasomal degradation<sup>334,335</sup>. M1/K63-linked chains, generated by the modification of K63-linked chains with M1-linked chains to form branched or mixed hetero-typic structures mediated the recruitment of kinases and activation of NF- $\kappa$ B and inflammatory signalling downstream of many immune receptors<sup>336-338</sup>, with the mixed chains improving signalling outcomes by more efficiently bringing together downstream signalling proteins like NEMO and the TAK1 complex<sup>339,340</sup>, increasing the speed and accuracy of signalling<sup>332</sup>.

## 1.5.2 LUBAC

Unlike other ubiquitin linkages, which are generated by multiple E3 ligases, only the Linear Ubiquitin Chain Assembly Complex (LUBAC) is capable of generating M1-linked ubiquitin chains in humans<sup>341</sup>. LUBAC is a 600 kDa complex of unknown stoichiometry composed of three subunits: HOIL-1-interacting protein (HOIP), Heme-oxidised IRP2 Ubiquitin ligase-1 (HOIL-1), and Shank-associated RH domain-interacting protein (SHARPIN)<sup>341-344</sup>, shown with interactions indicated in Figure 1.5.2. The complex is formed by interactions between the ubiquitin-like (UBL) domains of HOIL-1 and SHARPIN and the ubiquitin associated (UBA) and nuclear protein localisation 4 (Npl4) zinc finger (NZF) domains of HOIP<sup>342-345</sup>, stabilised by long-term interactions between the LUBAC tethering motif (LTM) domains of HOIL-1 and SHARPIN<sup>346,347</sup>.

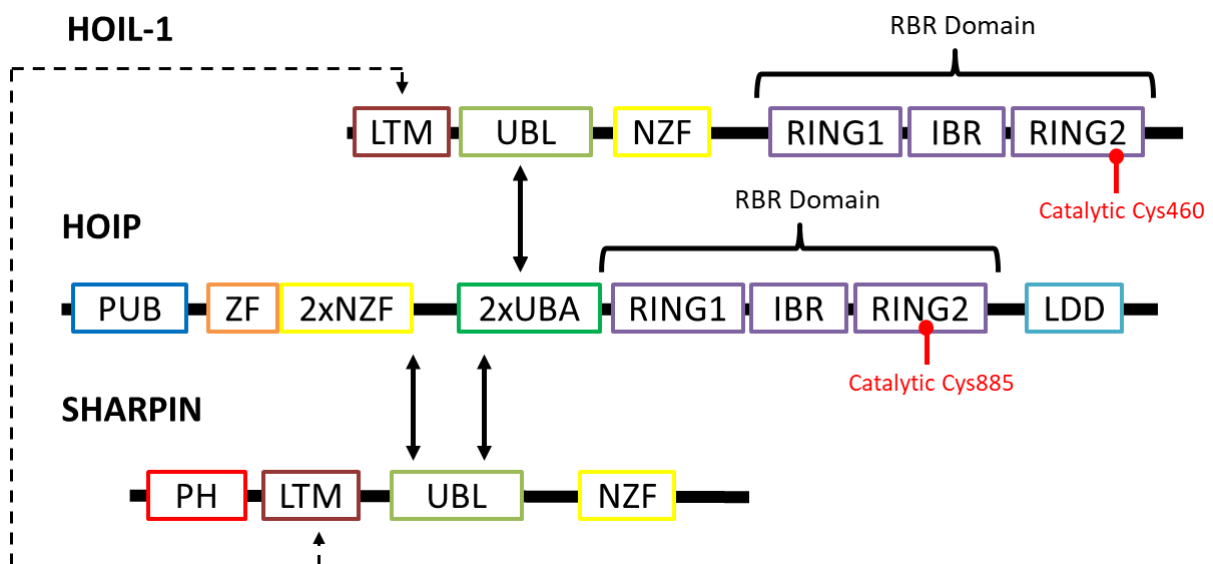


**Figure 1.5.2: Schematic representation of the domain structure and interactions between the LUBAC components.** Adapted from <sup>331</sup>.

Domains of each LUBAC component consist of LUBAC tethering motif (LTM), ubiquitin-like (UBL), nuclear protein localisation 4 (Npl4) zinc finger (NZF), really interesting new gene (RING), in-between-RING (IBR), peptide:N-glycanase/UBA- or UBX-containing proteins (PUB), zinc finger (ZF), ubiquitin-associated (UBA), linear ubiquitin chain determining domain (LDD) and pleckstrin homology (PH). Interactions between proteins indicated by thick double-headed arrows and long-distance stabilising interactions by dashed double-headed arrows.

Both HOIP and HOIL-1 are RBR E3 ligases, but only HOIP is capable of generating M1-linked ubiquitin chains, a unique function enabled by the position of its linear ubiquitin chain determining domain (LDD)<sup>345,346,348-350</sup>. HOIL-1 and SHARPIN function as part of the LUBAC complex to stabilise HOIP in an active conformation, with HOIP otherwise auto-inhibited by interactions between its RBR domain and N-terminus<sup>349</sup>. In addition to removing the auto-inhibition, binding of either SHARPIN or HOIL-1 to HOIP facilitates the E2 enzyme-mediated loading of HOIP, enabling ubiquitination to occur<sup>346</sup>.

HOIL-1 and SHARPIN are also required for the stability of HOIP expression in some contexts<sup>342-344,347,349,351</sup>.

Despite earlier reports that HOIL-1 only has very weak ligase activity, dispensable for LUBAC activity<sup>349</sup>, it has more recently been shown to play a vital role in LUBAC's function. First, initial ubiquitination of NEMO was shown to require catalysis by the RBR domain of HOIL-1 as well as HOIP<sup>352</sup>. HOIL-1 is also able to regulate the E3 ligase activity of LUBAC by mono-ubiquitination of all three subunits, which in turn directs HOIP to auto-ubiquitinate itself, preventing generation of M1-linked ubiquitin chains<sup>353</sup>. Finally, HOIL-1 can generate an atypical oxyester ubiquitin linkage, enabling conjugation of ubiquitin to serine and threonine residues on substrate proteins, instead of the typical lysine, resulting in the HOIL-1-catalysed conjugation of ubiquitin chains to IRAK1, 2 and MyD88, as well as itself and SHARPIN<sup>354</sup>. Generation of oxyester linkages by HOIL-1 has been suggested to catalyse M1-linked ubiquitination through a co-ordinated relay between HOIL-1 and HOIP, as well as promote the generation of heterotypic K63/M1-ubiquitin chains in both TNF and TLR signalling<sup>338,355</sup>, with varying signalling outcomes<sup>355,356</sup>.

SHARPIN does not have a ligase domain so is incapable of generating ubiquitin chains itself, however it helps determine the target of M1-ubiquitination, directing it to NEMO during TLR signalling<sup>330,331</sup>. It also appears to have a specific function in protecting cells from immune receptor-driven cell death<sup>343,357-360</sup>, although the exact mechanism by which this occurs is unknown. SHARPIN functions as a regulator of anti-apoptotic and anti-pyroptotic pathways<sup>343,359,361</sup>, meaning that it is regarded as a proto-oncogene<sup>362</sup>, upregulated in many types of human cancer with a specific role as a metastasis gene and prognostic marker for breast cancer<sup>363</sup>. Cancer regulation is thought to primarily occur through SHARPIN's role in LUBAC, controlling activation of the NF- $\kappa$ B pathway resulting in upregulation of pro-survival genes<sup>364</sup>, and through LUBAC-mediated ubiquitination and degradation of PKC $\zeta$ , enhancing tumour size and adaptation<sup>365</sup>.

### 1.5.3 Regulation of LUBAC

The constitutive activation of LUBAC even in the absence of upstream signalling, due to the binding of HOIL-1 and SHARPIN to HOIP removing auto-inhibition of HOIP<sup>342-344</sup>, means that its function must be tightly regulated. This negative regulation is carried out by the deubiquitinases (DUBs) OTU Deubiquitinase With Linear Linkage Specificity (OTULIN) and Cylindromatosis (CYLD), proteases which bind to and cleave M1-linked ubiquitin chains<sup>366-369</sup>. OTULIN hydrolyses only M1-linked ubiquitin chains, due to its highly selective binding of M1-chains and a specific mechanism of substrate-assisted catalysis caused by the binding position of the proximal ubiquitin in M1-linked

chains that activates the protease<sup>366,367</sup>. Conversely, CYLD hydrolyses both K63-linked and M1-linked ubiquitin chains<sup>368,369</sup>. In addition to hydrolysing M1-linked ubiquitin chains, OTULIN, but not CYLD, also prevents LUBAC from auto-ubiquitination<sup>367,370–372</sup>. The DUB A20 can also bind to M1-linked ubiquitin chains but does not hydrolyse them<sup>373,374</sup>.

To enable regulation, both OTULIN and CYLD form complexes with LUBAC. For OTULIN, this occurs through the binding of the PIM domain of OTULIN to the PUB domain of HOIP<sup>371,375</sup>, whereas for CYLD, complex formation is mediated by the adaptor protein Spermatogenesis-associated 2 (SPATA2), which interacts with the USP domain of CYLD and the PUB domain of HOIP, resulting in a CYLD-SPATA2-LUBAC complex<sup>376–379</sup>. Only either OTULIN or SPATA2 can bind to the PUB domain of HOIP, so each LUBAC complex is regulated by only one of either OTULIN or CYLD<sup>374,380</sup>.

Disassembly of M1-linked ubiquitin chains by OTULIN and CYLD negatively regulates activation of NF- $\kappa$ B in many signalling pathways. It is thought that the DUBs regulate LUBAC differently in different signalling contexts, as only CYLD translocates with LUBAC to the TNF-RSC<sup>374,375,378</sup>, and depletion of OTULIN results in differing outcomes in different cell-types<sup>381</sup>. As A20 can't hydrolyse M1-linked ubiquitin chains upon binding, it instead negatively regulates TNFRSC signalling by blocking the binding of NEMO to M1-linked ubiquitin chains<sup>382,383</sup>. Conversely, the formation of K63-/M1-linked heterotypic chains prevents cleavage of K63-linked chains by A20, regulating signalling pathways<sup>373,374</sup>.

LUBAC is also targeted by pathogen effector proteins, preventing its function. Viral effectors include HCV protein NS3<sup>332</sup>, which binds the NZF2 domain in HOIP to compete for NEMO binding and porcine reproductive and respiratory syndrome virus (PRRSV) proteins Nsp1 $\alpha$ , which prevents the HOIP-SHARPIN interaction. Bacterial effectors inhibit NF- $\kappa$ B activation by degrading M1-ubiquitin chains, like the M1-linked ubiquitin-specific DUB RavD encoded by *Legionella*; or by targeting LUBAC for degradation like *Shigella* K48-linked ubiquitin specific ligases IpaH1.4 and IpaH2.5<sup>331</sup>. Conversely *Salmonella typhimurium* and *Mycobacterium tuberculosis* are thought to enhance LUBAC activity<sup>384,385</sup>, although the reasons for this are unknown.

#### 1.5.4 The importance of LUBAC in humans

The importance and biological significance of LUBAC in human physiology are best illustrated by the study of disease-causing mutations in both HOIP and HOIL-1. Mutation of HOIP results in dysregulation of the immune system, resulting in immunodeficiency and increased susceptibility to repeated bacterial and viral infection infections, caused by impaired NF- $\kappa$ B in fibroblasts and B cells<sup>386,387</sup>. Contrastingly, mutation of HOIP also causes PBMC-driven auto-inflammation, induced by

aberrant cell death and hypersensitivity of monocytes causing excessive pro-inflammatory cytokine production. However, additional clinical characteristics like amylopectinosis and systemic lymphangiectasia only occurred when mutation resulted in reduced HOIP expression, destabilising LUBAC<sup>386</sup>. HOIP has also been implicated in activated B-cell-diffuse large B-cell lymphoma (ABC-DLBCL), caused by increased association of HOIP and HOIL-1, resulting in chronic activation of the B-cell receptor<sup>388,389</sup>.

Mutations in HOIL-1 have been identified and characterised in 16 individuals, with similarly wide-ranging phenotypes to HOIP: immunodeficiency and increased susceptibility to infection, auto-inflammation and amylopectinosis<sup>390-392</sup>. Again, immunodeficiency and auto-inflammation were caused by impaired signalling in fibroblasts and B cells, but hypersensitive monocytes, suggesting HOIL-1 mutant phenotypes are predominantly caused by impaired function of LUBAC<sup>392</sup>. However, the presence of additional clinical symptoms not seen in HOIP mutant patients, such as muscle weakness and cardiomyopathy, both resulting from dysregulated glycogen storage, demonstrates the significance of LUBAC-independent roles of HOIL-1<sup>390-392</sup>.

Mutations in the E2 ligase that associates with HOIP and HOIL-1, UBE2L3, have been linked with systemic lupus erythematosus and other autoimmune diseases<sup>393,394</sup>. Similarly, mutations in the LUBAC-specific DUB OTULIN, abolishing its catalytic activity, are found in patients with an autoimmune disease characterised by severe inflammation<sup>381,395</sup>.

Attempts to delete LUBAC components in mice compound the importance shown by human mutation. Full deletion of both HOIP and HOIL-1 results in embryonic lethality due to endothelial damage caused by aberrant TNF-driven cell death<sup>351,396,397</sup>, as does endothelial-specific deletion of HOIP and expression of a catalytically inactive HOIP mutant<sup>337,396,398</sup>. Conversely, mice with B cell and alveolar epithelial cell-specific deletions of HOIP are viable<sup>397,399</sup>, highlighting the importance of LUBAC in maintenance of the vascular architecture of the endothelium during embryogenesis. Mice expressing a truncated version of HOIL-1 show similar clinical manifestations to HOIL-1 mutation in humans, with amylopectin-like deposits and an extreme susceptibility to certain infections<sup>400,401</sup>.

No disease-causing SHARPIN mutations have yet been identified in humans, and SHARPIN-deficient mice are viable, caused by a mutation in exon one of SHARPIN that introduces a premature STOP codon<sup>402</sup>, displaying an inflammatory skin phenotype termed chronic proliferative dermatitis (*cpdm*), but without developmental issues<sup>402,403</sup>.

### 1.5.5 LUBAC-mediated regulation of immune signalling pathways

LUBAC was first shown to be capable of generating M1-linked ubiquitin chains in 2006<sup>341</sup>, and was later described to modulate immune signalling, specifically NF- $\kappa$ B activation and TNF-RSC signalling<sup>401,404-406</sup>. Since then, LUBAC has been shown to regulate cell death signalling<sup>322,407</sup>; activation of NF- $\kappa$ B by many ligands including IL-1 $\beta$ , CD-40, peptidoglycan (PGN), and LPS<sup>336,337,342,343,408,409</sup>; NOD2 signalling<sup>410</sup>; TLR signalling<sup>337,357,411-413</sup>; and RLR signalling<sup>214,399,414,415</sup>.

The best characterised mechanism of LUBAC-mediated regulation is during TNFR signalling, shown in Figure 1.5.5. Upon activation by TNF $\alpha$ , the TNF receptor recruits TNFR type 1-associated DEATH domain protein (TRADD), TRAF2, RIP1 and cellular inhibitor of apoptosis proteins (cIAPs) 1 and 2. LUBAC is recruited by binding to the K63-linked ubiquitin chains produced by cIAP1/2. At this point, LUBAC adds M1-linked ubiquitin chains to both RIP1 and NEMO<sup>401,404</sup>, as well as to pre-established K63-linked chains, generating K63-/M1-linked heterotypic chains<sup>336,337</sup>. This results in the formation of the TNF receptor signalling complex I (TNF-RSC-I) and increased recruitment of NEMO<sup>339,416</sup>, promoting its oligomerisation and allowing activation of IKK $\alpha$  and  $\beta$ , which in turn enable activation of NF- $\kappa$ B through phosphorylation of its inhibitor I $\kappa$ B $\alpha$ . In the absence of LUBAC, or indeed cIAPs, TBK1 and IKK $\epsilon$  are not recruited to the TNF-RSC, meaning that RIPK1 is not phosphorylated<sup>417</sup>. Unphosphorylated RIP1 is active, driving formation of TNF-RSC-II and activation of apoptosis through caspase 8, or necroptosis through formation of the RIP1 necrosome with RIP3 and MLKL<sup>418</sup>.

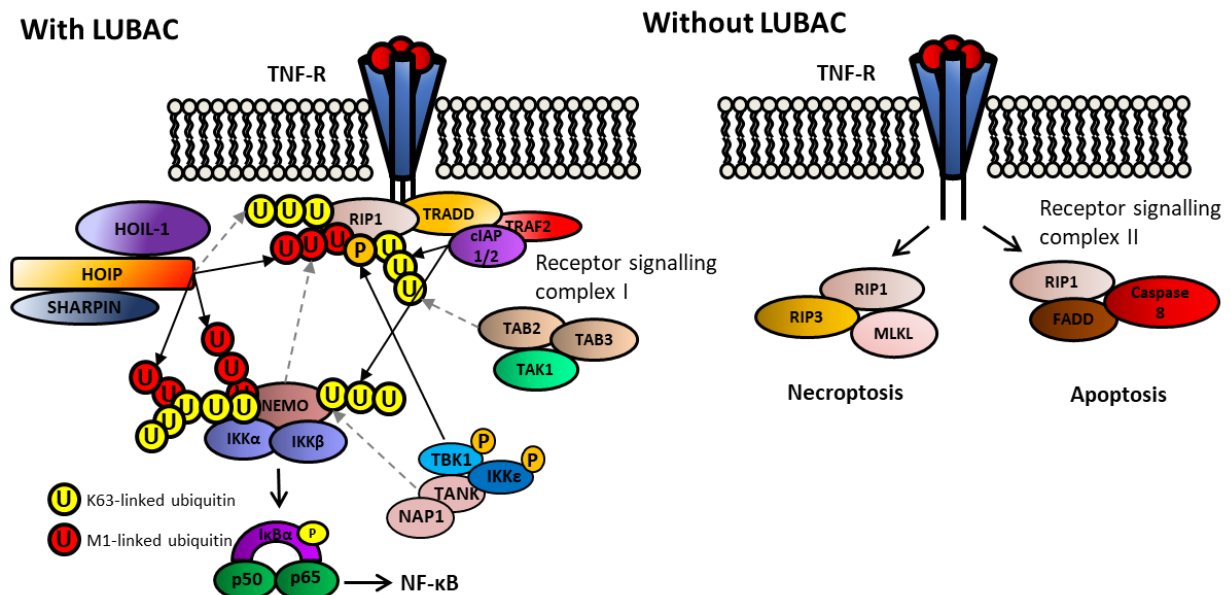


**Figure 1.5.5: LUBAC-mediated regulation of the signalling outcomes of the TNF-RSC.**

Adapted from <sup>419,420</sup>.

LUBAC mediates formation of the receptor signalling complex I by enabling recruitment of NEMO to activate NF- $\kappa$ B, and recruitment of TBK1, to phosphorylate RIP1 and keep it in its inactive state. LUBAC is recruited to

K63-linked chains on RIP1 generated by cIAPs. In turn, modification of RIP1, NEMO and pre-existing K63-linked chains with M1-linked ubiquitin chains results in efficient recruitment of NEMO and downstream signalling. Dashed grey arrows represent protein recruitment to the signalling complex, with solid black arrows representing modifications performed by the protein from which they originate.

LUBAC functions similarly in other immune signalling pathways, conjugating M1-Ub chains to other targets including RIPK2, TRADD, TNFR1 itself, IRAK1/2/4 and MyD88<sup>420</sup>. M1-/K63-linked heterotypic chains are also conjugated to NEMO in IL-1 $\beta$  and MAVS signalling, RIPK1 in TLR3 signalling, and RIPK2 in NOD2 signalling<sup>336,337</sup>.

LUBAC is also implicated in the immune response to intracellular bacteria, with HOIP binding to the ubiquitin coat already assembled on the surface of bacteria and in turn assembling M1-linked chains on the surface, acting as a signalling platform and recruiting NEMO and Optineurin to stimulate xenophagy and NF- $\kappa$ B activation<sup>421-423</sup>. Additionally, LUBAC is recruited to cytoplasmic protein aggregates, modifying them with M1-ubiquitin. In the case of Huntingtin, this shields the surface of the misfolded protein from unwanted interactions known to contribute to Huntingdon's disease<sup>424</sup>. LUBAC also functions in adaptive immunity, regulating regulatory T cell development and homeostasis<sup>425</sup>, and T and B cell differentiation<sup>397,426</sup>. It also functions in non-immune signalling pathways, regulating genotoxic stress-induced NF- $\kappa$ B activation<sup>406</sup>. Furthermore, the recently identified broad landscape of interacting proteins of LUBAC and its respective DUB OTULIN, suggests that LUBAC has additional functions we don't yet understand<sup>427</sup>.

### 1.5.6 LUBAC and RNA sensing

To date, LUBAC has been shown to regulate signalling downstream of three RNA sensors: TLR3, MDA5 and RIG-I. Whilst LUBAC's role in TLR3 and MDA5 signalling is clear<sup>357,415</sup>, research surrounding its role in RIG-I signalling is conflicting<sup>135,214,358,399</sup>.

In TLR3 signalling, LUBAC forms part of the TLR3-RSC and HOIP and SHARPIN are both required for TLR3-driven NF- $\kappa$ B and MAPK signalling<sup>357</sup>. Additionally, LUBAC was found to inhibit TLR3-mediated cell death induction, through restricting formation of the TLR3-induced death-inducing signalling complex (DISC) composed of cIAP1/2, FADD, RIP1 and caspase 8<sup>428,429</sup>, with cells lacking either HOIP or SHARPIN sensitised to Poly(I:C) and IAV-induced cell death<sup>357</sup>. This is reinforced by a previous study that implicated SHARPIN in TLR3-driven NF- $\kappa$ B activation in BMDCs<sup>404</sup>. LUBAC is also required for the MDA5-driven antiviral response to murine norovirus (MNoV) and Theiler's murine encephalomyelitis virus (TMEV), with reduced IFN-I and IFN-III responses in MEF cells expressing a truncated version of HOIL-1 and in HOIL-deficient BMDC, as well as limiting virus replication<sup>415</sup>.

### 1.5.7 LUBAC and RIG-I signalling

In studies using a variety of cell lines and techniques, individual LUBAC components shown to contribute differently to RIG-I-driven signalling outcomes.

Firstly, through overexpression studies, HOIP and either HOIL-1 or SHARPIN were shown to negatively regulate RIG-I signalling<sup>214,358,430</sup>, but this was disputed by experiments using knockout or knockdown cell lines. Studies using knock-down techniques showed that HOIP contributed modestly to RIG-I signalling, with cells expressing a reduced level of HOIP having similar or reduced IRF3 and NF-κB-driven signalling outcomes in response to infection with VSV and IAV WSN in both MEF and A549 cells<sup>135,214,399</sup>. However, studies in cells expressing a truncated version of HOIL-1, or cells where HOIL-1 expression is reduced, have yielded conflicting results about its influence on RIG-I signalling. HOIL-1 was shown to negatively regulate RIG-I-driven IFN-I and NF-κB activation in some studies<sup>135,214,358,431</sup>, but to have no effect on or be required for RIG-I-driven responses in others<sup>399,415</sup>. Finally, SHARPIN had mixed effects on RIG-I driven immune signalling, with cells lacking SHARPIN shown to have both increased and reduced IFN-I activation in response to VSV and SeV infection, but consistently reduced NF-κB-driven signalling<sup>135,358</sup>. Varying mechanisms have been suggested for LUBAC's influence on RIG-I signalling outcomes, with LUBAC suggested to bind and mediate the degradation of TRIM25<sup>214</sup>, to conjugate M1-linked ubiquitin chains to NEMO to prevent its interaction with TRAF3 and the formation of the MAVS-TRAF3 signalling complex<sup>358</sup>, and to function redundantly with TRAF proteins to generate ubiquitin chains for the recruitment of downstream signalling proteins<sup>135</sup>.

As seen with many other immune receptors, including TLR3<sup>357</sup>, LUBAC is suggested to regulate RIG-I-driven cell death, although again with varying outcomes. Cells lacking SHARPIN were sensitised to VSV-driven cell death<sup>358</sup>, but mice expressing a truncated version of HOIL-1 showed improved survival and reduced cell death in the lungs during IAV infection<sup>399</sup>. Furthermore, LUBAC has been implicated in driving the RLR-induced IRF3-mediated pathway of apoptosis (RIPA)<sup>432</sup>. This occurs through LUBAC-mediated conjugation of M1-Ub chains to IRF3, mediating the binding of Bax by IRF3, allowing it to initiate the release of the cytochrome C from the mitochondria, which both induces apoptosis<sup>433</sup> and restricts viral replication<sup>434,435</sup>.

### 1.5.8 M1-ubiquitin chain-independent functions of LUBAC

The majority of the functions of LUBAC rely on its ability to generate M1-linked ubiquitin chains, with the catalytic activity of the HOIP RBR domain shown to be required for driving NF-κB and MAPK activation downstream of multiple immune receptors<sup>348,396,397,412,436</sup>, as well as for prevention of TNF-

driven cell death, by enabling recruitment of TBK1 and IKK $\epsilon$  to the TNF receptor signalling complex<sup>396,417</sup>.

However, LUBACs role in some signalling pathways does not rely on its ability to generate M1-linked ubiquitin chains. The ubiquitin ligase activity of HOIP is dispensable for B cell-receptor mediated activation of NF- $\kappa$ B and ERK, despite being responsible for TNF and CD-40-induced NF- $\kappa$ B and ERK in B cells<sup>397</sup>. Similarly, the catalytic activity of HOIP is dispensable for T cell receptor (TCR)-mediated NF- $\kappa$ B activation, but not TNF-mediated NF- $\kappa$ B activation in T cells<sup>436</sup>. This is further reinforced by the fact that silencing of OTULIN in T cells affects TNF-driven but not TCR-mediated NF- $\kappa$ B activation<sup>436</sup>. Despite the non-requirement for LUBACs enzymatic activity in these pathways, no alternative mechanism of regulation, such as acting as a scaffold protein, has been proposed.

### 1.5.9 LUBAC-independent functions of HOIL-1 and SHARPIN

Both HOIL-1 and SHARPIN have additional roles outside of LUBAC. For HOIL-1, these roles focus predominantly on its role as an K48-linked ubiquitin ligase, regulating multiple cellular pathways by targeting signalling proteins for degradation<sup>437</sup>. Targets includes oxidised iron regulatory protein 2 (IRP2), whose iron-dependent ubiquitination and degradation results in expression of iron-containing protein ferritin<sup>438,439</sup>, since disputed<sup>440</sup>. Similarly, HOIL-1 induces the degradation of Bach1, preventing its repression of haem oxygenase 1 (HO-1) transcription, activating haem metabolism and resolution of oxidative stress<sup>441-443</sup>.

HOIL-1 also independently regulates specific immune signalling through: the binding and mediation of degradation of PKC $\beta$  and PKC $\zeta$ , regulating protein kinase C signalling and tumour cell survival during hypoxia<sup>365,444-446</sup>; the binding and degradation of TAB2 and 3, regulating TNF and IL-1 induced NF- $\kappa$ B activation<sup>440</sup>; ubiquitination and degradation of pregnane X receptor (PXR), a transcriptional regulator that affects multiple immune and inflammatory responses<sup>447,448</sup>; and interaction with eyes absent (Eya) 1 and 2, co-activators of essential transcription factors for organ development<sup>449,450</sup>.

Outside of LUBAC, SHARPIN plays a role in prevention of cancer progression. This occurs through the binding of SHARPIN to Protein arginine methyltransferase 5 (PRMT5), resulting in epigenetic regulation of chromatin with cancer metastasis-related genes<sup>451</sup>; and through association with Yes-associated protein (YAP), promoting its degradation and cancer progression<sup>452</sup>. SHARPIN is also implicated in regulating the development and function of Treg cells<sup>425,453-455</sup>, promoting lymphocyte migration<sup>456</sup> and preventing unnecessary platelet aggregation<sup>457</sup>. Additionally, SHARPIN interacts with and inhibits integrin to regulate cellular adhesion<sup>458</sup>, as well  $\alpha$ Ib $\beta$ 3 to enable platelet aggregation, MHC-I antigen presentation and inflammation<sup>457</sup>. Finally, SHARPIN has also been

identified as a genetic risk factor for Alzheimer's disease <sup>459,460</sup>, due to its role in mediating A $\beta$  protein clearance, preventing pathogenic A $\beta$  accumulation seen in Alzheimer's.

## 1.6 Thesis aims and objectives

The role of LUBAC and M1-linked ubiquitin chains downstream of many immune signalling receptors is well characterised, with clear and consistent signalling outcomes and even in some cases, a specifically defined mechanism of action. This is not the case for RIG-I signalling, with conflicting signalling outcomes and multiple contradictory mechanisms attributed to LUBAC. These previous studies utilised overexpression systems and incomplete knockdown or knockout systems to study the role of LUBAC, and often the contribution of individual LUBAC components has been attributed to the complex as a whole. Therefore, the aim of this project was to understand how HOIP, HOIL-1 and SHARPIN, the LUBAC complex as a whole, and M1-linked ubiquitin chains regulate the RIG-I signalling complex and its outcomes. To understand the mechanism by which LUBAC regulates the composition of the RIG-I signalling complex and its outcomes, a better understanding of what proteins were involved and what their individual contribution to signalling outcomes was needed.

As such, this work aimed to:

- Define and generate a system by which the RIG-I signalling mechanism and its outcomes can be measured,
- Characterise the contribution of individual components thought to be in the RIG-I signalling complex to signalling outcomes in our system,
- Assess the individual contribution of HOIP, HOIL-1, SHARPIN and M1-linked ubiquitin chains to RIG-I signalling outcomes,
- Generate a proposed mechanism by which LUBAC regulates the RIG-I signalling complex and its outcomes.

# Chapter Two: Materials and Methods

## 2.1 Maintenance of cell lines

### 2.1.1 Wild-type cell lines

Cell lines used for experiments in this study are shown in Table 2.1.1. A549 and MEF cells were a kind gift from the lab of Henning Walczak (University of Cologne) and U251 cells were from Dr. Nerea Irigoyen (University of Cambridge).

Cell line	Species	Origin Tissue	Cell Type
A549	Human	Lung	Adenocarcinomic human alveolar basal epithelium
HaCaT	Human	Skin	Transformed aneuploid immortal keratinocytes
HEK293T	Human	Kidney	Immortalised embryonic kidney
(Madin-Darby Canine Kidney) MDCK	Dog	Kidney	Kidney epithelium
MEF	Mouse	Skin	Immortalised embryonic fibroblasts
U251	Human	Brain	Glioblastoma astrocytoma
Vero	African green monkey (Chlorocebus sp)	Kidney	Kidney epithelium

**Table 2.1.1: Wild-type cell lines used in this study**

Model cell lines used for these studies, their species, origin tissue and cell type.

### 2.1.2 Edited cell lines

To study the function of various proteins in RIG-I signalling, cell lines deficient for these proteins were used, which were either developed as part of this project using CRISPR/Cas9 technology described in Chapter 2.2 or were kind gifts from collaborators. Wild-type parental cell lines used for generation of knockout cells were used for comparison in the following studies. The origin of edited cell lines is detailed in Table 2.1.2.

Cell line	Developed (group)	Location	Reference
A549 RIG-I -/-	This study	University of Cambridge	(unpublished)
A549 TKO (TANK/NAP1/SINTBAD -/-)	Henning Walczak	University of Cologne	
A549 OPTN -/-	Henning Walczak	University of Cologne	<sup>333</sup>
A549 NEMO -/-	Henning Walczak	University of Cologne	<sup>333</sup>
A549 NEMO -/- + TAP-NEMO	Henning Walczak	University of Cologne	<sup>333</sup>
A549 RIP1 -/-	Henning Walczak	University of Cologne	
A549 HOIP -/-	Henning Walczak	University of Cologne	<sup>334</sup>
A549 HOIP -/- + TAP-HOIP-WT	Henning Walczak	University of Cologne	<sup>334</sup>

A549 HOIP -/- + TAP-HOIP-C885S	Henning Walczak	University of Cologne	<sup>333</sup>
A549 SHARPIN -/-	This study	University of Cambridge	(unpublished)
MEF TNF -/- HOIL +/-	Henning Walczak	University of Cologne	<sup>335</sup>
MEF TNF -/- HOIL -/-	Henning Walczak	University of Cologne	<sup>335</sup>

**Table 2.1.2: Genetically edited cell lines used in this study**

### 2.1.3 Maintenance conditions

All cell lines were grown in Dulbecco's Modified Eagle's Medium (DMEM) with 4.5 g/L D-glucose, 8mM L-glutamine and Sodium Pyruvate (Gibco), supplemented with 10% foetal calf serum (FCS, Pan Biotech) and 100 U/mL Penicillin and Streptomycin (Gibco). Cells were incubated at 37°C, 5% CO<sub>2</sub> and 3% O<sub>2</sub> in a humidified incubator.

### 2.1.4 Passaging cells

Cells were passaged when they reached approximately 95% confluence. Monolayers were washed twice with sterile PBS (Sigma) and incubated with Trypsin/EDTA (Lonza) until they began to detach from the bottom of the flask. Detached cells were resuspended in DMEM 10% FCS and either counted and seeded for experiments, or approximately 10% were transferred to a new flask to continue passaging.

### 2.1.5 Seeding cells for experiments

Cells were trypsinised as described above (2.1.4), mixed 1:1 with Trypan Blue (Sigma), and live cells that had not taken up the Trypan blue were counted using a haemocytometer. For qPCR, ELISA and Vitality Assay analyses, cells were seeded in 6-well plates, at 70% confluence for transfection of synthetic RNAs (5.5x10<sup>5</sup> cells per well), and 80-90% confluence for virus infection (6x10<sup>5</sup> cells per well). For phosphoblotting, cells were seeded in 10 cm dishes at 80% confluence (3x10<sup>6</sup> cells per dish). For phos-flow analysis, cells were seeded in 6 cm dishes at 80-90% confluence (1x10<sup>6</sup> cells per dish). For co-immunoprecipitation cells were seeded in 15 cm dishes at 70% confluence (5x10<sup>6</sup> cells per dish). For qPCR and ELISA, either duplicate or triplicate wells were seeded for each experimental condition (n=2 or 3) and for phosphoblotting, co-IP or phos-flow one dish was seeded per condition (n=1).

## 2.2 Generation of cell lines by CRISPR/Cas9

Clustered Regularly Interspaced Short Palindromic Repeats (CRISPR)/Cas9 technology was used to generate RIG-I and SHARPIN deficient A549 cells as part of this study.

## 2.2.1 CRISPR Guide Design

The human genomic sequences of RIG-I and SHARPIN were identified on ENSEMBL (<http://www.ensembl.org/index.html>: DDX58 (RIG-I) ENSG00000107201 and SHARPIN ENSG00000179526). The correct start codons were identified by translation of the exon DNA sequence using ExPasy ([www.web.expasy.org/translate/](http://www.web.expasy.org/translate/)) and comparing it to the protein sequence on Uniprot ([www.uniprot.org/](http://www.uniprot.org/)). Small guide (sg)RNAs were designed using Benchling ([www.benchling.com](http://www.benchling.com)) by selecting the first few of the gene of interest after the start codon. From suggested guides, the ones with the best on- and lowest off-target effects, not located over an intron-exon junction, were chosen. Guides were synthesised as forward and reverse complimentary DNA oligonucleotides (IDT) with BbsI restriction sites, to enable annealing into the pSpCas9(BB)-2A-GFP (PX458) plasmid (Addgene #48138), created by the Zhang lab<sup>336</sup> and donated by Geoffrey Smith (University of Cambridge). Guide sequences responsible for successful knock-out of RIG-I and SHARPIN are shown in Table 2.2.1.

Gene	Exon targeted	Guide sequence	Orientation
<i>DDX58</i>	1	AAAGTCCAGAATAACCTGCA	antisense
<i>SHARPIN</i>	2	CCTAGTCCGAGGTGCCACCG	sense

**Table 2.2.1: sgRNAs used for CRISPR/Cas9 knockout generation**

Target gene and exon, guide sequence and orientation used for successful generation of knockout A549 cells

## 2.2.2 Cloning of constructs

sgRNA DNA oligos were diluted to 10  $\mu$ M in nuclease free water (NF-H<sub>2</sub>O) and 5  $\mu$ L of each forwards and reverse guide was combined in a polymerase chain reaction (PCR) tube (Starlab) and heated to 75 °C for 15 minutes using a Veriti thermocycler (Applied Biosystems). The thermocycler was then switched off and allowed to cool to room temperature to allow annealing. Annealed primers were diluted to 20 nM in NF-H<sub>2</sub>O.

3  $\mu$ g of pSpCas9(BB)-2A-GFP (PX458) plasmid was digested with BbsI-HF (NEB), run on a 1% agarose gel at 120 V, visualised using a UV light box and excised using a scalpel. DNA was extracted from the agarose gel using a QIAquick Gel Extraction Kit (Qiagen) and eluted in 10  $\mu$ L NF-H<sub>2</sub>O. The DNA concentration and purity was measured using a NanoDrop 2000 spectrophotometer.

sgRNAs were ligated into the digested plasmid at a 3:1 (insert:plasmid) molar ratio using T4 DNA ligase (Promega). The ligated plasmid was transformed into Stb13 E. Coli by heat-shocking, allowed to grow for 1 hour at 37 °C, spread onto LB agar with Carbenicillin (50  $\mu$ g/mL) and incubated at 37 °C for 16 hours. Colonies were picked and grown in 5 mL LB Carbenicillin at 37 °C for 16 hours for a Miniprep; or 8 hours for a maxiprep, before being diluted in 250 mL LB Carbenicillin and grown at 37

°C for 16 hours. DNA was purified using a QIAprep Spin Miniprep/Maxiprep kit (Qiagen) and DNA concentration was measured using a NanoDrop 2000 spectrophotometer.

Constructs were sequenced to ensure that the guide had been inserted into the plasmid in the correct orientation, without introducing any additional mutations.

### **2.2.3 Transfection of CRISPR constructs**

A549 cells were seeded at 70% confluency in a 10 cm dish and 5 µg of each plasmid was transfected using TransIT-LT1 transfection reagent (Mirus) at a ratio of 3 µL per µg DNA, in 1 mL of OptiMEM (Gibco). TransIT-LT1 and OptiMEM were incubated for 5 minutes, DNA was added, and the mix was incubated for a further 1 hour before being added dropwise onto cells in DMEM 10% FCS 1% P/S.

### **2.2.4 Cell Sorting and Cloning**

After 24 hours, GFP fluorescence was checked using a fluorescence microscope to indicate positively transfected cells. A further 24 hours later, GFP-expressing cells were collected using a Mo Flo Sorter (Beckman Coulter) and clonal populations were established by single cell sorting into a 96-well plate. Clonal cell lines were established by passaging until they were in a 6-well plate.

### **2.2.5 Confirmation of successful knock-out**

Putative knock-out clones were first screened by Western blotting (2.6) to check for absence of expression of the target protein. From clones lacking expression, genomic DNA was extracted and the region around the site targeted by the guide was amplified by PCR, cloned into a pcDNA4/TO plasmid and sequenced. The primers used to amplify the target site in RIG-I were forwards TAGCTCGGATCCAGGGAAACGAACTAGCCCG and reverse GAGCTGGAATTCTGCTGCGGAGATCTTACCAC. SHARPIN-knockout clones were not sequenced. Clone sequences were aligned with those from WT A549 cells to check for mutations at the target site. After identification of the start codon, mutated sequences were translated using Expasy ([www.web.expasy.org/translate/](http://www.web.expasy.org/translate/)) to confirm that the mutations introduced changed the amino acid sequence and/or introduced premature stop codon, terminating the sequence.

## 2.3 Stimulation of cells

### 2.3.1 Transfection of synthetic RNAs

High molecular weight (HMW) Poly(I:C) and 3p-hpRNA (both Invivogen) were diluted in NF-H<sub>2</sub>O to concentrations of 1 mg/mL and 0.1 mg/mL respectively and stored at -20°C.

For qPCR and ELISA, cells were seeded in 6-well plates and transfected 16 hours later with 1 µg of synthetic RNA per well. For phosphoblotting, cells were seeded in 10 cm dishes and transfected 16 hours later with 5 µg of RNA. For phos-flow cells were seeded in 6 cm dishes and transfected 16 hours later with 2 µg of RNA. TransIT-LT1 (Mirus) was used at a ratio of 3 µL per µg of RNA and was added to OptiMEM (Gibco) (200 µL per well, 400 µL per 6 cm dish and 1 mL per 10 cm dish), mixed and incubated for 5 minutes. RNA was added and the mix was incubated for a further 30 minutes. Half of the media was removed to leave 1 mL per well, 2 mL per 6 cm dish, or 5 mL per 10 cm dish of complete media remaining. The transfection mix was added dropwise to the cells, which were then incubated for the indicated time.

### 2.3.2 IFN $\alpha$ stimulation

Cells were seeded at 70% confluence and after 16 hours, IFN $\alpha$  (Sigma) diluted in (1 mL per well, 3 mL per 6 cm dish, 5 mL per 10 cm dish and 10 mL per 15 cm dish) DMEM 10% FCS 1% P/S to a concentration of 100 U/mL, was added to cells and incubated for 24 hours.

### 2.3.3 TNF $\alpha$ stimulation

Cells were seeded at 80-90% confluency in 10 or 15 cm dishes. 16 hours later, TNF $\alpha$  (PeproTech) diluted to 200 ng/mL in 5 mL per dish DMEM 10% FCS 1% P/S, was added to cells and incubated for the indicated time.

## 2.4 Virus infection

### 2.4.1 Sendai virus

The Cantell strain of Sendai virus (SeV), a kind gift from Steve Goodbourne (St. Georges University), and was stored at -80 °C. After initial dose-response tests, A549 cells were infected at a 1:300 dilution and MEF and HEK293T cells at a 1:100 dilution, in DMEM 2.5% FCS 1% P/S (1 mL per well, 3 mL per 6 cm dish and 5 mL per 10 cm dish) and incubated for the indicated time. A single infection mix was made, and cells were infected sequentially and harvested together.

## 2.4.2 IAV

### 2.4.2.1 Generation and titration of virus stocks

Influenza A/Puerto Rico/8/1934 (IAV PR8 WT) virus was a kind gift from Wendy Barclay (Imperial) and NS1 mutant viruses IAV PR8 NS1 R38A, K41A and R38A+K41A were generated in the lab of Paul Digard (University of Edinburgh) and provided by Rupert Beale (The Francis Crick Institute). IAV stocks were grown in MDCK cells, infected at a multiplicity of infection (MOI) of 0.01 virus particles per cell in minimum essential media (MEM) 0.3% BSA 1% P/S 2 µg/mL TPCK-Trypsin. After 48 hours or once significant cytopathic effects (CPE) was seen, the supernatant was harvested, and detached cells were pelleted by centrifugation for 10 minutes at 724 x g at 4°C. The remaining virus-containing supernatant was aliquoted into 2 mL vials and stored at -80 °C.

To quantify the amount of virus generated, duplicate 10-fold serial dilutions of the IAV stock were carried out in MEM 0.3% w/v BSA 2 µg/mL TPCK-Trypsin. 500 µL of each dilution was added to confluent MDCK cells in a 6-well plate and incubated on a rocker at 37 °C. After 1 hour, the inoculum was removed and replaced with a 50:50 mix of 2% low melting point (LMP) agarose and 2x MEM (20% 10X MEM, 8mM L-glutamine, 0.45% Na<sub>2</sub>CO<sub>3</sub>, 0.4% non-essential amino acids (NEAA), 4% HEPES, pH 7.4) 0.6% BSA. Cells were incubated for 48 hours, or until plaques were seen by the naked eye. 1 mL of Neutral red (Sigma) diluted 1:20 with MEM 0.3% w/v BSA was added on top of the overlay and incubated for approximately 6 hours at 37 °C before the stain was aspirated, and plaques were counted in wells containing between 30 and 150 plaques. The number of plaques was multiplied by the dilution factor of the well and doubled to calculate the number of plaque forming units (PFU) per mL.

### 2.4.2.2 Infection of cells

A549 and MEF cells were seeded with a spare well or dish, which 16 hours later was trypsinised and counted. Total cell number was calculated and if cell numbers were within 10% of each other, cells were infected at a MOI of 5.

### 2.4.2.3 Virus growth curve analysis

Cells were infected with IAV PR8 WT and R+K at the indicated MOI, with each condition in triplicate. At the stated time, the supernatants were collected and stored at -80 °C. Supernatants were titrated onto confluent MDCK cells in 6-well plates and plaques were counted, as described in 2.4.2.1. Data shown is the mean value across biological and technical replicates and standard deviation is represented as error bars.

## 2.4.3 Zika virus

### 2.4.3.1 Generation of and titration of virus stocks

ZIKV/H.Sapiens/Brazil/PE243/2015 (ZIKV PE243) was a gift from Dr. Nerea Irigoyen. ZIKV stocks were grown in Vero cells, infected at MOI 0.01 in DMEM 0% FCS, 1% P/S, 8mM L-Glutamine with 20 mM HEPES. Virus was incubated on the cells for 1 hour at 37°C, then removed and DMEM 10% FCS, 1% P/S, 8mM L-Glutamine with 20 mM HEPES was added to the cells, which were returned to the incubator. Virus was harvested by collection of the supernatant on the cells at day 3 and day 5 post-infection, followed by centrifugation for 10 minutes at 724 x g at 4°C. Supernatants were stored at -80 °C. To quantify the amount of virus generated, virus stocks underwent triplicate 10-fold serial dilutions in serum-free DMEM. 400 µL of dilutions were added to Vero cells in duplicate and incubated for 1 hour at 37°C. At this point, the inoculum was removed and replaced with a 50:50 mix of 3% LMP agarose and 2x MEM 4% FCS. Cells were incubated for 5 days before being fixed overnight at room temperature using formal saline (4% formaldehyde, 0.9% sodium chloride, 90% H<sub>2</sub>O) and then stained with Toluidine Blue. Plaques were counted and PFU was calculated as previously described. This work was all done by Dr. Nerea Irigoyen and Charlotte Lefevre in the Department of Virology, University of Cambridge.

### 2.4.3.2 Infection of cells

A549 cells were trypsinised, counted, seeded at 90% confluency in a 6 well plate ( $6.5 \times 10^5$  cells per well) and incubated for 6 hours. Cells were infected with ZIKV PE243 at MOI 3 in 500 µL DMEM 2.5 % FCS 1% P/S per well and incubated for 1 hour, rocking every 10 minutes. After 1 hour, the inoculum was removed and 2 mL DMEM 2% FCS 20 mM HEPES was added to each well and infected cells were incubated for the indicated time. All infections were done in triplicate per condition. This was done together with Dr. Nerea Irigoyen and Charlotte Lefevre in the Department of Virology, University of Cambridge.

### 2.4.3.3 Virus growth curve analysis

A549 cells were seeded at a confluence of 60-70% and infected with ZIKV at an MOI of 0.01 in triplicate. After the indicated time Supernatant was collected and stored at -80 °C and titrated onto confluent Vero cells as previously described (2.4.3.1). Data shown is the mean value across biological and technical replicates and standard deviation is represented as error bars. This work was all done by Dr. Nerea Irigoyen and Charlotte Lefevre in the Department of Virology, University of Cambridge.

## 2.5 RT-qPCR

### 2.5.1 Cell Lysis and RNA Extraction

Cells were seeded in 6-well plates in either duplicates or triplicates per condition and stimulated or infected as previously described. For all experiments except ZIKV infection, at the indicated time points, cells were washed twice with 1 mL PBS and then lysed by addition of 250  $\mu$ L lysis buffer (4 M Guanidine Thiocyanate, 25 mM Tris pH7, 143 mM 2-mercaptoethanol (2-ME) followed by 250  $\mu$ L 70% ethanol. Lysates were passed through a silica spin column (Epoch) by centrifugation for 3 minutes at 18000 x g at 4 °C. The column was washed once with 500  $\mu$ L wash buffer 1 (1M Guanidine Thiocyanate, 25 mM Tris pH7, 10% ethanol) and twice with 500  $\mu$ L wash buffer 2 (25 mM Tris pH 7, 70% ethanol) by centrifugation for 1 minute at 18000 x g at 4 °C. RNA was eluted by addition of 50  $\mu$ L NF-H<sub>2</sub>O and centrifugation for 1 minute, the eluate was reapplied to the column and eluted for a second time. Eluted RNA was stored at -80 °C.

After infection with ZIKV for the indicated time, cells were washed twice with 1 mL PBS cells and scraped in 250  $\mu$ L lysis buffer (Polysome buffer (20 mM Tris-HCl pH 7.5, 150 mM NaCl, 5 mM MgCl<sub>2</sub>, 1 mM DTT), 5 % Triton X-100, 12.5 U/mL DNase I, 1% DTT). Mechanical lysis was performed by passing the lysate through a 26-gage needle 30 times. Insoluble material was pelleted by centrifugation at 18000 x g for 20 minutes at 4 °C. A phenol/chloroform (1:1 600  $\mu$ L) extraction was performed, followed by a chloroform extraction (600  $\mu$ L). RNA was precipitated by recovery of the aqueous phase and addition of 60  $\mu$ L 3M sodium acetate pH 4.8 and 1.8 mL ice cold 100% ethanol. Samples were incubated for 1 hour at -80 °C and RNA pelleted by centrifugation at 18000 x g for 15 minutes at 4 °C. The pellet was washed in 200  $\mu$ L ice cold 95% ethanol before air drying and resuspension in 11  $\mu$ L NF-H<sub>2</sub>O. RNA was stored at -80 °C. This was done by Dr. Nerea Irigoyen and Charlotte Lefevre in the Department of Virology, University of Cambridge.

### 2.5.2 cDNA synthesis

RNA concentration and purity were determined using a NanoDrop 2000 Spectrophotometer. 500  $\mu$ g of RNA, 1  $\mu$ L of 10 mM deoxynucleotides (dNTPs) and 500 ng of oligo(dT) (both Thermo Scientific) were incubated at 65°C for 5 minutes using a Veriti thermocycler (Applied Biosystems). 10 U of RNaseOUT (Invitrogen), 50 U of Superscript III Reverse Transcriptase (Invitrogen), 4  $\mu$ L of 10x First Strand buffer and 1  $\mu$ L of 0.1 M dithiothreitol (DTT) were added and the mix was incubated at 50°C for 1 hour then 72°C for 15 minutes. The resulting cDNA was diluted 1:3 with 40  $\mu$ L NF-H<sub>2</sub>O.

## 2.5.3 qPCR

### 2.5.3.1 Targets

cDNA samples were analysed by quantitative polymerase chain reaction (qPCR) using primers to amplify specific regions of the genes of interest, ordered as DNA oligos (IDT). Target genes and primer sequences for human and murine cells can be found in Table 2.5.3.1A and B respectively.

Gene symbol	Gene name	Primer direction	Primer sequence
<i>GAPDH</i>	glyceraldehyde-3-phosphate dehydrogenase	Forwards	ACC CAG AAG ACT GTG GAT GG
		Reverse	TTC TAG ACG GCA GGT CAG GT
<i>IFNB1</i>	interferon beta 1	Forwards	ACA TCC CTG AGG AGA TTA AGC A
		Reverse	GCC AGG AGG TTC TCA ACA ATA G
<i>CXCL10</i>	C-X-C motif chemokine ligand 10	Forwards	GTG GCA TTC AAG GAG TAC CTC
		Reverse	GCC TTC GAT TCT GGA TTC AGA CA
<i>DDX58</i>	DEXD/H-box helicase 58	Forwards	CTC TGC AGA AAG TGC AAA GC
		Reverse	GGC TTG GGA TGT GGT CTA CT
<i>MAVS</i>	mitochondrial antiviral signalling protein	Forwards	GGACGAAGTGGCCTCTGTCTA
		Reverse	CAT GGG GTA ACT TGG CTC CTT
<i>IFNA2</i>	interferon alpha 2	Forwards	AGT CAA GCT GCT CTG TGG GC
		Reverse	GTG AGC TGG CAT ACG AAT CA
<i>IFNL1</i>	interferon lambda 1	Forwards	CGC CTT GGA AGA GTC ACT CA
		Reverse	GAA GCC TCA GGT CCC AAT TC
<i>CCL5</i>	C-C motif chemokine ligand 5	Forwards	CCC AGC AGT CGT CTT TGT CA
		Reverse	TCC CGA ACC CAT TTC TTC TCT
<i>ISG15</i>	ISG15 ubiquitin like modifier	Forwards	AGC ATC TTC ACC GTC AGG TC
		Reverse	GAG GCA GCG AAC TCA TCT TT
<i>ISG54/IFIT2</i>	interferon induced protein with tetratricopeptide repeats 2	Forwards	CTG AAG AGT GCA GCT GCC TG
		Reverse	CAC TTT AAC CGT GTC CAC CC
<i>NFKBIA</i>	NFKB inhibitor alpha	Forwards	CTC CGA GAC TTT CGA GGA AAT
		Reverse	GCC ATT GTA GTT GGT AGC CTT
<i>TNFA</i>	tumour necrosis factor a	Forwards	AGG CGC TCC CCA AGA AGA CAG G
		Reverse	CAG CAG GCA GAA GAG CGT GGT G
<i>IL6</i>	interleukin 6	Forwards	ACA ACC ACG GCC TTC CCT ACT T
		Reverse	CAC GAT TTC CCA GAG AAC ATG TG

**Table 2.5.3.1A: Primers used to detect mRNA transcription in human cell lines**

Gene symbol	Gene name	Primer direction	Primer sequence
<i>Hprt</i>	hypoxanthine guanine phosphoribosyl transferase	Forwards	GTT GGA TAC AGG CCA GAC TTT GTT G
		Reverse	GAT TCA ACT TGC GCT CAT CTT AGG C
<i>Ifnb1</i>	interferon beta 1	Forwards	GCC TAG GTG AGG TTG ATC T
		Reverse	AGC TCC AAG AAA GCA CGA ACA T
<i>Ifna4</i>	interferon alpha 4	Forwards	GGW ACA CAG TGA TCC TGT GG
		Reverse	AGG GCT CTC CAG AYT TCT GCT CTG
<i>Ifnl2/3</i>	interferon lambda 2/3	Forwards	CCG GAT CCT GTC CCC AGG GCC ACC AGG C
		Reverse	GAG AAT TCC AGG TCA GAC ACA CTG GTC TCC
<i>Cxcl10</i>	C-X-C motif chemokine ligand 10	Forwards	ACT GCA TCC ATA TCG ATG AC
		Reverse	TTC ATC GTG GCA ATG ATC TC
<i>Isg56/Ifit1</i>	interferon-induced protein with tetratricopeptide repeats 1	Forwards	CTG AAG AGT GCA GCT GCC TG
		Reverse	CAC TTT AAC CGT GTC CAC CC
<i>Isg15</i>	ISG15 ubiquitin like modifier	Forwards	GCA AGC AGC CAG AAG CAG ACT CC
		Reverse	CGG ACA CCA GGA AAT CGT TAC CCC
<i>Il6</i>	interleukin 6	Forwards	GTA GCT ATG GTA CTC CAG AAG AC
		Reverse	ACG ATG ATG CAC TTG CAG AA
<i>Nfkbia</i>	NFKB inhibitor alpha	Forwards	CTG CAG GCC ACC AAC TAC AA
		Reverse	CAG CAC CCA AAG TCA CCA AGT

**Table 2.5.3.1B: Primers used to detect mRNA transcription in murine cell lines**

### 2.5.3.2 qPCR protocol

qPCR reactions were set up in a MicroAmp 384-well plate (Thermo Scientific). In addition to the experimental duplicates/triplicates for each condition, technical duplicates were done for each cDNA sample and target gene combination. 2 µL of diluted cDNA was added to 5 µL SyGreen HiROX mix (PCR Biosystems) and 1 µL of each forward and reverse primer (IDT) at 10 µM (final concentration of 0.5 µM for each). The plate was loaded into a Vii7 Real-Time PCR machine (Thermo Scientific) and the programme was run as per the Thermocycling parameters shown in Table 2.5.3.2.

	Rate	Temperature	Time
		25°C	
	Increase @ 1.9°C/s	95°C	
		95°C	20 seconds
40x cycles to amplify		95°C	1 second
	Decrease @ 1.6°C/s	60°C	20 seconds
	Increase @ 1.9°C/s	95°C	15 seconds
Melt curve	Decrease @ 1.6°C/s	60°C	60 seconds
	Increase @ 0.05°C/s	95°C	

**Table 2.5.3.2: qPCR thermocycling parameters**

### 2.5.3.3 $\Delta\Delta\text{Ct}$ calculations

Melt curves generated by qPCR were checked for presence of a single symmetrical peak, indicative of a single specific dsDNA amplicon generated during amplification of each gene with the specific primers. The raw cycle threshold (Ct) value for each amplicon was collected. Mean Ct values were calculated for technical duplicates, excluding those that appeared to be outliers compared to their technical and experimental replicates.  $\Delta\text{Ct}$  was calculated by subtracting the Ct value for the gene of interest from the Ct value of the reference gene: *GAPDH* in human cells and *HPRT* in murine cells.  $\Delta\Delta\text{Ct}$  was calculated by subtracting the  $\Delta\text{Ct}$  from each treated sample (e.g., each infection time point or stimulation condition) from the  $\Delta\text{Ct}$  of its relevant untreated sample. Once calculated,  $\Delta\Delta\text{Ct}$  values were used to generate a fold change value, using the calculation  $2^{\Delta\Delta\text{Ct}}$ , as an increase of one in Ct value results in a doubling of the amount of DNA in the PCR reaction. The mean fold change values calculated from experimental replicates were plotted as a bar chart, with standard deviation indicated by error bars.

## 2.6 Western blotting

### 2.6.1 Harvesting cell lysates

Cell lysates were harvested differently depending on the application of the lysate.

#### 2.6.1.1 Harvesting whole cell lysate

For Western blotting analysis of total protein levels, whole cell lysate was harvested from resting cells. Cells were trypsinised and resuspended in DMEM 10% FCS, pelleted by centrifugation (724 x g, 4 minutes, 4 °C) and washed twice by resuspension in PBS followed by centrifugation. Pelleted cells were resuspended in lysis buffer, approximately 100  $\mu\text{L}$  per  $2.5 \times 10^6$  cells. The lysis buffer used for A549 and U251 cells was radioimmunoprecipitation assay (RIPA) buffer (50 mM Tris-HCl pH 8, 1% Nonidet P-40 (NP-40), 0.5% sodium deoxycholate, 0.1% SDS, 150 mM NaCl) and for MEF cells was 30 mM Tris-HCl pH 7.4, 1% Triton X-100, 20 mM NaCl, 2 mM KCl, 2 mM EDTA and 10% glycerol.

#### 2.6.1.2 Harvesting lysates during infection or stimulation

When harvesting cells for Western blotting during stimulation or infection, all reagents used during lysis were ice cold and the whole procedure was done on ice. At the indicated time point, cells were washed once in 5 mL PBS, then scraped into 5 mL of PBS and transferred to a falcon tube. Cells were pelleted by centrifugation (724 x g, 4 minutes, 4 °C) and resuspended in 115  $\mu\text{L}$  of the lysis buffers, with protease inhibitors (Roche) and phosphatase inhibitors (Sigma).

For both applications, cells were lysed for 30 minutes on ice and 10 minutes on a rotating wheel at 4 °C and insoluble material was pelleted by centrifugation (18000 x g, 10 minutes, 4 °C). A sample was taken for determination of protein concentration, and then 6x loading buffer (300 mM Tris-HCl pH 6.8, 12% SDS, 60% glycerol, 0.6% bromophenol blue, 600 µM 2-ME) was added to the remaining cleared lysate. Whole cell lysates were stored at -20 °C until use and lysates for phosphoblotting were snap-frozen in a dry ice-ethanol bath and stored at -80 °C until use.

Protein concentration was determined by bicinchoninic acid (BCA) assay (Thermo Scientific) to enable equal loading of protein samples.

### **2.6.1.3 Harvesting lysates from ZIKV infection**

Following ZIKA infection, cells were washed twice with 1 mL PBS and scraped into 250 µL lysis buffer (Polysome buffer (20 mM Tris-HCl pH 7.5, 150 mM NaCl, 5 mM MgCl<sub>2</sub>, 1 mM DTT), 5 % Triton X-100, 12.5 U/mL DNase I and 1% DTT. Mechanical lysis was performed by passing the lysate through a 26-gauge needle 30 times. Insoluble material was pelleted by centrifugation at 18000 x g for 20 minutes at 4 °C. 6x loading buffer (300 mM Tris-HCl pH 6.8, 12% SDS, 60% glycerol, 0.6% bromophenol blue, 600 µM 2-ME) was added to the 50 µL of complete lysate, which was stored at -20 °C before use. Total protein concentration was not calculated or used to normalise loading with these lysates. This work was done together with Dr. Nerea Irigoyen and Charlotte Lefevre in the Department of Virology, University of Cambridge, who also analysed these samples by Western blotting.

### **2.6.2 Sodium dodecyl sulphate polyacrylamide gel electrophoresis (SDS-PAGE)**

Except for those used for analysis of co-immunoprecipitation experiments (BioRad 4-20% Tris-Glycine gels), SDS-PAGE gels were made using a Bio-Rad Protean III system: made up of a separating gel (10% (all stimulation except ZIKV) or 12% (ZIKV) polyacrylamide, 390 mM Tris (pH 8.8), 0.1% SDS, 0.1% ammonium persulphate (APS), 0.04% tetramethyl ethylenediamine (TEMED)) and a stacking gel (5% polyacrylamide, 130 mM Tris (pH 6.8), 0.1% SDS, 0.1% APS, and 0.1% TEMED).

Protein samples were defrosted on ice then boiled at 98 °C for 5 minutes. Insoluble material was pelleted by centrifugation at 18000 x g for 30 seconds. For Western blotting of whole cell lysates and phosphoblotting using A549 cell lysates, 50 µg of protein was loaded per well. For phosphoblotting using MEF cell lysates, 100 µg of protein was loaded per well.

Gels were run in a Mini-PROTEAN Tetra Vertical Electrophoresis Cell (BioRad) at 90 V for 30 minutes and 120 V for the remaining time (approximately 1.5 hours) using a Tris-Glycine running buffer (25 mM Tris, 192 mM glycine, 0.1 % SDS).

### 2.6.3 Transfer

A stack comprising of (bottom to top) blotting paper (BioRad), 0.2  $\mu$ m nitrocellulose membrane (Amersham), SDS-Page gel and blotting paper was pre-soaked in transfer buffer (25 mM Tris, 192 mM glycine, 20% methanol) for 5 minutes, assembled and then placed in a Pierce Power Blotter semi-dry transfer machine (Thermo Scientific). Proteins were transferred at 25 V for 30 minutes (if 50  $\mu$ g of protein was loaded) or 45 minutes (if 100  $\mu$ g of protein was loaded)

### 2.6.4 Immunoblotting

After transfer, membranes were blocked for 1 hour in Tris buffered saline 0.1% Tween-20 (TBST) 5% skim milk powder. After quickly washing twice with TBST, membranes were incubated with a primary antibody for 16 hours at 4 °C. Details of primary antibodies, their dilutions and diluents are shown in Table 2.6.4A. After 16 hours, membranes were washed 3 times for 5 minutes in TBST, incubated with secondary antibody for 1 hour at room temperature in the dark and washed 3 times for 10 minutes in TBST. Details of secondary antibodies are shown in Table 2.6.4B. Membranes were dried and stored in the dark at room temperature before imaging.

Antibody	Company	Code	Dilution/diluent
RIG-I (D-12)	Santa Cruz	sc-376845	1:1000/TBST
MAVS (E-3)	Santa Cruz	sc-166583	1:1000/TBST
TRAF2	Home-made (Henning Walczak lab, University of Cologne)		1:1000/TBST
IKKgamma/NEMO (DA10-12)	Cell Signaling Technology	#2695	1:1000/TBST
RIP1 (D94C12)	Cell Signaling Technology	#3493	1:1000/TBST
IRF3 [EPR2418Y]	Abcam	ab68481	1:1000/TBST
NAK/TBK1 [EP611Y]	Abcam	ab40676	1:1000/TBST
I $\kappa$ B $\alpha$ (L35a5)- MEF	Cell Signaling Technology	#4814	1:1000/TBST
$\alpha$ -Tubulin (DM1A)	Millipore	05-829	1:5000/TBST
ZIKV E protein	GeneTex	GTX133314	1:1000 PBST
GAPDH	Sigma	G8795	1:20000 PBST
IRF3 (phospho S386) [EPR2346]	Abcam	ab76493	1:1000/TBST
Phospho-TBK1 (Ser172) D52C2	Cell Signaling Technology	#5483S	1:1000/TBST
Phospho-I $\kappa$ B $\alpha$ (Ser32/36) (5A5)	Cell Signaling Technology	#9246	1:1000/TBST
Phospho-IRF3 (Ser396) (4D4G)	Cell Signaling Technology	#4947	1:500/TBST
Ku70 [N3H10]	Abcam	ab3114	1:1000/TBST
phospho-IKK $\epsilon$ (Ser172) (D1B7)	Cell Signaling Technology	#8766S	1:500/TBST

IKKε (D61F9) XP	Cell Signaling Technology	#3416	1:500/TBST
TANK	R&D	AF4755	1:1000/TBST
HOIP (human; full length), pAb	Ubiquigent	68-0013-100	1:1000/TBST
RBCK1 (H-1) (HOIL-1)	Santa Cruz	sc-393754	1:1000/TBST
SHARPIN	ProteinTech	14626-1-AP	1:1000/TBST
KU86 (B-4)	Santa Cruz	sc-515736	1:1000/TBST
Phospho-RIP (Ser166) (D1L3S)	Cell Signaling Technology	#65746	1:500/TBST
RIP3 (B-2)	Santa Cruz	sc-374639	1:1000/TBST
Flag	Sigma	#F7425	1:1000/TBST

**Table 2.6.4A Primary antibodies used for Western blotting**

Listed in order of appearance

Antibody	Company	Code	Dilution/diluent
Goat anti-rabbit 680 RD	Li-Cor	926-68071	1:10000/TBST
Goat anti-mouse 800 CW	Li-Cor	926-32210	1:10000/TBST
Donkey anti-Goat 800-CW	Li-Cor	926-32214	1:10000/TBST
Goat anti-Human IgG 800-CW	Li-Cor	926-32232	1:10000/TBST

**Table 2.6.4B Secondary antibodies used for Western blotting**

## 2.6.5 Detection

Blots were imaged by a Li-Cor Odyssey CLx, and images were processed using the programme Image Studio.

## 2.7 Enzyme-linked immunosorbent assay (ELISA)

A DuoSetELISA assay (R&D) was used to detect the presence of human CXCL10/IP-10 in the supernatants of infected or stimulated A549 cells.

### 2.7.1 Sample preparation

Cells were seeded in 6-well plates with biological duplicates per condition and were either stimulated or infected as previously described. At the stated time point, 1 mL of the supernatant was collected and stored at -20 °C.

### 2.7.2 ELISA

Initial optimisation assays were done to determine the dilution factor of samples to enable CXCL10 levels to fall within the standard curve, with samples diluted in PBS 1% PBS. Samples were diluted as

appropriate and the assay procedure was performed as described in the kit protocol, with technical duplicates done for each experimental sample, using TMB (Abcam) used as the substrate solution and 0.3 M H<sub>2</sub>SO<sub>4</sub> as the stop solution.

### 2.7.3 Analysis

The optical density of each sample was measured using a LUMIstar Omega. The blank-corrected optical density at 450 nm was subtracted from that at 540 nm. A 4-parameter fit standard curve was applied to the standards of known concentration and used to calculate the amount of CXCL10 in experimental samples. Dilutions were accounted for, and mean values generated from technical and experimental replicates were plotted as a bar chart, with standard deviation indicated by error bars.

## 2.8 Phos-flow

### 2.8.1 Fixing cells

After stimulation or infection, cells were washed twice in PBS, detached with trypsin and resuspended in DMEM 2.5% FCS. Cells were pelleted by centrifugation at 600 x g for 6 minutes and fixed in 100 µL per 1x10<sup>6</sup> cells of PhosFlow Lyse/Fix buffer (BD Bioscience) at 37 °C for 10 minutes. Fixation was stopped by addition of 1 mL of PBS 1% FCS and cells were stored at 4 °C overnight in PBS.

### 2.8.2 Staining cells

Cells were pelleted by centrifugation and further fixed and permeabilised in 1 mL of 88% methanol PBS at 4 °C for 30 minutes. Cells were washed 3 times in PBS 1% FCS, each time pelleted by centrifugation at 850 x g for 6 minutes at 4 °C. Cells were incubated with primary antibody diluted in PBS 1% FCS (25 µL per 1x10<sup>6</sup> cells), for 1 hour at room temperature in the dark. Details of antibodies used in these experiments are shown in Table 2.8.2. The washing steps were repeated, and cells were resuspended in filtered PBS in FACS tubes and stored at 4 °C until analysis was done, either immediately or the following day. Control samples, no antibody, single antibody and positive control samples, were also stained under the same conditions.

Antibody	Company	Code	Dilution/diluent
Phospho-IRF-3 (Ser396) (D6O1M) Rabbit mAb (Alexa Fluor® 647 Conjugate)	Cell Signaling	#10327	1:25/PBS 1% FCS
PE Rabbit Anti- Active Caspase-3 Clone C92-605	BD Pharmingen	550821	1:10/PBS 1% FCS

**Table 2.8.2: Antibodies used for phos-flow analysis**

### 2.8.3 Analysis of samples

Samples were analysed by flow cytometry using the Attune NxT Acoustic Focusing Cytometer (Fisher Scientific) and analysed in FlowJo Version 10. The gating strategy used for analysis is shown in Figure 2.8.3.

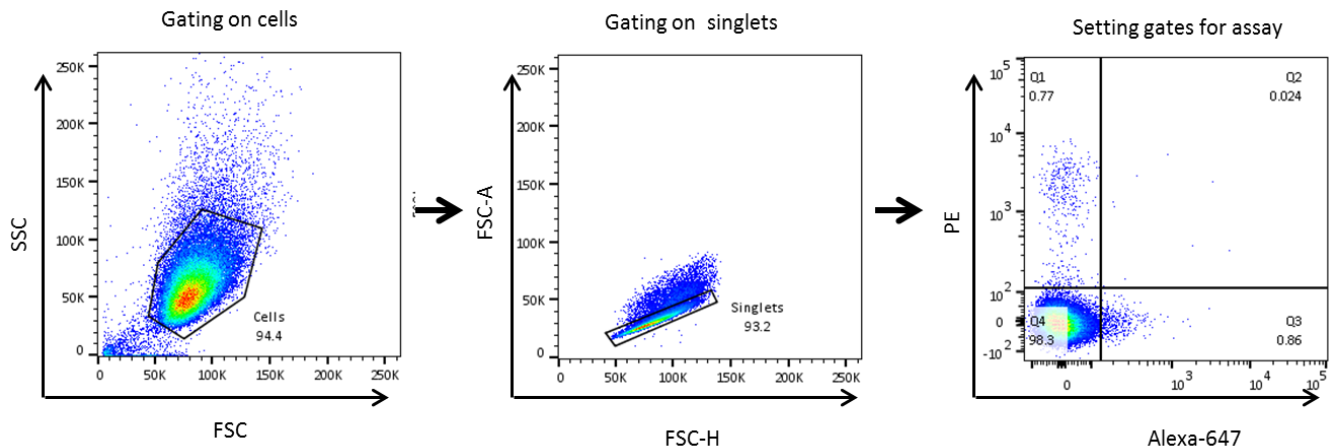


**Figure 2.8.3: Gating strategy for phos-flow analysis in FlowJo**

Dot plots showing forward scatter (FSC) against side scatter (SSC) to differentiate cells from debris, FSC-height against FSC-area to differentiate singlets (in the diagonal plane) from aggregated cells and Alexa-647 against PE to gate around negative cells in negative control (no antibody and no stimulation) samples.

## 2.9 LUBAC overexpression in HEK cells

### 2.9.1 Constructs

For overexpression of HOIP, HOIL-1 and SHARPIN in HEK cells, plasmids encoding N terminally V5- and His-tagged proteins were used, generated in the lab of Henning Walczak (University of Cologne), 337,338.

### 2.9.2 Transfection of overexpression constructs

HEK293T cells were seeded in 6-well plates at 60 % confluency ( $3 \times 10^5$  cells per well). Cells were transfected with the indicated amount of DNA, either empty vector (pcDNA4), or HOIP or HOIL-1 overexpression plasmids. 200  $\mu$ L per well of OptiMEM, 3  $\mu$ L per  $\mu$ g of DNA Polyethyleneimine (PEI, Polysciences) and expression plasmids were mixed and incubated at room temperature for 20 minutes. Half of the media was removed to leave 1 mL of complete media per well and 200  $\mu$ L of the transfection mix was added to each well. Cells were incubated for 24 hours, after which the media was replaced with an inoculum containing Sendai virus at a 1:100 dilution in DMEM 2.5% FCS and cells were incubated for a further 16 hours.

## 2.10 Cell death analysis

### 2.10.1 Methods of inducing cell death

#### 2.10.1.1 Staurosporine

A549 cells were treated with staurosporine (STS, Cell Guidance Systems) to induce caspase-3 dependent apoptosis. 2  $\mu$ M STS, dissolved in DMSO, was diluted in DMEM 10 % FCS, added to cells and incubated for the indicated time. As STS was diluted in DMSO, A549 cells were also treated with an equivalent dilution of DMSO in DMEM 10 % FCS, to check that any toxicity seen was due to STS and not just DMSO.

### 2.10.2 Methods of measuring cell death

#### 2.10.2.1 Imaging CPE

Phase contrast images of live cells were taken using a Zeiss Axio microscope with a 10 times magnification lens.

#### 2.10.2 Measuring active caspase 3-expressing cells

After stimulation, fixing and staining of cells was done as per section 2.8, using PE Rabbit Anti-Active Caspase-3 antibody.

#### 2.10.3 Vitality Assay

After stimulation, cells were washed twice with PBS, trypsinised and resuspended in DMEM 2.5% FCS to a total volume of 1 mL per  $5 \times 10^5$  cells (1 well). The cell suspension was mixed with NC-250 Solution 6, containing VB-48 vitality dye and propidium iodide (PI), at a 20:1 dilution and this was added to a NC-slide. The slide was loaded into the Nucleocounter NC-250 and the Vitality assay was run.

Images of the stained cells were acquired, and these were automatically used to generate scatter plots and histograms showing PI and VB-48 fluorescence intensity. Once this was acquired for all samples, cells from a control sample were used to gate around as healthy (VB-48 'high' and PI 'low'). The same gates were applied to all experimental samples. Gating of 'healthy' control cells is shown in Figure 2.10.2A and the relevant scatter plot and histogram, as well as the gating strategy used is shown in Figure 2.10.2B. Loss of VB-48 fluorescence intensity after 8 hours of treatment with 2  $\mu$ M STS is demonstrated in Figure 2.10.2C. The percentages of cells in each gate were used to generate a 100 % stacked bar chart.

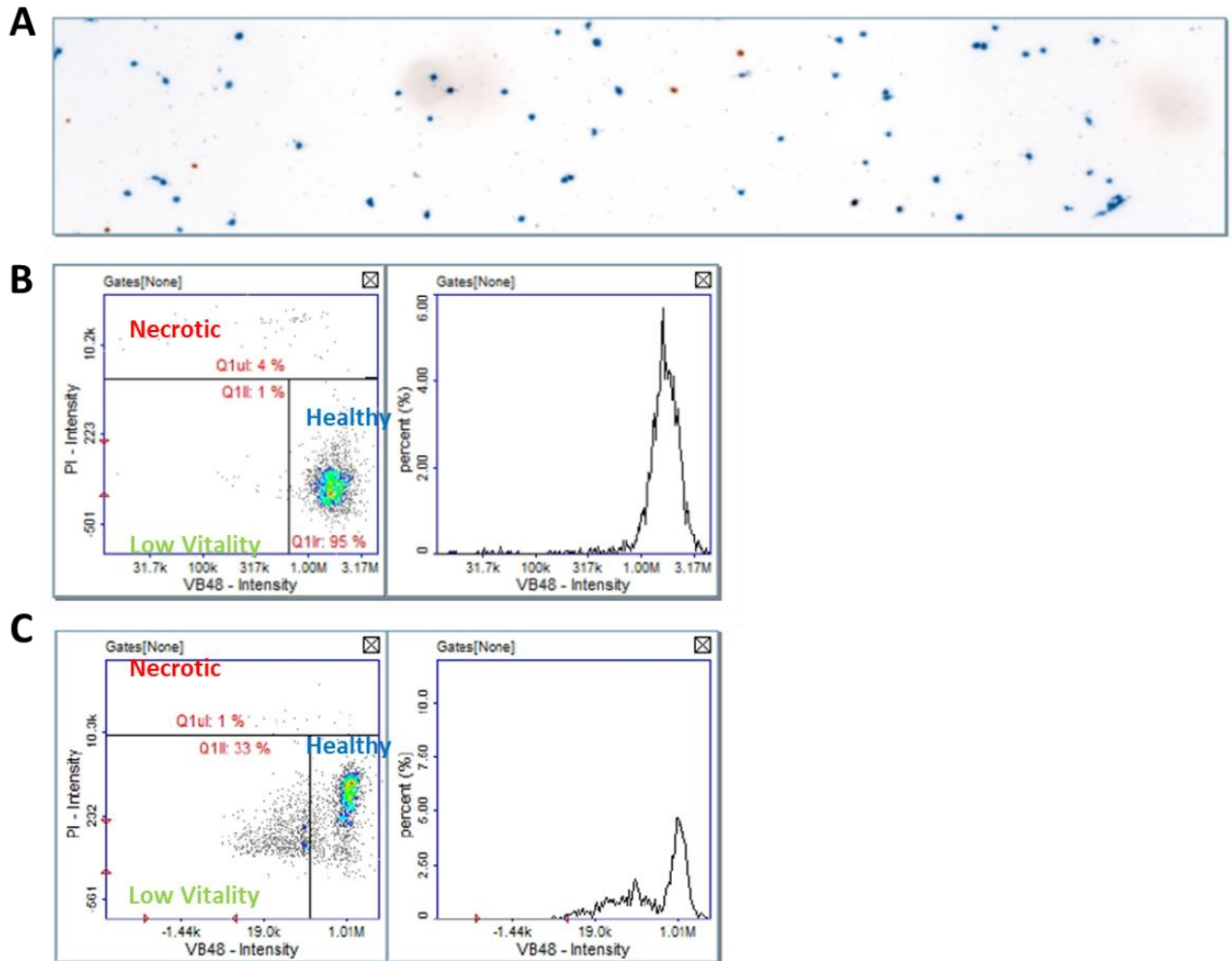


**Figure 2.10.2: NC-250 vitality assay parameters**

A) Image taken of A549 WT cells stained with Solution 6 containing VB-48 dye (blue) and PI, indicating non-viable cells (orange). Automatically generated scatter plots with gating strategy and histogram of VB-48 fluorescence intensity of A549 WT cells that are A) unstimulated and B) 8 hour treatment with 2  $\mu$ M STS.

## 2.11 Co-immunoprecipitation

### 2.11.1 TNF $\alpha$ stimulation and harvesting for Flag-IP

A549 cells stably expressing a tandem affinity purification (TAP)-tagged HOIP and NEMO were seeded in 15 cm dishes at 70% confluence ( $5 \times 10^6$  cells per dish) and incubated for 40 hours. Cells were stimulated with 500 ng/mL TNF $\alpha$  for the indicated times. Cells were washed twice in 5 mL cold PBS and scraped in 1 mL cold lysis buffer (30 mM Tris-HCl pH7.4, 120 mM NaCl, 2 mM EDTA, 2 mM KCl, 10% Glycerol, 1% Triton-X100) with protease inhibitors (Roche) and phosphatase inhibitors (Sigma). Cells were lysed for 30 minutes on ice and 10 minutes on a rotating wheel at 4  $^{\circ}$ C. Insoluble

debris was pelleted by centrifugation at 16200 x g for 30 minutes at 4 °C. 35 µL of cleared lysate was taken for an input sample and 7 µL of 6x loading buffer was added to the remainder.

### **2.11.2 SeV infection and harvesting for Flag-IP**

A549 cells stably expressing a tandem affinity purification (TAP)-tagged HOIP and NEMO were seeded in 15 cm dishes at 70% confluence ( $5 \times 10^6$  cells per dish) and incubated for 16 hours. Cells were stimulated with 100 U/mL IFN $\alpha$  and incubated for 24 hours before being infected with SeV for the indicated time. A single infection mix was made, cells were infected sequentially and harvested together. Cells were washed twice in 5 mL cold PBS and scraped in 0.5 mL lysis buffer 1 (100 mM NaCl, 40 mM Tris-HCl, pH 7.5, 1 mM CaCl<sub>2</sub>, 1 mM MgCl<sub>2</sub>) with protease inhibitors (Roche) and phosphatase inhibitors (Sigma). Cells were lysed for 30 minutes on ice and 40 minutes on a rotating wheel at 4 °C. Insoluble debris was pelleted by centrifugation at 16200 x g for 10 minutes at 4 °C and cleared lysate was transferred to a new Eppendorf tube. Pellets were resuspended in 0.5 mL lysis buffer 2 (100 mM NaCl, 40 mM Tris-HCl, pH 7.5, 1 mM CaCl<sub>2</sub>, 1 mM MgCl<sub>2</sub>, 1% Triton X-100 and 0.1% SDS) with protease inhibitors (Roche) and phosphatase inhibitors (Sigma) and twice subjected to sonification at 20 Hz for 10 seconds, with a minute on ice between. Sonicated samples were subjected to centrifugation at 16200 x g for 20 minutes at 4 °C. Cleared lysates from pre- and post-sonification were combined. 35 µL of cleared lysate was taken for an input sample and 7 µL of 6x loading buffer was added to the remainder.

### **2.11.3 Flag-IP and washing**

25 µL per sample of Flag-M2 beads (Sigma), pre-washed once with PBS and 3 times with the respective lysis buffer, were added to the cleared lysates and this was incubated on a rotating wheel at 4 °C for 16 hours. Beads were pelleted by centrifugation at 2,400 x g for 5 minutes at 4 °C and unbound material was removed using a 1 mL needle with a 20-gage syringe. Beads were washed by addition of 1 mL of respective lysis buffer (without protease or phosphatase inhibitors) followed by centrifugation as before. The washing procedure was repeated four more times. 40 µL of 2x loading buffer with 330 mM DTT was added to beads.

Immunoprecipitation samples were heated at 95 °C for 5 minutes and were analysed by Western blotting.

## 2.12 Statistical analysis

Significance was determined by a one tailed student's T test for two independent means. All data produced met the requirements of two independent samples with the same variance and normal data distribution. The null hypothesis stated that there was no difference between the means of the two populations (H0:  $\mu_1 - \mu_2 = 0$ , where  $\mu_1$  is the mean of the first population and  $\mu_2$  the mean of

the second). The equation used for this calculation was  $p\ value = \frac{\bar{x}_1 - \bar{x}_2}{\sqrt{\left(\frac{(N_1-1)S_1^2 + (N_2-1)S_2^2}{N_1 + N_2 - 2}\right)\left(\frac{1}{N_1} + \frac{1}{N_2}\right)}}$ .

Data was deemed significant if the p value was  $<0.05$  and significance is represented on graphs by P  $<0.05 = *$ , P  $<0.01 = **$  and P  $<0.001 = ***$ .

# Chapter Three: Developing tools to study RIG-I signalling in A549 cells

---

## 3.1 Introduction

The importance of RIG-I in sensing certain viral infections has been highlighted by the use of knock-out mice and the characterisation of disease-causing RIG-I mutation in humans<sup>339,340</sup>. Loss-of-function mutations confer increased susceptibility to virus infection, whereas gain-of-function mutations that render RIG-I constitutively active result in exaggerated or spontaneous production of anti-viral and pro-inflammatory cytokines. The sensing of viruses by RIG-I in the first infected cells in the body is crucial for effective infection control and clearance with minimal damage to the host. Due to the nature of the viruses detected by RIG-I, this usually occurs in epithelial cells, often at mucosal surfaces like those found in our airways.

The aims of this chapter were to generate tools that could be used to study signalling mechanisms downstream of RIG-I. To do this, we used synthetic RNA ligands and RNA viruses known to activate RIG-I and tested their efficacy in our chosen model system. The response to each stimulus was measured and quantified by qPCR to measure the transcription of genes known to be activated by IFN-I, IRF-3 and NF- $\kappa$ B; Western blotting and phos-flow analysis to observe the activation of known RIG-I signalling pathway components; and ELISA to measure chemokine secretion. The specificity the ligands for RIG-I was determined by the generation and testing of A549 cells deficient in RIG-I. Data generated in this chapter demonstrates that stimulation of A549 cells with 3p-hpRNA, Poly(I:C), SeV, IAV R+K and ZIKV PE243 induces an IFN-I response, with SeV and ZIKV also activating IFN-III and NF- $\kappa$ B-dependent responses, all of which were completely dependent on RIG-I expression.

## 3.2 RNA sensing in A549 cells

### 3.2.1 A549 cells as a model for studying RIG-I signalling

When investigating a signalling pathway, to ensure that any data generated is reliable, accurate and close to what would happen physiologically, the choice of an appropriate model system is very important. Many viruses known to activate RIG-I *in vivo*, such as Sendai virus (SeV) and Influenza A virus (IAV), are respiratory viruses, therefore ideally primary human alveolar cells would be used. However, primary cells are not very tractable for studies involving cell signalling analyses or genetic

manipulation. Therefore, A549 cells, a transformed human lung adenocarcinoma cell line that has similarities to human basal alveolar epithelial cells was chosen.

Although cancer cell lines allow flexibility to study cell signalling pathways in detail using genetic manipulation techniques, they can also have flaws as model. Cancer is driven by genetic alterations, some of which map to signalling networks resulting in dysregulated signalling outcomes. For example, many carcinoma cell lines, including A549 cells, downregulate nucleic acid sensing machinery to allow them to remain undetected by the immune system<sup>341–343</sup>. Despite this, the prior use of A549 cells in many studies of RNA sensing suggested they could be a suitable model for RIG-I signalling analysis<sup>97,344,345</sup>.

Although previous literature indicates that A549 cells can function as a good model for RIG-I signalling, there are often differences between batches of commonly used mammalian cancer cell lines, so we empirically tested the RIG-I signalling capability of our A549 cells. Consistent with previous literature, we found that A549 cells expressed high levels of RIG-I signalling pathway proteins MAVS, TRAF2, NEMO, RIP1, IRF3, TBK1 and I $\kappa$ B $\alpha$  (Figure 3.2.1A). Although RIG-I expression was barely detectable by Western blotting in resting A549 cells, it was strongly upregulated by stimulation with IFN $\alpha$  (Figure 3.2.1B).

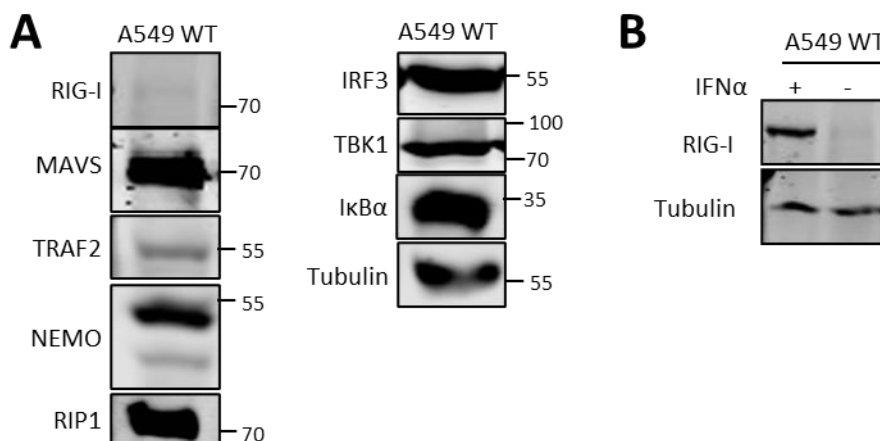


**Figure 3.2.1: A549 cells express many of the components of the RIG-I signalling machinery**

Western blotting analysis of A) signalling pathway proteins in resting A549 WT cells and B) RIG-I in A549 cells either resting or after 24h stimulation with IFN $\alpha$  at 100 U/mL.

### 3.2.2 A549 cells generate an immune response to stimulation with synthetic RNAs

To confirm that A549 cells can sense non-self RNA in the cytoplasm, they were transfected with three synthetic RNA species that activate RIG-I: Poly(I:C), 5'ppp-dsRNA and 3p-hpRNA.

Poly(I:C) is a long synthetic double stranded (ds)RNA analogue that predominantly activates TLR3 and MDA5<sup>78,346–348</sup>. However, smaller or branched fragments of Poly(I:C) have been shown to preferentially activate RIG-I<sup>95,167,349–353</sup>. 5'ppp-dsRNA is a short, blunt ended, double stranded (ds)RNA duplex with a 5'triphosphate group. The helicase domain of RIG-I is known to recognise short dsRNA duplexes, but the 5' triphosphate group, which distinguishes the foreign RNA from 5'capped cellular RNAs, is recognised by RIG-I C-terminal domain (CTD)<sup>83,354</sup>. These two structures are thought to be necessary and sufficient to induce RIG-I activation<sup>89,90,355</sup>. 3p-hpRNA is a short single-stranded RNA with a 5' triphosphate generated by in vitro transcription of a region of the IAV genome (sequence shown in Fig 3.2.2A), which self-anneals into regions of double stranded secondary structures such as hairpin or panhandles (predicted structure shown in Fig 3.2.2B), therefore should also activate RIG-I.

After stimulation of RIG-I by transfection with these synthetic RNAs, transcription of immune genes was measured by qPCR. IFN-I and chemokine genes *IFNB1* and *CXCL10* were chosen as a direct readout of RIG-I activation due to their biological significance in antiviral immunity. Their transcription, activated by the IRF and NF-κB families of transcription factors, is strongly induced by signalling from many pattern recognition receptors, including nucleic acid sensors like RIG-I<sup>213,356,357</sup>. *IFNB1*, a type-I interferon, is one of the most potent antiviral products of PRR signalling, however it is often only expressed by a small subset of cells<sup>358,359</sup>. It's transcription is regulated by an enhanceosome comprised of transcription factors such as NF-κB and IRF3 or IRF7<sup>360,361</sup>. *CXCL10* transcription provides a near-digital readout of RIG-I activation as levels of background expression in the absence of PRR activation are very low, but its transcription is strongly induced as a result of RIG-I ligation. Its transcription is activated directly by NF-κB or IRF3, alongside other transcription factors depending on the context<sup>357</sup>.

A549 WT cells were stimulated by transfection of high molecular weight (HMW) Poly(I:C), and qPCR analysis showed transcription of both *IFNB1* and *CXCL10* (Figure 3.2.2C). This confirmed both the successful transfection of Poly(I:C) into the cytoplasm of A549 cells and the presence of functional intracellular RNA sensing in our A549 cells. Transfection of 5'ppp-dsRNA did not induce expression of *IFNB1* or *CXCL10*, even at high doses (Figure 3.2.1D), despite possessing both a short dsRNA region and a 5' triphosphate group. Contrastingly, stimulation of A549 cells with triphosphate hairpin RNA (3p-hpRNA) was successful at activating transcription of *CXCL10* at higher doses (0.5 and 1 µg), although *IFNB1* was still not detectable above background levels (Figure 3.2.1E).

Based on these data, transfection with 1  $\mu\text{g}$  Poly(I:C) and 3p-hpRNA was used to further examine activation of RIG-I by synthetic RNAs.

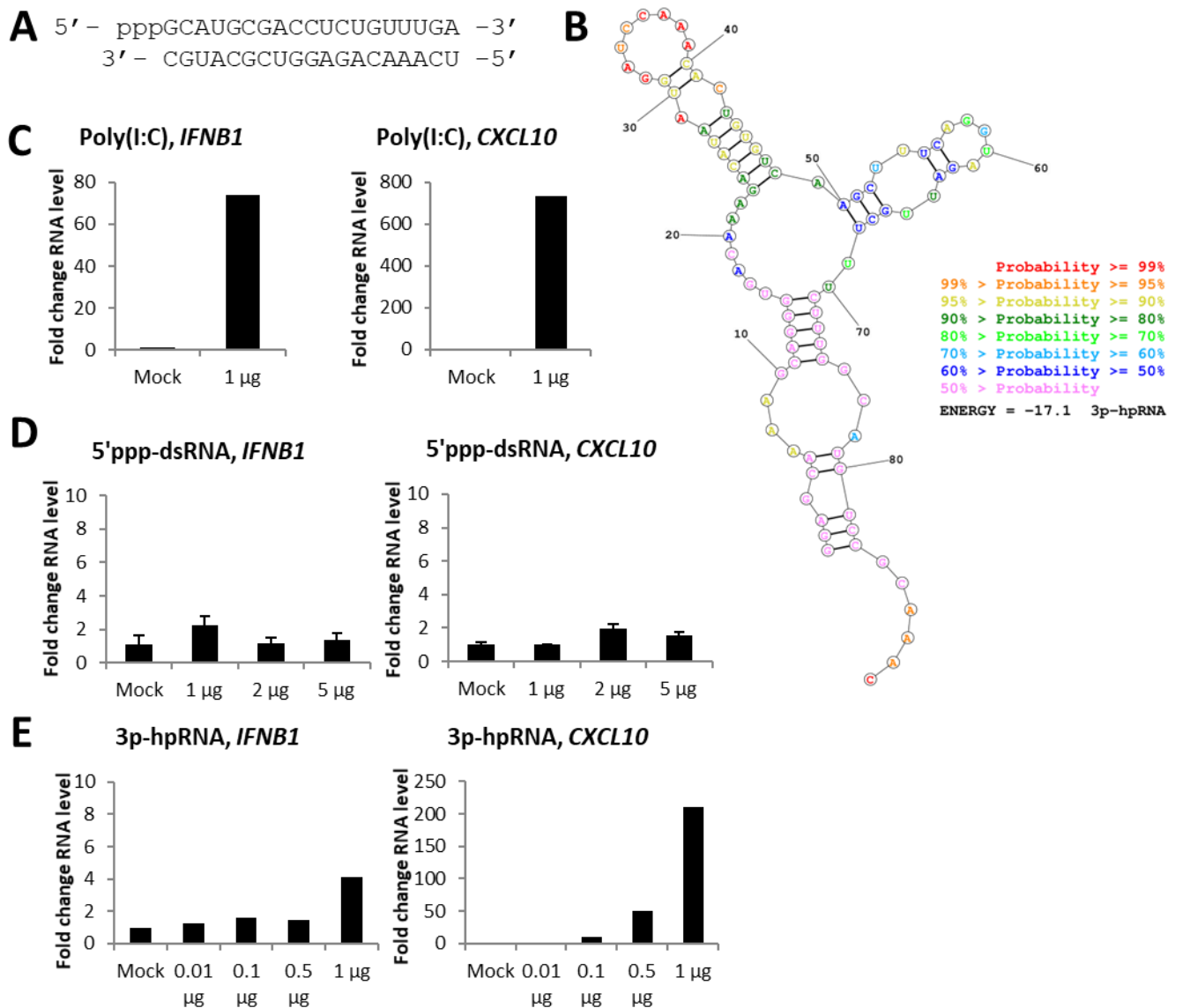


**Figure 3.2.2: A549 cells generate an immune response when stimulated by synthetic RNAs**

A) Sequence of 5'pppRNA. B) Lowest free energy structure of 3p-hpRNA, predicted by RNAstructure v6.2 (<http://rna.urmc.rochester.edu/RNAstructure.html>). qPCR to measure transcription of indicated genes in A549 WT cells both not transfected (Mock) and 6h post-stimulation with C) 1  $\mu\text{g}$  Poly(I:C) (n=2, data representative of >3 experimental replicates), D) 1, 2 and 5  $\mu\text{g}$  5'ppp dsRNA (n=2, data representative of one experimental replicate) and E) 0.01, 0.1, 0.5 and 1  $\mu\text{g}$  3p-hpRNA (n=2, all data representative of one experimental replicate).

### 3.2.3. A549 cells generate an immune response when infected with respiratory RNA viruses, SeV and IAV

After successful stimulation of A549 cells with synthetic RNAs, the response of the cells to infection with known RIG-I-activating respiratory RNA viruses was measured.

Sendai virus (SeV) and Influenza A virus (IAV) were chosen as stimulation models due to their specificity activating RIG-I over other PRR and their physiological relevance in the cell type chosen. The Cantell strain of SeV was used as it is a potent activator of RIG-I, due to high levels of defective interfering RNAs consisting of copyback genomes, induced by continuous passage at high multiplicity<sup>281,282</sup>. The strain of Influenza A virus used, A/Puerto Rico/8/1934, is a mouse adapted H1N1 virus known to activate both RIG-I and TLR3 in A549 cells<sup>345</sup>.

As the Cantell strain of SeV doesn't result in a productive infection due to the generation of defective interfering (DI) particles with copy-back genomes rather than intact viral genomes<sup>281</sup>, multiplicity of infection (MOI) could not be used as a measure of virus concentration, so dilution of virus stock was used. To determine the optimal concentration of SeV for infection studies, A549 cells were infected with varying dilutions of the SeV stock for 6 hours (Figure 3.2.3A). Infection at all dilutions resulted in induction of high levels of *IFNB1* and *CXCL10* transcripts, with the 1:100 dilution being the most potent stimulator. However, as there were only small increases in transcription of *IFNB1* and *CXCL10* at higher concentrations above 1:300, a 1:300 dilution was chosen for further use.

Following infection with IAV PR8, qPCR analysis showed a 200,000-fold increase in transcription of NS1 (Figure 3.2.2B), an early and abundantly expressed IAV gene. Despite this, transcription of both *IFNB1* and *CXCL10* was not detected above background levels by 6 hours post infection (Figure 3.2.2C). This is likely due to the known immunosuppressive functions of the NS1 protein itself, which inhibits virus induced activation of both IRF3 and NF- $\kappa$ B, including directly disrupting RIG-I signalling by binding to dsRNA, TRIM25 and Riplet<sup>244,362-364</sup>. Because of this, a virus with a reduced its capacity to antagonise RIG-I signalling caused by Lysine (K) to Alanine (A) mutations at positions 38 and 41 of NS1, abrogating its binding to dsRNA to prevent it from sequestration away from RIG-I<sup>362,365</sup>, was used. In response to infection of A549 cells with the NS1 R38A mutant virus, transcription of *CXCL10* increased slightly (less than 5-fold) compared to PR8 WT infection. However, in response to infection with the double mutant virus NS1 R38A K41A (R+K), *CXCL10* transcription was over 30-fold higher than in resting cells (Figure 3.2.3C). Transcription of *IFNB1* was still not detected, as was seen with transfection of 3p-hpRNA in A549 cells (Figure 3.2.2E).

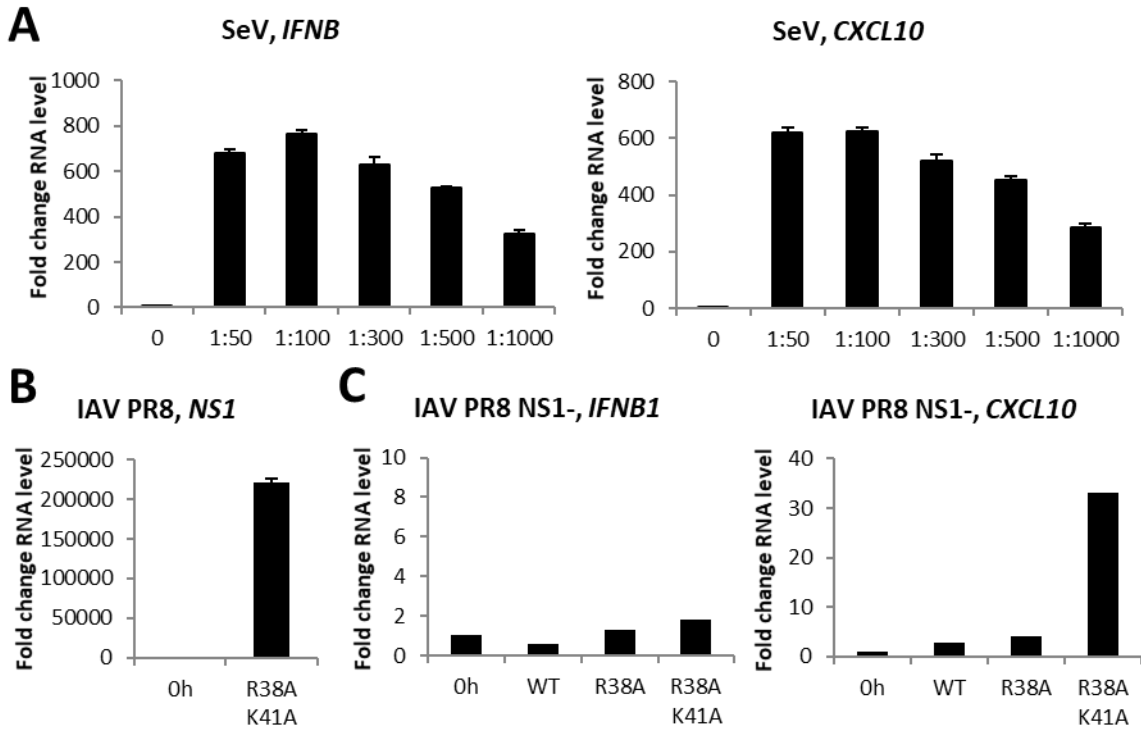


**Figure 3.2.3: A549 cells generate an immune response when stimulated by RNA viruses**

qPCR to study transcription of indicated genes in A549 WT cells during A) infection with SeV for 6 hours at the indicated dilution (n=2, data representative of 2 experimental replicates), B) and C) infection with IAV PR8 WT and indicated NS1 mutants at MOI 5 for 6 hours (n=2, data representative of >3 experimental replicates), C) *IFNB1* and *CXCL10* in NI cells and after 6 hour infection with IAV PR8 WT, NS1 R38A and NS1 R38A K41A mutants at MOI 5 (n=2, data representative of one experimental replicate).

### 3.2.4 A549 cells as a model to study ZIKV infection

Zika virus (ZIKV) is an Arbovirus, spread by the bite of an infected mosquito. Because of this, initial infection generally occurs in skin epithelial cells, meaning that A549 cells are not the most physiologically relevant model for studying early responses to ZIKV infection. The majority of the pathology associated with severe ZIKV infection, such as congenital microcephaly and Guillian Barre syndrome, is related to infection of astrocytes in the central nervous system, so many studies of ZIKV infection use U251 cells, a human glioblastoma astrocytoma cell line<sup>366,367</sup>.

Previous data suggests that RIG-I plays a role in sensing ZIKV infection in physiologically relevant cell lines such as U251<sup>368-370</sup>. To confirm that RIG-I senses RNA virus infection U251 cells, they were infected with SeV and IAV R+K and the transcription of *IFNB1* and *CXCL10* was measured by qPCR (Figure 3.2.4A and B). 50-fold induction of *IFNB1* transcription and over 200-fold induction of *CXCL10* transcription was seen in response to infection with both SeV IAV R+K. Consequently, ZIKV infection was used as additional infection model to study RIG-I signalling in A549 cells.

Previous studies have shown that ZIKV can infect A549 cells<sup>313,369,371,372</sup>. To confirm this, A549 WT cells were infected with ZIKV, transcription of the virus-encoded open reading frame (ORF) was measured by qPCR (Figure 3.2.4C), expression of the ZIKV E protein was confirmed by Western blotting (Figure 3.2.4D) and replication of ZIKV was determined by a one-step growth curve (Figure 3.2.4E). ZIKV infections were done together with Dr. Nerea Irigoyen and Charlotte Lefevre (University of Cambridge), who completed all RNA extraction, Western blotting and growth curve analyses. Detection of increasing levels of ZIKV ORF transcript and E protein through the time course confirmed successful infection and increasing levels of plaque forming units over the time course confirmed that ZIKV can infect and productively replicate in A549 cells.

Finally, transcription of *IFNB1* and *CXCL10* was also measured in ZIKV infected A549 cells (Figure 3.2.4F). Although delayed compared to infection with SeV or IAV R+K (Figure 3.2.3A and C), transcription of both genes was detectable above background levels by 16 hours post infection. This confirmed both A549 cells could sense and mount an immune response to ZIKV infection and that despite measuring immune readout at later time points, we were still capturing the initial RIG-I signalling events in these cells.

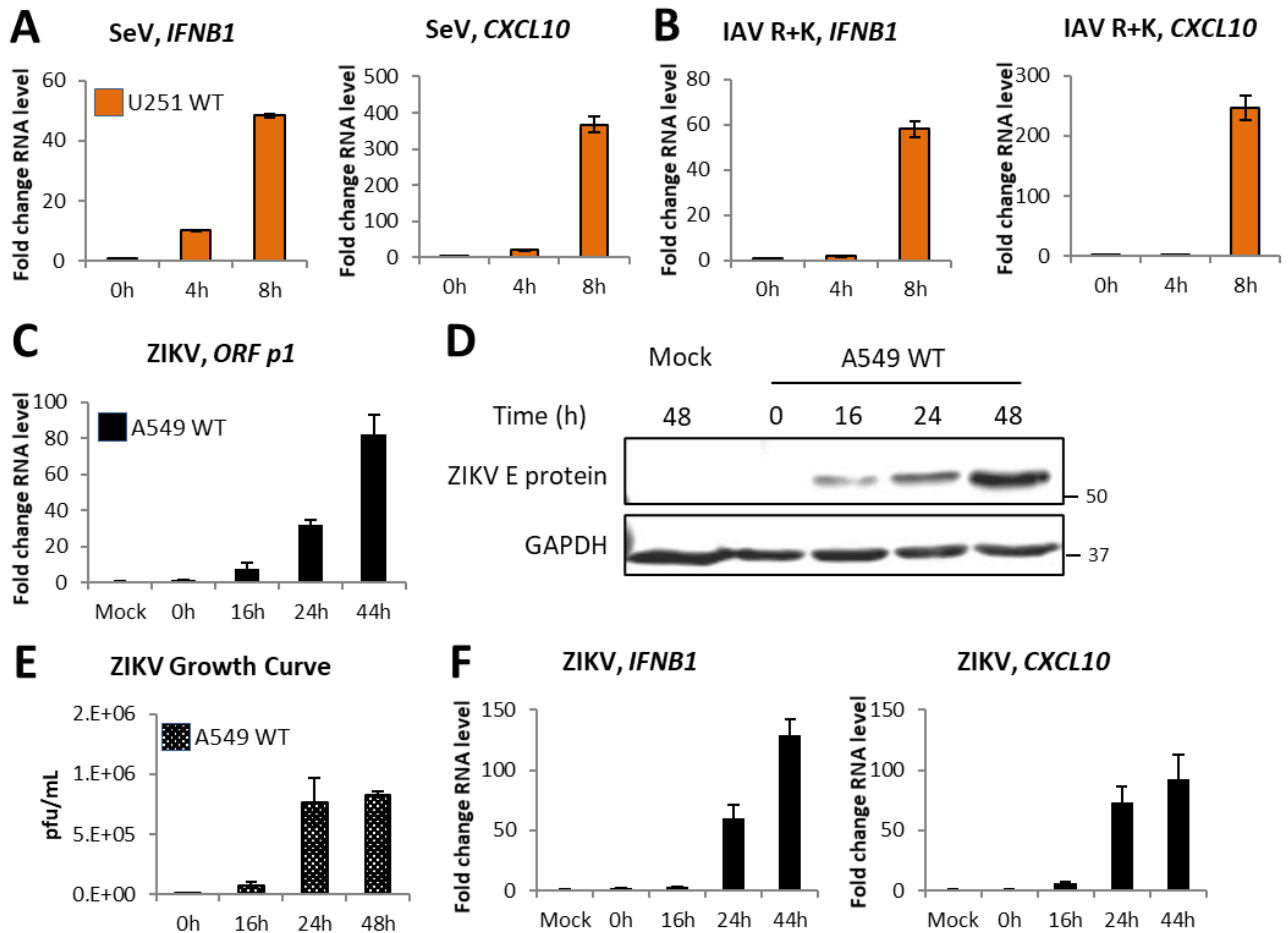


**Figure 3.2.4: A549 cells are a suitable model to study innate immune sensing of ZIKV**

qPCR to measure transcription of indicated genes in U251 WT cells during infection with A) SeV at 1:300 dilution and B) IAV R+K at MOI 5 (both n=2, data representative of 1 experimental repeat). C) qPCR to measure ZIKV PE243 ORF transcription during infection of A549 WT cells with ZIKV PE243 at MOI 3 (n=3). D) Western blotting analysis of infection of A549 cells with ZIKV PE234 at MOI 3 (blot carried out by Dr. Nerea Irigoyen and Charlotte Lefevre). E) ZIKV PE243 growth curve generated by titration and plaque assay of ZIKV infection of A549 WT cells (n=3, data representative of 3 experimental replicates, generated by Dr. Nerea Irigoyen and Charlotte Lefevre). F) qPCR to measure transcription of indicated genes during infection of A549 WT cells with ZIKV PE243 at MOI 3 (n=2, data representative of >3 experimental replicates).

### 3.3 Characterising the signalling response of A549 cells to synthetic RNAs and RNA viruses

To better understand the immune response in A549 cells stimulated by synthetic RNAs and RNA viruses was carried out.

The transcriptional response of stimulated cells was studied in more detail by measuring the expression of a wider panel of immune genes by qPCR. In addition to *IFNB1*, transcription of IFN-I gene *IFNA2* was also measured because whilst *IFNB1* transcription requires co-ordinated binding of both IRF3 and NF- $\kappa$ B to its promoter, IFN $\alpha$  genes can be activated by binding of either IRF3 or NF-

$\kappa$ B<sup>373</sup>. To counteract that fact that *IFNB1* is often only expressed by a small subset of cells<sup>358,359</sup>, transcription of IFN-I dependent genes *ISG15* and *ISG54* was also measured. In addition to occurring in an IFN-I-dependent manner, transcription of *ISG54* is directly activated by IRF3 independent of IFN-I activity. Activation of IFN-III was determined by measuring transcription of *IFNL1*. NF- $\kappa$ B activity was examined by studying transcription of *NFKBIA*, *TNFA* and *IL6*. *NFKBIA* is used here as a technical readout of NF- $\kappa$ B activity, transcribed only as a direct result of the activity of NF- $\kappa$ B, whereas *TNFA* and *IL6* are functional NF- $\kappa$ B-responsive cytokines. Additionally, transcription of the chemokine *CXCL10* was further validated using ELISA to measure secretion of CXCL10 into the supernatant of stimulated cells.

Many proteins in the RIG-I signalling pathway, including TBK1, IRF3 and I $\kappa$ B $\alpha$ , are activated by phosphorylation. Both Western blotting and phos-flow analyses, using antibodies specific for the phosphorylated forms of the individual proteins, were used to detect their activation. Western blotting analysis indicates the level of accumulation of the phosphorylated form of the protein, and phos-flow indicates the percentage of cells expressing the phospho-form of IRF3.

### 3.3.1 Stimulation of RIG-I by synthetic RNAs activates Type I IFN, chemokines and ISGs

Stimulation with synthetic RNAs was done as previously described, transcription of an extended gene panel was examined by qPCR and activation of signalling proteins measured by Western blotting and phos-flow.

After stimulation with 3p-hpRNA, transcription of IFN-I dependent genes *ISG15* and *ISG54* was robustly induced (Figure 3.3.1A), as seen previously with *CXCL10*. As with *IFNB1*, transcription of IFN-I gene *IFNA2* was undetectable, which contradicts previous studies<sup>374</sup>. However, this may well be because the fact that IFN-I genes are only expressed by a small subset of cells is exacerbated by low levels of transfection efficiency in A549 cells, making their transcription undetectable. Poly(I:C) transfection resulted in a 30-fold increase in transcription of IFN-I gene *IFNB1*, but not *IFNA2*. Additionally, transcription of IFN-I-dependent genes *ISG15* and *ISG54* was also detected. Neither synthetic RNA induced robust transcription of IFN-III or NF- $\kappa$ B-dependent genes *IFNL1* and *NFKBIA*, despite the literature suggesting both that IFN $\lambda$  is critical to the antiviral response to respiratory viruses, acting potently on epithelial cells<sup>375–377</sup> and that NF- $\kappa$ B is activated downstream of RIG-I stimulation by synthetic RNAs<sup>378</sup>. This also contradicts previous studies showing transcription of IFN-III-dependent genes *IL28* and *IL29* after stimulation of HepG2 cells with 3p-hpRNA and Poly(I:C)<sup>379</sup>.

Transcription of *TNFA* and *IL6* was not measured because *NFKBIA* transcription was not detectable above background levels.

The transcription of *CXCL10* in response to stimulation with both synthetic RNAs transfection was supported by ELISA analysis (Figure 3.3.1B), which showed substantial secretion of CXCL10 by 24 hours post stimulation.

Examination of signalling protein phosphorylation in A549 cells stimulated by 3p-hpRNA and Poly(I:C) by Western blotting showed phosphorylation of both TBK1 and IRF3 after 6 hours (Figure 3.3.1C), however this was much stronger with Poly(I:C) than with 3p-hpRNA. Despite this, examination of IRF3 phosphorylation by phos-flow showed no detectable increase in cells expressing phosphorylated IRF3 after 6 hours of Poly(I:C) stimulation (Figure 3.3.1D). This is likely due to a lower sensitivity level of the phos-flow assay compared to Western blotting, compounded by the relatively low transfection efficiency of A549 cells. Phosphorylation of I $\kappa$ B $\alpha$  was barely detected by Western blotting, consistent with the lack of detectable *NFKBIA* transcription. However, this may also be because, in the absence of proteasome inhibitors such as MG-132, I $\kappa$ B $\alpha$  is degraded quickly once phosphorylated to allow activation of NF- $\kappa$ B<sup>380–382</sup>.

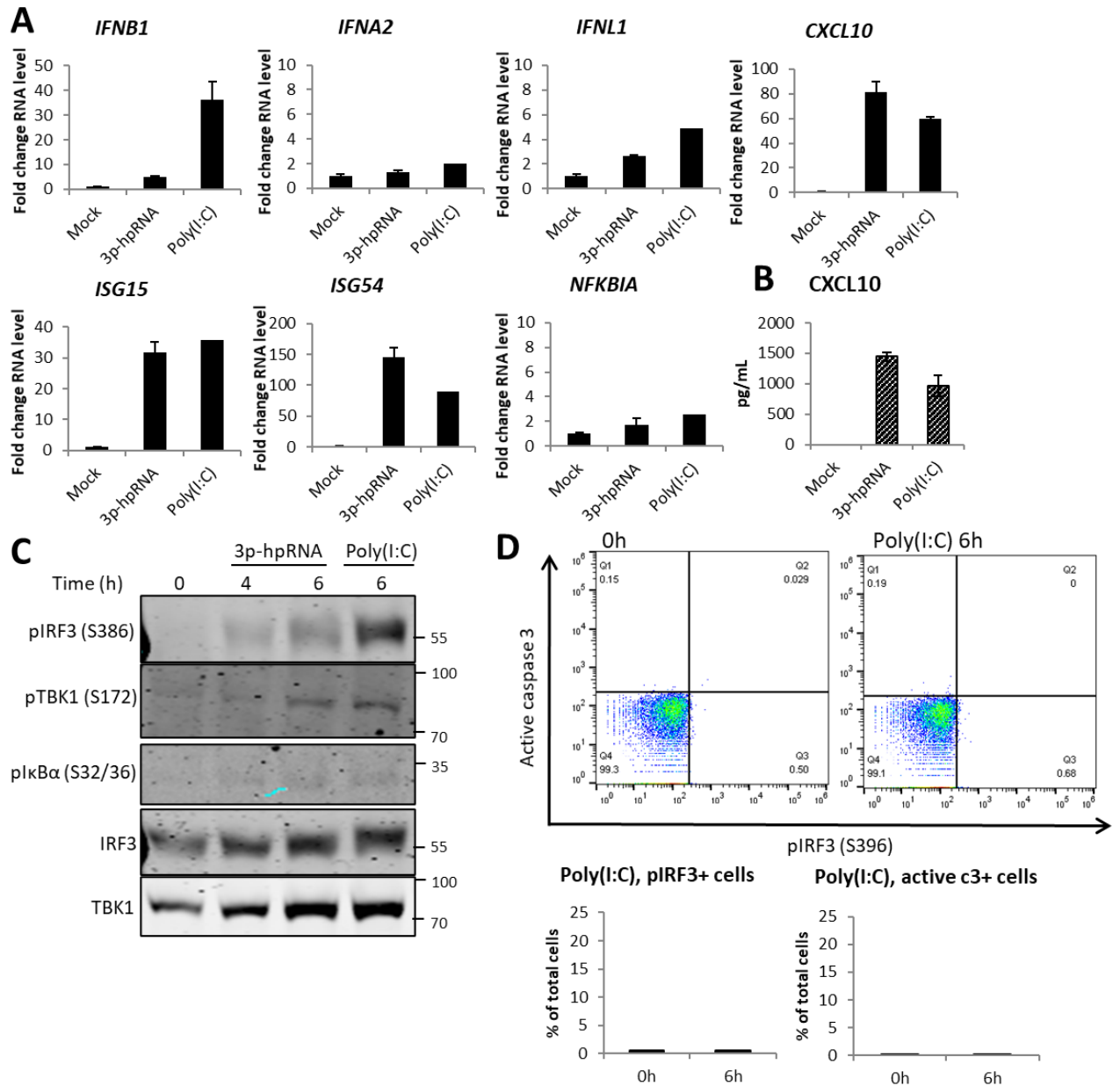


**Figure 3.3.1: Synthetic RNAs activate IRF3-dependent pathways, but not NF-κB dependent**

A) qPCR to measure transcription of indicated genes 6 hours post-stimulation of A549 WT cells with 1 μg 3p-hpRNA and 1 μg Poly(I:C) (n=2, data representative of >3 independent assays). B) ELISA to measure CXCL10 secretion 24 hours post-stimulation of A549 WT cells with 1 μg 3p-hpRNA and 1 μg Poly(I:C) (n=2, data representative of >3 experimental replicates). C) Western blotting analysis of lysates from A549 WT cells stimulated with 5 μg 3p-hpRNA or Poly(I:C) (data representative of one experimental replicate). D) Phos-flow analysis of expression of phospho-IRF3 (Ser396) and active caspase 3 in A549 WT cells 6 hours post-stimulation with 2 μg Poly(I:C) (n=1, data representative of 1 experimental repeat).

### 3.3.2. Infection of A549 cells with SeV activates IRF3 and NF-κB, driving expression of IFN, chemokines and NF-κB stimulated genes

The signalling outcomes of SeV infection of A549 cells were examined by qPCR, ELISA, Western blotting and phos-flow (Figure 3.4.2).

SeV infection resulted in increasing transcription of IFN-I and IFN-III genes (*IFNB1* and *IFNL1*), IRF-activated *ISG15* and *ISG54*, the chemokine *CXCL10* and NF- $\kappa$ B-driven genes *NFKBIA*, *TNFA* and *IL6* through the 6 hour time course (Figure 3.3.2A). Of the genes tested, only *IFNA2* transcripts were not detectable above background levels, conversely to a previous studies showing transcription of IFN $\alpha$  genes in murine fibroblasts and lung tissue after infection with SeV, albeit to approximately 100-fold lower level than IFN $\beta$  transcripts<sup>383,384</sup>. Compared to the transcriptional response to synthetic RNAs, expression of all transcripts was more robust during SeV infection. Additionally, significant upregulation of *IFNL1* (4000-fold) and *NFKBIA* (600-fold), not seen with synthetic RNAs, was evident by 6 hours post infection with SeV. Although *TNFA* transcription was modestly upregulated by 6 hours post infection, *IL6* transcription was barely detectable above background levels.

Detection of CXCL10 secretion by ELISA during SeV infection of A549 cells confirmed *CXCL10* transcription data, with detectable levels of CXCL10 by 6 hours post infection and much higher levels of accumulation at 24 hours (Figure 3.3.2B).

Western blotting of A549 cells during SeV infection (Figure 3.3.2C) detected visible phosphorylation of IRF3, TBK1 and I $\kappa$ B $\alpha$ , with stronger bands suggesting higher levels of phosphorylation, or phosphorylation in a higher proportion of cells than seen during stimulation with synthetic RNAs. Visible phosphorylation of I $\kappa$ B $\alpha$ , seen most strongly in the presence of MG-132 is in line with the robust transcription of *NFKBIA* and *TNFA* seen during SeV infection, but not stimulation with synthetic RNAs. Unchanged total (unphosphorylated) protein expression levels through the infection time course confirm that the increase of phosphorylated protein during infection was not due to a change in total protein levels.

Phosphorylation of IRF3 during SeV infection was also detected by phos-flow analysis in approximately a third of A549 WT cells (Figure 3.3.2D). Without staining of cells with antibody against SeV or dsRNA, so we cannot confirm whether infection fully correlates with IRF3 phosphorylation. It is possible that only a small percentage of A549 WT cells were successfully infected; that only a small proportion of infected cells expressed phosphorylated IRF3; or that we have only detected a fraction of the phosphorylation happening in cells.

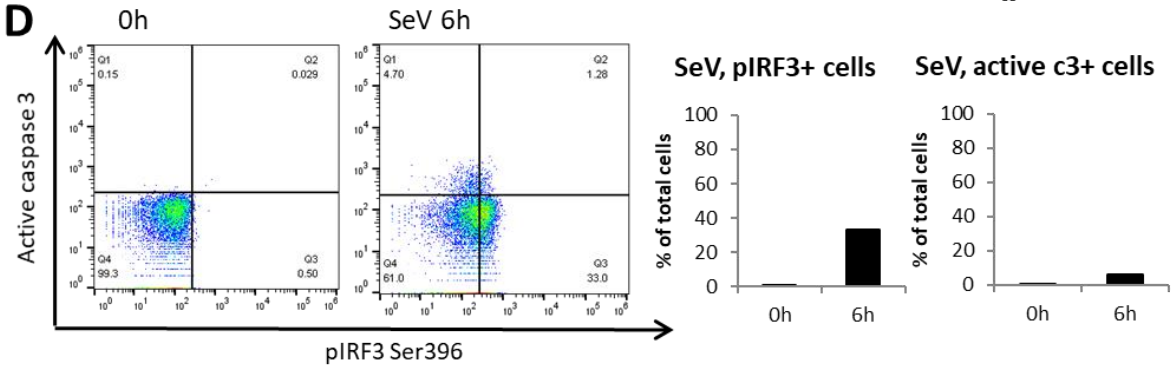
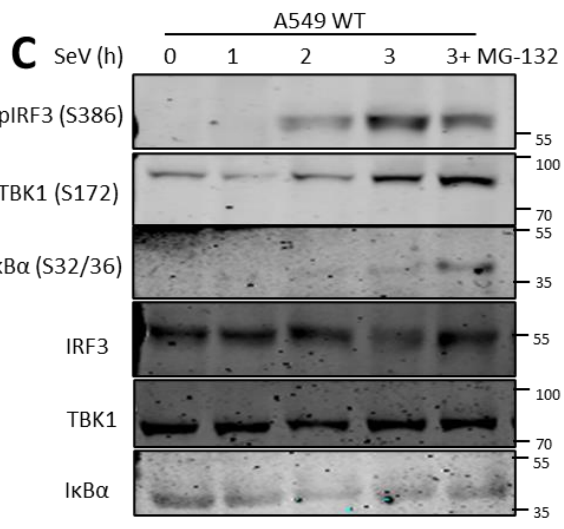
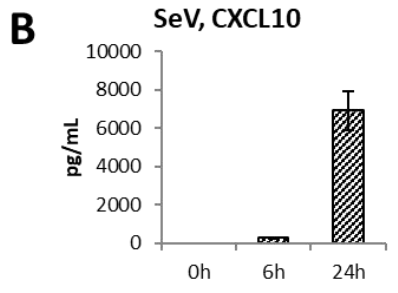
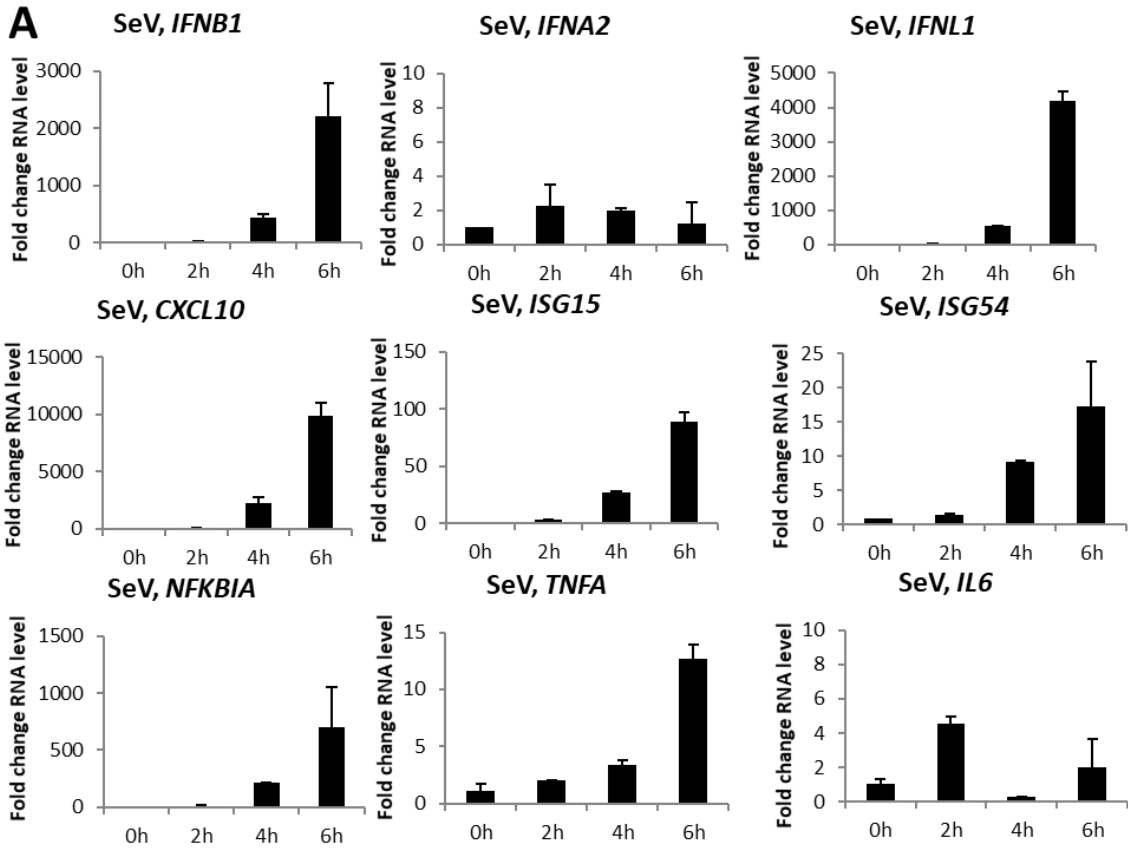


### Figure 3.3.2: SeV infection drives activation of IRF3- and NF- $\kappa$ B-dependent pathways

A) qPCR to measure transcription of indicated genes in response to infection of A549 WT cells with SeV at 1:300 dilution (n=2, data representative of >3 independent assays). B) ELISA to measure CXCL10 secretion in response to infection of A549 cells with SeV at 1:300 dilution (n=2, data representative of >3 independent assays). C) Western blotting to detect phosphorylation of signalling pathway components in response to infection with SeV at 1:300 dilution with and without the presence of 10  $\mu$ M MG-132 (3+) (data representative of >3 independent assays). D) Phos-flow analysis of A549 WT cells expressing phospho-IRF3 (Ser396) and active caspase 3 in response to 6 hour infection with SeV at a 1:300 dilution (data representative of 3 independent assays).

### 3.3.3. Infection of A549 cells with IAV R+K results in potent IRF3 activation, resulting in IFN, chemokine and ISG expression

To compare the stimulation profile of SeV with another respiratory RNA virus, A549 WT cells were infected with IAV PR8 NS1 R38A K41A (R+K) and the immune response was analysed by qPCR (Figure 3.3.3A) and Western blotting (Figure 3.3.3B).

Transcription of IFN-I gene *IFNB1*, chemokine *CXCL10* and ISGs *ISG15* and *ISG54* was robustly induced during IAV infection, however IFN-III and NF- $\kappa$ B dependent genes *IFNL1* and *NFKBIA* transcripts were not detectable above background levels, as with *IFNA2*. This transcription profile induced by IAV R+K infection is more like that seen with A549 cells stimulated with synthetic RNAs (Figure 3.3.1A), than to SeV infected A549 cells (Figure 3.3.2A).

Western blotting analysis of IAV R+K-infected A549 cells detected high levels of phosphorylation of IRF3 and TBK1, increasing through the time course (Figure 3.3.3B), as seen during SeV infection (Figure 3.3.2C). Evidence of I $\kappa$ B $\alpha$  phosphorylation was less clear, appearing to peak at two hours post infection, with consistently reduced levels seen until eight hours post infection. This mirrors the levels of *NFKBIA* transcription seen during IAV R+K infection (Figure 3.3.3A), possibly suggesting that the peak of I $\kappa$ B $\alpha$  phosphorylation and *NFKBIA* transcription may be before 2 hours post infection, but this was not tested.

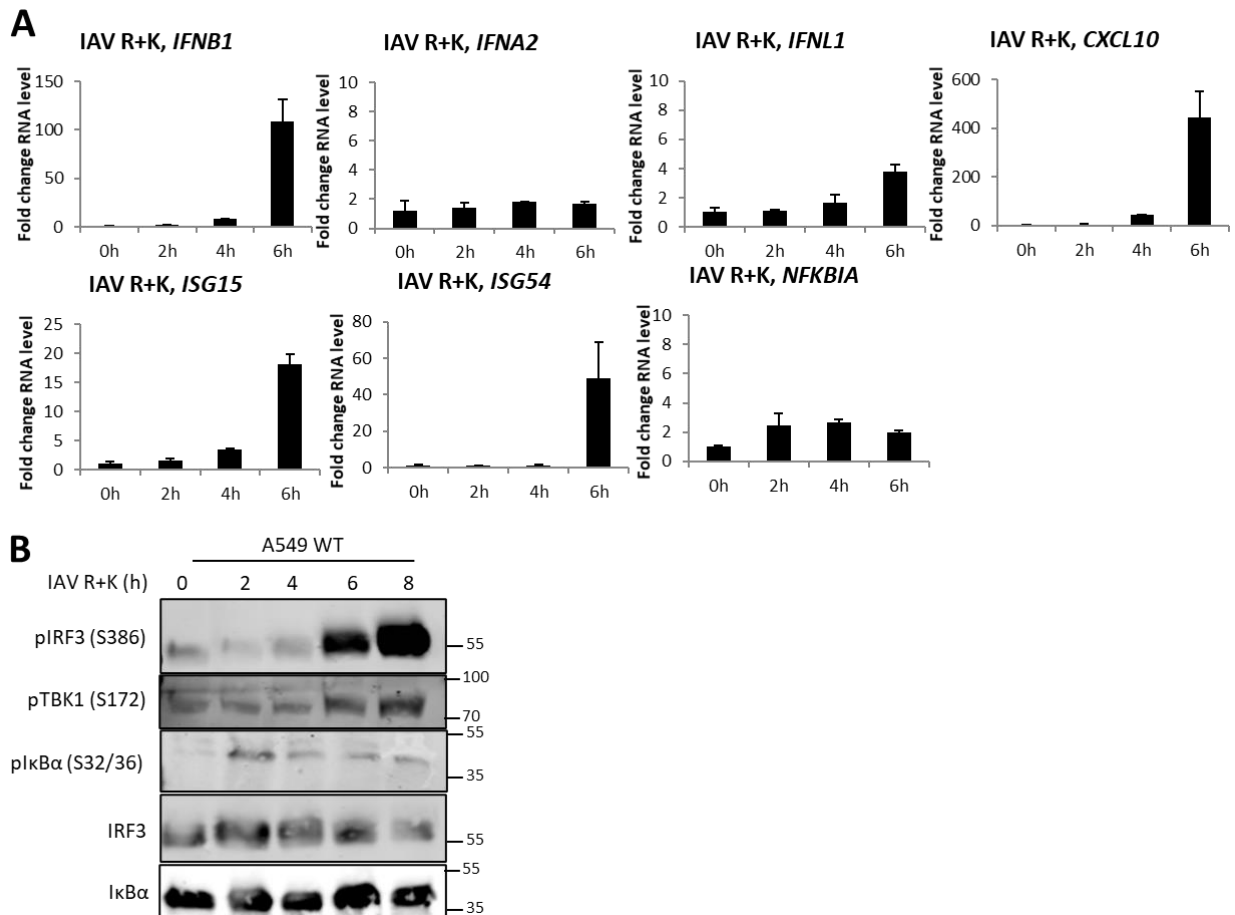


**Figure 3.3.3: IAV R+K infection drives activation of IRF3-, but not NF-κB-dependent pathways**

A) qPCR to measure transcription of indicated genes in response to infection of A549 cells with IAV PR8 R+K at MOI 5 (n=2, data representative of >3 independent assays). B) Western blotting to detect phosphorylation of signalling pathway components in response to infection with IAV R+K at MOI 5 for the indicated time in hours (data representative of >3 independent assays). Data generated by Rahul Singh.

### 3.3.4. Infection of A549 cells with ZIKV PE243 drives transcription of Type I and III IFN, ISGs and NF-κB dependent genes

Expression of an expanded panel of immune genes was also measured by qPCR during a ZIKV infection time course (Figure 3.3.4). At 16 and 24 hours post infection, ZIKV induced transcription of IFN-I and III genes *IFNB1* and *IFNL1* and IFN-I-dependent genes *ISG15* and *ISG54*, but not NF-κB-dependent genes *NFKBIA*, *TNFA* or *IL6*. At 48 hours post infection, a robust increase in transcription of *IFNA2* and *TNFA* was detected, although transcripts from other NF-κB-dependent genes *NFKBIA* and *IL6* are barely detectable above background levels. Transcription of *CXCL10*, known to be strongly associated with the microcephaly phenotype during ZIKV infection<sup>385</sup>, was detected from 16 hours post infection and strongly upregulated (800-fold) by 48 hours post infection.

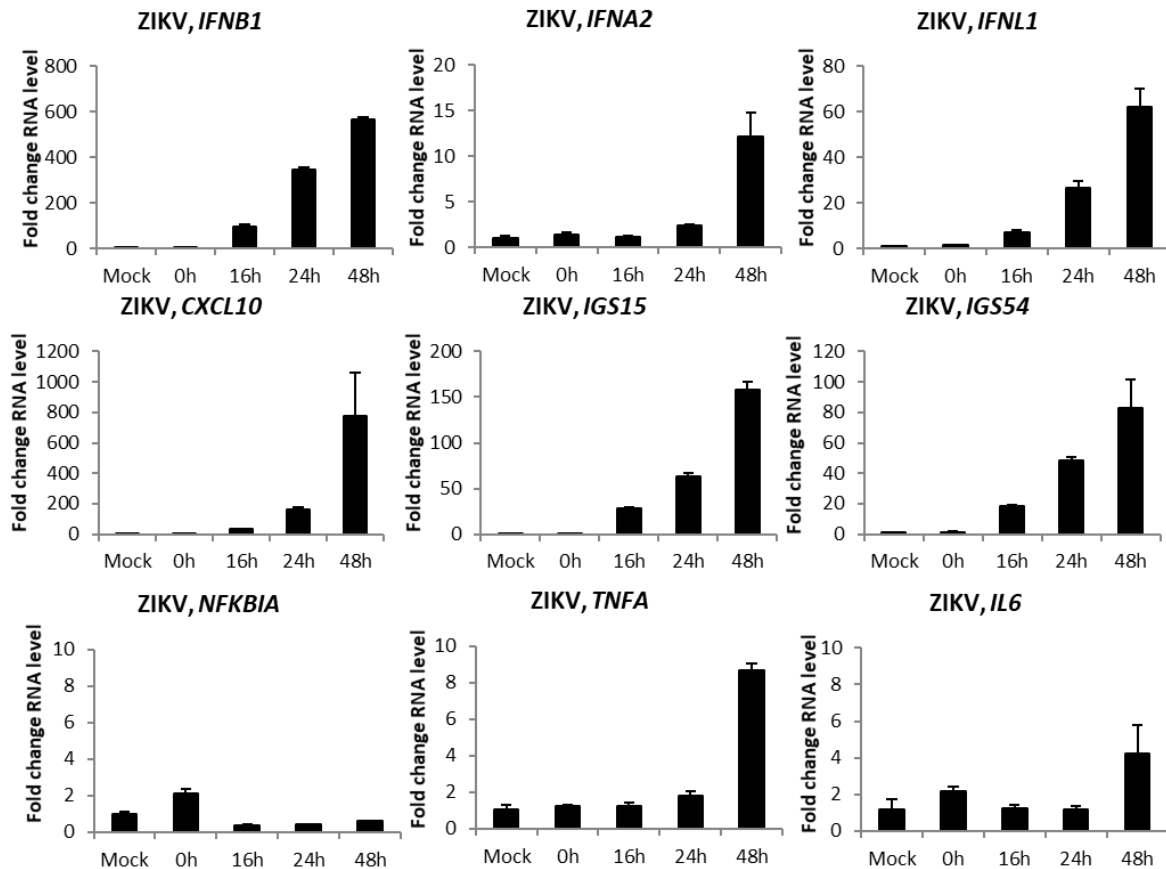


**Figure 3.3.4: ZIKV PE243 infection drives transcription of IRF3- and NF- $\kappa$ B-dependent genes**  
qPCR to measure transcription of indicated genes in response to infection of A549 cells with ZIKV PE243 at MOI 3 (n=3, data representative of >3 independent assays). Infections done in collaboration with Dr. Nerea Irigoyen and Charlotte Lefevre.

### 3.4. RIG-I is required for immune activation of A549 cells by synthetic RNAs and RNA viruses

#### 3.4.1 RIG-I is an ISG, upregulated during immune stimulation

RIG-I was undetectable by Western blotting in resting A549 cells (Figure 3.2.1A). However, like many other PRR, RIG-I is an immune stimulated gene (ISG), expressed at a low level in resting cells and upregulated in response to IFN-I, to amplify immune signalling<sup>66,67</sup>. To confirm that RIG-I is upregulated by an IFN-I response in A549 cells, its transcription was analysed by qPCR (Figure 3.4.1A) and protein expression by Western blotting (Figure 3.3.1B).

During SeV infection of A549 cells, previously shown to rapidly to activate an IFN-I response, transcription of *IFNB1* was detected at 6 hours post infection. This early wave of IFN-I activation was followed by a strong upregulation of *DDX58* (the gene name for RIG-I) transcription, detectable by 6 hours post infection but much stronger by 24 hours post infection. Western blotting of RIG-I protein

levels in untreated, IFN $\alpha$  stimulated and SeV infected A549 cells showed that RIG-I, undetectable in resting cells, was much more abundant after stimulation with both IFN $\alpha$  and SeV. Both of these data are both consistent with RIG-I behaving as an ISG in A549 cells.

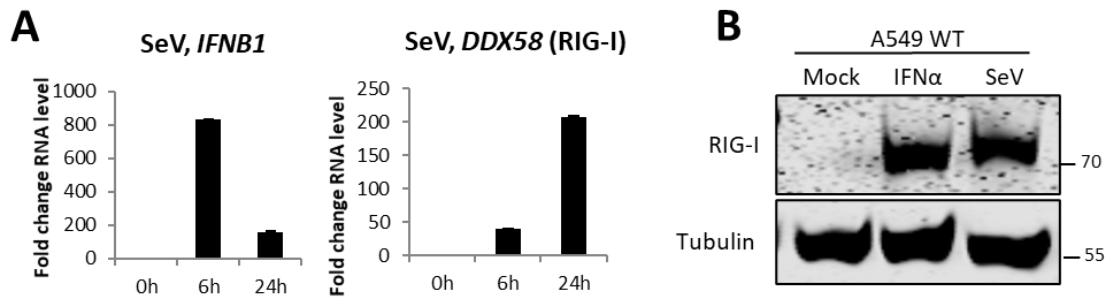


**Figure 3.4.1: RIG-I is an ISG that is upregulated by Type I IFN and SeV infection**

A) qPCR of *IFNB1* and *DDX58* (RIG-I) transcription after 0, 6, 24 hours SeV infection at 1:300 dilution (n=2, representative of one experimental replicate). B) Western blotting analysis of RIG-I expression in cells left unstimulated, stimulated with IFN $\alpha$  at 100 U/mL and infected with SeV at a 1:300 dilution, both for 24 hours (data shown is representative of >3 experimental replicates).

### 3.4.2 Generation of RIG-I deficient A549 cells

As the tested synthetic RNAs and RNA viruses are known RIG-I ligands, we hypothesised that response to stimulation seen in A549 cells was dependent RIG-I. To assess this, a RIG-I knock out cell line was generated by CRISPR/Cas9 in A549 WT cells (described in Chapter 2.2).

Figure 3.4.2A shows the position of the sgRNA that was successfully used to generate the knock-out cell line, targeting exon one of RIG-I after the start codon. RIG-I protein expression in potential RIG-I knockout (-/-) clonal cell lines was tested by Western blotting after stimulation with IFN $\alpha$  for 24 hours. If negative, loss of expression was confirmed by Sanger sequencing of genomic DNA extracted from putative knockout cells. The region around the sgRNA target site was cloned into an expression vector and 20 amplicons from each clone was sequenced to look for the mutations introduced by the Cas9 endonuclease. All mutated sequences were translated using EXPASY, to check for presence a premature STOP codon. For the clone taken forward for all future experiments, all translations generated from the sequencing of 20 amplicons showed mutations that introduced a premature STOP codon, shown in Figure 3.4.2B.

The selected RIG-I -/- cells showed no detectable expression of the RIG-I protein by western blotting, even after stimulation with 100 U/mL IFN $\alpha$  for 24h, a condition in which RIG-I is clearly visible in A549 WT cells (Figure 3.2.1C). Western blotting analysis of other RIG-I signalling proteins confirmed comparative expression levels of TBK1, IRF3 and MAVS in WT and RIG-I -/- cells (Figure 3.4.2D),

ensuring that any phenotype seen in downstream experiments was due to loss of the targeted protein only.

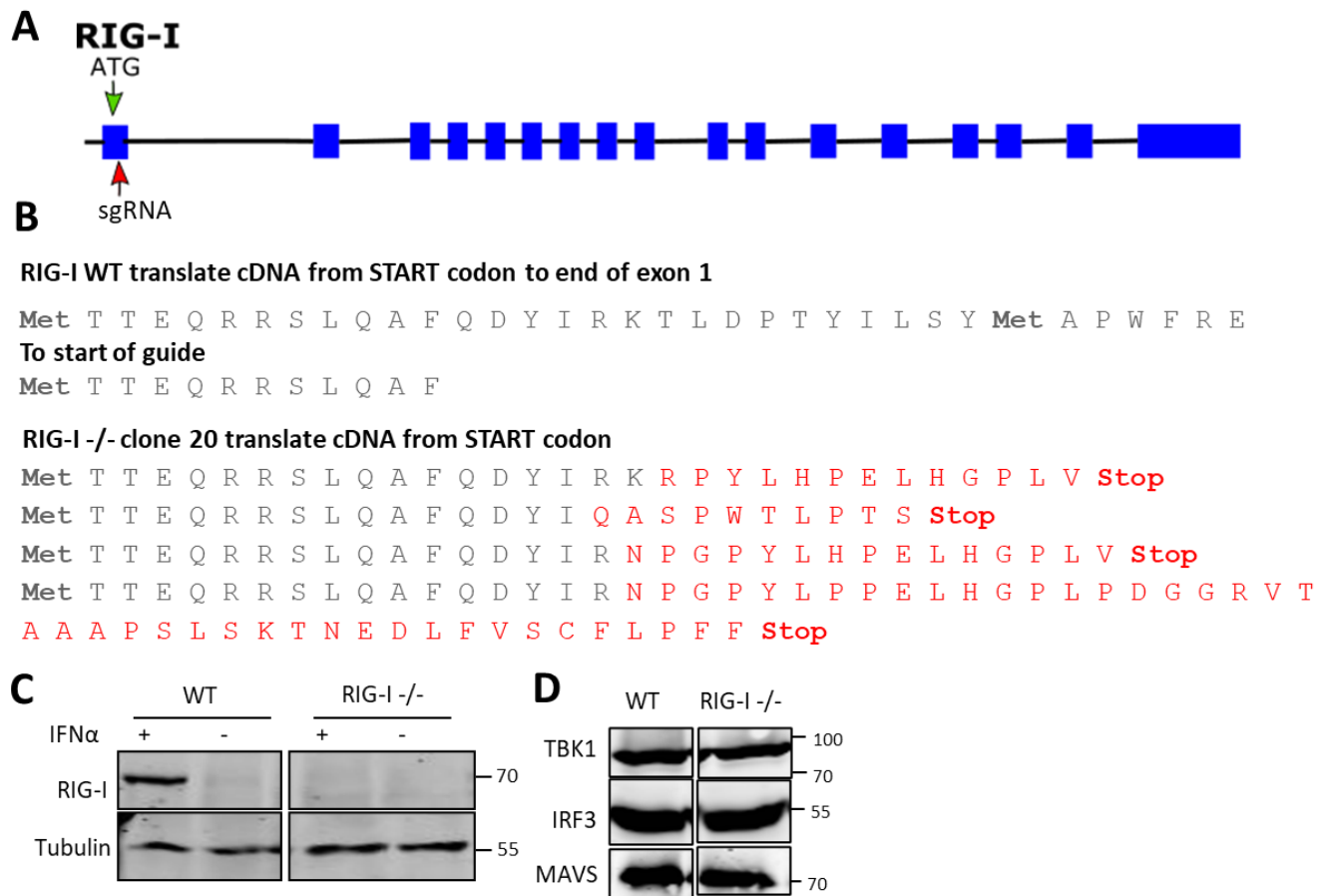


**Figure 3.4.2: Generation and characterisation of a RIG-I -/- cell line**

A) Schematic of location of small guide RNA targeting RIG-I for CRISPR (Exons indicated by blue boxes and introns by black lines. Start codon (ATG) position indicated by green arrow and location of target sequence of sgRNA by red arrow). B) ExPASy translation of A549 WT and RIG-I -/- sequences. Western blot analysis of C) A549 WT and RIG-I -/- cells with and without 24h stimulation with 100 U/mL IFN $\alpha$  ( data representative of >3 independent assays) and D) RIG-I signalling pathway components in A549 WT and RIG-I -/- cells (data representative of 2 independent assays).

### 3.4.3. A549 RIG-I -/- cells respond to various receptor stimuli

To verify that the newly generated RIG-I -/- cells were not deficient in other innate immune sensing pathways, their ability to respond to DNA, IFN-I and LPS was tested.

A549 WT and RIG-I -/- cells were stimulated with 2  $\mu$ g of herring testes (ht)DNA (Figure 3.3.5A), a known immuno-stimulatory DNA<sup>388-390</sup>. Neither A549 WT nor RIG-I -/- cells showed more than a 5-fold increase in *IFNB1* or *CXCL10* transcription when analysed by qPCR. This lack of response is likely due to the fact that A549 cells downregulate STING expression, preventing them sensing DNA<sup>341-343</sup>,

which is common in cancer cell lines to allow them to remain undetected by the immune system <sup>391-</sup>

393

Stimulation of WT and RIG-I <sup>-/-</sup> cells with IFN $\alpha$  resulted in significant induction of *CXCL10* transcription in both WT and RIG-I <sup>-/-</sup> cells (Figure 3.3.5B). The levels of *CXCL10* transcripts were significantly lower in RIG-I <sup>-/-</sup> cells than WT, possibly due to the clonal nature of the RIG-I-deficient cells, but it is still expressed almost 100 times more than in unstimulated cells, confirming that RIG-I <sup>-/-</sup> cells have functional interferon  $\alpha$  receptor (IFNAR) signalling. LPS treatment of cells resulted in a small induction of both *IFNB1* and *CXCL10* transcription after 6 hours, even in the absence of RIG-I (Figure 3.3.5C). RIG-I deficient cells transcribed *IFNB1* at levels twice that of WT, but the converse with true of *CXCL10* transcription.

These results demonstrate that RIG-I <sup>-/-</sup> cells can induce an immune response to RIG-I-independent stimuli, suggesting that any phenotype seen when RIG-I <sup>-/-</sup> cells are stimulated with RIG-I ligands is due to loss of RIG-I expression rather than other abnormalities in this cell line.

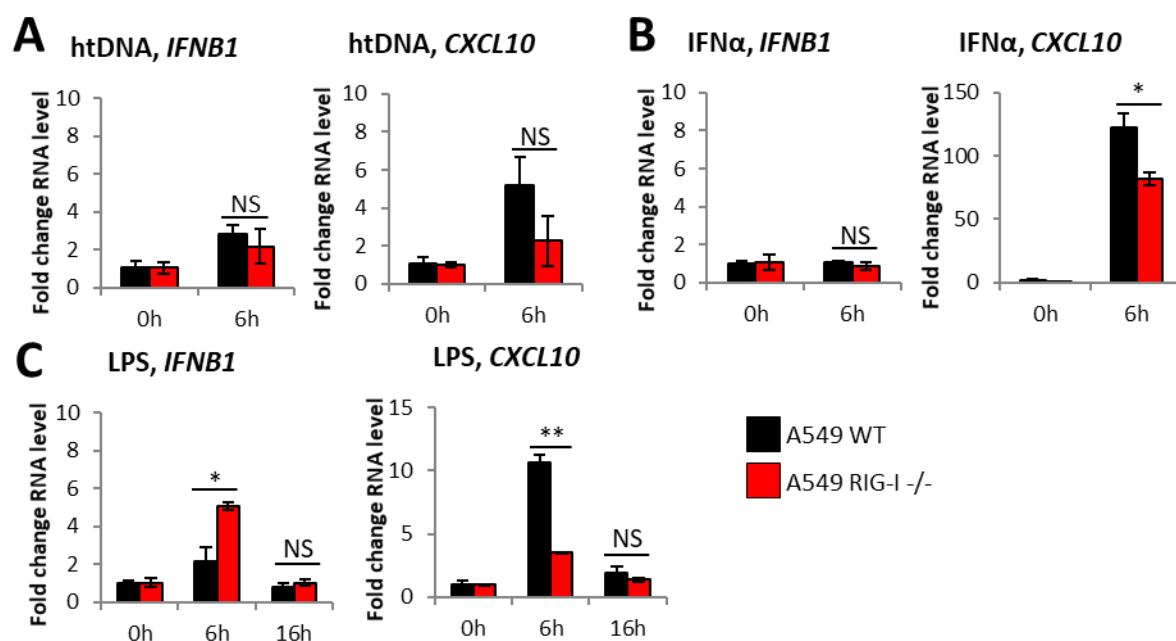


**Figure 3.4.3: A549 RIG-I <sup>-/-</sup> cells have immune signalling capacity**

qPCR to measure transcription of indicated genes after stimulation of A549 WT and RIG-I <sup>-/-</sup> cells with A) 2  $\mu$ g htDNA (n=2, data representative of 2 independent assays), B) 100 U/mL IFN $\alpha$  (n=2, data representative of 1 independent assay) and C) 1  $\mu$ g LPS (n=2, data representative of 2 independent assays).

### 3.4.4. Stimulation of A549 cells by synthetic RNAs is dependent on RIG-I

To study the role of RIG-I in the sensing of synthetic RNAs in A549 cells, WT and RIG-I <sup>-/-</sup> cells were transfected with 3p-hpRNA and Poly(I:C) and transcription of genes previously seen to be upregulated in WT cells (Figure 3.3.1A) was measured by qPCR.

For both 3p-hpRNA (Figure 3.4.4A) and Poly(I:C) (Figure 3.4.4B), transcription of all genes in A549 WT cells was as previously seen. However, transcription of all genes was undetectable above background levels in RIG-I <sup>-/-</sup> cells. This shows that in A549 cells, sensing of both RNA species is entirely dependent on RIG-I, without any contribution from other RNA sensing PRRs like MDA5 or TLR3. This was expected for 3p-hpRNA, which is designed to be a specific agonist of RIG-I. However, it was more surprising for HMW Poly(I:C), which is thought to be a more potent activator of MDA5, a sensor of longer double stranded RNAs with no 5' modifications, like Poly(I:C).

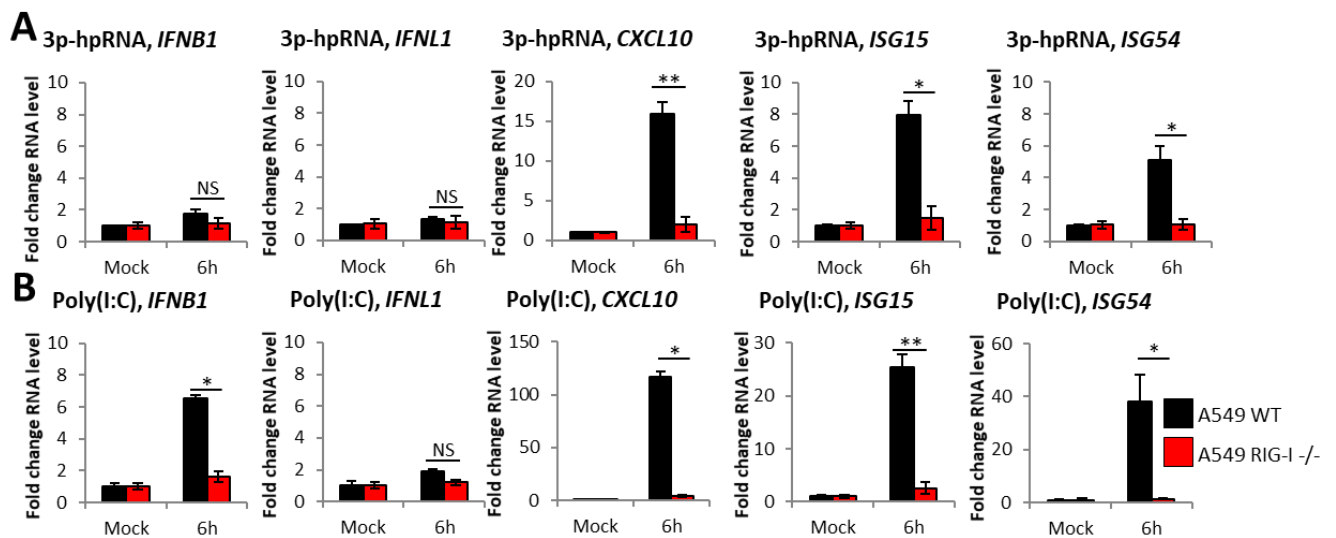


**Figure 3.4.4: Stimulation of A549 cells by synthetic RNAs is dependent on RIG-I**

qPCR to measure transcription of indicated genes in response to stimulation of A549 WT and RIG-I <sup>-/-</sup> with A) 1 µg 3p-hpRNA and B) 1 µg Poly(I:C) (for all data shown, n=2 and data are representative of >3 independent experimental replicates).

### 3.4.5. Stimulation of A549 cells by SeV and IAV R+K is dependent on RIG-I

Due to the complex structure of viruses, they often encode ligands for multiple PRRs. Subsequently, many viruses have evolved to avoid detection by encoding inhibitors to block the signalling of these receptors. Because of this, we examined the contribution of RIG-I to the sensing of SeV and IAV in A549 cells.

In WT cells, infection with both SeV (Figure 3.4.5A) and IAV R+K (Figure 3.4.5B) resulted in similar patterns of transcription to what we saw previously (Figure 3.3.2A and 3.3.3A). As with synthetic RNAs, transcription of all genes in RIG-I <sup>-/-</sup> cells was barely detectable above background levels, confirming that RIG-I is the major sensor of SeV and IAV in A549 cells.

To corroborate this, the percentage of WT and RIG-I <sup>-/-</sup> cells expressing phosphorylated IRF3 and activated caspase 3 was analysed using phos-flow after infection with SeV. Approximately 20% of A549 WT cells infected with SeV for 6 hours were positive for phosphorylated IRF3. However, only 0.2% of RIG-I <sup>-/-</sup> cells expressed phosphorylated IRF3, indicating this activation is dependent on RIG-I. Almost none of either cell line, expressed activated caspase 3, suggesting RIG-I doesn't initiate cellular apoptosis pathways under these conditions.



### 3.4.6. Stimulation of A549 cells by ZIKV is dependent on RIG-I

To examine the extent to which RIG-I is responsible for sensing ZIKV in A549 cells, A549 WT and RIG-I<sup>-/-</sup> cells were infected with ZIKV PE243 and qPCR was used to measure transcription of immune genes shown to be activated in A549 WT cells (Figure 3.4.6A).

At 16 and 24 hours post infection, transcription of *IFNB1*, *IFNL1*, *CXCL10*, *ISG15* and *ISG54*, but not *IFNA2*, *TNFA* or *IL6*, was significantly induced. For all transcribed genes, this was dependent on RIG-I, with expression in RIG-I<sup>-/-</sup> cells barely detectable above background levels. This reinforces previous data showing RIG-I plays a dominant role in the induction of ZIKV-driven transcription<sup>394</sup>. By 48 hours post infection, transcription *IFNA2*, *TNFA* and *IL6* in WT cells is detectable. However, they are also transcribed to the same level in RIG-I<sup>-/-</sup> cells, with significant induction of *IFNL1* transcription also seen in RIG-I<sup>-/-</sup> cells at this later time point. This suggests that up to 24-hours, signalling is dependent on RIG-I, but by 48 hours a wave of RIG-I-independent immune signalling has been activated.

Growth curve analysis of ZIKV replication (Figure 3.4.6B) showed similar levels of virus present at 16 and 24 hours post infection in WT and RIG-I<sup>-/-</sup> cells, with only 1.5 times more virus present in WT cells at 24 hours. However, at 48 hours post infection there was 5 times the amount of virus present in RIG-I-knockout cells compared to WT. This is likely because the lack of a RIG-I-driven IFN-I response in knockout cells prevents the inhibition of viral replication seen in WT cells.

The RIG-I-specific nature of early ZIKV-driven immunity in A549 cells strengthens the use of ZIKV as a model to study RIG-I signalling in A549 cells.

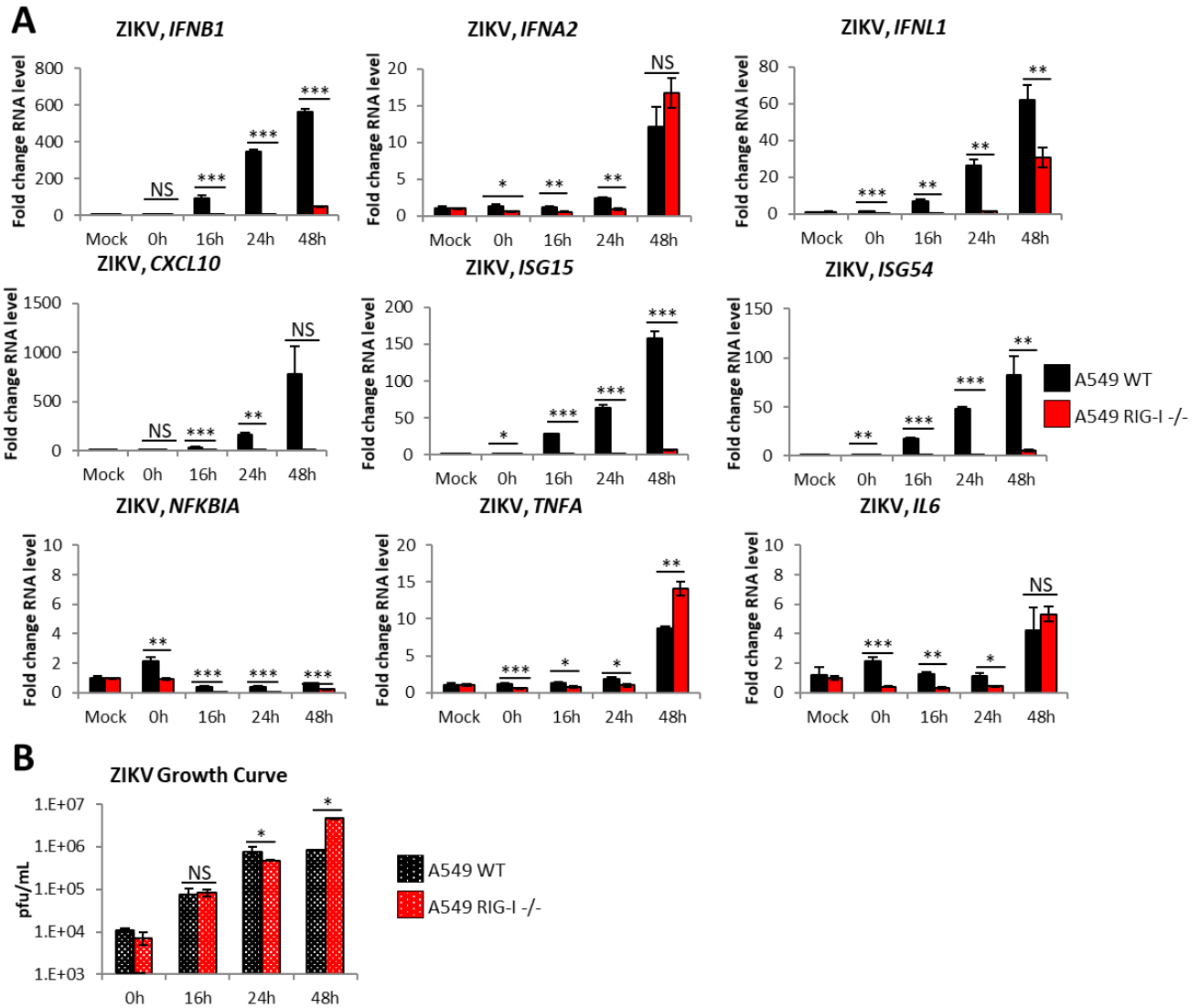


**Figure 3.4.6: Stimulation of A549 cells by ZIKV is dependent on RIG-I at early time points**

A) qPCR to measure transcription of indicated genes in A549 WT and RIG-I<sup>-/-</sup> cells infected with ZIKV PE243 at MOI 3 (n=3, data representative of >3 experimental repeats). B) ZIKV PE243 growth curve generated by titration and plaque assay, done by Dr. Nerea Irigoyen and Charlotte Lefevre. (n=3, data representative of 3 experimental repeats).

### 3.5. Discussion

Sensing of RNA by RIG-I has been studied extensively, with synthetic RNAs, RNA viruses and gain or loss of function systems used to stimulate RIG-I in a variety of model cell lines, primary cells, and *in vivo* models. The signalling outputs of RIG-I stimulation have been characterised in multiple ways including gene expression quantification, cell signalling analysis and *in vivo* cellular immunity studies. Despite this large body of work, there are still many unanswered questions about most aspects of RIG-I signalling; from the features of RIG-I ligands and the identity of signalling and regulatory proteins involved in the pathway, to the outputs of RIG-I activation. Through the work in this

chapter, we determined and optimised the tools and assays required to investigate RIG-I signalling outcomes and characterise the RIG-I-dependent immune response generated. Generation of this system has allowed us to explore the RIG-I signalling complex and how it is regulated.

### **3.5.1 A549 as a model system to study RIG-I signalling**

A549 cells were chosen as a tractable model to study RIG-I signalling and we established successful stimulation models with two synthetic RNAs, 3p-hpRNA and Poly(I:C), and three RNA viruses, SeV, IAV R+K and ZIKV PE243. all of which induced a measurable anti-viral innate immune response in these cells.

Synthetic RNAs were chosen as they specifically activate RIG-I without the unwanted activation of other PRRs, which can occur when a single stimulus contains multiple ligands in complex with the RNA species, as is the case for viruses<sup>91</sup>. This specific activation of RIG-I without being recognised by other PRR is possible because the features of RNAs that activate RIG-I have been extensively studied and relatively well characterised<sup>83,89,90,95,354</sup>. Stimulation with of RIG-I by 3p-hpRNA and Poly(I:C) in A549 cells generates a measurable immune response, despite the relatively low transfection efficiency that affected our ability to monitor intracellular signalling with these ligands.

RNA viruses were chosen as a model to study RIG-I signalling due to the biological significance of their sensing; IFN-I and IFN-III production during virus infection, essential to driving downstream immunity, is critically dependent on the detection of the virus by intracellular RNA sensors. Three viruses were chosen as RIG-I stimulation models: Sendai, Influenza and Zika, as their sensing has previously been shown to be RIG-I-dependent<sup>282,345,394</sup>. Infection of A549 cells with SeV and ZIKV, and use of an IAV mutant virus, results in activation of a measurable immune response, allowing us to study how viruses are sensed by RIG-I.

### **3.5.2 There is variation between the immune gene expression profile in response to different RIG-I ligands**

Closer examination of the immune signalling response in A549 cells by qPCR, Western blotting analysis and ELISA showed that both the magnitude and the breadth of the immune response differed between the ligands. Stimulation with all ligands induced TBK1 and IRF3 activation resulting in IFN-I and chemokine production, whereas only SeV infection activated NF-κB and downstream inflammatory responses.

As 3p-hpRNA is a relatively newly developed synthetic RNA, the response it induces is yet to be comprehensively characterised. Early studies show it stimulates activation of IFN-I and chemokine

responses<sup>374,379,395–397</sup>, mirroring what we see during stimulation of A549 cells. Induction of IFN-III and NF-κB-dependent responses by 3p-hpRNA, which we did not see, was detected in some but not all these studies, possibly due to differences in the response between cell types. Alternatively, this may be because their expression may meet the threshold of detection in some studies but not others, depending on the cell type, transfection method or analysis method. As we saw, the lack of a measurable immune response to the similar RNA 5'ppp-dsRNA has been previously shown in HEK cells<sup>91</sup>, although other studies have successfully used 5'ppp-dsRNA to stimulate RIG-I<sup>90,343</sup>. Possibly 5'ppp-dsRNA may be a weaker ligand than 3p-hpRNA if RIG-I is preferentially activated by regions of secondary structure such as pan-handles than perfectly complementary dsRNA duplexes. Alternatively, it may be less efficiently transfected into A549 cells than 3p-hpRNA, or may be degraded upon entry into the host cell prior to being sensed by RIG-I.

The activation of IFN-I and chemokine responses by Poly(I:C) seen in A549 also mirrored other studies<sup>398–402</sup>. However, from the transcriptional output of A549 cells we did not observe Poly(I:C)-induced NF-κB activation, which has been relatively consistently documented previously, demonstrated by both phosphorylation of IκBα and transcription of *IL6* and *TNFA*<sup>398,400,402–406</sup>. In some of these earlier studies, activation of NF-κB by Poly(I:C) was proven to be dependent on TLR3, which we have shown does not contribute to sensing of Poly(I:C) in our A549 cells, as no Poly(I:C)-driven stimulation is present in RIG-I-deficient cells. This is supported by a study that showed that treatment of cells with extracellular Poly(I:C) resulted in TLR3-mediated activation of IFN-I and the NF-κB-dependent gene *IL-8*, but transfection of Poly(I:C) in the same cells activated RIG-I/MAVS-dependent IFN-I activation, without *IL-8* co-activation<sup>349</sup>. This suggests that NF-κB activation by Poly(I:C) seen in previous studies is likely to be mediated by TLR3 activation, supporting our lack of RIG-I-driven NF-κB activation in response to Poly(I:C).

Infection of A549 cells with SeV resulted in activation of IFN-I, IFN-III, chemokines, and NF-κB-dependent responses, with the highest levels of IFN-I and chemokine transcription of any stimulation method, mirroring what has been seen in previous studies<sup>301,407–412</sup>. Interestingly, SeV is the only stimulation method tested that activated NF-κB-dependent responses in A549 cells.

One possibility as to why differing expression profiles are detected for different stimuli is that the responses are controlled by an activation threshold controls. For example, ligands like 3p-hpRNA and Poly(I:C), which induced minimal transcription of NF-κB dependent genes and no detectable IκBα phosphorylation, also tended to induce lower levels of *IFNB1* and *CXCL10* transcription than seen with SeV, which also activates NF-κB. Therefore, the threshold level of RIG-I activation that results in

NF- $\kappa$ B activation may be higher than the threshold for IRF3 activation. This threshold may depend on the activation status of a RIG-I signalling complex, varying in relation to the elements of a specific ligand; how many activated molecules of RIG-I there are in a single cell; or to how many stimulated cells there are in a population. For example, complexes containing fewer activated RIG-I CARD domains may only signal to activate IRF3 and not NF- $\kappa$ B. It is not known whether a single RIG-I signalling complex can activate both IRF3 and NF- $\kappa$ B, or whether each signalling complex drives either IRF3- or NF- $\kappa$ B-activation. It is likely rarer that both IRF3 and NF- $\kappa$ B are activated simultaneously in a single cell than just one of them, but we know this does occur as their co-operative binding to promoters is required for transcription of genes like *IFNB1*, which does occur in a small subset of cells. Alternatively, RIG-I may be able to differentiate between ligands, signalling via a distinct pathway to initiate different responses to different ligands, although this has not been shown before.

IAV PR8 WT infection of A549 cells didn't activate an immune response, likely due to the immunosuppressive functions of the IAV NS1 protein<sup>362,363</sup>. IFN-I, IFN-III and chemokine production have been detected during infection with IAV PR8 WT and WSN WT strains in previous studies, but generally at later time points than we used for our assays<sup>413-418</sup>. This is reinforced by the fact that infection with the IAV NS1 R38A K41A mutant virus did induce activation of IFN-I and chemokine responses, but not NF- $\kappa$ B or IFN-III-dependent responses. The mutation of residues R38 and K41 abrogates the ability of NS1 to bind dsRNA, preventing its ability to shield viral RNAs from recognition by RIG-I<sup>365,419,420</sup>. Previously demonstrated activation of NF- $\kappa$ B by IAV infection only occurred at later time points like 12 hours post infection, with minimal transcription of NF- $\kappa$ B-dependent genes *TNFA* and *IL6* by 4 hours post infection<sup>413</sup>, which agrees with our data showing no transcription of NF- $\kappa$ B-dependent genes after 6 hours. Similarly to what we showed mutations in NS1 in the WSN strain of IAV has also been shown to result in higher levels of IFN-I, IFN-III and NF- $\kappa$ B dependent gene transcription than seen with WSN WT<sup>416</sup>. Our demonstrated lack of *IFNL1* transcription contradicts what has been previously shown, with IFN-III is known to be important in the antiviral response to infection with IAV and other RNA viruses in epithelial cells<sup>376,377,421</sup>. This is likely caused by a lack of NF- $\kappa$ B activation, as transcription of IFN-III gene *IFNL1* is predominantly activated by the binding of NF- $\kappa$ B binding sites in the promoter<sup>422</sup>, whereas IFN $\beta$  expression predominantly depends on the binding of IRF3 and 7 to its promoter<sup>373</sup>. The lack of NF- $\kappa$ B activation by IAV infection may be due to the antagonism of their activation by other IAV proteins, or alternative functions of NS1 not abrogated by the mutations.

ZIKV PE243 infection activated IFN-I and IFN-III responses and chemokine secretion, but not NF- $\kappa$ B. This supports previous data, including some studies in A549 cells, showing that ZIKV strongly infects A549 cells<sup>371</sup>, resulting in activation of IFN-I, IFN-I-dependent genes, and chemokines, with significantly less transcription of NF- $\kappa$ B-dependent genes IL-6 and IL-8<sup>369,372,423</sup>. Our finding of ZIKV-driven IFN-III activation is novel, as no previous studies have described activation of IFN-III by ZIKV infection.

In addition to induction of differing immune expression profiles by different ligands, the magnitude of the response detected varied significantly between the ligands. SeV infection was the most potent inducer of immune gene transcription and chemokine secretion and resulted in the highest levels of phospho-IRF3, -TBK1 and -I $\kappa$ B $\alpha$ . This is likely because of the high proportion of dysfunctional DI-virus particles produced by the Cantell strain of SeV, which are both potent activators of RIG-I and diminish the effectivity of SeV-encoded proteins known to inhibit the innate immune response<sup>408</sup>. The magnitude of induction of IFN and chemokines with IAV and ZIKV was significantly lower than with SeV infection, likely because both viruses encode proteins that are designed to antagonise the immune response to avoid detection. A stronger response to IAV and ZIKV infection than to synthetic RNA transfection is likely because infection with both viruses deliver RNA-ligands of RIG-I into more cells than occurs during transfection of synthetic RNAs, resulting in more activated RIG-I signalling complexes.

Although differing responses have undoubtedly been seen before across studies with many synthetic RNAs and viruses, as well as during examination of the minimal essential RIG-I ligand *in vivo*<sup>91</sup>, the reason for this remains unknown.

### **3.5.3 The response to synthetic RNAs and RNA viruses in A549 cells was entirely dependent on RIG-I**

The contribution of RIG-I and other PRRs to the sensing of these stimuli was determined using RIG-I -/- cells. For the synthetic RNAs and RNA viruses examined, all measurable immune response was lost in RIG-I -/- cells. This shows that the first wave of signalling in A549 cells in response to these stimuli is entirely dependent on RIG-I and rules out the possibility that the varying ranges of signalling outcomes for different ligands was due to the contribution of other PRR.

Clean stimulation of RIG-I by the commercial 'RIG-I ligand' 3p-hpRNA was anticipated, based on its molecular characteristics. 3p-hpRNA is composed solely of known features of RIG-I ligands: an uncapped 5' triphosphate group and regions of double-stranded RNA, in the form of panhandle or hairpin structures formed by self-annealing of the single stranded RNA, without any known features

that activate other PRR<sup>83,354</sup>. Previously, 5' blunt ended dsRNA structures were reported to be the most potent RIG-I activators<sup>89,90</sup>, however in our hands measurable RIG-I signalling was not activated by the blunt-ended dsRNA 5'ppp-dsRNA, suggesting a preference for panhandle or hairpin structures formed by partially complementary single stranded RNAs like 3p-hpRNA. This is supported by Linehan et al. who, during analysis of the components of the minimal RIG-I ligand, suggest that RNA ligands with a stem loop "provide simplicity, structural stability, and resistance to nucleases while presenting a single duplex terminus that fits precisely into the RNA binding pocket of RIG-I", which is not the case for dsRNA duplexes<sup>91</sup>.

Surprisingly, RIG-I was also specifically activated by Poly(I:C) in our A549 cells, despite it not containing 5' tri- or di-phosphate modifications. This disputes the idea that 5' modifications are essential for RIG-I activation and is supported by previous studies that found RIG-I is activated by dsRNAs without a 5' phosphate group, albeit to a lesser extent than those with<sup>91,95</sup>. There is still much debate around how varied the RNA structures that successfully activate RIG-I can be. A lack of one preferential feature can have been proposed to be compensated for by the presence of another, enabled by the plasticity of the RNA binding domain of RIG-I<sup>93</sup>. Despite this, mono-phosphorylated RNA ends are thought to be selectively discriminated against by RIG-I, possibly even blocking the signalling of RIG-I<sup>101</sup>.

Although generally thought of as a more potent ligand of MDA5<sup>95</sup>, multiple studies implicate RIG-I as the major sensor of transfected high molecular weight (HMW) Poly(I:C), especially in epithelial and fibroblast cell types<sup>167,349-353</sup>. Lengths of Poly(I:C) below 2 kilobase-pairs (kbp) preferentially activate RIG-I over MDA5, with the reverse being true for full length undigested Poly(I:C)<sup>95</sup>. The two distinct mechanisms for binding of RNA by RIG-I, both preferentially binding 5'triphosphate blunt RNA ends and binding dsRNA internally, may allow for activation of RIG-I by RNAs without 5' phosphate groups<sup>353,424</sup>. Additionally, although Poly(I:C) is supposed to mimic long double-stranded RNA, it is in fact extensively branched and contains some single stranded segments and overhangs that may be responsible for activation of RIG-I<sup>107,425</sup>. Poly(I:C) used in these studies was advertised to be 1.5-8 kbp in length<sup>426</sup>, although we did not investigate its structure in more detail.

Despite studies showing RIG-I contributes to the sensing of Poly(I:C), the lack of contribution of MDA5 was surprising. One potential explanation for this is that MDA5 is expressed at very low levels in these A549 cells. Opposing this, previous studies have shown MDA5 activation by Poly(I:C) in A549 cells<sup>427-430</sup> and upregulation of MDA5 expression in response to stimulation with VSV and Poly(I:C)<sup>427-429</sup>. However, as previously discussed there can be differences between batches of commonly used

mammalian cell lines and a previous study examining the levels of RIG-I and MDA5 mRNAs in resting A549 cells by qPCR showed that the level of MDA5 mRNA is significantly lower than that of RIG-I<sup>431</sup>, reinforcing the fact that in our cells MDA5 was undetectable by western blotting in A549 cells, even after treatment with IFN $\alpha$ . From this, we suggest that MDA5 is not playing any role in the sensing of RNAs in A549 cells in our system.

Our data suggests that TLR3, despite being known to be potently activated by extracellular and endosomal Poly(I:C)<sup>432</sup>, does not contribute to the sensing of transfected Poly(I:C) in A549 cells. This is supported by previous studies showing an intact immune response to Poly(I:C) in TLR3 deficient embryonic fibroblast cells, but not MAVS-deficient A549 cells or mice<sup>167,433-435</sup>. Like MDA5, TLR3 also has a low basal expression level in resting A549 cells, undetectable by Western blotting and with only very low levels of mRNA compared to RIG-I<sup>431</sup>. Perhaps, as its expression has been shown to be upregulated in response to IFN-I, Poly(I:C) transfection and IAV infection in A549 cells<sup>405,436</sup>, TLR3 may contribute to later waves of immune signalling, but it does not contribute to the first wave of signalling in response to Poly(I:C) in our A549 cells.

Studies with RIG-I -/- mice have shown the importance of RIG-I in the sensing of multiple RNA viruses such as Sendai, Vesicular Stomatitis Virus (VSV) and Newcastle Disease Virus (NDV) in most cell types. Only in plasmacytoid dendritic cells was RIG-I dispensable for IFN-I and interleukin production in response to infection with Newcastle disease virus, where TLR7 and 9 were required<sup>437</sup>. Although virus infection often results in the simultaneous activation of multiple PRRs, infection of A549 cells with SeV, IAV R+K and ZIKV activated RIG-I alone. The RIG-I specificity shown by SeV was expected as the DI particles produced by the Cantell strain potently activate RIG-I, but do not generate the long dsRNAs generally sensed by MDA5 and TLR3<sup>97</sup>.

Surprisingly, infection with IAV R+K also specifically activated RIG-I. As well as RIG-I, TLR3 is thought to be required for the pro-inflammatory response and maximum IFN induction by IAV infection, especially in lung epithelial cells<sup>432,438-441</sup>. However, previous studies have shown IAV-driven immune signalling to be solely RIG-I dependent<sup>95</sup> and it is known that like SeV, natural IAV infection results in production of DI-RNAs essential for RIG-I driven early activation of IFN-I in IAV infected cells<sup>301</sup>. As described for Poly(I:C), we suggest that the absence of IAV-induced TLR3-dependent signalling is likely due to its low expression in A549 cells, although it also could be inhibited by the remaining immunosuppressive functions of the mutant NS1 protein, or other IAV proteins known to antagonise immune responses<sup>442</sup>. The absence of signalling by TLR3, likely accounts for the lack of pro-

inflammatory signalling seen after IAV infection of A549 cells, as this has been shown to mediate NF- $\kappa$ B, but not IRF-3 dependent gene activation during IAV infection of human lung epithelium<sup>440</sup>.

Up to 24 hours post infection, ZIKV-induced antiviral transcription was entirely dependent on RIG-I, although at 48 hours post-infection a second wave of RIG-I-independent signalling was activated. Recent studies have shown that RIG-I is the primary sensor of ZIKV infection, with MDA5 and TLR3 both dispensable despite upregulation of TLR3 by early ZIKV infection<sup>313,368,369</sup>. This supports what had previously been inferred from the sensing of other flaviviruses such as Dengue<sup>102,443-445</sup> and is further reinforced by the targeting of MAVS and IKK $\epsilon$  by ZIKV-encoded proteins NS4A and NS5 to inhibit RIG-I signalling<sup>370,446</sup>. The cGAS-STING pathway has also been implicated in ZIKV sensing<sup>311,318</sup>, but this is unlikely to be playing a role in our system as A549 cells do not express STING thus can't respond to stimulation with DNA<sup>343</sup>. The wave of RIG-I-independent signalling seen at later time points is likely to be activated by the other PRRs detecting the high levels of viral material in cells or the damage caused by virus infection. The activation of IFN $\alpha$  by ZIKV in a RIG-I-independent manner has previously been shown during Dengue infection, where its transcription is induced to prolong and increase expression of IFN-I, exacerbating the immune response<sup>447</sup>.

The absence of functional MDA5 and TLR3 in A549 cells provides us with a 'clean' system to study the RIG-I signalling pathway and its outcomes. However, the main limitation of this system is that we could not use primary cells to best mimic the immune response that would happen in a physiological setting. Despite this, the system we have developed has allowed us to study specific RIG-I activation and the downstream signalling in detail, addressing previous inconsistencies.

### 3.6 Conclusion

In this chapter we have developed a system to study RIG-I-signalling in human cells. Optimisation of stimulation methods and techniques examining the RIG-I-driven immune-response, resulted in a system where treatment of A549 cells with synthetic RNAs 3p-hpRNA and Poly(I:C) and RNA viruses SeV, IAV R+K and ZIKV generates a measurable innate immune response. All stimulation methods activated the TBK1/IRF3 signalling axis, resulting in transcription of IFN-I, IFN-I-dependent genes, and chemokines. SeV and ZIKV infection also activated IFN-III, and SeV alone activated NF- $\kappa$ B and downstream pro-inflammatory responses. Generation of RIG-I deficient cells allowed us to demonstrate that all signalling outcomes activated by all of the tested ligands were dependent on RIG-I, suggesting that they all specifically stimulate RIG-I in A549 cells. The development and characterisation of this system has given us a platform from which to address conflicting data from

previous studies surrounding the requirement for various downstream signalling proteins and the regulation of the RIG-I signalling pathway by LUBAC.

# Chapter Four: Characterising the RIG-I signalling pathway

---

## 4.1 Introduction

Upon binding non-self RNA, RIG-I activates downstream signalling through the adaptor protein MAVS. Through the recruitment of many downstream signalling proteins, this triggers a cascade that activates IRF3 and NF- $\kappa$ B to induce expression of IFN and pro-inflammatory mediators. Although the signalling pathway downstream of RIG-I is better characterised than many other PRR, there is still much debate about which proteins are definitively required for the RIG-I driven immune response, the mechanism by which they act, and whether this differs depending on conditions or ligand.

Before studying the role of LUBAC in RIG-I signalling, we wanted to better characterise what proteins are involved in the signalling complex in our system. LUBAC is known to conjugate M1-Ub chains to signalling complex proteins to enable efficient recruitment of downstream signalling proteins, thus controlling the composition of the signalling complex and the outcome of signalling. Therefore, this exploration of the signalling complex will be vital to help us understand how LUBAC functions to regulate it.

Using knockout A549 cell lines, we tested the role of MAVS, NEMO, TBK1, IKK $\epsilon$ , the TANK-NAP1-SINTBAD complex, RIP1 and optineurin in RIG-I signalling. We found MAVS and NEMO, a known target of M1-Ub chains, to be essential for both IRF3- and NF- $\kappa$ B-driven responses. TBK1 and IKK $\epsilon$  were shown to function redundantly to activate IRF3 in response to all ligands but play no role in NF- $\kappa$ B activation. The role of the TANK-NAP1-SINTBAD complex, RIP1 and optineurin in RIG-I signalling remain unclear, with possible functions for RIP1 and optineurin in IRF3 activation, and potential redundant functions of all three proteins or protein complexes in the recruitment of TBK1 and IKK $\epsilon$  to the signalling complex.

## 4.2 MAVS is the central adaptor protein of the RIG-I signalling pathway

The adaptor protein MAVS functions directly downstream of RIG-I activation. Upon recognition of viral RNA, RIG-I oligomerises its CARD domain, in a ubiquitin-dependent and -independent fashion. The CARD domain is then recruited to MAVS, which in turn oligomerises its CARD domains in a prion-like fashion<sup>73</sup>, becoming a scaffold for sequential recruitment of a cascade of immune signalling

proteins. This cascade is thought to begin with recruitment of TRAFs 2, 5, and 6 to MAVS<sup>135,138,448</sup>, and ultimately results in the activation of IRF3 and NF- $\kappa$ B.

#### 4.2.1 MAVS is required for transcription downstream of RIG-I activation by SeV and 3p-hpRNA, but not Poly(I:C)

To confirm the requirement of MAVS for RIG-I-driven immune gene transcription, A549 MAVS  $-/-$  cells were purchased from Invivogen. Upon analysis by Western blotting (Figure 4.2.1A), MAVS  $-/-$  cells were found to express a truncated form of the MAVS protein, with a molecular mass of 30 kDa compared to 70 kDa in WT cells.

qPCR was used to analyse transcription of *IFNB1* and *CXCL10* in A549 WT and MAVS  $-/-$  cells stimulated by transfection with 3p-hpRNA (Figure 4.2.1B) and Poly(I:C) (Figure 4.2.1C) and infection with SeV (Figure 4.2.1D). Transcription of both *IFNB1* and *CXCL10* was entirely dependent on MAVS during stimulation of RIG-I with both 3p-hpRNA and SeV. However, in response to transfection with Poly(I:C), expression of *IFNB1* and *CXCL10* transcripts was three times higher in MAVS  $-/-$  cells compared to WT.

This may be due to differential protein expression between clonal cell lines, even derived from the same cell original cell line, which has been described previously in A549 cells<sup>449</sup>. The WT and MAVS  $-/-$  cells in this experiment are from different batches, with the WT cells coming from the lab of Henning Walczak (University of Cologne) and the MAVS  $-/-$  cells from Invivogen. TLR3 is the only known sensor of Poly(I:C) that does not signal through the adaptor proteins MAVS, instead using TRIF<sup>346,450,451</sup>. Therefore, we suggest that the MAVS  $-/-$  cell line expresses higher levels of TLR3 than WT cells, which senses Poly(I:C) in endosomes of transfected cells. To investigate this possibility, WT and MAVS  $-/-$  cells were treated with extracellular, non-transfected, Poly(I:C), which can only be detected by TLR3, and transcription was measured by qPCR (Figure 4.2.1E). Again, MAVS  $-/-$  cells showed much higher levels of *CXCL10* transcripts than WT suggesting that MAVS  $-/-$  cells express higher levels of TLR3, and possibly other components unique to the TLR3 signalling complex.

From this we conclude that MAVS is required for RIG-I-driven signalling in response to both 3p-hpRNA and SeV, which specifically activate RIG-I, but not Poly(I:C), whose activation in MAVS  $-/-$  cells is not RIG-I-specific. To confirm that MAVS was required for activation of both IRF3 and NF- $\kappa$ B by RIG-I, transcription of further genes would have to be analysed by qPCR, although based on these results and previous studies, we would expect this to be the case.

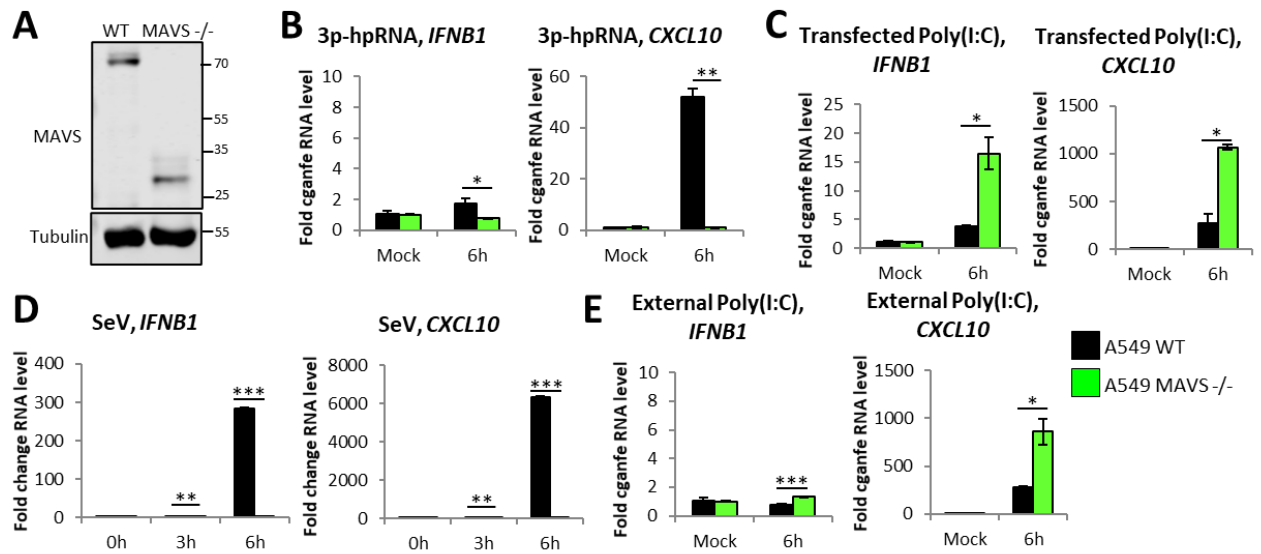


**Figure 4.2.1 MAVS is required for RIG-I-driven immune signalling following stimulation with synthetic RNAs and RNA viruses**

A) Western blotting analysis of A549 WT and MAVS <sup>-/-</sup> cells. qPCR to measure transcription of indicated genes in A549 WT and MAVS <sup>-/-</sup> cells in response to B) transfection with 1 µg 3p-hpRNA, C) transfection with 1 µg Poly(I:C), D) SeV infection at 1:300 dilution and E) external treatment with 1 µg Poly(I:C) (for all qPCR, n=2 and data is representative of 2 experimental repeats).

## 4.3 NEMO is required for activation of both IRF3 and NF-κB during RIG-I signalling

The adaptor protein NEMO is found in many PRR signalling pathways and has also been implicated in RIG-I signalling, where it acts upstream of TBK1 and IKKε to activate both the IRF3/7 and NF-κB signalling pathways<sup>143,149</sup>. To investigate the role of NEMO in RIG-I signalling, we used A549 cells deficient in NEMO, and NEMO <sup>-/-</sup> cells reconstituted with TAP-NEMO expression, both a kind gift from Henning Walczak (University of Cologne).

### 4.3.1 NEMO is required for transcription of IFN-I-dependent genes during stimulation of RIG-I with synthetic RNAs

Western blotting analysis of WT, NEMO <sup>-/-</sup> and NEMO <sup>-/-</sup> + TAP-NEMO (TAP-NEMO) cells (Figure 4.3.1A) confirmed loss of NEMO expression in knockout cells, and re-expression of endogenous levels of NEMO in the TAP-NEMO cell line.

To test whether NEMO is required for the synthetic RNA-driven IRF3-dependent immune response, A549 WT and NEMO <sup>-/-</sup> cells were stimulated with 3p-hpRNA and Poly(I:C) and transcription of immune genes was examined by qPCR. During both 3p-hpRNA (Figure 4.3.1B) and Poly(I:C) (Figure 4.3.1C) stimulation, increased transcription was seen in WT cells but was barely detectable above

background levels in NEMO  $-/-$  cells, showing that expression of NEMO was required for transcription of all tested genes.

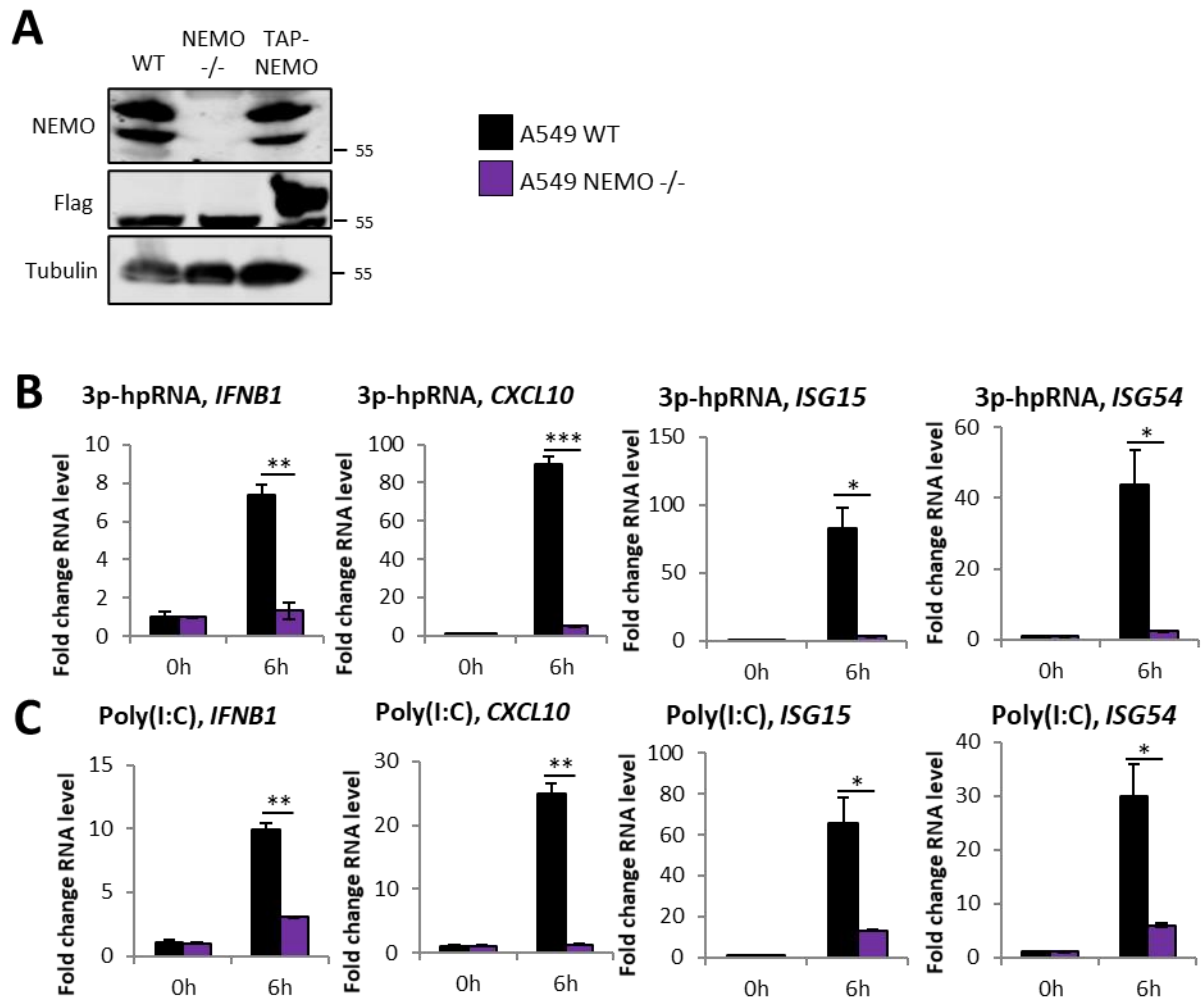


**Figure 4.3.1: NEMO is required for synthetic RNA-driven activation of IRF3- and NF- $\kappa$ B-dependent pathways**  
 A) Western blot analysis of A549 WT and NEMO  $-/-$  cells. qPCR to analyse transcription of indicated genes in A549 WT and NEMO  $-/-$  cells stimulated with B) 1  $\mu$ g 3p-hpRNA and C) 1  $\mu$ g Poly(I:C) (for both, n=2 and data is representative of 3 experimental repeats).

### 4.3.2 NEMO is required for activation of both IRF3- and NF- $\kappa$ B-dependent responses to SeV infection

To assess whether NEMO is also required for RIG-I-driven antiviral responses, the effect of NEMO expression on SeV-driven IRF3 and NF- $\kappa$ B-dependent signalling was examined.

During SeV infection, expression of IFN-dependent transcripts *IFNB1*, *IFNL1*, *CXCL10*, *ISG15* and *ISG54* was barely detectable above background levels in NEMO  $-/-$  cells, despite high levels of transcripts being found in WT cells (Figure 4.3.2A). *NFKBIA*, the only NF- $\kappa$ B-dependent gene whose transcription was strongly induced by SeV infection in WT cells, was also not transcribed above

background levels in NEMO  $-/-$  cells. Together, these data show that NEMO is essential for transcription of both IRF3 and NF- $\kappa$ B-dependent genes during RIG-I activation. qPCR analysis of the transcription in SeV infected A549 WT, NEMO  $-/-$  and TAP-NEMO cells (Figure 4.3.2C), demonstrates that re-expression of NEMO cells rescues the transcription of immune genes to near WT levels, confirming the requirement of NEMO.

Western blotting analysis of SeV infected A549 WT and NEMO  $-/-$  cells (Figure 4.3.2C) showed that NEMO was required for phosphorylation of IRF3 at serine residues 386 and 396. Conversely, NEMO appears not to be required for phosphorylation of TBK1 or I $\kappa$ B $\alpha$ . Having said this, NEMO does appear to be required for the degradation of total I $\kappa$ B $\alpha$ , which only occurred in WT cells during SeV infection.

Because in the absence of NEMO, TBK1 is still activated by RIG-I signalling, but IRF3 is not, we posit that NEMO may be involved in the recruitment of IRF3 to the RIG-I signalling complex, bringing it into proximity to TBK1 to enable activation. NEMO also appears to be required for NF- $\kappa$ B activation and subsequent transcription, because although cells lacking NEMO still express phospho-I $\kappa$ B $\alpha$ , they show lower levels of I $\kappa$ B $\alpha$  degradation, required for the release of active NF- $\kappa$ B subunits into the nucleus.

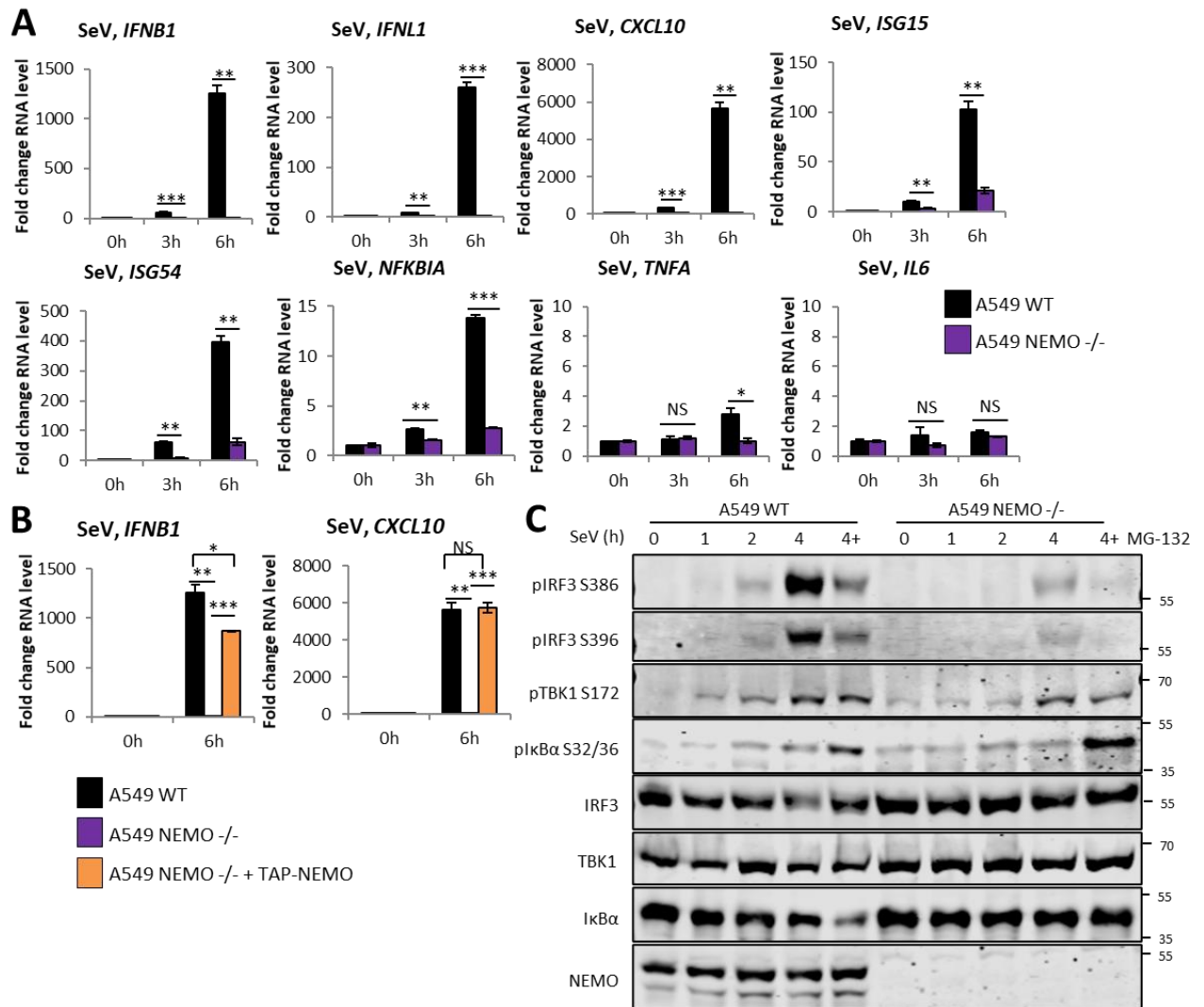


**Figure 4.3.2: NEMO is required for SeV-driven activation of IRF3- and NF-κB-dependent pathways**

qPCR analysis of transcription of indicated genes in A) A549 WT and NEMO<sup>-/-</sup> cells infected with SeV at 1:300 dilution (n=2, data representative of 3 experimental repeats) and B) SeV infection of A549 WT, NEMO<sup>-/-</sup> and NEMO<sup>-/-</sup> + TAP-NEMO at 1:300 dilution (n=2, data representative of 2 experimental repeats). C) Western blot analysis of signalling protein activation in A549 WT and NEMO<sup>-/-</sup> cells infected with SeV at 1:300 dilution blot in the presence (+) or absence of 10 μM MG-132 (data representative of 2 experimental repeats).

#### 4.4 TBK1 and IKKε function redundantly to activate IRF3 during RIG-I signalling in A549 cells

Our previous experiments have shown that stimulation of A549 cells with both synthetic RNAs and RNA viruses results in phosphorylation of TBK1 at Serine 172 (Figures 3.3.1C, 3.3.2C and 3.3.3B), a modification known to strongly promote TBK1 activity<sup>452</sup>. Consequently, we predicted that, as has been shown in signalling pathways in many model systems, TBK1 was required for the phosphorylation of IRF3 and subsequent activation of IRF3-dependent immune signalling during RIG-I activation.

TBK1, alongside IKK $\alpha$ ,  $\beta$  and  $\epsilon$ , is part of the Inhibitor of Nuclear Factor Kappa-B Kinase (IKK) subfamily of Serine-Threonine protein kinases. IKK $\alpha$  and IKK $\beta$  form the canonical IKK complex to activate NF- $\kappa$ B, whereas TBK1 and IKK $\epsilon$  form the non-canonical IKK complex<sup>171</sup>. TBK1 and IKK $\epsilon$  were initially implicated in NF- $\kappa$ B activation, evident during overexpression of the two proteins<sup>172,453–455</sup>. However, this was later disputed and the non-canonical IKK complex was found to be required for the phosphorylation of IR 21,151,152 F3. Furthermore, TBK1 and IKK $\epsilon$  are also responsible for restricting cell death outcomes downstream of TNF activation<sup>333,456</sup>. TBK1 exhibits functional redundancy with IKK $\epsilon$ , but the proteins have differing expression patterns; TBK1 is constitutively expressed in many cell types, but basal IKK $\epsilon$  expression is only detectable in specific cell types, such as pancreas, thymus and spleen<sup>170</sup>. Despite low basal levels, IKK $\epsilon$  expression has been shown to be rapidly and dramatically upregulated in response to cytokines and microbial products<sup>171,172</sup>, triggered by both NF- $\kappa$ B and STAT3 binding sites in its promoter<sup>457,458</sup>. This capacity for rapid upregulation enables IKK $\epsilon$  to contribute to signalling, even in cell types where its expression is very low. In non-immune cells, IKK $\epsilon$  was reported to be predominantly involved in phosphorylation of STAT proteins after initiation of the Type I IFN response<sup>173</sup>, but has also been shown to phosphorylate IRF3 and IRF7 downstream of viral RNA sensors<sup>143,459</sup>.

#### 4.4.1 TBK1 and IKK $\epsilon$ function redundantly in the RIG-I response to synthetic RNAs

We set out to assess the relative contributions of TBK1 and IKK $\epsilon$  to RIG-I signalling using A549 WT, TBK1  $-/-$ , IKK $\epsilon$   $-/-$  and TBK1/IKK $\epsilon$   $-/-$  cells (a gift from Henning Walczak, University of Cologne, Germany). These cell lines were stimulated with 3p-hpRNA (Figure 4.4.1A) and Poly(I:C) (Figure 4.4.1B) and transcription of immune genes was analysed by qPCR. In TBK1 and IKK $\epsilon$  single knockout cells, the level of transcription of all genes was as, or more than, seen in WT cells. However, cells lacking both TBK1 and IKK $\epsilon$  expression had significantly reduced *CXCL10* and *ISG54* transcription during stimulation with both 3p-hpRNA and Poly(I:C). Low expression of *IFNB1*, *IFNL1* and *ISG15*, even in stimulated WT cells, may account for a lack of significant phenotype seen in knockout cells.

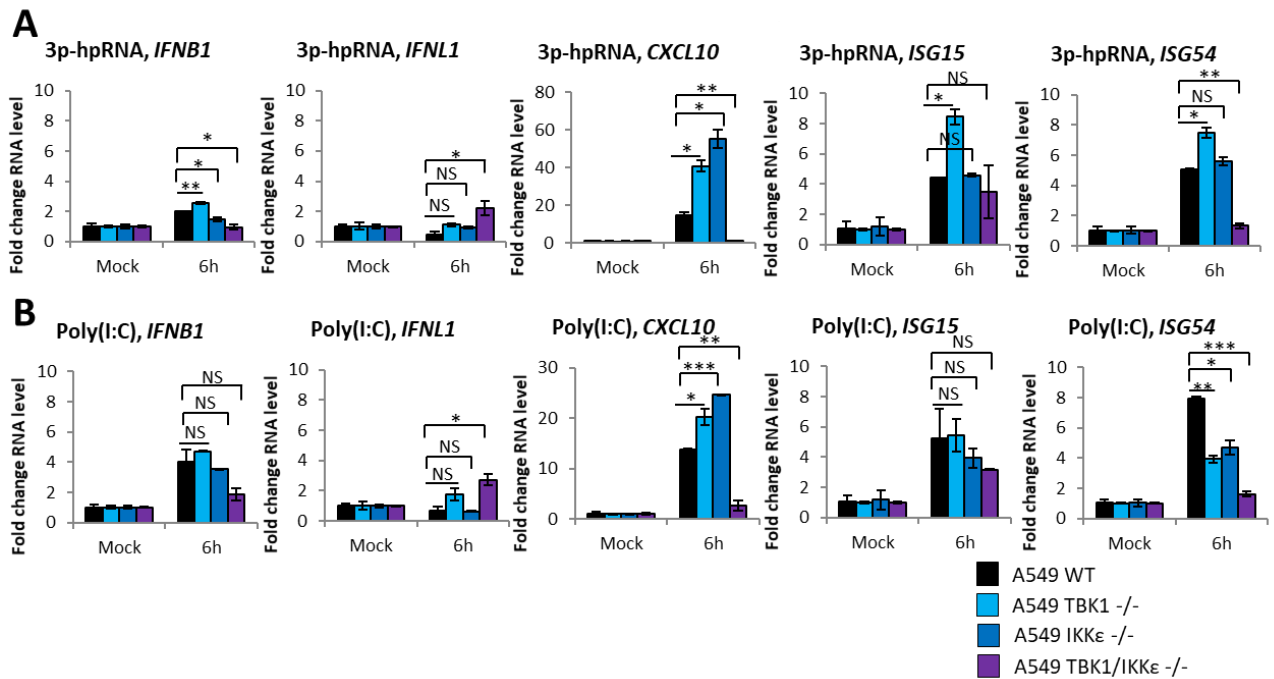


**Figure 4.4.1: TBK1 and IKKε act redundantly during RIG-I stimulation by synthetic RNAs**

qPCR to measure expression of indicated genes during stimulation of A549 WT, TBK1 -/-, IKKε -/- and TBK1/IKKε -/- cells by transfection of A) 1 μg 3p-hpRNA and B) 1 μg Poly(I:C) (for both, n=2 and data is representative of 3 experimental repeats).

#### 4.4.2 TBK1 and IKKε function redundantly in the IRF3-dependent response to SeV infection, but are not required for the NF-κB dependent response

Infection of TBK1 and IKKε deficient cells with SeV enabled us to investigate involvement of TBK1 and IKKε in both IRF3 and NF-κB activation downstream of RIG-I, due to the broader measurable immune response induced.

Analysis of transcription by qPCR (Figure 4.4.2A) showed that loss of either TBK1 or IKKε resulted in either no significant change or a significant increase in transcription of all genes, as seen with 3p-hpRNA and Poly(I:C). In a much clearer picture than during synthetic RNA stimulation, in cells lacking both TBK1 and IKKε the transcription of *IFNB1*, *IFNL1*, *CXCL10*, *ISG16* and *ISG54* was undetectable above background levels. This confirms that the contribution of either one of TBK1 or IKKε is essential for activation of an IFN-I and IFN-III-driven transcriptional response, as previously reported<sup>167,460</sup>. Conversely, transcription of *NFKBIA* and *TNFA* in cells lacking both TBK1 and IKKε was not significantly different from WT or single knockout cell lines, demonstrating that TBK1 and IKKε do not contribute to RIG-I-driven NF-κB activation in A549 cells.

The requirement of either TBK1 or IKKε for efficient chemokine production was confirmed by ELISA analysis of CXCL10 secretion from A549 WT, TBK1 <sup>-/-</sup>, IKKε <sup>-/-</sup> and TBK1/IKKε <sup>-/-</sup> cells infected with SeV (Figure 4.4.2B). Unlike with qPCR analysis, ELISA showed that TBK1 <sup>-/-</sup> and IKKε <sup>-/-</sup> cells have an intermediate phenotype, secreting about two thirds the level of CXCL10 secretion seen in WT cells. Across 2 experimental replicates, TBK1 <sup>-/-</sup> cells showed consistently lower levels of CXCL10 secretion than IKKε, in line with observations that TBK1 plays the predominant role in IRF3 activation in non-immune cells. A549 cells deficient in both TBK1 and IKKε secreted little or no CXCL10 after infection.

To further analyse the role of TBK1 and IKKε in the activation of IRF3 and NF-κB, Western blotting analysis of TBK1, IRF3 and IκBα phosphorylation in these cell lines was done during SeV infection (Figure 4.4.2C). In WT cells, levels of phosphorylated IRF3 and TBK1 increased through the 6-hour infection time course, whereas the level of phospho(p)-IκBα was highest at 3 hours post infection and lost at later time points, consistent with it being quickly degraded by the proteasome post-phosphorylation. In TBK1 <sup>-/-</sup> cells, levels of phospho-IRF3 and phospho-IκBα are consistent with what is seen in WT cells, with TBK1 phosphorylation absent. Levels of phospho-IRF3 and phospho-IκBα in IKKε <sup>-/-</sup> cells are similar to both WT and TBK1 <sup>-/-</sup> cells, however increased levels of phospho-TBK1 were detected. This is suggestive of increased TBK1 activation to compensate for loss of IKKε expression, in line with their redundancy. IRF3 phosphorylation is undetectable in cells lacking both TBK1 and IKKε, supporting the requirement for either TBK1 or IKKε in IRF3 activation, IκBα phosphorylation is unchanged or higher than seen in WT and single knockout cell lines. This is consistent with the qPCR data for showing the unaffected transcription of *NFKBIA* in these cells (Figure 4.4.2A), confirming that TBK1 and IKKε are not required for NF-κB activation.

IKKε phosphorylation was still undetectable by Western blotting after 6 hours of infection, even in TBK1 <sup>-/-</sup> cells, and there was no visible upregulation of total IKKε protein levels (data not shown). However, after a longer SeV infection time course and a 24 hour IFNα treatment, conditions previously shown to upregulate known ISG RIG-I (Figure 3.4.1B), phospho-IKKε was detected by Western blotting in TBK1-deficient cells but not WT cells (Figure 4.4.2D), with expression is much stronger after stimulation with IFNα. Upregulation of IKKε only in TBK1 <sup>-/-</sup> cells suggests loss of TBK1 can be compensated for by upregulation of IKKε.

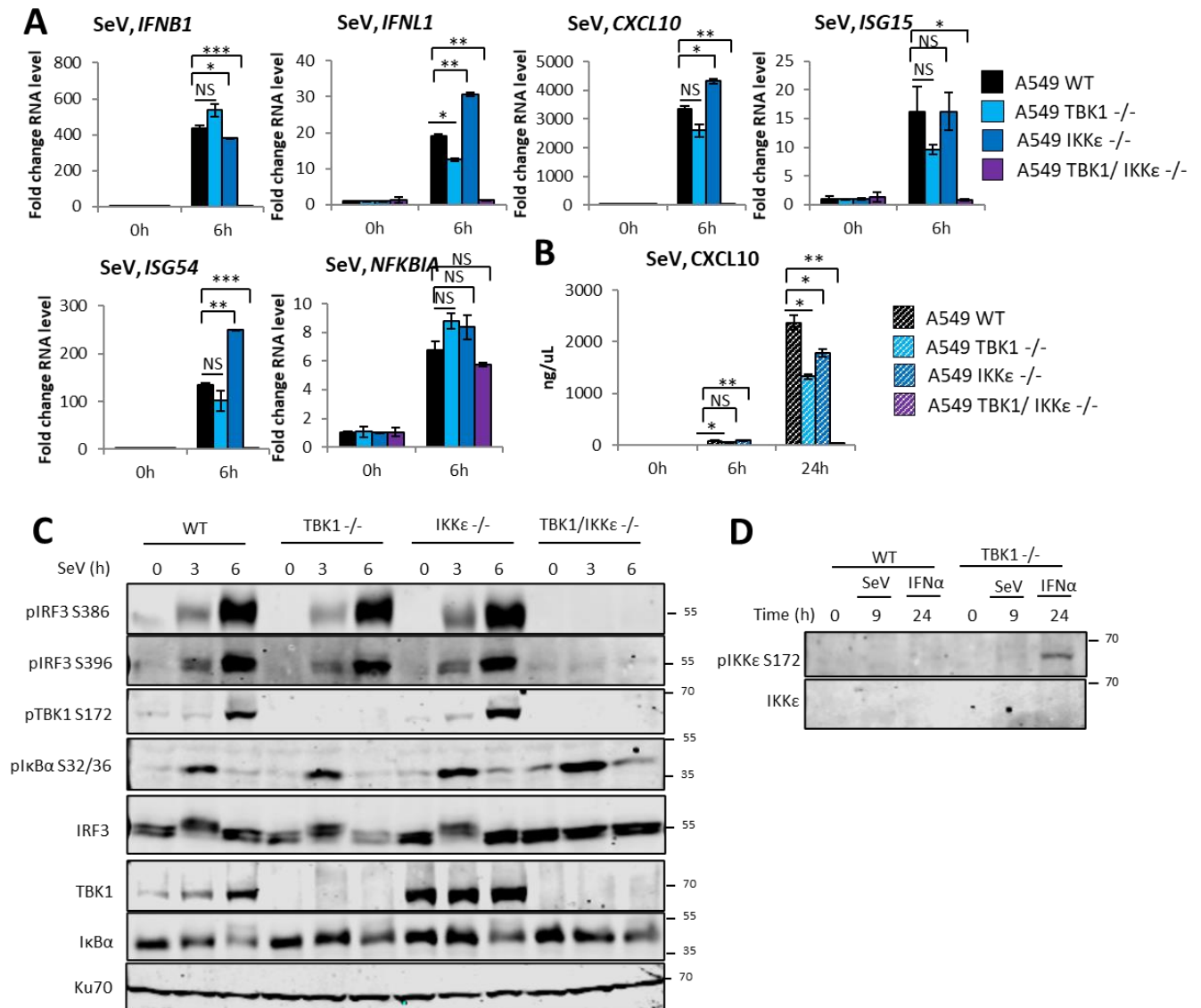


**Figure 4.4.2: TBK1 and IKKε act redundantly during stimulation of RIG-I by SeV**

Infection of A549 WT, TBK1<sup>-/-</sup>, IKKε<sup>-/-</sup> and TBK1/IKKε<sup>-/-</sup> cells with SeV at 1:300 dilution and A) qPCR to analyse transcription of indicated genes (n=2, data representative of >3 experimental repeats), B) ELISA to analyse CXCL10 secretion (n=2, data representative of 2 experimental repeats), C) Western blotting analysis of signalling protein activation (data representative of 2 experimental repeats) and D) Western blotting analysis of IKKε phosphorylation during infection with SeV at 1:300 dilution and treatment with 100 U/mL IFNα.

## 4.5 How are TBK1 and IKKε recruited to the RIG-I signalling pathway

Activation of TBK1 and IKKε is known to occur by trans-autophosphorylation when the proteins are at a high concentration in signalling complexes<sup>161,452</sup>, but there is debate surrounding about how TBK1 and IKKε are recruited to the RIG-I signalling pathway. TRAF proteins, the TANK/NAP1/SINTBAD complex, RIP1 and Optineurin have all been implicated in its recruitment to the mitochondrial MAVS complexes. To study their contribution to TBK1 and IKKε recruitment, we have used A549 cell lines deficient in TANK/NAP1/SINTBAD, RIPK1 and Optineurin.

#### 4.5.1 TANK/NAP1/SINTBAD are not essential for recruitment of TBK1 and IKKε to the RIG-I signalling complex during stimulation with synthetic RNAs

The TANK, NAP1 and SINTBAD proteins, identified through their shared TBK1-binding domains<sup>453,461,462</sup>, have been previously implicated in TBK1 recruitment to the RIG-I signalling complex<sup>462-465</sup>, as well as TBK1 and IKKε recruitment to the TNF-RSC<sup>466</sup>. Using A549 cells deficient in TANK, NAP1 and SINTBAD (TKO), a kind gift from the lab of Henning Walczak (University of Cologne), we examined the requirement of this protein complex in TBK1 and IKKε recruitment to the RIG-I-RSC.

Western blotting analysis of TANK protein expression in WT and TKO cells (Figure 4.5.1A) confirmed loss of TANK expression in the knockout cells, but antibodies against NAP1 and SINTBAD were unsuccessful in detecting proteins in either WT or TKO cells. Therefore, to verify that the TKO cells behave previously shown, with reduced levels of TBK1 phosphorylation during TNFα stimulation<sup>333</sup>, WT and TKO cells were stimulated with TNFα and the phosphorylation of IRF3, TBK1 and IκBα was analysed by Western blotting (Figure 5.4.1B). In cells lacking TANK, NAP1 and SINTBAD, TBK1 phosphorylation was significantly reduced compared to WT cells, confirming reduced recruitment of TBK1 to the TNF signalling complex in TKO cells, and increased in IκBα phosphorylation was also seen, mimicking the previous study<sup>333</sup>. Because, unlike in RIG-I signalling, TBK1 doesn't drive IFN-I induction downstream of TNF, the lack of IRF3 phosphorylation seen was expected. This highlights the different roles of TBK1 and IKKε between the two pathways, possibly mediated by differential recruitment mechanisms to the respective signalling complexes.

After functional verification of the TKO cells, qPCR analysis was used to assess the role of the TANK/NAP1/SINTBAD complex in RIG-I-induced transcription in response to stimulation with 3p-hpRNA (Figure 4.5.1C) and Poly(I:C) (Figure 4.5.1D). Whilst transcription of *CXCL10* in response to both RNAs was significantly lesser in TKO cells across multiple experimental repeats, this was not true of other IFN-I or IFN-I-stimulated genes. From this we cannot say whether the TANK/NAP1/SINTBAD complex is required for the recruitment of one of TBK1 or IKKε due to their functional redundancy, however it suggests that the complex is not essential for the recruitment of both proteins during stimulation with synthetic RNAs.

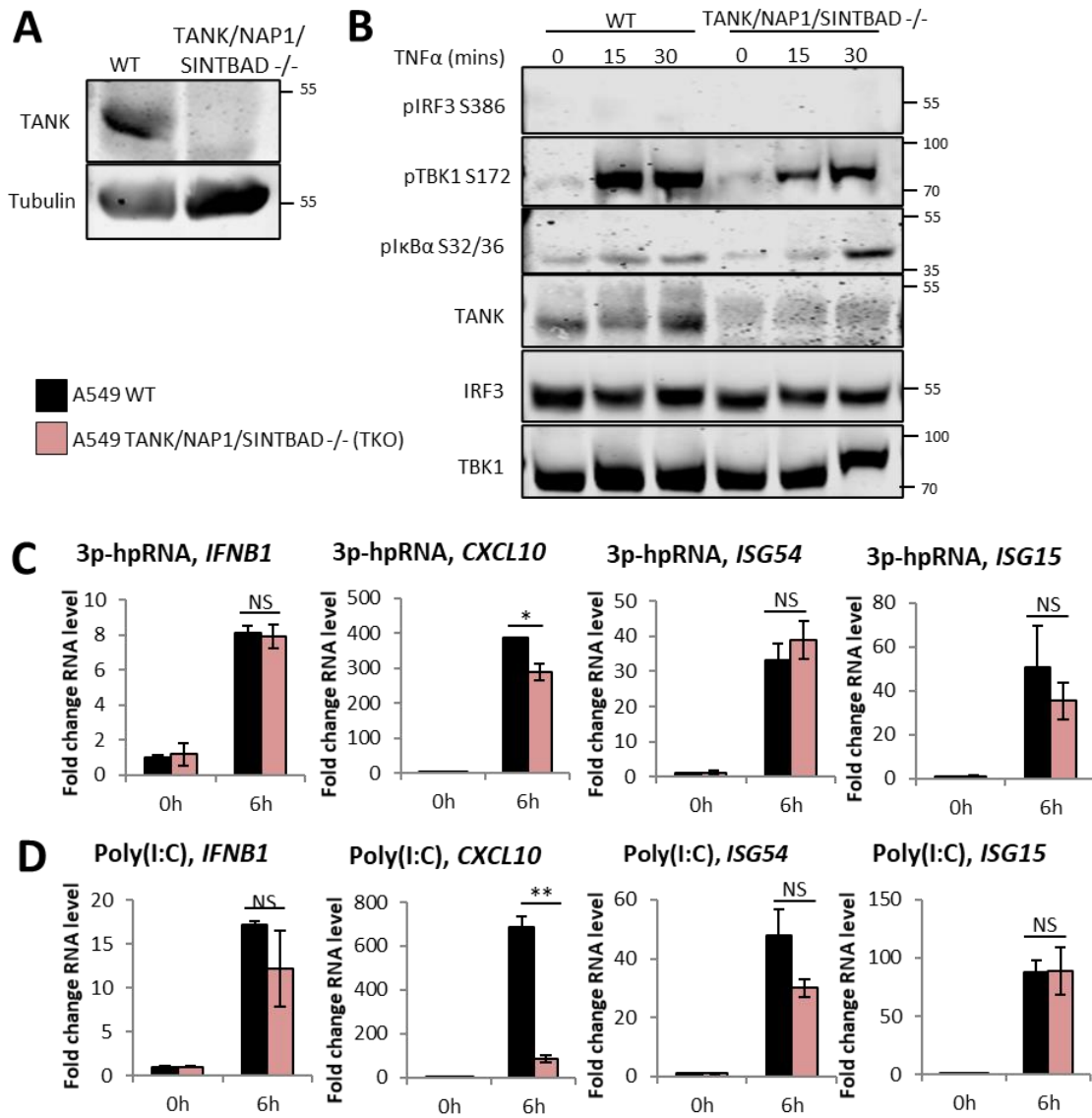


**Figure 4.5.1: TANK/NAP1/SINTBAD are not essential for RIG-I-driven pathways downstream of activation by synthetic RNAs**

A) Western blotting of A549 WT and TANK/NAP1/SINTBAD -/- (TKO) cells and B) Western blotting analysis signalling protein phosphorylation in A549 WT and TKO cells stimulated with TNFα @ 200 ng/mL. qPCR analysis of transcription of indicated genes in A549 WT and TKO cells stimulated by C) 1 μg 3p-hpRNA and D) 1 μg Poly(I:C) (both n=2, data representative of 3 experimental replicates).

#### 4.5.2 TANK/NAP1/SINTBAD are not essential for recruitment of TBK1 and IKKε to the RIG-I signalling complex during SeV infection

To see if this is also the case during RNA virus infection, WT and TKO cells were infected with SeV, transcription of immune genes was measured by qPCR (Figure 4.5.2A) and activation of signalling proteins was measured by Western blotting (Figure 4.5.2B). Unlike seen with synthetic RNAs, during SeV infection there was no significant reduction in *CXCL10* transcription in TKO cells. Results differed

slightly between experimental replicates, but generally there was a trend for either no significant change or an increase in transcription in cells lacking TANK, NAP1 and SINTBAD compared to WT for both IRF3 and NF- $\kappa$ B dependent genes. Western blotting during SeV infection supported this, with TKO cells expressing similar levels of phospho-IRF3 but elevated levels of both p-TBK1 and p-I $\kappa$ B $\alpha$  compared to WT.

This data, as well as that seen with synthetic RNA stimulation, shows that the TANK/NAP1/SINTBAD complex is not essential for recruitment of both TBK1 and IKK $\epsilon$  to the RIG-I signalling complex, but may play a role in the recruitment of one of the proteins. This is likely to be TBK1, as this has previously been shown<sup>151-153</sup>, whereas they have never been specifically implicated in IKK $\epsilon$  recruitment previously.

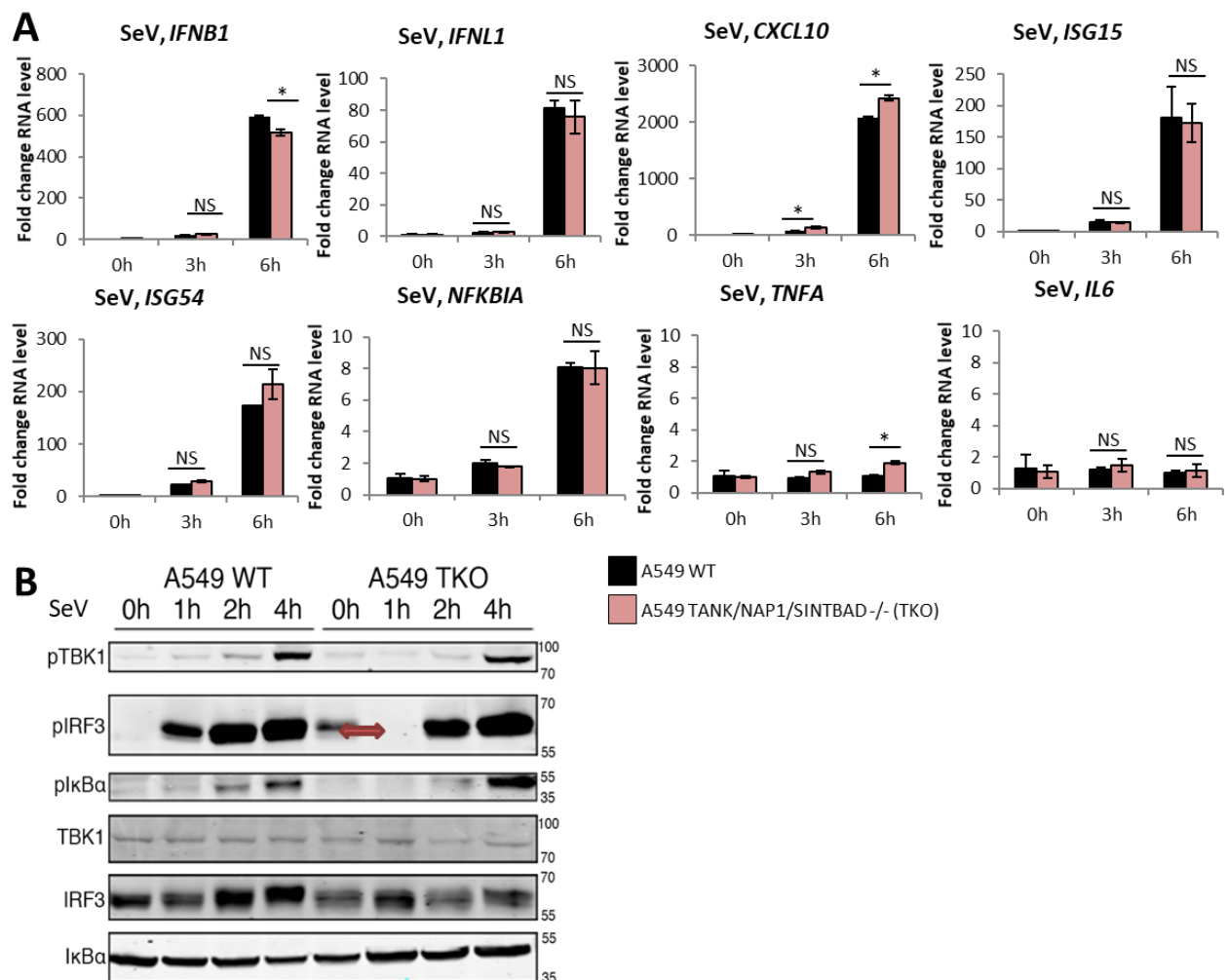


**Figure 4.5.2: TANK/NAP1/SINTBAD are not essential for RIG-I-driven pathways downstream of activation by SeV**

SeV infection A549 WT and TKO cells at 1:300 dilution and A) qPCR analysis of transcription of indicated genes (n=2, data representative of >3 experimental replicates) and B) Western blotting analysis of signalling protein

phosphorylation. 0h and 1h samples were accidentally loaded in the wrong lanes, represented by a red double-headed arrow (data representative of 2 experimental repeats).

### 4.5.3 The role of RIP1 in the RIG-I signalling pathway is unclear

The role of the kinase RIP1 in RIG-I signalling is heavily contested. Some studies have shown that it is recruited to the MAVS signalling complex alongside FADD and caspase 8, where RIP1 recruits TANK and NEMO to MAVS, a process required for maximum activation of NF- $\kappa$ B and IRF3<sup>149,467–470</sup>, before it is cleaved by caspase 8 to inhibit IRF3 activation in a self-regulating loop. However, loss of RIP1 expression in MEFs was shown to have no effect on IFN-I production<sup>142</sup>, disputing this. To investigate the role of RIP1 in the RIG-I signalling in A549 cells, A549 RIP1 -/- cells, generated in the lab of Henning Walczak (University of Cologne), were stimulated by SeV infection.

Loss of RIP1 protein expression in RIP1 -/- cells was confirmed by Western blotting analysis (Figure 4.5.3A). A549 WT and RIP1 -/- cells were then analysed by qPCR to measure immune gene activation (Figure 4.5.3B). During SeV infection, RIP1 -/- cells showed significantly reduced transcription of *IFNB1*, consistent across 4 experimental repeats. However, the transcription of IFN-I-stimulated genes *ISG15* and *ISG54* was not consistently reduced in RIP1-deficient cells, with mixed outcomes across experimental repeats. Similarly, loss of RIP1 expression also did not significantly alter transcription of chemokine *CXCL10*, or NF- $\kappa$ B dependent genes *NFKBIA*.

This is somewhat supported by Western blotting analysis of lysates from SeV infected WT and RIP1 -/- cells (Figure 4.5.3C). Generally, deletion of RIP1 only minorly affected phosphorylation of signalling pathway components, with I $\kappa$ B $\alpha$  phosphorylation unaffected and higher levels of phosphorylated TBK1 were detected in RIP1 -/- cells at 2 and 4 hours post infection. However, IRF3 phosphorylation appeared to be delayed in RIP1 -/- cells. As RIP1 -/- cells show a defect in the activation of IRF3, which affects the transcription of IFN-I gene *IFNB1*, we suggest that RIP1 may play a role in activation of IRF3 during RIG-I signalling. However, unclear data around the transcription of ISGs means that more work would have to be done to confirm this. Both transcriptional and Western blotting data consistently suggests that RIP1 is not to be required for RIG-I-dependent activation of NF- $\kappa$ B.

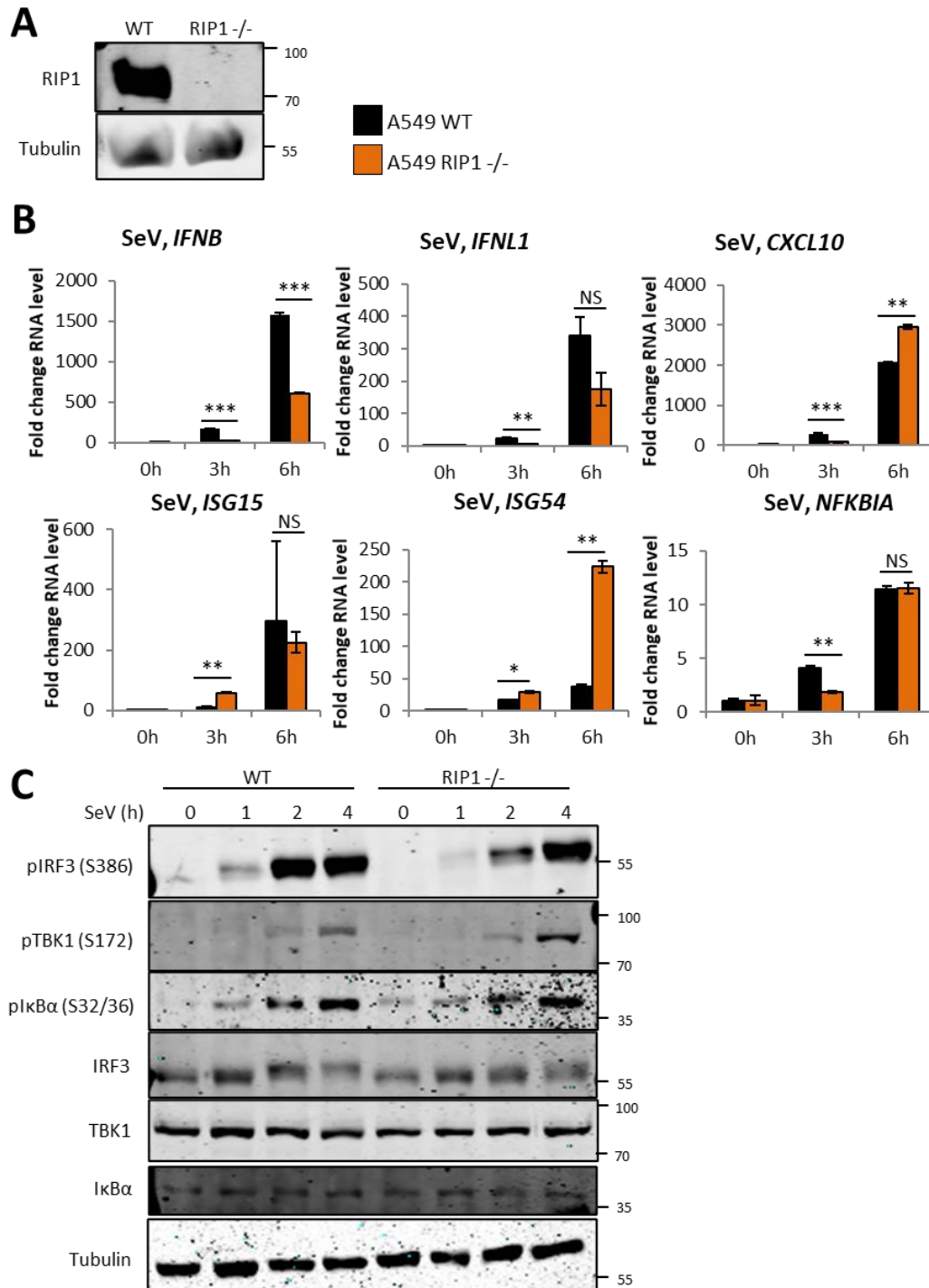


**Figure 4.5.3: RIP1 may play a role in RIG-I-driven IRF3 activation by SeV**

A) Western blot analysis of A549 WT and RIP1<sup>-/-</sup> cells. SeV infection of A549 WT and RIP1<sup>-/-</sup> cells at 1:300 dilution and A) qPCR analysis of transcription of indicated genes (n=2, data representative of >3 experimental replicates) and B) Western blotting analysis of signalling protein phosphorylation (data representative of 2 experimental repeats).

#### 4.5.4 Optineurin appears not to be required in the RIG-I response to SeV infection

Optineurin (OPTN) is a NEMO-related, Golgi localised protein known to bind to ubiquitinated proteins. It has been shown to regulate many cellular processes, including immune, inflammatory and antiviral signalling, generally occurring through suppression of NF- $\kappa$ B activation by mimicking NEMO<sup>471-474</sup>, or activation of IFN-I through its interaction with TBK1<sup>162,475,476</sup>. Optineurin has also been implicated in the RLR-driven antiviral response, interacting with ubiquitinated TBK1 to initiate its trans-autophosphorylation, resulting in IRF3 phosphorylation and IFN-I activation<sup>162-164</sup>. However, this appears to be cell-type specific and has been opposed, with Optineurin also suggested to be a negative regulator of RIG-I-driven IFN-I activation<sup>477</sup>. Interestingly, OPTN can bind TBK1 but not IKK $\epsilon$ , supporting suggestions that the two redundant proteins may be recruited differently<sup>155,156</sup>. OPTN has also been shown to interact with the LUBAC complex during RNA virus infection<sup>157</sup>.

To explore its role in RIG-I signalling in A549 cells, optineurin deficient A549 cells (OPTN<sup>-/-</sup>), a kind gift from the lab of Henning Walczak (University of Cologne) were infected with SeV. From a single experimental replicate, qPCR data shows that expression of *IFNB1* was significantly less in OPTN<sup>-/-</sup> cells, but expression of *CXCL10* was significantly more (Figure 4.5.4A), meaning that we do not have enough data to conclude anything around the role of optineurin in RIG-I signalling in A549 cells.

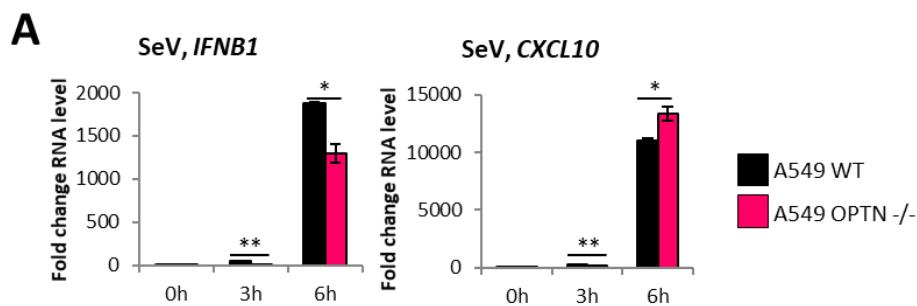


**Figure 4.5.4: Optineurin is not essential for RIG-I-driven pathways downstream of activation by SeV**  
A) SeV infection of A549 WT and OPTN<sup>-/-</sup> cells at 1:300 dilution and qPCR analysis of transcription of indicated genes (n=2, data representative of one experimental replicate).

#### 4.6 Discussion

Much of the data surrounding the requirement of individual signalling proteins for RIG-I-driven IFN-I and NF- $\kappa$ B activation is conflicting, suggesting that this may be context dependent. Because we have demonstrated that we have a system to study RIG-I signalling that is not interfered with by other RNA sensors, with RIG-I-deficient A549 cells showing no signalling response to all tested RNAs and

viruses, we believe we have a clean system to assess the contribution of proteins to signalling in A549 cells. Therefore, before examining how LUBAC and M1 ubiquitin chains regulate the RIG-I signalling pathway, we set out to further define the composition of the RIG-I signalling complex in our system. Through the work in this chapter, we used knockout cell lines to test the requirement of various signalling proteins, some of which are known to be modified by LUBAC, for the activation of both IRF3 and NF- $\kappa$ B. Such data will then allow us to identify where LUBAC fits into the signalling pathway, what both LUBAC and M1-Ub chains are binding to, and how it contributes to RIG-I signalling outputs.

#### 4.6.1 Limitations of experimental system

Throughout this project, protein function was studied using CRISPR knockout cells, predominantly A549. Although this system has many benefits over some techniques such as protein overexpression or incomplete knockdown studies, various limitations prevail.

Limitations of using cancer cell lines are derived from the fact that cancer is driven by genetic alterations, which can dysregulate signalling pathways. For example, A549 cells have downregulated STING to inhibit the DNA sensing pathway, helping them remain undetected by the immune system<sup>341–343</sup>. However, in this instance, as A549 cells have an intact RIG-I-driven RNA sensing pathway but appear to have downregulated other RNA sensors like MDA5 and TLR3<sup>431</sup>, this enabled us to have a clean system to study RIG-I signalling without interference from other PRR. Use of primary cells would provide more relevance to the data, although they are not as tractable for genetic manipulation to study the function of individual proteins within signalling pathways. Cell lines enable fine manipulation of cellular functions and tend to generate more reproducible data, as they aren't as reactive to small changes in culture conditions as primary cells, and their features do not change as much with serial passaging. However, as cancer cell lines are often resistant to cell death, another mechanism developed to inhibit their destruction by the immune system, limiting their usefulness for studying regulation of cell death pathways, as was done in this project.

The use of CRISPR techniques to study protein function also comes with limitations. Although recent advances in CRISPR technology have enabled its accurate and target-specific use to knockout expression of an individual protein, off-target effects of CRISPR can still occur<sup>478</sup>. This can result in incorrect attribution of phenotypes to target proteins protein, that are in fact the result of off-target genetic editing. Furthermore, once a population of CRISPR edited cells has been generated, studies must then use either the heterozygous pool of edited cells or clonal populations grown from individual edited cells. In this study, CRISPR-edited A549 cells from the heterogenous wild-type

population were grown as clonal populations, which were then characterised and used for functional studies. This was done as a homozygous clonal cell line ensures that expression of the target protein is entirely ablated, leading to reproducible results. However, if only a single CRISPR clone is then used to study protein function, variation between the individual clones, unrelated to the function of the target protein, can be misconstrued.

A number of mechanisms can be used to address these limitations. To mitigate against off-target effects, whole genome sequencing can be done in CRISPR-edited cells, although this is expensive and time consuming. Clonal variation can be countered by the use of multiple knockout clones to explore target protein function. Additionally, single cell sorting and clonal expansion from the wild-type population of cells would enable CRISPR pools to be pools generated from a single wild-type clone, preventing clonal variability. To address both limitations, repetition of assays in knockout cells with the target protein re-expressed, either stably or transiently, to see if the phenotype seen in knockout cells was reversed, could be done. CRISPR-edited cells can also be validated by repeating previously published functional characterisation.

Where possible in the scope of this study, some of the aforementioned measures were used to mitigate against limitations. Although predominantly knockout A549 cells were used for to explore the function of target proteins, CRISPR-edited HaCaT and MEF cells were also used to further explore phenotypes seen in A549 cells. For CRISPR knockout cell lines generated as part of the project, loss of protein expression was confirmed by Western blotting and the presence and location of the mutation introduced by editing was confirmed by sequencing of the genomic DNA of the knockout clone. Unfortunately for both cell lines generated during this project, only one successful knockout clonal cell line was generated, so multiple clones could not be used for functional characterisation. These cells were further characterised by functional assays to ensure non-targeted signalling pathways remained intact. For CRISPR knockout cell lines used in the project that were kind gifts from collaborators, loss of protein expression was also confirmed by Western blotting. Where possible, functional confirmation of the cell line was also done by repeating a relevant assay previously published using the specific cell line, for example when A549 WT and A549 TANK/NAP1/SINTBAD  $-/-$  cells were stimulated with TNF $\alpha$  (Figure 4.5.1B) to confirm reduced TBK1 phosphorylation in triple knockout cells. Functional characterisation of knockout cells stably re-expressing both HOIP and NEMO confirmed that re-expression of the target protein reversed the phenotype seen in knockout cells.

#### 4.6.2 Requirement for MAVS and NEMO in RIG-I signalling

Much of the controversy surrounding the specific role of many proteins in RIG-I signalling is likely due to the use of many different cell types and even species in prior studies, between which we would expect a level of variation. Because of this, we did not assume anything about the composition of the RIG-I signalling complex in our system. Instead, we examined RIG-I signalling outcomes in a range of knockout cell lines to ascertain the relative contribution of each protein to the signalling outputs.

We confirmed the requirement of MAVS, the central adaptor protein of both the RIG-I and MDA5 signalling complexes, for activation of IFN-I and chemokine responses. This was expected as the role of MAVS in the RIG-I signalling complex is well described, with MAVS forming the basis for recruitment of signalling proteins that activate IRF3 and NF- $\kappa$ B<sup>434,479</sup>. In our system, we did not examine the mechanism by which MAVS activated signalling outcomes, although previous data suggests that the activation of the resultant signalling cascades is mediated by the recruitment of TRAF proteins to MAVS at the mitochondrial outer membrane<sup>135,143</sup>.

Secondly, consistent with previous studies describing its role in both branches of RIG-I signalling<sup>149</sup>, we showed that NEMO is required for the activation of both IRF and NF- $\kappa$ B-dependent signalling responses. Previously, NEMO-mediated activation of both branches of signalling has been shown to occur through recruitment of the IKK complex, which then phosphorylates I $\kappa$ B $\alpha$  to activate NF- $\kappa$ B, and TBK1 to enable IRF3 activation<sup>143,480</sup>. Our data somewhat disputes this, showing that TBK1, but not IRF3, was activated in the absence of NEMO. This instead supports a previously proposed NEMO-independent mechanism of TBK1 and IKK $\epsilon$  activation by MAVS and TRAF proteins<sup>143</sup>. However, as NEMO is required for IRF3 activation, we propose that NEMO recruits active TBK1 to the RIG-I signalling complex, bringing it into proximity with IRF3. In addition to this, whilst NEMO was required for the transcription of NF- $\kappa$ B-dependent genes and the required degradation of I $\kappa$ B $\alpha$ , NEMO was not required for the prior phosphorylation of I $\kappa$ B $\alpha$ . Degradation of I $\kappa$ B $\alpha$  is initiated by its N-terminal phosphorylation by IKK $\beta$ , which recruits the E3 ligase SCF- $\beta$ TrCP that conjugates K48-ubiquitin chains to I $\kappa$ B $\alpha$ , targeting the protein for selective degradation by the 26S proteasome<sup>481</sup>. As phosphorylation but not degradation of I $\kappa$ B $\alpha$  does not occur in cells lacking NEMO, possibly NEMO is involved in the recruitment of the UBC4/5 E2 and SCF- $\beta$ TrCP E3 ligase to I $\kappa$ B $\alpha$  at the RIG-I signalling complex, something that has previously been attributed to IKK $\beta$ <sup>482</sup>.

### 4.6.3 The role of TBK1 and IKKε in IRF3 activation in non-immune cells

Activation of IRF3 occurs occur through direct phosphorylation at Serine 386 by both TBK1 and IKKε<sup>69,173,460,483,484</sup>. We have shown that TBK1 and IKKε function redundantly to phosphorylate IRF3 and activate IFN-I dependent signalling downstream of RIG-I, suggesting that they are both recruited to the RIG-I signalling complex in this system.

Previously, TBK1 has been shown to be the major mediator of IRF3 activation in non-immune cells, with IKKε considered dispensable for IFN-I induction, likely due to its low expression<sup>167,169,460,485</sup>. Disputes around the role of IKKε in IRF3 activation likely stem from differential expression of IKKε between non-immune cell types. However, as IKKε is upregulated as quickly as 1 hour during infection with RNA virus SeV in embryonic fibroblasts and A549 cells<sup>169,486</sup>, it can contribute to signalling in cells where it is undetectable in the absence of stimulation. In our system, IKKε fully activates IRF3 in the absence of TBK1, supporting this. This in turn disputes previous studies showing that the requirement for IKKε in non-immune cells is either less significant or delayed compared to TBK1<sup>169,173,487,488</sup>.

We have also shown that TBK1 and IKKε are not required for the activation of NF-κB by RIG-I in A549 cells, supporting the majority of previous reports showing that TBK1 and IKKε play no role in NF-κB, or MAPK activation<sup>143,167,169,488</sup>. Interestingly, this differs from STING signalling, where TBK1 and IKKε function redundantly to activate NF-κB through activation of the IKK complex, despite the fact that TBK1 alone has been implicated in activation of IRF3<sup>146,488</sup>. We do not know why or how TBK1 is able to perform different functions downstream of different immune receptors, although it is also seen in TNFR signalling, where activated TBK1 phosphorylates RIP1 to prevent cell death activation<sup>333,456</sup>. The differing roles for TBK1 and IKKε in different immune signalling pathways shows that there is much we still do not know about the rules governing the recruitment, activation and regulation of TBK1 and IKKε, or the functional consequences of this.

### 4.6.4 The mechanism of recruitment and activation of TBK1 and IKKε at the RIG-I signalling complex in A549 cells remains unclear

Having already highlighted the importance of both TBK1 and IKKε for RIG-I-mediated IRF3 activation, understanding their recruitment to the signalling complex was important. Recruitment to activated signalling complex generally occurs through pre-association with multiple different adaptor proteins<sup>490</sup>, although the mechanism by which TBK1 and IKKε are recruited to MAVS remains unclear, with TRAF proteins, the TANK/NAP1/SINTBAD complex and optineurin all previously suggested to facilitate this process<sup>143,149,151,162,163,462,491</sup>. Despite attempts to examine the contribution

of the TANK/NAP1/SINTBAD complex, RIP1 and Optineurin to recruitment and activation of TBK1 and IKK $\epsilon$  to RIG-I signalling in A549 cells, we remain unable to conclusively describe the mechanism by which this occurs.

Our data indicated that none of TANK, NAP1 and SINTBAD, RIP1 or optineurin were solely required for the recruitment of both TBK1 and IKK $\epsilon$  to the RIG-I signalling complex. For TANK, NAP1 and SINTBAD, this disputes previous studies demonstrating their individual requirement for RIG-I-driven IFN induction in HEK293T and HeLa cells, mediated by the recruitment of TBK1 and IKK $\epsilon$ <sup>151–153</sup>. However, others have shown that HEK293T cells lacking all three components have unimpaired IFN-I induction in response to RNA virus infection<sup>143</sup>. Our detection of a small defect in IRF3 phosphorylation in cells lacking this complex may suggest they do play a role in the recruitment of either or both TBK1 and IKK $\epsilon$ , albeit redundantly.

Optineurin, which shares the TBK1 interaction domain found in TANK, NAP1 and SINTBAD, was identified as a TBK1 binding partner by yeast 2-hybrid screens<sup>155,156</sup>. However, its role in RIG-I has been much disputed, as it was initially described to initiate the trans-activation of TBK1 after RIG-I activation<sup>162,163,491</sup>, but more recently has been shown to dampen RIG-I-driven NF- $\kappa$ B and IRF3 activation<sup>157,158</sup>. As signalling outcomes in response to loss of optineurin expression vary between cell lines, this is likely to be cell-type specific. As well as TBK1 recruitment, optineurin has also been implicated in its activation, binding to ubiquitinated TBK1 to promote its trans-autophosphorylation in OPTN-TBK1 complexes found at the Golgi<sup>158,162,164</sup>. Our data neither confirms or rules out a role for optineurin in RIG-I-mediated TBK1 recruitment and activation.

Furthermore, our data points to a requirement for RIP1 in the activation of IRF3 and IFN-I transcription, but not TBK1 activation or ISG transcription by RIG-I. The requirement of RIP1 for IFN induction supports previous studies showing that it acts as a signalling enhancer for IFN-induction during RIG-I signalling, recruited to MAVS complexes during RNA virus infection<sup>467,470,492</sup>. However, the reason why RIP1 was not required for the transcription of ISGs is unclear. This inconsistent phenotype and the conflicting literature surrounding the role of RIP1 in RIG-I signalling may be caused by how RIP1-mediated negative regulation of RIG-I signalling, where its cleavage by caspase 8 results in inhibition of signalling<sup>142,492</sup>. Despite this, our data suggests that RIP1 may play a role in the recruitment of activated TBK1 to the signalling complex, which is further supported by the fact that RIP1 is not required for activation of NF- $\kappa$ B, a process that is also independent of TBK1 and IKK $\epsilon$ .

The importance of TRAF proteins in RIG-I signalling is well characterised, with roles in activation of IRF3 and NF- $\kappa$ B previously described<sup>135,137,138,140,141</sup>, both requiring the generation of K63-linked

ubiquitin chains<sup>144-147</sup>. However, some level of redundancy between TRAF2, 3 and 5 for IFN-I activation is evident<sup>135,142,143</sup>. Despite this, attempts were made to examine the role of TRAF proteins in RIG-I signalling using TRAF2-deficient A549 cells generated in the lab of Henning Walczak (University of Cologne). However, multiple attempts to grow up the cells from multiple batches of frozen stocks failed, possibly suggesting that loss of TRAF2 is toxic to these cells.

As there was no clear phenotype in any of our adaptor protein knockout cell lines, as was seen in cells lacking both TBK1 and IKK $\epsilon$ , we suggest that TBK1 and IKK $\epsilon$  are likely recruited to RIG-I by different mechanisms. In systems where TBK1 and IKK $\epsilon$  function redundantly, unless a single adaptor protein or protein complex is solely required for the recruitment of both proteins, the phenotype seen in cells lacking that adaptor would be masked, as a lack of recruitment of either protein would be compensated for by the activity of the other. The redundant function of TBK1 and IKK $\epsilon$  in our system suggests that they are recruited to the RIG-I signalling complex by different mechanisms, explaining the modest phenotypes seen in cells lacking TANK/NAP1/SINTBAD, RIP1 and OPTN. Previous data also suggests this is the case, with studies showing that optineurin binds TBK1 but not IKK $\epsilon$ <sup>155,156</sup>, and that IKK $\epsilon$  but not TBK1 can be recruited directly to MAVS via K63 chains conjugated to MAVS<sup>159</sup>. This is further supported by visualisation of IKK $\epsilon$  and TBK1 in distinct subcellular locations during RNA virus infection<sup>486</sup>.

The biological significance of the differing mechanisms for recruitment of TBK1 and IKK $\epsilon$  to other signalling pathways may relate to the roles of the proteins within each specific signalling pathway. The substrate specificity of TBK1 is at least partially determined by proximity<sup>493</sup>, suggesting that its function is decided by the other proteins in the signalling complex. However, it may also be determined by the adaptor protein that recruits TBK1/IKK $\epsilon$  to the signalling complex. For example, in TNF-receptor signalling, TBK1 is predominantly recruited by the TANK/NAP1/SINTBAD complex and acts to phosphorylate RIPK1, but not IRF3, despite the fact that it is phosphorylated at the same residue to become active<sup>333,494,495</sup>, resulting in differing signalling outcomes than if IRF3 was activated. During intracellular DNA sensing, STING directly recruits TBK1 through a specific interaction between the C-terminal tail of STING and the kinase domain of TBK1<sup>496</sup>. TBK1 then not only directly activates IRF3, but also activates NF- $\kappa$ B redundantly with IKK $\epsilon$ <sup>146,489</sup>, not seen during RIG-I signalling. Using distinct mechanisms of recruitment of TBK1 and IKK $\epsilon$  would be advantageous as it would make it more difficult for viruses to inhibit the activation of IRF3, requiring the antagonism of multiple mechanisms to prevent TBK1 recruitment to signalling complexes.

Although many different mechanisms of TBK1 recruitment have been proposed and are evident in different signalling pathways, one unifying factor is the ubiquitin binding capacity of the adaptor proteins, including NEMO, SINTBAD, NAP1 and OPTN496–498. Ubiquitin chains form a recruitment platform for TBK1 in many signalling pathways and their presence at the RIG-I signalling complex could enable recruitment of multiple of these adaptor proteins, supporting our suggestion for redundant methods of TBK1 and IKKε recruitment. Together with our data, this supports a role for any or all of the TANK/NAP1/SINTBAD complex, RIP1 and optineurin in the recruitment of TBK1/ IKKε to MAVS during RIG-I signalling.

#### **4.6.5 How a better insight into the RIG-I signalling complex helps us study the contribution of LUBAC to RIG-I signalling**

As well as adding new information about how RIG-I signalling functions, the work in this chapter has laid the foundations for examining how LUBAC and M1 ubiquitin chains interact with the rest of the RIG-I signalling complex, and how this contributes to signalling outcomes. The ‘clean’ system of RIG-I activation that we have allows us to confidently assign functional roles for each of these proteins. By generating and analysing LUBAC-knockout cell lines and comparing the phenotypes with those from this chapter, we will be able to determine where LUBAC fits in the pathway and to use a rational approach to find LUBAC binding partners and the targets of M1-linked ubiquitin chains.

Several of the proteins we studied have already been well characterised to interact with LUBAC, both downstream of RIG-I and in other immune signalling complexes. NEMO binds both LUBAC and M1-Ub chains, with the recruitment of NEMO to the RIG-I signalling complex previously shown to rely on its binding to ubiquitin chains synthesised by both TRAF proteins and LUBAC<sup>135,143</sup>. Additionally, optineurin’s previously described role in dampening RIG-I-driven NF-κB and IRF3 activation is facilitated by its interaction with LUBAC, sequestering LUBAC from signalling complexes<sup>157,158</sup>. Outside of RNA sensing, LUBAC is well characterised to interact with NEMO and RIP1 at the TNF-RSC<sup>500–502</sup>, both of which we suggest are involved in RIG-I signalling. This knowledge we have gained about how proteins known to interact with LUBAC function within RIG-I signalling is vital for helping us define how LUBAC contributes to the signalling complex and its outcomes.

### **4.7 Conclusion**

Through the generation of a ‘clean’ system for RIG-I activation, we have been able to use knockout cell lines to determine the specific function of several proteins in RIG-I signalling. Based on this and previous literature, we propose a mechanism by which RIG-I drives activation of both IRF3 (Figure

4.7.1) and NF- $\kappa$ B (Figure 4.7.2). We have shown that in A549 cells, regardless of the ligand that is used to stimulate RIG-I, activation of NF- $\kappa$ B requires the presence of both MAVS and NEMO, but not TBK1, IKK $\epsilon$ , TANK/NAP1/SINTBAD, RIP1 or Optineurin. Activation of IRF3 and the resultant IFN-I signalling required expression of MAVS, NEMO and either TBK1 or IKK $\epsilon$ . The mechanism by which TBK1 and IKK $\epsilon$  are recruited to the complex remains inconclusive, although we suggest that the TANK/NAP1/SINTBAD complex, RIP1 and optineurin may play a role, although both proteins appear not to be recruited by the same mechanism. Better characterisation of the RIG-I signalling pathway in our system gives us a platform from which to examine how LUBAC and M1-ubiquitin chains regulate it.

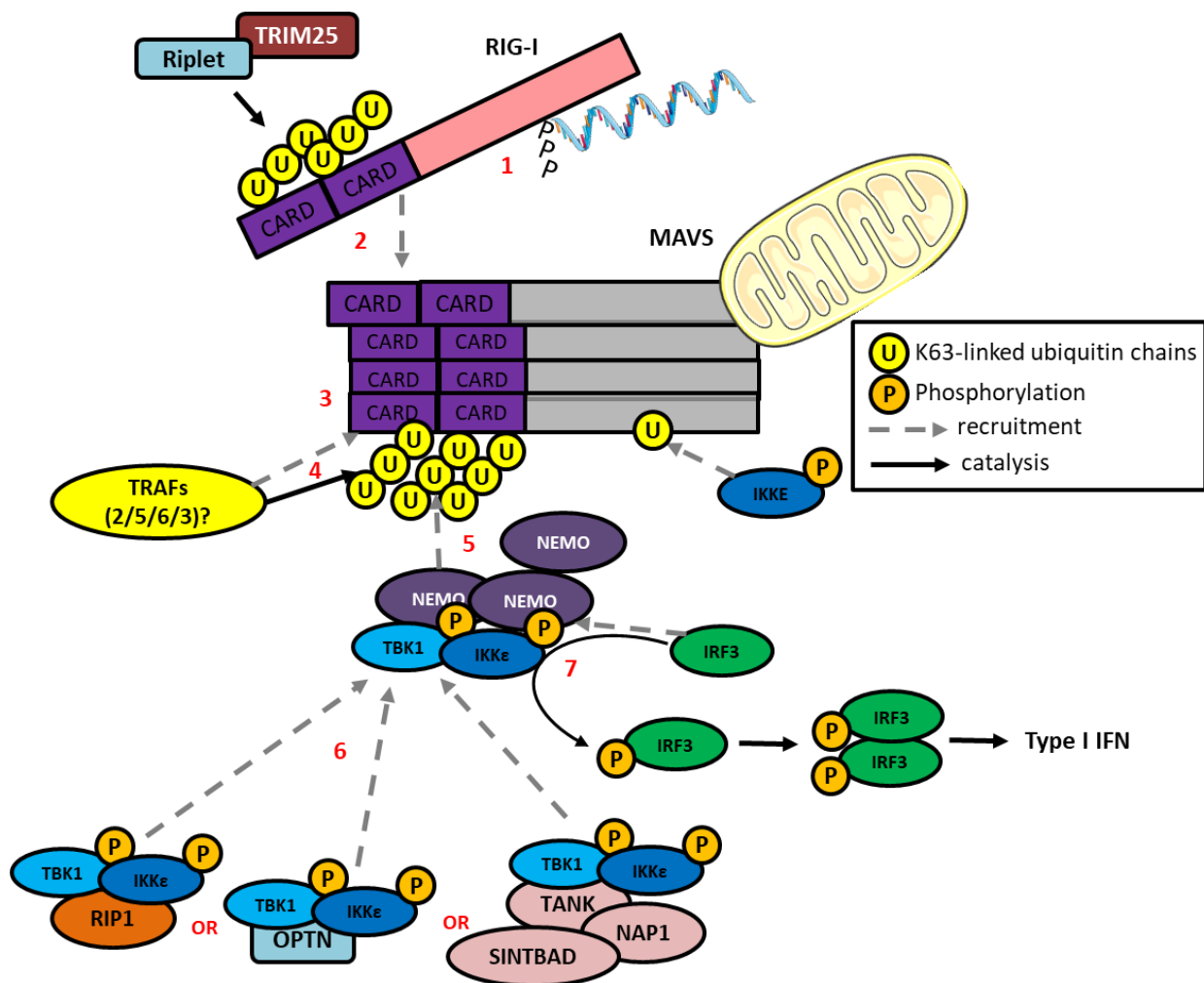


**Figure 4.7.1: Schematic of the mechanism of IRF3 activation by RIG-I**

1. RIG-I binds to RNA with 5' ppp and regions of double-stranded secondary structure
2. This alongside ubiquitination of RIG-I CARD domains by Riplet and TRIM25 activates RIG-I CARD, which is recruited to MAVS at the mitochondrial outer membrane
3. Activation of MAVS by RIG-I (and a wealth of other modifications) causes oligomerization of MAVS via the CARD domain
4. TRAF proteins are recruited to MAVS, where they add K63 ubiquitin chains to the CARD domain of MAVS oligomers

5. NEMO is recruited by binding K63 ubiquitin chains
6. Pre-activated TBK1 and IKKε are recruited to the signalling complex via distinct mechanisms, likely involving the TANK/NAP1/SINTBAD complex, RIP1 and optineurin, or direct recruitment of IKK ε to ubiquitinated MAVS
7. IRF3 is recruited to the signalling complex, and once in proximity with activated TBK1/IKKε, is phosphorylated, inducing dimerization, translocation to the nucleus and activation of an IFN-I response

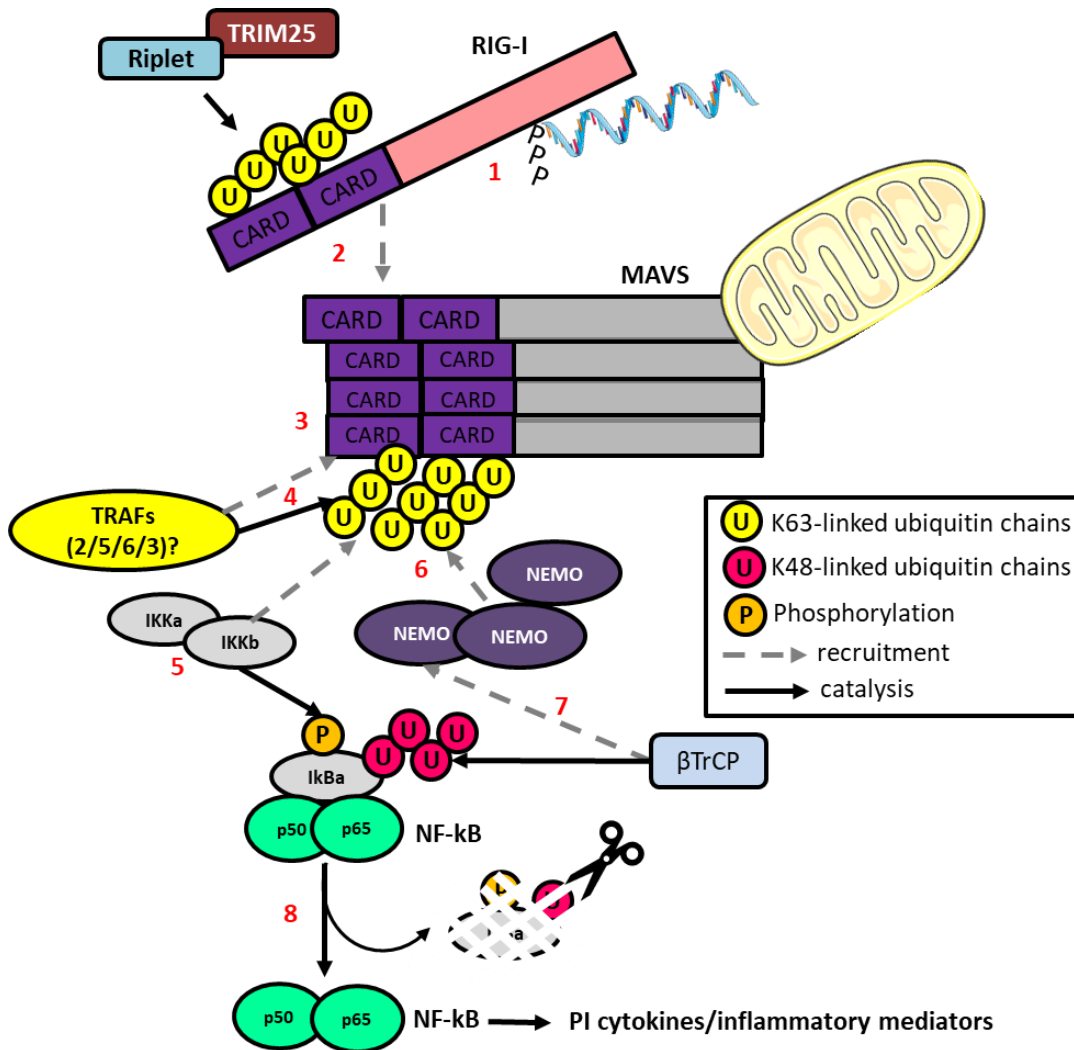


**Figure 4.7.2: Schematic of the mechanism of NF-κB activation by RIG-I**

1. RIG-I binds to RNA with 5'ppp and regions of double-stranded secondary structure
2. This alongside ubiquitination of RIG-I CARD domains by Riplet and TRIM25 activates RIG-I CARD, which is recruited to MAVS at the mitochondrial outer membrane
3. Activation of MAVS by RIG-I (and a wealth of other modifications) causes oligomerization of MAVS via the CARD domain
4. TRAF proteins are recruited to MAVS, where they add K63 ubiquitin chains to the CARD domain of MAVS oligomers
5. IKKα and β are recruited to the signalling complex, where IKKβ phosphorylates IκBα to initiate its degradation

6. NEMO is recruited by binding K63 ubiquitin chains on MAVS
7. NEMO recruits the E3 ligase SCF- $\beta$ TrCP and the proteasomal degradation machinery to the signalling complex, where it ubiquitinates I $\kappa$ B $\alpha$ , inducing its degradation by the 26S proteasome
8. NF- $\kappa$ B subunits are released to translocate into the nucleus to activate transcription of pro-inflammatory responses

# Chapter Five: HOIP is required for RIG-I-driven immune responses

---

## 5.1 Introduction

LUBAC is critical to regulating many signalling pathways, including those involved in development, immune responses to infection and cell death activation<sup>503</sup>. In these pathways, it is well characterised to drive activation of NF- $\kappa$ B and induction of pro-inflammatory mediators, as well as restrict the activation of a multitude of cell death pathways. In RNA sensing pathways, LUBAC is required for activation of NF- $\kappa$ B and IFN by both TLR3 and MDA5<sup>432,504</sup>, controlling virus levels and preventing cell death by forming a crucial part of the TLR3 signalling complex. However, previous studies exploring the role of HOIP in RIG-I signalling have yielded highly conflicting conclusions, with results suggesting that HOIP is required for, restricts, or has no effect on RIG-I-driven immune responses<sup>213,432,504–506</sup>. Data surrounding the influence of HOIP on virus infection and RIG-I-driven cell death is also inconsistent.

In this chapter, we studied the role of HOIP in RIG-I signalling, examining how it regulates the RIG-I signalling pathway and its outcomes, as well as monitoring its effects on the kinetics of virus infection and RIG-I-driven cell death. To address this, we used A549 cells deficient in HOIP, and cells stably expressing either a tagged WT or catalytic mutant of HOIP. Cells were stimulated with synthetic RNAs, 3p-hpRNA and Poly(I:C), and RNA viruses, SeV, IAV R+K and ZIKV PE243. The effect of HOIP on RIG-I-driven antiviral signalling was analysed by multiple techniques: qPCR to measure transcription of genes previously shown to be activated by RIG-I in response to the chosen ligand; Western blotting and phos-flow to assess the activation of signalling pathway components; and ELISA to measure secretion of chemokines. qPCR and Western blotting were also used to measure viral gene transcription and protein expression, which alongside growth curve analyses quantifying viral replication, formed a picture of the effect of HOIP on virus infection kinetics. Cell death was measured using flow cytometry analysis of caspase 3 activation and a Nucleocounter vitality assay.

We demonstrate that HOIP is required for efficient RIG-I-driven transcription, signalling pathway activation and chemokine secretion, for all tested methods of RIG-I activation. Despite this, and its apparent influence on viral transcription, HOIP appeared to have minimal effect on viral protein expression or virus replication and did not affect RIG-I-driven cell death, which was not detected in this system.

## 5.2 Determining the best system to study the role of HOIP in RIG-I signalling

### 5.2.1 Overexpression of LUBAC components in HEK does not affect the immune response to SeV

Many studies exploring LUBACs role in signalling pathways have utilised exogenous protein expression techniques. First used to demonstrate LUBACs role in immune signalling, overexpression of HOIP and either HOIL or SHARPIN was shown to enhance TNF- and CD40-mediated NF- $\kappa$ B activation<sup>507,508</sup>. However, overexpression of HOIP and HOIL-1 during RIG-I activation has been shown to reduce IFN-I and NF- $\kappa$ B activation<sup>213,505,509</sup>, indicating that LUBAC may negatively regulate RIG-I signalling.

In an attempt to replicate these previous studies, LUBAC components HOIP and HOIL were overexpressed in HEK 293T cells for 24 hours, followed by a 16-hour infection with SeV. Western blotting confirmed the presence of overexpressed HOIP and HOIL-1 in these cells (Figure 5.2.1A), known to be sufficient to generate M1-Ub chains<sup>510</sup>. However, qPCR analysis detected no significant effect of HOIP or HOIL overexpression on transcription of *IFNB1* or *CXCL10* (Figure 5.2.1B). Transcription of both genes was reduced during overexpression of HOIP and HOIL-1, but this also occurred after transfection with an empty expression plasmid, suggesting their reduced transcription was likely caused by the burden of DNA plasmid expression on the cells, rather than the proteins themselves. Generally, expression of HOIP and HOIL together lead to an increase of *IFNB1* and *CXCL10* transcription after SeV infection, but this was not consistent across the two genes, or experimental repeats, unlike previously described<sup>507,508</sup>. These inconclusive findings, as well as the conflicting literature, suggest that overexpression systems are not a good model to study the role of LUBAC in RIG-I signalling.

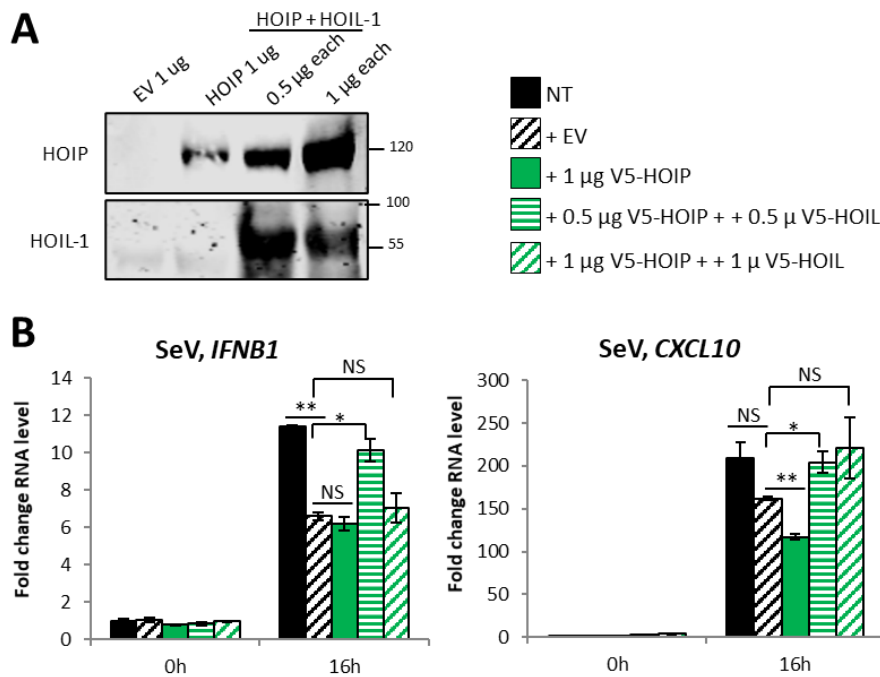


**Figure 5.2.1: Reproducing previous LUBAC-overexpression experiments in HEK293T cells**

A) Western blotting of HEK293T cells transfected with an empty pcDNA4 plasmid (EV), and either 0.5 or 1 μg overexpression plasmids with V5 tagged HOIP and HOIL-1 (data representative of 2 independent assays). B) qPCR to measure transcription of *IFNB1* and *CXCL10* in HEK293T cells after 24 hours of transfection with the plasmids and a subsequent 16-hour infection with SeV at a 1:100 dilution (n=2, data representative of 2 independent assays).

## 5.2.2 Use of HOIP-deficient A549 cells to study the role of LUBAC in RIG-I signalling

Instead, HOIP-deficient (HOIP<sup>-/-</sup>) A549 cells generated using a lentiviral CRISPR system in the lab of Henning Walczak (University of Cologne)<sup>334</sup>, were used to study the role of HOIP in RIG-I signalling. To demonstrate that any phenotype seen in HOIP<sup>-/-</sup> cells was due to loss of HOIP expression alone, knockout cells were reconstituted by lentiviral expression of a TAP-tagged HOIP construct (TAP-HOIP-WT), resulting in stable expression of TAP-HOIP.

Expression of LUBAC components was analysed by Western blotting in WT, HOIP<sup>-/-</sup> and TAP-HOIP-WT cells (Figure 5.2.2), confirming that HOIP could be detected in WT cells, its expression was lost in HOIP<sup>-/-</sup> cells, and TAP-HOIP-WT cells were found to express higher than WT levels of HOIP. Unlike previous studies<sup>213,503,505,506</sup>, loss of HOIP expression in HOIP<sup>-/-</sup> did not result in reduced levels of HOIL-1 or SHARPIN but conversely, over-expression of HOIP in TAP-HOIP-WT cells did result in higher HOIL-1 and SHARPIN expression. This may be due to more HOIP enabling increased incorporation of HOIL and SHARPIN into LUBAC complexes, as has been previously

described<sup>338,510</sup>. As HOIL and SHARPIN transcription was not examined, we cannot say whether this increase at the protein level was due to increased transcription, or increased protein stability.

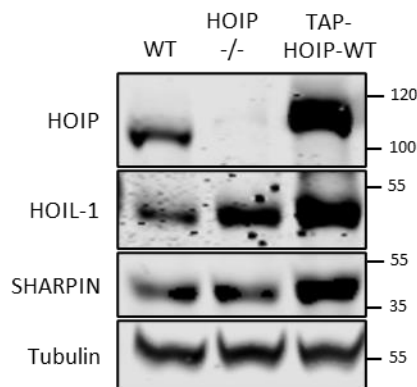


**Figure 5.2.2: Characterisation of A549 HOIP <sup>-/-</sup> and +TAP-HOIP-WT cells**

Western blotting to show presence of LUBAC components in resting A549 WT, HOIP <sup>-/-</sup> and TAP-HOIP-WT cells (data representative of 2 independent assays).

## 5.3 HOIP is required for RIG-I-driven transcription of antiviral genes

### 5.3.1 HOIP is required for efficient transcription of IFN-I, ISGs and chemokines in response to 3p-hpRNA and Poly(I:C) stimulation

The only synthetic RNA previously used in studies exploring the role of HOIP in RNA sensing is Poly(I:C)<sup>432,504</sup>. Although MDA5 and TLR3 were implicated the sensing of Poly(I:C) in these studies, collectively they demonstrated that HOIP is required for Poly(I:C) driven signalling, with loss of HOIP expression resulting in reduced NF- $\kappa$ B, IFN-I and chemokine activation. To examine the requirement of HOIP for synthetic RNA-induced RIG-I-driven immune gene transcription in our system, A549 WT, HOIP <sup>-/-</sup> and TAP-HOIP-WT cells were stimulated by transfection of 3p-hpRNA and Poly(I:C) and transcription was measured by qPCR.

When stimulated with 3p-hpRNA, HOIP <sup>-/-</sup> cells showed significantly reduced transcription of *CXC10*, *ISG15* and *ISG54* in comparison to WT cells (Figure 5.3.1A). Re-expression of HOIP in knockout cells rescued the transcription of both *IFNB1* and *CXCL10*, with TAP-HOIP-WT cells expressing higher levels of both genes than WT cells (Figure 5.3.1B), suggesting that elevated levels of HOIP enhanced RIG-I activation. This conflicts with data from HEK293T overexpression experiments (Figure 5.2.1B) but is consistently true for stable HOIP overexpression in A549 cells with multiple stimulation methods.

Stimulation of A549 WT and HOIP <sup>-/-</sup> cells with Poly(I:C) yielded similar results, with transcription of *IFNB1*, *IFNL1*, *CXCL10* and *ISG15* significantly lower in HOIP-deficient cells (Figure 5.3.1C). Although

*ISG54* transcription was more variable, HOIP  $-/-$  cells consistently expressed similar or higher levels of *ISG54* transcripts than WT cells, a phenotype only seen with Poly(I:C) and one which we cannot explain. Again, stable re-expression of HOIP resulted in similar or higher levels of transcription of both *IFNB1* and *CXCL10* than in WT cells (Figure 5.3.1D).

These data demonstrate that HOIP is required for the efficient RIG-I-driven transcription of IFN-I, IFN-III and ISGs after stimulation with synthetic RNAs.

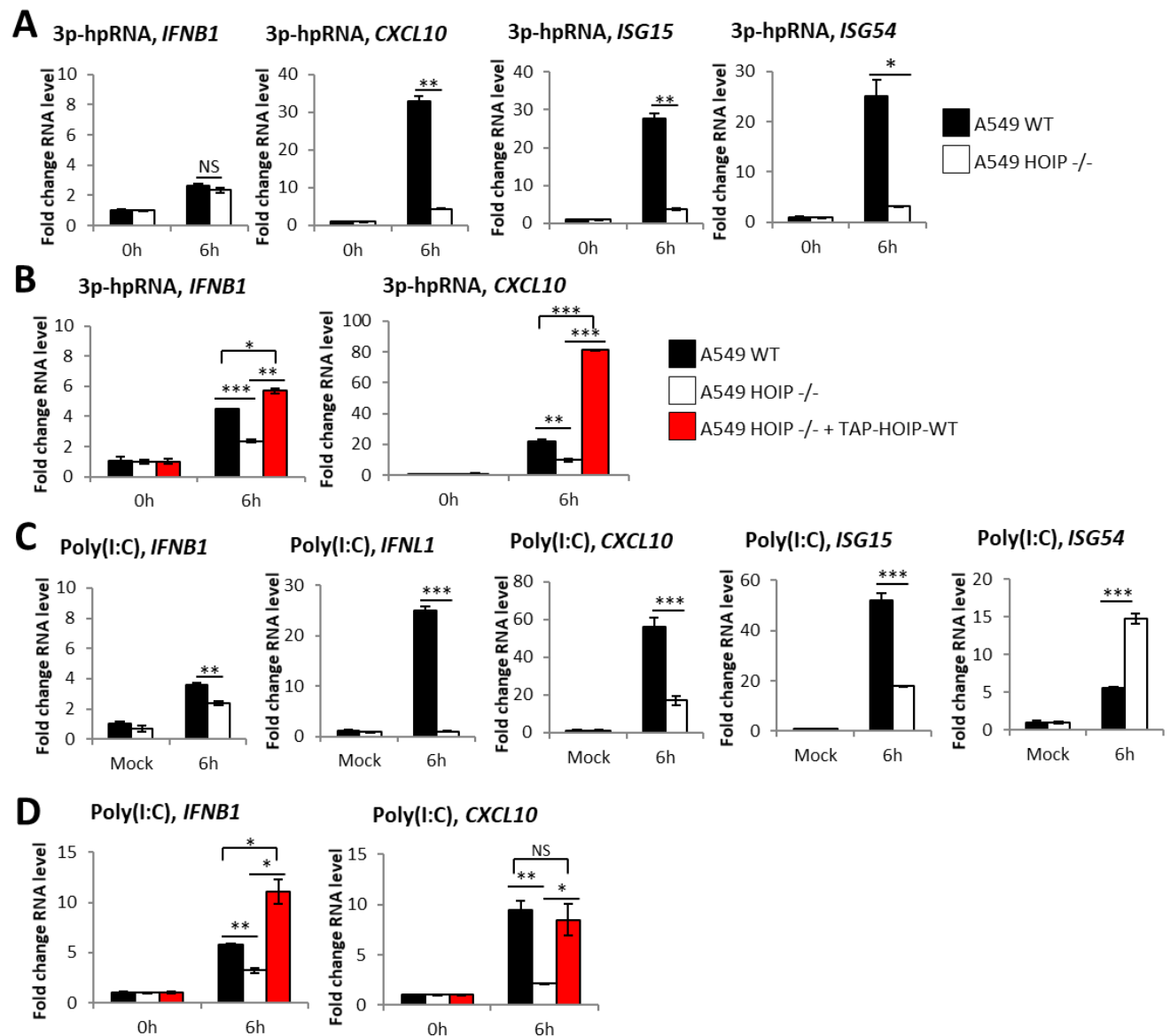


**Figure 5.3.1: RIG-I-driven expression of immune genes in response to synthetic RNAs is dependent on HOIP** qPCR to measure transcription of indicated genes in response to stimulation with A) 1  $\mu$ g 3p-hpRNA in A549 WT and HOIP  $-/-$  cells (n=2, data is representative of >3 independent assays), B) 1  $\mu$ g 3p-hpRNA in A549 WT, HOIP  $-/-$  and HOIP  $-/-$  + TAP-HOIP-WT (TAP-HOIP-WT) cells (n=2, data representative of 2 independent assays), C) 1  $\mu$ g Poly(I:C) in A549 WT and HOIP  $-/-$  cells (n=2, data is representative of >3 independent assays) and D) 1  $\mu$ g Poly(I:C) in A549 WT, HOIP  $-/-$  and TAP-HOIP-WT cells (n=2, data representative of 2 independent assays).

### 5.3.2 HOIP is required for efficient transcription of IFN-I, IFN-III, NF- $\kappa$ B-dependent genes and chemokines in response to SeV infection

As viruses like SeV are capable of activating a broader measurable immune response, the effect of HOIP on RNA virus-driven transcription was also studied. Only one previous study has explored the role of HOIP during SeV infection<sup>213</sup>, but multiple studies have used other RNA viruses such as VSV and IAV135,505. In this previous study, knockdown of HOIP in MEF cells had little effect on SeV-driven IFN $\beta$  expression, although did increase the ubiquitination of RIG-I and its consequent binding to TRIM25<sup>213</sup>.

In our system, SeV-induced transcription of IFN-I and IFN-III, ISGs, chemokines and NF- $\kappa$ B-dependent genes was reduced in HOIP  $-/-$  cells (Figure 5.3.2A), with the reduction even more marked than that seen with synthetic RNAs. Again, re-expression of HOIP resulted in similar or higher levels of *IFNB1* and *CXCL10* transcription than seen in WT cells (Figure 5.3.3B).

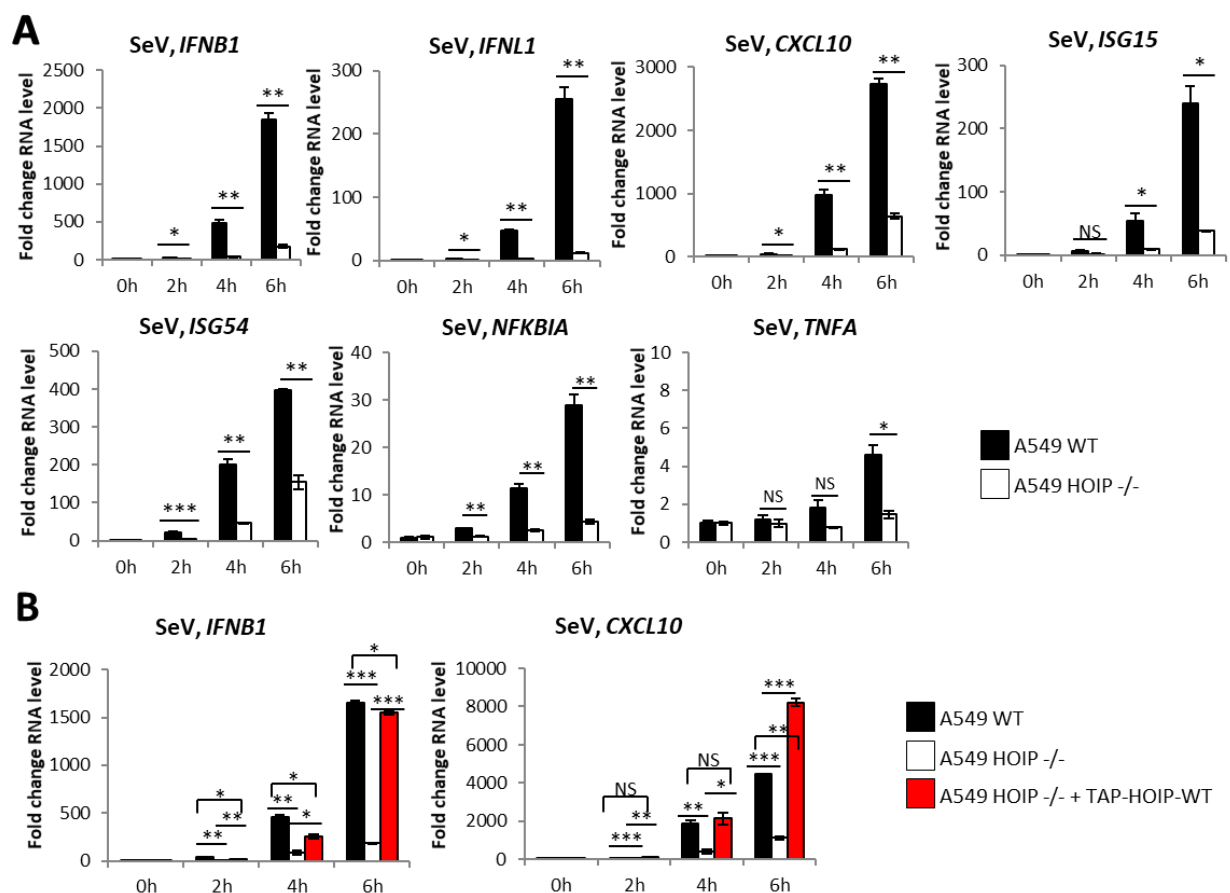


**Figure 5.3.2: RIG-I-driven expression of immune genes in response to SeV infection is dependent on HOIP** qPCR to measure transcription of indicated genes in A) A549 WT and HOIP  $-/-$  and B) A549 WT, HOIP  $-/-$  and TAP-HOIP-WT cells during SeV infection at 1:300 dilution (both n=2, data representative of >3 independent assays).

### 5.3.3 HOIP is required for efficient transcription of IFN-I, ISGs and chemokines in response to IAV R+K infection

The role of HOIP during infection with the replication competent RNA virus IAV, was also studied. HOIP has previously been shown to be required for the IAV-driven response in A549 cells and *in vivo*, with loss of HOIP in alveolar stem cells shown to result in reduced transcription of *Ifnb1*, *Il6* and *Mcp1* compared to WT stem cells during IAV WSN infection<sup>506</sup>.

Here, A549 WT and HOIP *-/-* cells were infected with IAV PR8 NS1 R+K and transcription was measured using qPCR (Figure 5.3.3A). The robust upregulation of *IFNB1*, *CXCL10*, *ISG15* and *ISG54*, seen in WT cells was significantly reduced in HOIP *-/-* cells in several experiments (Figure 5.3.3A). However, the data was not always consistent, with differing signalling outcomes shown in Figure 5.3.3B. To understand the cause of this variation, transcription of early expressed IAV gene *NS1* was measured for each experiment (Figure 5.3.3B). When *NS1* transcripts were less abundant in HOIP *-/-* cells, they also expressed much lower levels of *IFNB1* and *CXCL10* transcripts, whereas when *NS1* transcripts were much higher in HOIP *-/-* cells than WT, transcription of *IFNB1* and *CXCL10* was unaltered by loss of HOIP expression. Varied signalling outcomes is likely caused by uneven infection kinetics between replicate experiments, captured by *NS1* transcriptional data. Induction of IFN-I and chemokine transcription in these cells correlates with the level of viral RNA in the cells, but despite this viral RNA does appear to induce a less potent immune response in HOIP *-/-* cells.

To explore whether variable *NS1* transcription was due to unequal infection between cell lines, attempts were made to measure replication of IAV NS1 R+K in WT and HOIP *-/-* cells by plaque assay. However, IAV R+K did not replicate in A549 cells, possibly because the mutant virus is incapable of suppressing the RIG-I-driven immune response in these cells (Figure 5.3.3C). Because of this, IAV PR8 was used, which did replicate at low levels in both A549 WT and HOIP *-/-* cells (Figure 5.3.3D). In this assay, loss of HOIP had no effect on viral replication, possibly because the RIG-I-driven immune response is already impeded by the IAV NS1 protein in WT cells, so the reduction in RIG-I-driven transcription seen in HOIP *-/-* cells would have no effect, or because the cells were infected at too high a MOI to enable sufficient replication to see a phenotype.

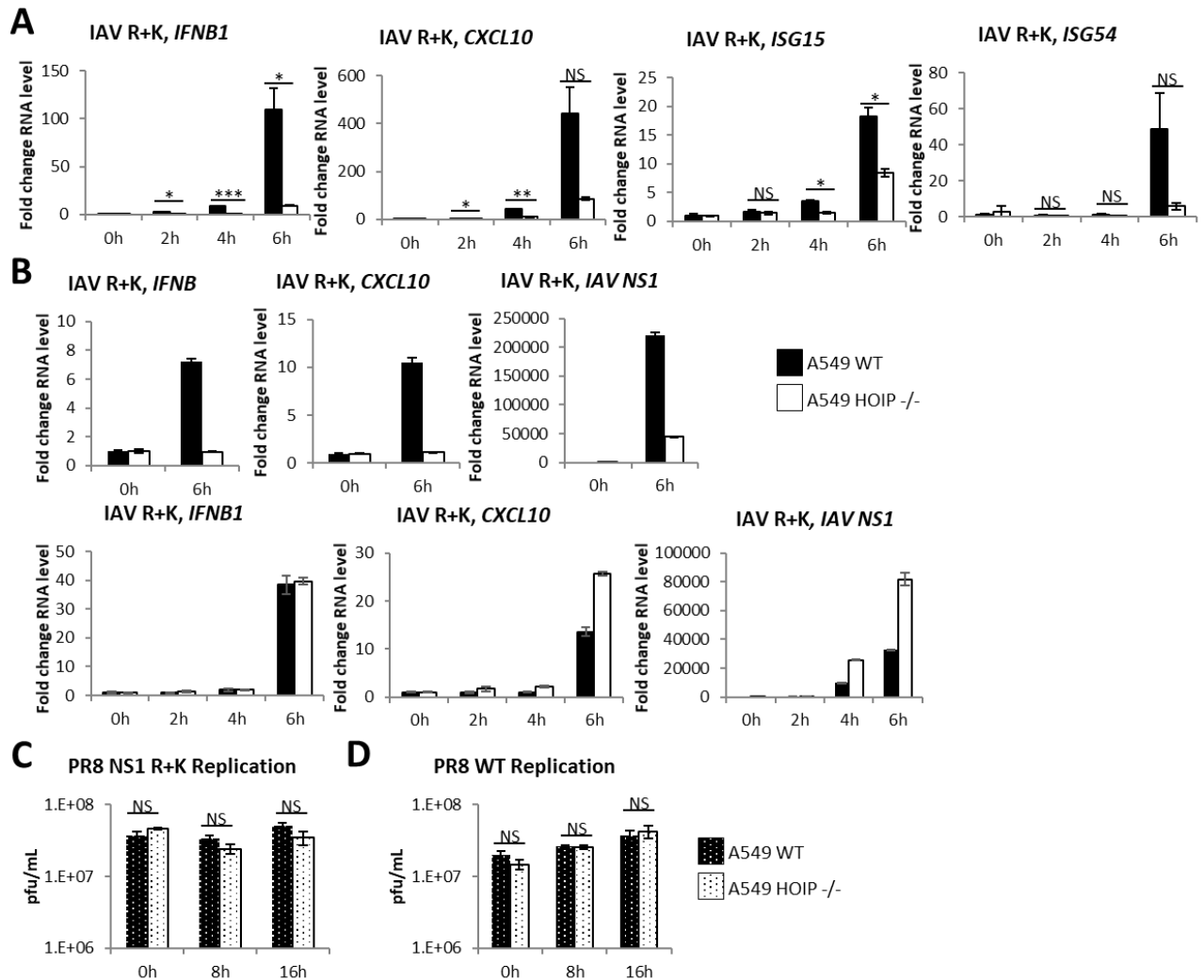


**Figure 5.3.3: HOIP may contribute to innate immune sensing of IAV**

qPCR to measure transcription of indicated genes in A549 WT and HOIP<sup>-/-</sup> cells during IAV R+K infection at MOI 3 A) (n=2, data representative of >3 independent assays) and B) (n=2, two datasets shown are examples of variability of results). C and D) Replication of IAV NS1 R+K and PR8 WT, growth curves analysis generated by titration of lysates on Vero cells followed by plaque assay. (n=2, data representative of 2 experimental repeats).

### 5.3.4 HOIP is required for efficient transcription of IFN-I, IFN-III, ISGs and chemokines during to ZIKV infection

Because the data generated by IAV infection was inconsistent, we used ZIKV infection to study the impact of HOIP on the infection kinetics of and immune response to a replicating RNA virus in our system.

A549 WT and HOIP<sup>-/-</sup> cells were infected with ZIKV and the transcription of genes previously upregulated at 16 and 24 hours post ZIKV infection (Figure 3.3.4) were analysed by qPCR. As the transcription of most genes was RIG-I-independent by 48 hours post infection (Figure 3.4.6A), cells

were only infected for 24 hours. Transcription of all genes was significantly reduced in HOIP *-/-* cells at both 16 and 24-hours post infection, with transcription of *IFNB1*, *IFNL1*, *CXCL10* and *ISG54* in HOIP *-/-* cells barely detectable above background levels. *ISG15* was still strongly expressed in the absence of HOIP, but still significantly less than in WT cells, together showing that HOIP is required for the RIG-I-driven transcriptional response to ZIKV.

As with IAV, ZIKV transcription was measured by qPCR. Figure 5.3.4B shows the location of the primer pairs targeted to both the ORF (open reading frame) region and 3'UTR (untranslated region) of the ZIKV genome, mapped against the polyprotein and mature proteins. Transcription of both regions of the ORF and 3'UTR was not significantly different between WT and HOIP *-/-* cells at 16 hours post infection but was transcribed to a much higher level WT cells by 24 hours (Figure 5.3.4C), mimicking what was seen most frequently during IAV infection (Figure 5.3.3B). The level of ORF transcripts was significantly lower than UTR transcripts, likely due to the degradation of the ZIKV RNA by cellular exonucleases<sup>512</sup>, from which the 3'UTR is protected due to secondary RNA pseudoknot structures that accumulate during infection<sup>513</sup>. Conversely, expression of the ZIKV protein analysed by Western blotting was consistent between WT and HOIP *-/-* cells at all time points (Figure 5.3.4D). Similarly, a single-step analysis of ZIKV replication using a plaque assay showed that HOIP expression did not affect ZIKV replication (Figure 5.3.4E).

From this we suggest that measuring transcription is a poor technique to study viral infection, as measures of viral protein expression and replication show consistency between the cell lines and between experimental repeats.

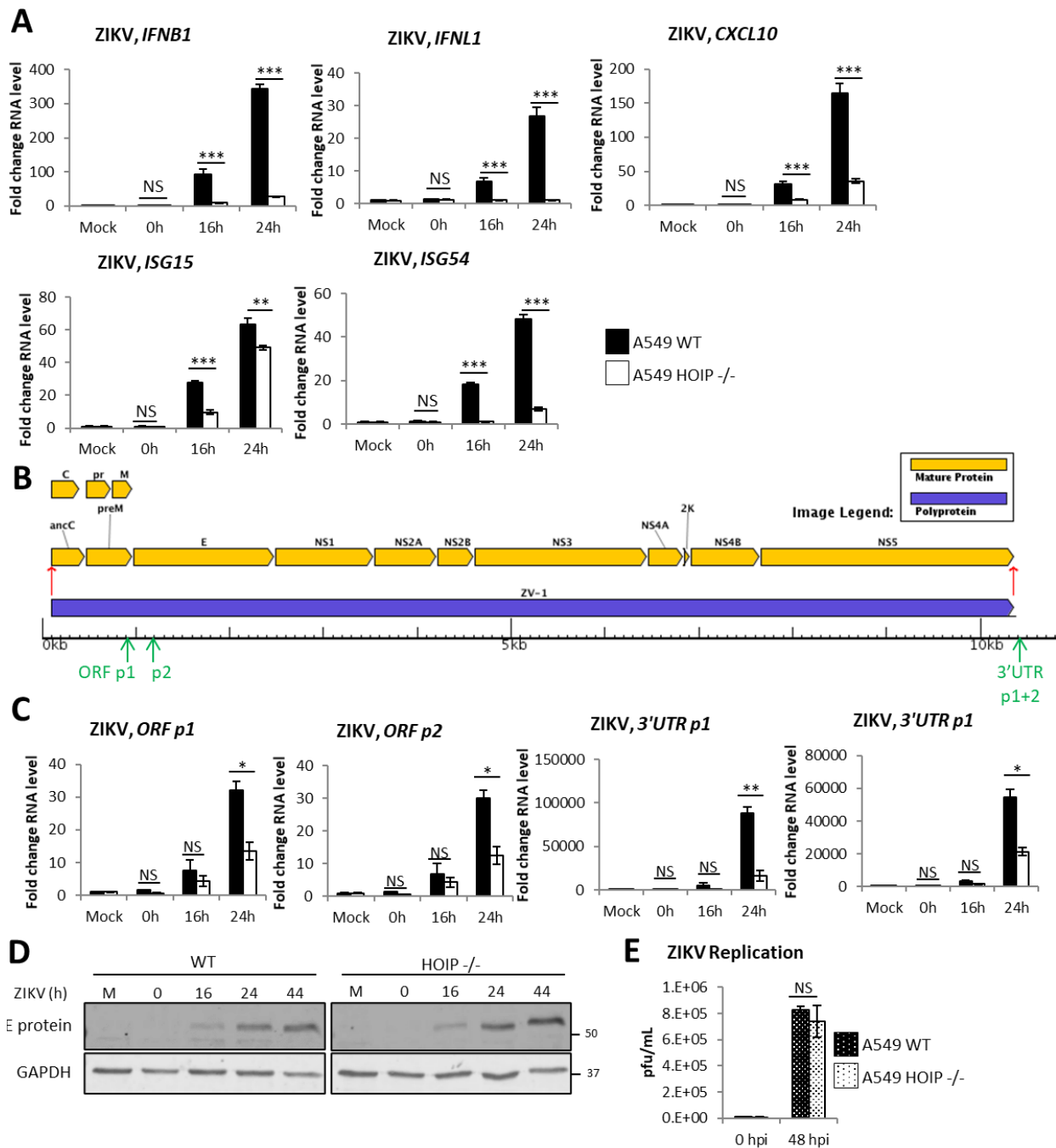


**Figure 5.3.4: RIG-I-driven expression of immune genes in response to ZIKV infection is dependent on HOIP**  
 A) qPCR to measure transcription of indicated genes during ZIKV PE243 infection A549 WT and HOIP  $-/-$  cells at MOI 3 (n=3, data representative of 3 experimental repeats). B) Schematic representation of location of primers targeting ZIKV polyprotein region for qPCR. C) qPCR to measure transcription of ZIKV ORF and 3'UTR during ZIKV PE243 infection A549 WT and HOIP  $-/-$  cells at MOI 3 (n=2, data representative of 2 independent assays). D) Western blotting analysis of ZIKV E protein during infection A549 WT and HOIP  $-/-$  cells with ZIKV PE243 at MOI 3, done by Dr Nerea Irigoyen and Charlotte Lefevre (data representative of 2 independent assays). E) ZIKV PE243 growth curve generated by titration and plaque assay, done by Dr Nerea Irigoyen and Charlotte Lefevre. (n=2, data representative of 2 experimental repeats).

## **5.4 HOIP is required for activation of RIG-I signalling pathway components**

We have found HOIP to be required for efficient transcription of all studied genes. Transcription of these genes requires activation of both IRF3 and NF- $\kappa$ B, suggesting that HOIP regulates both of their activation. To investigate this, we measured the activation of signalling pathway components TBK1, IRF3 and I $\kappa$ B $\alpha$ , all of which undergo phosphorylation during IRF3 and NF- $\kappa$ B activation, by both Western blotting and flow cytometry.

### **5.4.1 Western blotting analysis and phos-flow are not sensitive enough to provide insight into the role of HOIP in signalling pathway activation during stimulation with synthetic RNAs**

Only once has the requirement of HOIP for synthetic RNA-driven signalling protein phosphorylation been demonstrated<sup>432</sup>, with siRNA knockdown of HOIP in HaCaT cells stimulated with extracellular Poly(I:C) resulting in reduced TLR3-mediated phosphorylation of IRF3, I $\kappa$ B $\alpha$  and MAPK proteins ERK and JNK. In this study, we examined signalling protein phosphorylation in A549 WT and HOIP  $-/-$  cells stimulated by 3p-hpRNA and transfected Poly(I:C) by Western blotting (Figure 5.4.1).

Transfection of A549 WT cells with 3p-hpRNA and Poly(I:C) resulted in detectable phosphorylation of TBK1 and IRF3, but the weak expression of phospho-proteins, especially with 3p-hpRNA stimulation, means that we were unable to reliably differentiate between phosphorylation levels in WT and HOIP  $-/-$  cells. Phos-flow analysis could not be used to study the role of HOIP during stimulation with synthetic RNA ligands because, as previously shown (Figure 3.3.1D), there was no detectable increase in A549 WT cells expressing phosphorylated IRF3 after 6-hour stimulation with Poly(I:C). To be able to examine the effect of HOIP on activation of signalling pathway components during stimulation with synthetic RNAs, different model cell lines, further transfection optimisation or more sensitive analysis techniques would be required.

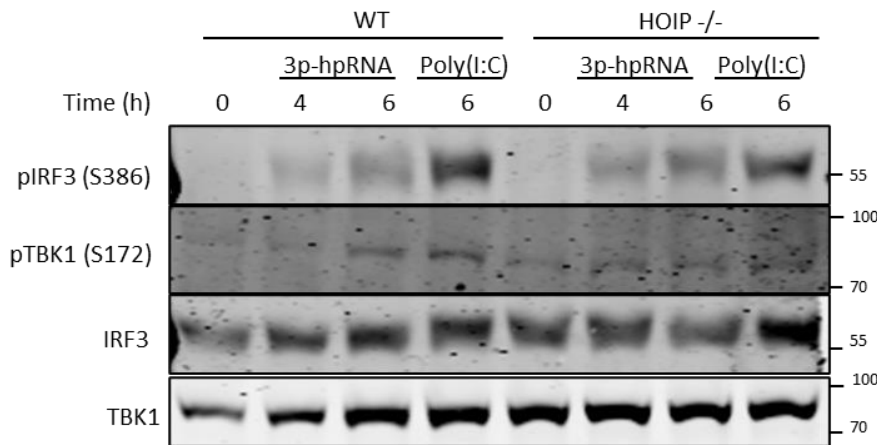


**Figure 5.4.1: Stimulation with synthetic RNAs is too weak to quantify using Western blotting**

A) Western blotting analysis of signalling protein phosphorylation during stimulation of A549 WT and HOIP -/- with 5  $\mu$ g 3p-hpRNA and Poly(I:C) (data representative of one assay).

### 5.4.2 HOIP increases activation of TBK1, IRF3 and I $\kappa$ B $\alpha$ in response to SeV infection

Previous studies exploring the role of HOIP in RNA virus-induced signalling protein activation generally acknowledge that HOIP is required. siRNA HOIP knockdown in A549 resulted in reduced IRF3 phosphorylation in response to IAV WSN infection<sup>506</sup>. Similarly, during VSV infection in U2OS cells and TRAF-deficient MEFs, HOIP knockdown resulted in reduced IRF3 and I $\kappa$ B $\alpha$  phosphorylation<sup>135</sup>, although no phenotype was seen with shRNA knockdown of HOIP in WT MEFs.

SeV is a more potent stimulator of RIG-I than the synthetic RNAs in our system, therefore the resulting higher levels of phosphorylated signalling proteins produced allowed the role of HOIP in signalling pathway activation to be analysed by both Western blotting and phos-flow. During SeV infection, lower levels of phospho-IRF3, -TBK1 and -I $\kappa$ B $\alpha$  in were detected in HOIP -/- cells compared to WT (Figure 5.4.2A). This is supported by phos-flow analysis of SeV infection, which also showed reduced IRF3 phosphorylation in HOIP-deficient cells, with twice the number of phospho-IRF3-expressing WT cells than HOIP -/- cells by 6 hours post-infection (Figure 5.4.2B).

This data demonstrates that HOIP is required for efficient activation of both the TBK1-IRF3 arm and the NF- $\kappa$ B arm of the RIG-I signalling pathway during SeV infection, supporting our transcriptional data.

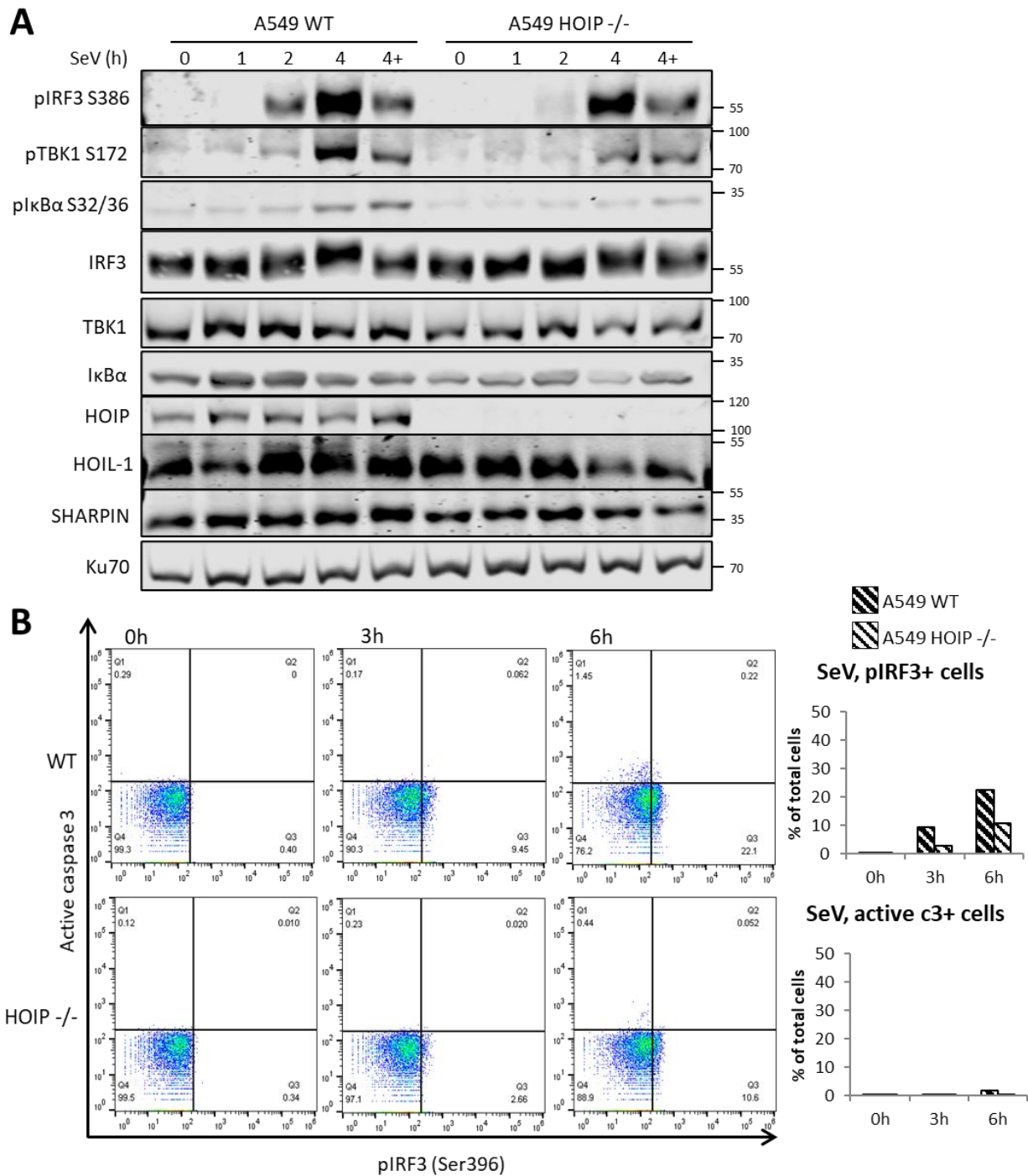


**Figure 5.4.2: HOIP is required for activation of signalling pathway components in response to Sendai virus** Infection of A549 WT and HOIP -/- cells with SeV at 1:300 dilution and A) Western blotting analysis of signalling protein phosphorylation in the presence and absence of 10  $\mu$ M MG-132 (data representative of >3 independent assays) and B) Phos-flow analysis of cells expressing phospho-IRF3 and active caspase 3 (n=1, data representative of 3 independent assays).

## 5.5 HOIP is required for RIG-I-driven chemokine secretion in response to synthetic RNA ligands and SeV infection

Multiple earlier studies show the requirement of HOIP for efficient RNA-induced secretion of chemokines and IFN- $\beta$  (135,432,505). In HaCaT and HeLa cells stimulated with extracellular Poly(I:C), reduction or loss of HOIP expression resulted in reduced TLR3-driven CCL5, TNF $\alpha$  and IL-8 secretion<sup>432</sup>. Similarly, HOIP knockdown in MEF cells resulted in reduced secretion of IFN $\beta$ , IL-6 and CXCL10 in response to VSV infection<sup>135</sup>, also seen during IAV infection of HOIP-deficient A549 cells<sup>505</sup>. Conversely, knockdown of HOIP in MEF cells had no effect on IFN $\beta$  secretion during SeV infection<sup>213</sup>.

ELISA analysis of CXCL10 secretion in A549 WT and HOIP  $-/-$  cells was used to validate our previous data showing that HOIP is required for efficient transcription of the chemokine *CXCL10* in response to synthetic RNAs and RNA viruses. In A549 WT, HOIP  $-/-$  and TAP-HOIP-WT cells stimulated with 3p-hpRNA (Figure 5.5A), Poly(I:C) (Figure 5.5B), HOIP  $-/-$  cells had secreted significantly less CXCL10 than WT after 24 hours. This is even more pronounced during SeV infection (Figure 5.5C), with CXCL10 secretion was almost undetectable by the assay in HOIP  $-/-$  cells after 6 hours and significantly reduced at 24 hours. Secretion of CXCL10 in TAP-HOIP-WT cells was even higher than that seen in WT cells at 24 hours post stimulation with all stimulation methods, as seen with *CXCL10* transcription.

This confirms that, as previously described<sup>135,432,506</sup>, secretion of CXCL10 in response to RIG-I activation is dependent on HOIP. Additionally, the use of longer infection and stimulation time points in ELISA assays confirms that loss of HOIP expression prevents, rather than just delays, RIG-I-driven immune signalling.

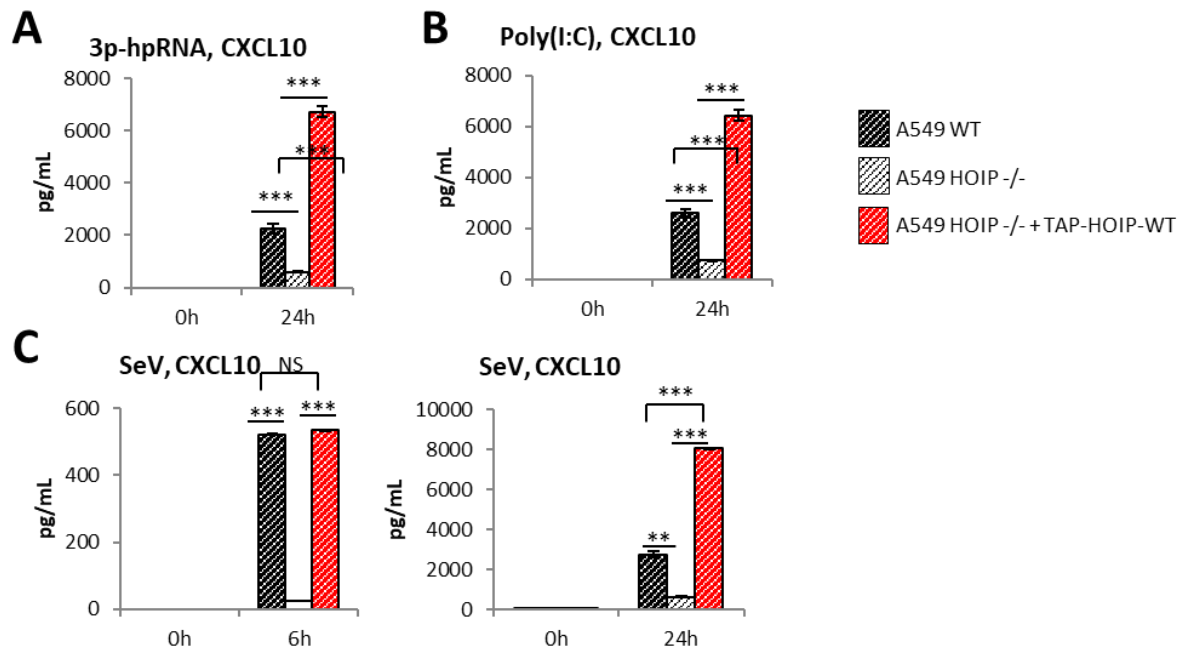


**Figure 5.5.1: HOIP is required for CXCL10 secretion during stimulation with synthetic RNAs and SeV**  
 ELISA to measure CXCL10 secretion in A549 WT, HOIP -/- and TAP-HOIP-WT cells during stimulation with A) 1  $\mu$ g 3p-hpRNA (n=2, representative of 3 independent assays), 1  $\mu$ g Poly(I:C) (n=2, representative of 3 independent assays) and C) SeV infection at 1:300 dilution (n=2, representative of >3 independent assays).

## 5.6 HOIP is also required for a RIG-I-driven antiviral immune response in HaCaT cells

### 5.6.1 HOIP is required for RIG-I driven transcription in HaCaT cells in response to synthetic RNAs and RNA viruses

To validate our findings that HOIP is required for RIG-I-driven transcription of antiviral genes and signalling protein phosphorylation, experiments were repeated in a second model cell line. The HaCaT cell line was generated from spontaneously transformed aneuploid immortal keratinocyte cells, derived from adult human skin. Like A549 cells, they are a physiologically relevant cell line to study the initial sensing of virus infection as many non-respiratory viruses enter the body through infection of skin cells. HaCaT cells deficient in HOIP were generated by Lentiviral CRISPR/Cas9 technology in the lab of Henning Walczak (University of Cologne).

Transcription of *IFNB1*, *IFNL1* and *CXCL10* was measured by qPCR in HaCaT WT and HOIP -/- cells after 6-hour stimulation with Poly(I:C) (Figure 5.6.1A) and infection with SeV (Figure 5.6.1B). Poly(I:C) induced robust transcription of all genes in WT cells, but transcription was barely detectable above background levels in HOIP -/- cells, mimicking what was seen in A549 cells. SeV infection of HOIP -/- cells resulted in lower levels of *IFNB1* and *CXCL10* transcription than WT cells, but this was

only significant for *IFNB1*, although the data is of lower quality data than with A549 cells. Western blotting analysis of SeV-infected HaCaT WT and HOIP  $-/-$  cells (Figure 5.6.1B) detected reduced levels of phospho-IRF3 in HOIP  $-/-$  cells compared to WT, for all time points, as seen in A549 cells. Overall, these data reinforce conclusions from experiments in A549 cells, showing that HOIP is required for the RIG-I-mediated immune response

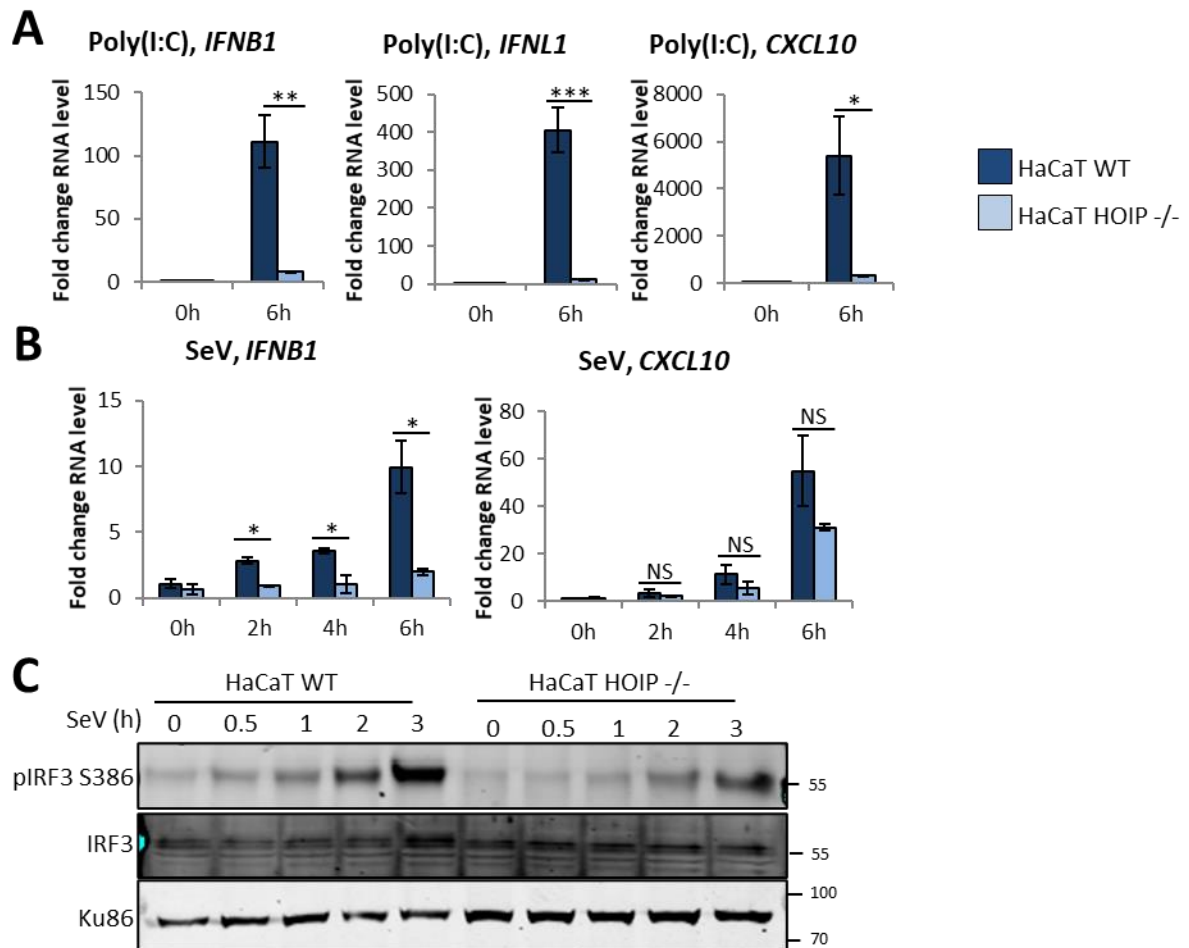


**Figure 5.6.1: HOIP is required for RIG-I signalling in HaCaT cells after stimulation with Poly(I:C) and SeV infection**

Western blotting analysis of expression of A) LUBAC components and B) RIG-I signalling pathway components in HaCaT WT and HOIP  $-/-$  cells. qPCR to measure transcription of *IFNB1*, *IFNL1* and *CXCL10* in HaCaT WT and HOIP  $-/-$  cells in response to 6-hour stimulation with C) 1  $\mu$ g Poly(I:C) and D) SeV at 1:300 dilution (both n=2, data representative of 3 independent assays).

## 5.7 Catalytic activity of HOIP is only partially required for its role in RIG-I signalling

Although we have demonstrated that HOIP is required for an efficient RIG-I mediated immune response to RNA and RNA viruses, we have not yet examined whether its contribution to RIG-I

signalling should be attributed this to the ability of HOIP to generate M1-linked ubiquitin chains or an alternative function.

The requirement for the HOIPs E3 ligase activity for its role in NF- $\kappa$ B activation has been well characterised in multiple systems, using mutants lacking or inactivating the catalytic RBR domain<sup>514-517</sup>. Ligase activity is also required for recruitment of TBK1 and IKK $\epsilon$  to the TNF receptor signalling complex and the subsequent prevention of TNF-driven cell death<sup>333,516</sup>. As seen with full deletion of HOIP, the mutation of HOIP at cysteine 879 in mice, abrogating its catalytic activity, results in embryonic lethality<sup>335,518</sup>. This is due to the requirement for the E3 ligase activity of HOIP for prevention TNF-driven endothelial cell death, allowing maintenance of blood vessel integrity during development. The only systems in which a catalytic-independent function of HOIP has been shown is in B and T cells, where the E3 ligase activity of HOIP is required for canonical TNF-driven NF- $\kappa$ B and ERK activation, but not for B and T cell receptor mediated NF- $\kappa$ B and ERK activation<sup>519,520</sup>.

### 5.7.1 Mutation of residue C885 inactivates the catalytic activity of HOIP

The analogous mutation in human HOIP, of the residue cysteine 885 located within the second RING domain of the active site of HOIP (Figure 5.7.1A), also results in loss of E3 ligase activity<sup>521</sup>. To determine the contribution of HOIP's E3 ligase activity and thus the contribution of M1-Ub chains to RIG-I signalling, we compared the RIG-I-driven immune response in A549 HOIP  $-/-$  cells stably expressing TAP-HOIP-C885S (TAP-HOIP-C885S cells) to that seen in WT, HOIP  $-/-$  and TAP-HOIP-WT cells.

First, Western blotting analysis of LUBAC expression in WT, HOIP  $-/-$ , TAP-HOIP-WT and TAP-HOIP-C885S cells (Figure 5.7.1B), showed similar levels of HOIP expression between TAP-HOIP-WT and TAP-HOIP-C885S cells, both higher than seen in A549 WT cells. As seen before with TAP-HOIP-WT cells, increased HOIP expression in TAP-HOIP-C885S cells resulted in higher levels of HOIL-1 and SHARPIN than in WT cells, also suggesting that the mutation did not disrupt LUBAC complex formation. Additionally, expression of signalling proteins IRF3, TBK1 and MAVS were consistent across the 4 cell lines (Figure 5.7.1C).

Due both to the incredibly low abundance of M1-linked ubiquitin chains in cells even after stimulation and lack of a good antibody, we were unable to demonstrate the presence of M1-Ub chains by Western blotting. Therefore, to prove that TAP-HOIP-C885S cells behaved as expected for cells lacking M1-Ub chains, the effect of loss of ligase activity, previously shown to be required for recruitment of NEMO and TBK1 and to the TNF-RSC and prevention of RIP1 phosphorylation<sup>333</sup>, was examined. TAP-HOIP-WT and TAP-HOIP-C885S cells were stimulated with TNF $\alpha$  and phosphorylation

of TBK1, I $\kappa$ B $\alpha$  and RIP1 was measured by Western blotting analysis (Figure 5.7.1D). As previously described, TNF $\alpha$  stimulation resulted in phosphorylation of TBK1 in TAP-HOIP-WT cells, increasing in abundance through the 60-minute time course, with levels of phospho-TBK1 much lower in TAP-HOIP-C885S cells, consistent with the reported role of LUBAC<sup>333</sup>. TNF $\alpha$  stimulation of TAP-HOIP-WT cells also resulted in early phosphorylation of I $\kappa$ B $\alpha$ , detected at 5 minutes post-stimulation but rapidly degraded by the proteasome after phosphorylation preventing detection after 15 or 30 minutes, detectable again after 60 minutes indicating a cyclical nature of phosphorylation and degradation. As with TBK1, phosphorylation of I $\kappa$ B $\alpha$  was reduced in TAP-HOIP-C885S cells at both 5 and 60-minutes post infection, supporting studies showing the requirement of the E3 ligase activity for NF- $\kappa$ B activation<sup>514-516</sup>. Finally, phosphorylation of RIP1, a modification that prevents cell death through the TNF-RSC-II<sup>522,523</sup>, is present to higher levels in TAP-HOIP-C885S cells than TAP-HOIP-WT, expected due to the protective role of the E3 ligase activity of HOIP against cell death<sup>516</sup>. From these observations, we were satisfied that TAP-HOIP-C885S cells are incapable of producing M1-linked ubiquitin chains during TNF $\alpha$  stimulation.

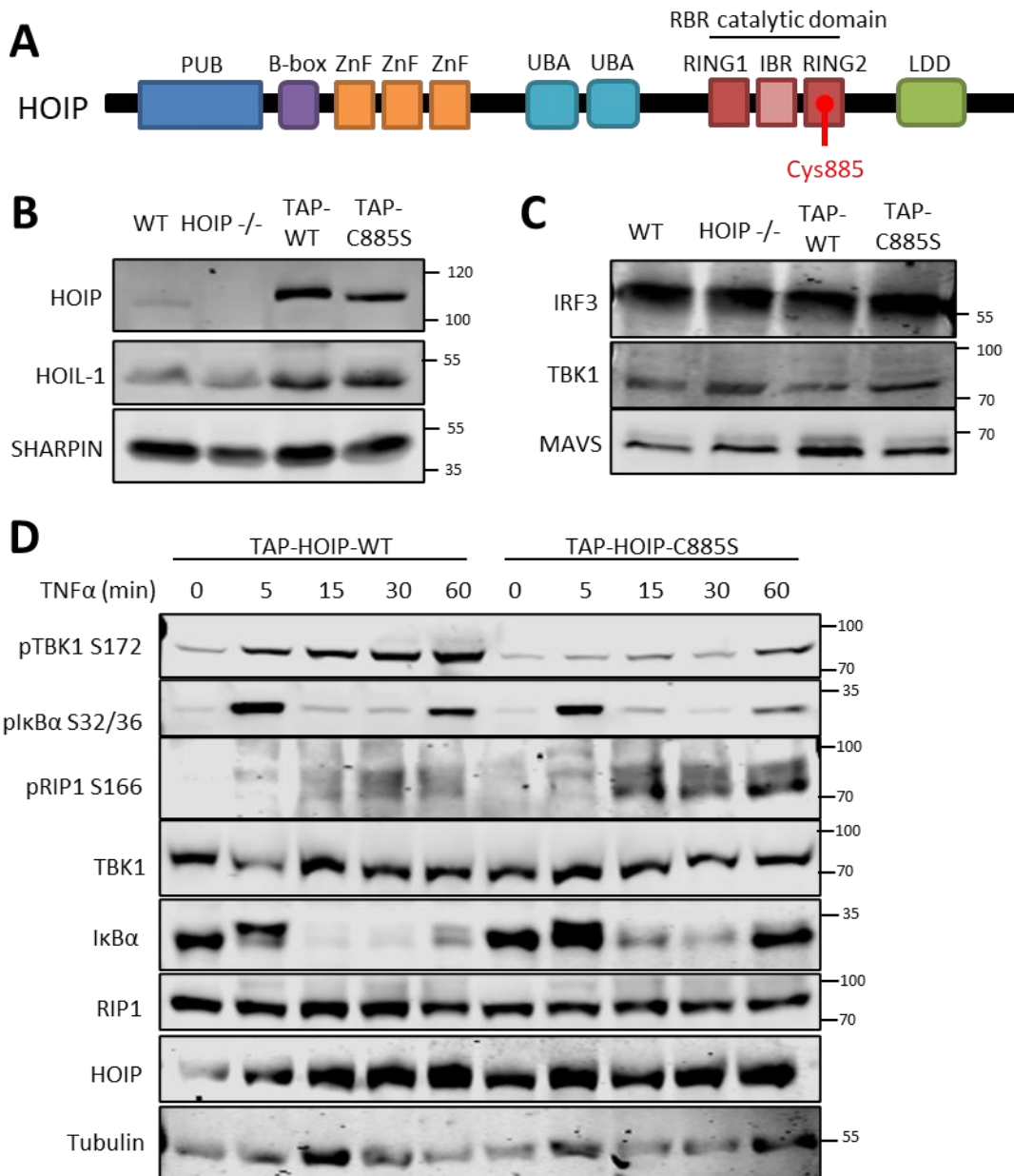


**Figure 5.7.1: Characterisation of TAP-HOIP-WT and TAP-HOIP-C885S cells**

A) Schematic of HOIP with position of mutation indicated (adapted from Gyrd Hansen et al., 2021). Western blotting analysis of B) expression of LUBAC components in A549 WT, HOIP  $-/-$ , TAP-HOIP-WT and TAP-HOIP-C885S cells, C) expression of RIG-I signalling pathway components in A549 WT, HOIP  $-/-$ , TAP-HOIP-WT and TAP-HOIP-C885S cells and D) phosphorylation of signalling proteins during TNF $\alpha$  stimulation A549 TAP-HOIP-WT and TAP-HOIP-C885S at 200 ng/mL (data representative of one experimental replicate).

### 5.7.2 Expression of immune genes is only partially dependent on the catalytic activity of HOIP

The requirement of the E3 ligase activity of LUBAC for RIG-I signalling outcomes has not previously been studied. We examined its role in RIG-I driven transcription by qPCR analysis of WT, HOIP  $-/-$ , TAP-HOIP-WT and TAP-HOIP-C885S cells transfected with 3p-hpRNA and Poly(I:C) and infected with

SeV (Figure 5.7.2A, B and C respectively). In general, transcription of both IRF3- and NF- $\kappa$ B-dependent genes was significantly lower in TAP-HOIP-C885S cells than TAP-HOIP-WT cells, suggesting that loss of the catalytic activity of HOIP has a detrimental effect on the role of HOIP in RIG-I signalling. The most notable exception to this is *ISG54*, which was transcribed to significantly higher levels in TAP-HOIP-C885S cells than TAP-HOIP-WT. However, transcription of all tested genes was also significantly higher in TAP-HOIP-C885S cells than seen in HOIP  $-/-$  cells, showing HOIP is capable of regulation RIG-I-driven transcription in the absence of M1-linked ubiquitin chains. Together this data suggests that the M1-Ub chains produced by HOIP are partially responsible for its role in RIG-I signalling, but that HOIP also drives signalling by another mechanism, as seen in T and B cell receptor-mediated NF- $\kappa$ B activation<sup>519,524</sup>.

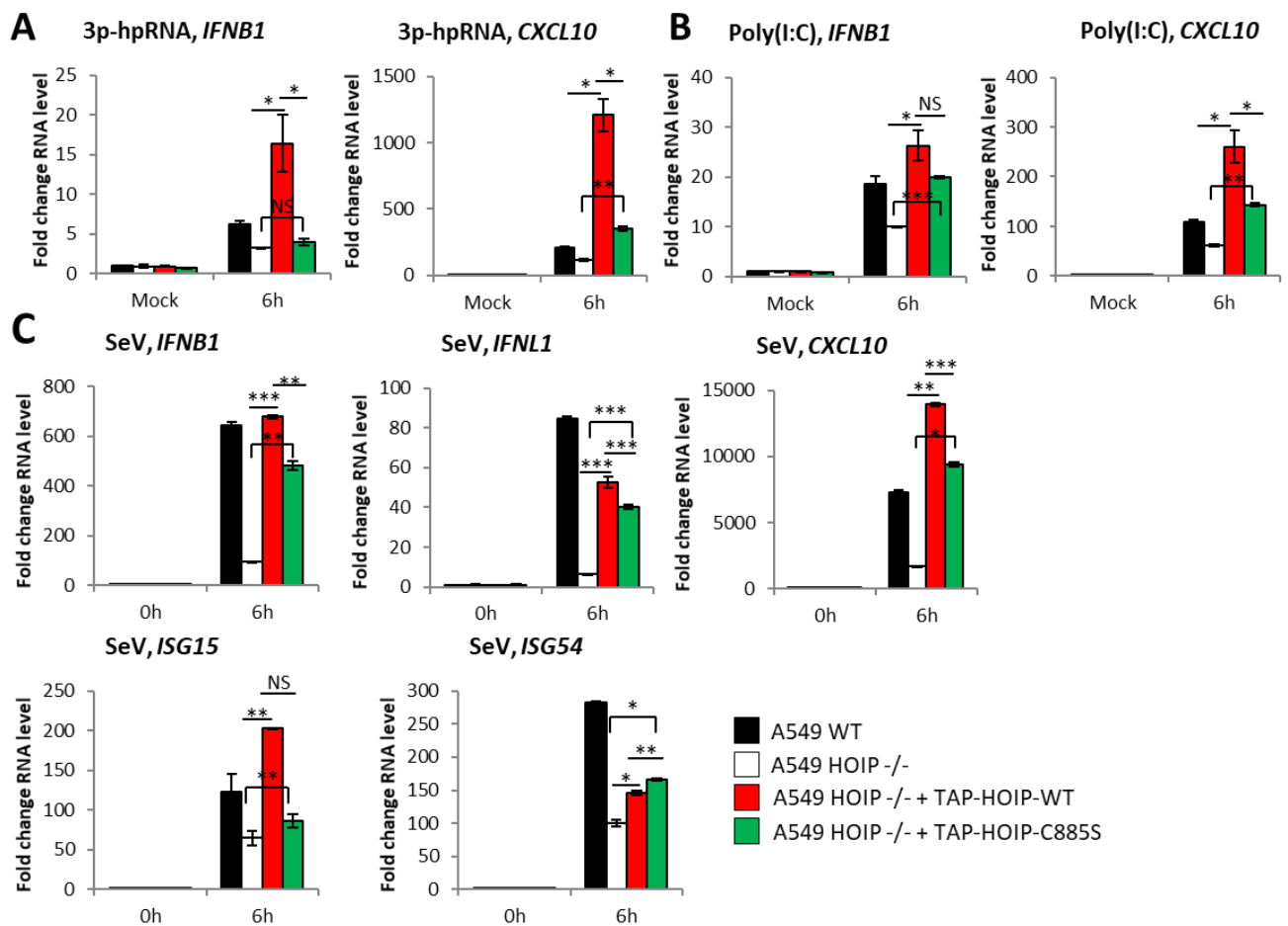


**Figure 5.7.2: Expression of immune genes in response to synthetic RNAs and SeV infection is only partially dependent on the catalytic activity of HOIP**

qPCR to measure transcription of indicated genes in WT, HOIP  $-/-$ , TAP-HOIP-WT and TAP-HOIP-C885S cells in response to stimulation with A) 1  $\mu$ g 3p-hpRNA in A549 WT and HOIP  $-/-$  cells (n=2, data is representative of >3 independent assays), B) 1  $\mu$ g Poly(I:C) (n=2, data is representative of >3 independent assays) and C) infection with SeV at 1:300 dilution (n=2, data representative of 3 independent assays).

### 5.7.3 Phosphorylation of IRF3, TBK1 and IκBα is not dependent on the catalytic activity of HOIP

Previously, the catalytic activity of HOIP has been shown to be required for RIG-I-driven signalling protein activation, with WT but not a catalytically inactive HOIP mutant able to rescue VSV-induced IRF3 dimerization<sup>135</sup>. This study also reported a functional redundancy between the E3 ligase activity of HOIP RBR domain and TRAF2 RING domain in RIG-I signalling.

To examine this in our system, TAP-HOIP-WT and TAP-HOIP-C885S cells were infected with SeV and phosphorylation of IRF3, TBK1 and IκBα was measured by Western blotting (Figure 5.7.3). The phosphorylation of IRF3 and TBK1 in TAP-HOIP-WT cells mimicked that previously seen in A549 WT cells (Figure 3.3.2), as did detection of phospho-IκBα in the presence of proteasome inhibitor MG-132 at 4 hours post-infection. However, phosphorylation of all three proteins appeared unaffected by mutation of HOIP, suggesting loss of M1-linked ubiquitin chains had no effect on signalling protein activation, disputing the earlier study<sup>135</sup>. This also somewhat contradicts our transcriptional data showing that expression of the mutant HOIP only partially rescues transcription of immune genes compared to expression of WT HOIP. This may suggest that IRF3 phosphorylation is not dependent on M1-linked chains but dimerization or nuclear translation of IRF3 is, or more likely may be accounted for by the sensitivity threshold of the two assays, with qPCR much better at detecting small changes in expression.

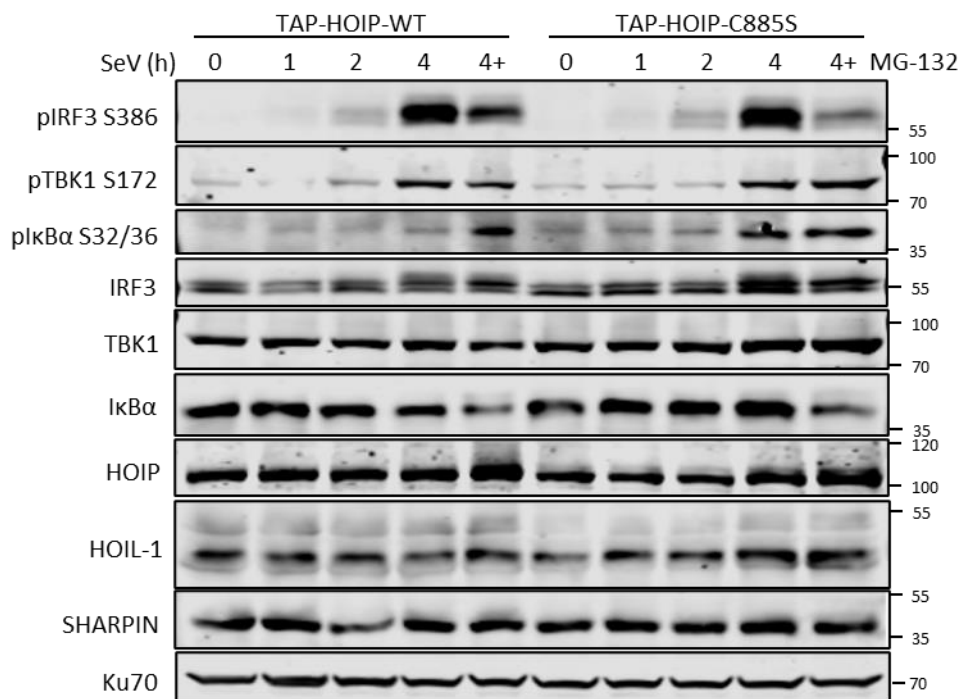


### Figure 5.7.3: Phosphorylation of signalling proteins during SeV infection appears not to be dependent on the catalytic activity of HOIP

Western blotting analysis of A549 TAP-HOIP-WT and TAP-HOIP-C885S cells infected with SeV at 1:300 dilution with and without 10  $\mu$ M MG-132 (data representative of 2 experimental replicates).

### 5.7.4 Chemokine expression is only partially dependent on the catalytic activity of HOIP

Because *CXCL10* transcription in response to SeV infection was partially reduced by mutation of the HOIP ligase domain (Figure 5.7.2C), secretion of CXCL10 was analysed by ELISA at 6 and 24 hours post infection with SeV (Figure 5.7.4). After 6 hours, TAP-HOIP-C885S cells had secreted significantly more CXCL10 than TAP-HOIP-WT cells. However, by 24-hours post infection, the phenotype more closely mimicked what was seen for transcription with the cells expressing mutant HOIP secreting an intermediate amount of CXCL10, between what was seen in HOIP  $-/-$  cells and in TAP-HOIP-WT cells. This change in secretion dynamics across the infection time course was consistent over three experimental replicates, which is consistent with a role of M1 chains in signal amplification.

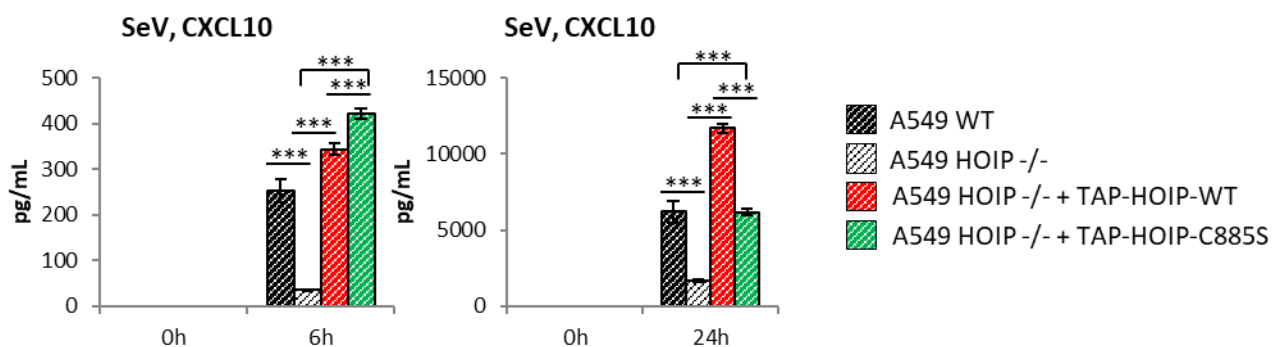


### Figure 5.7.4: CXCL10 secretion in response to SeV infection is only partially dependent on the catalytic activity of HOIP

ELISA to measure secretion of CXCL10 in A549 WT, HOIP  $-/-$ , TAP-HOIP-WT and TAP-HOIP-C885S cells infected with SeV at 1:300 dilution ( $n=2$ , data representative of 3 independent assays).

## 5.8 The LUBAC complex functions as a scaffold during RIG-I signalling

### 5.8.1 LUBAC components co-IP with NEMO and SHARPIN during SeV infection

As our data indicates a M1-linked ubiquitin chain-independent function of HOIP in RIG-I signalling, we hypothesised that the HOIP or the LUBAC complex may act as a scaffold, binding to and enabling efficient recruitment of other proteins to the signalling complex. Co-immunoprecipitation studies were used to test whether the HOIP binds to other proteins known to be involved in RIG-I signalling, analysed by Western blotting. In TNF signalling, presence of LUBAC leads to enhanced and sustained

recruitment of NEMO to the TNF-RSC, a process that requires the enzymatic activity of LUBAC<sup>501</sup>. This, alongside our demonstration that HOIP and NEMO are required for IRF3 and NF- $\kappa$ B activation downstream of RIG-I, meant that we chose to do these co-immunoprecipitation studies in A549 cells expressing TAP-HOIP-WT and TAP-NEMO. As Western blotting analysis is a targeted approach for finding binding partners, candidate proteins known to interact with LUBAC in other signalling complexes, such as NEMO and RIP1 in the TNF-RSC<sup>338,507</sup>, were examined.

As a proof of principle of the assay, TAP-HOIP and -NEMO were immunoprecipitated in cells that were stimulated with TNF $\alpha$  (Figure 5.8.1A), as they are known to interact in the TNF-RSC<sup>338,507</sup>. Western blotting analysis showed that HOIP co-immunoprecipitated with NEMO in TAP-NEMO cells at 5 minutes post-stimulation, but not in unstimulated cells or 15 minutes after stimulation. In TAP-HOIP cells, both RIP1 and TRAF2 were found to interact with HOIP after 5 and 15 minutes of TNF $\alpha$  stimulation, but not in unstimulated cells. This was as expected, as TRAF2 is also known to be required for TNF-RSC-driven signalling and showed that co-immunoprecipitation is an effective method to study interactions of HOIP and NEMO in signalling complexes in this system.

Consequently, co-immunoprecipitation techniques were used to analyse the RIG-I signalling complex during SeV infection. As RIG-I is expressed at such low levels in resting A549 cells, A549 TAP-NEMO and TAP-HOIP-WT cells were pre-stimulated with IFN $\alpha$  for 24 hours to increase the amount of RIG-I available to form signalling complexes, infected with SeV, and NEMO and HOIP were immunoprecipitated using Flag-M2 beads (Figure 5.8.1B). Western blotting analysis detected binding of HOIP, SHARPIN and TBK1 to TAP-NEMO during SeV infection. Binding of HOIP was only detected at 3 hours post infection, but for TBK1 and SHARPIN, a very low level of binding was detected in the absence of infection, but this binding was enhanced in the presence of infection. Apparent binding in the absence of infection is likely due to the proteins 'sticking' to the antibody beads, despite extensive washing. TBK1 also co-immunoprecipitated with TAP-HOIP during SeV infection, with some background binding in the absence of infection, but much higher levels detected at 3- and 6-hours post-infection.

Unlike in the TNF-RSC (Figure 5.8.1A), we did not detect binding of HOIP to RIP1 during SeV infection, suggesting it does not form part of the RIG-I signalling complex and is not bound or modified by LUBAC during RIG-I signalling. This is supported by our data using RIP1 knockout cells, which showed that, unlike in TNF signalling<sup>525,526</sup>, RIP1 appeared not to be essential for the RIG-I-driven immune response, so may not be present in this signalling complex. Conversely, binding of TRAF2 to TAP-HOIP was also not detected during SeV infection, despite its previously reported role

alongside LUBAC in the RIG-I-RSC<sup>135</sup>. Because HOIL-1 is the same molecular weight as the antibody heavy chain, we were unable to study its binding to NEMO in this experiment, as it could not be detected by Western blotting. Use of light-chain only secondary antibodies to overcome this was attempted, but their reduced sensitivity meant that we did not detect binding of other proteins. Despite this, from these data we conclude that LUBAC is present in the RIG-I signalling complex, binding to both NEMO and TBK1, both of which we have shown are required for the RIG-I mediated immune response.

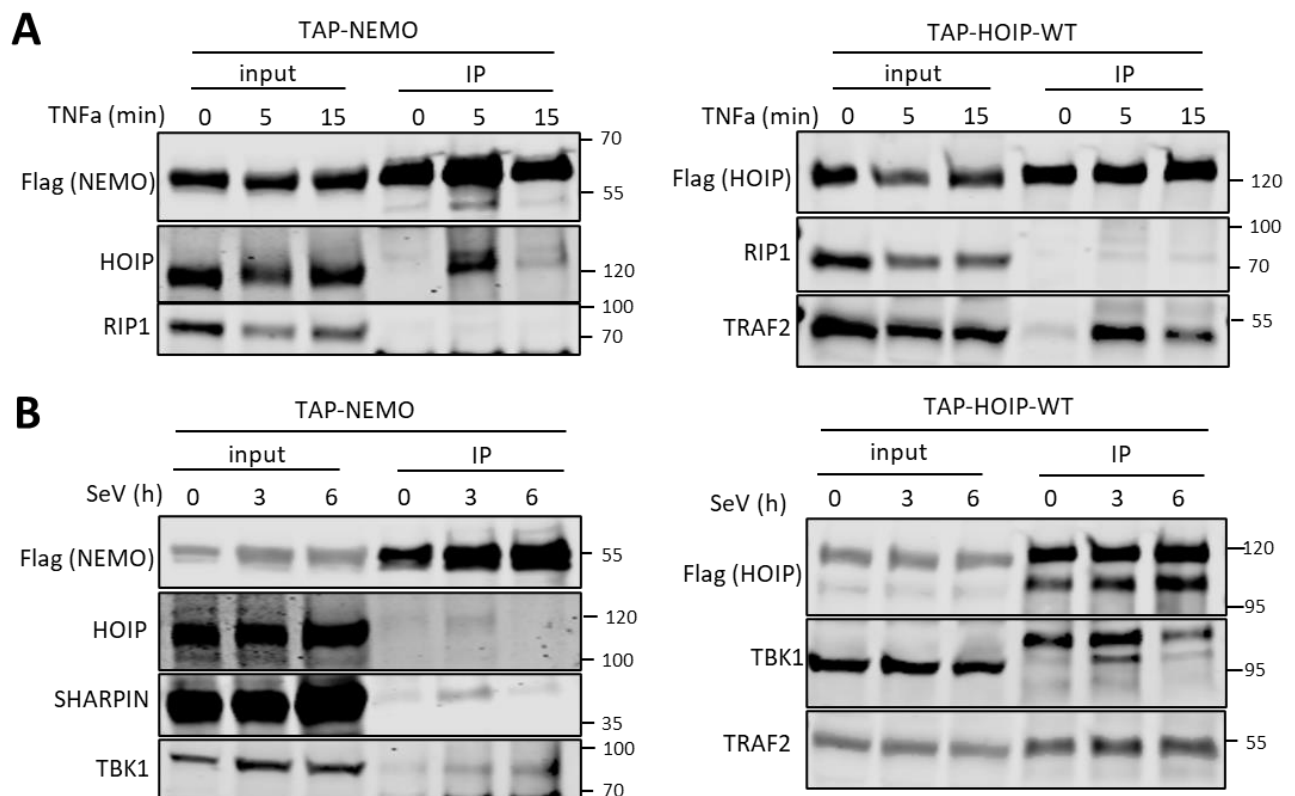


**Figure 5.8.1: LUBAC co-IPs with NEMO and TBK1 during SeV infection**

Western blotting analysis of Flag-M2 immunoprecipitation (IP) of TAP-NEMO and TAP-HOIP in A549 NEMO <sup>-/-</sup> + TAP-NEMO and A549 HOIP <sup>-/-</sup> + TAP-HOIP-WT cells respectively after A) treatment with 500 ng/mL TNFα and B) infection with SeV at 1:300 dilution (for both, data is representative of 2 independent assays).

## 5.9 HOIP does not play a role in preventing RIG-I-driven cell death in A549 cells

When LUBAC was first discovered to play a role in TNF signalling, it was identified as a modulator of cell death pathways, as loss of LUBAC activity resulted in a loss of the TNF-driven pro-inflammatory phenotype and sensitisation of cells to TNF-driven cell death, predominantly by programmed necrotic death pathway necroptosis<sup>338,527,528</sup>. More recently, loss of LUBAC activity has also been

shown to result in RLR- and TLR3-driven cell death, occurring through either apoptosis during VSV infection and Poly(I:C) stimulation, or activation of necroptosis during SeV infection<sup>432,505,529</sup>. *In vivo*, enhanced lung injury was seen during IAV infection of mice with an alveolar epithelium-specific HOIP deletion<sup>506</sup>, as was seen during Poly(I:C) treatment of SHARPIN deficient mice<sup>432</sup>. Conversely, LUBAC-mediated ubiquitination of IRF was shown to be required for activation of the RLR-induced IRF3-mediated pathway of apoptosis (RIPA) during late stages of SeV infection<sup>530</sup>.

### 5.9.1 RIG-I-driven cell death is not activated in A549 cells lacking HOIP

To see if HOIP is playing a role in RIG-I-driven cell death in our model, we studied whether HOIP *-/-* cells were sensitised to cell death after stimulation with our RIG-I ligands. SeV infection of both A549 WT and HOIP *-/-* resulted in no visible cytopathic effects (CPE) (Figure 5.9.1A), whereas treatment of the same cells with staurosporine, a potent inducer of caspase-dependent and -independent apoptosis<sup>531,532</sup>, became apoptotic in morphology (not shown). Similarly, no visible morphological changes were observed in either A549 WT or HOIP *-/-* cells after treatment with 3p-hpRNA or Poly(I:C), or infection with IAV R+K (not shown). Some visible cell death was seen at later time points of ZIKV infection, although this was not quantified and only occurred at time points where signalling outcomes were no longer RIG-I-specific, suggesting RIG-I was not driving this death.

Despite no visible CPE, phos-flow and a vitality assay were used to quantify cell death during SeV infection. Phos-flow staining for activated caspase 3 was used to identify cells undergoing programmed apoptosis as caspase 3 is an effector caspase activated by cleavage by an initiator caspase during both intrinsic and extrinsic cell apoptosis<sup>533</sup>. After 6 hours of SeV infection, there was no notable increase in the number of either WT or HOIP *-/-* cells expressing activated caspase 3 (Figure 5.9.1B).

This was further verified using a vitality assay, which detects changes in the intracellular level of reduced thiols as a measure of apoptosis activation, as depletion of reduced thiol GSH is an early hallmark of apoptosis progression. Resting and infected cells were stained with a VB-48™ dye, to quantify the amount of free thiols, and propidium iodide (PI), which accumulates in cells with permeabilised membranes. Stained cells were analysed using a NC-250 vitality assay programme, and a fluorescence intensity plot showing the distribution of thiol levels and PI in individual cells was generated. Staining of resting healthy cells was used to devise a gating strategy, which was then used to assign cells as healthy (high VB-48 and low PI), apoptotic (low VB-48 and low PI) and dead (high PI), (Figure 5.9.1C). A549 WT and HOIP *-/-* cells were infected with SeV or stimulated with staurosporine and categorised using the same gating parameters as the control cells (also Figure

5.9.1C). The percentage of healthy, early apoptotic and necrotic cells was compared between WT and HOIP  $-/-$  (Figure 5.9.1D). In the absence of stimulation, approximately 90% of both cell lines were healthy. Staurosporine stimulation of cells resulted in 40-50% of cells taking up PI and only 30-40% of the cells remaining healthy, both relatively consistent between WT and HOIP  $-/-$  cells across the two time points. After a 6-hour infection with SeV, 80-90% of both WT and HOIP  $-/-$  cells remained healthy. This reinforces the phos-flow data, confirming that SeV infection is not inducing RIG-I-driven cell death, even in the absence of HOIP.

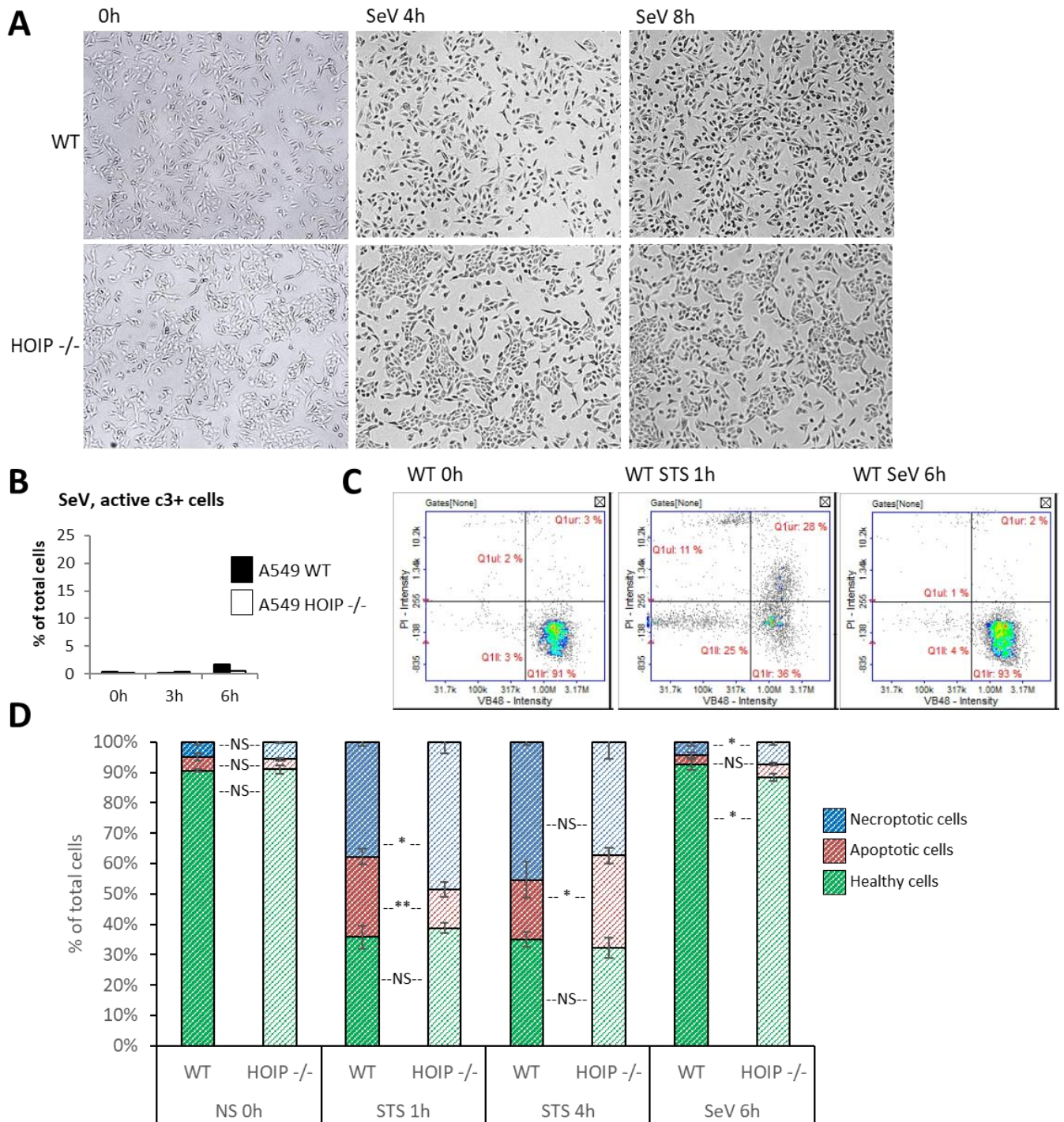


**Figure 5.9.1: RIG-I does not drive cell death in A549 cells, even in the absence of HOIP**

A549 WT and HOIP  $-/-$  cells infected with SeV at 1:300 dilution, A) Images taken at 10x magnification and B) phos-flow to look at % of cells with activates caspase 3 (n=1, data representative of >3 independent assays). Nucleocounter NC-250 Vitality Assay of A549 WT and HOIP  $-/-$  cells treated with 2  $\mu$ M Staurosporine (STS) or infected with SeV at 1:300 dilution, C) images of dot plots generated during vitality assay where upper left and right quadrants represent necroptotic cells (PI positive), lower left represents apoptotic cells (PI negative, VB-48 negative) and the lower right quadrant represents healthy cells (PI negative, VB-48 positive) and D) stacked bar chart generated from Vitality Assay (both n=3, data representative of >3 independent assays).

## 5.10 Discussion

Through the work in this chapter, we aimed to study how the E3 ligase component of LUBAC HOIP regulates RIG-I signalling. Our work using cell lines deficient in HOIP and cells expressing wild-type and a catalytic dead mutant of HOIP goes some way to address previous inconsistencies in the literature surrounding the role of HOIP in RIG-I signalling and suggests that HOIP positively regulates RIG-I-driven immune activation in a similar way to other signalling pathways like TNF, NOD2 and TLR3.

### 5.10.1 Addressing previously conflicting studies showing opposing roles for HOIP in the regulation of RNA sensing.

We have shown that in A549 cells, HOIP is required for efficient RIG-I-driven activation of IRF3 and NF- $\kappa$ B and the resultant immune gene transcription and chemokine secretion. Previous data surrounding this topic is conflicting, some of which is supported by our results.

HOIP was previously shown to be required for RIG-I signalling during infection with IAV WSN, where knockdown of HOIP in A549 cells resulted in reduced IRF3 and NF- $\kappa$ B activation, and loss of HOIP expression in the alveolar epithelium of mice inhibited the IFN-I and inflammatory-driven immune response<sup>534</sup>. Similarly, HOIP was required for VSV-driven IFN-I activation in U2OS cells, but only played a modest role in the activation of IRF3- and NF- $\kappa$ B-dependent pathways, due to its functional redundancy with TRAF proteins<sup>135</sup>. However, other studies were less clear cut, with HOIP knockout having minimal effect on IFN-I activation, but HOIP overexpression reducing IFN-I induction, both in MEF cells infected with SeV<sup>213</sup>. Additionally, HOIP was shown to assist Hepatitis B-mediated restriction of IFN-I activity when RIG-I is activated by pre-genomic RNA<sup>535</sup>. This conflicting literature may suggest that the role of HOIP in RIG-I signalling is cell-type dependent, as both studies indicating either a redundant or non-existent role for HOIP in RIG-I-mediated signalling were done using MEF cells<sup>135,213</sup>. However, it may also highlight the importance of using clean knockout systems to study the role of LUBAC, as both studies also relied on knock-down systems, where evidence of residual HOIP expression after knockdown was visible<sup>213</sup>.

Our data supports what is known about the regulation of other RNA sensing pathways by HOIP. In TLR3 signalling, recruitment of HOIP results in efficient activation of IRF3 and NF- $\kappa$ B, as well as cytokine signalling, seen in both HaCaT and HeLa cells<sup>432</sup>. This is also supported by data showing that small molecule inhibitors of HOIP called HOIPINs inhibit the TLR3-dependent response to Poly(I:C)<sup>536</sup>. By using a clean knockout system to show that HOIP is required for efficient RIG-I signalling, we

provide clear evidence that that HOIP has a consistent function between different RNA sensing pathways.

In addition to in other RNA sensing pathways, our data showing the requirement of HOIP for immune activation mimics what is seen in other immune signalling pathways, strengthening our findings. M1-ubiquitin chains generated by HOIP are required for the activation of NF- $\kappa$ B, MAP kinase cascades and pro-inflammatory gene transcription by TNFR1, IL-1, NOD1 and 2 and other TLRs, through enabling the efficient recruitment of RIPK and IRAK proteins<sup>501,518,537–540</sup>. HOIP also drives IRF-dependent defences to intracellular bacteria, through enabling recruitment of TBK1/IKK $\epsilon$  to the bacteria<sup>541</sup>. Outside of RIG-I signalling, no previous studies show negative regulation of immune activation by HOIP.

From our study, we concluded that overexpression systems, a technique that has been used to generate much of the data surrounding LUBAC and RIG-I, are poorly suited to studying the role of E3 ligases like HOIP or HOIL-1. Previous studies using this system showed that overexpression of HOIP and HOIL-1 reduced IFN-I, and NF- $\kappa$ B activation in response to both SeV infection and overexpression of many components of the RIG-I signalling complex<sup>213,505,542</sup>. These findings contradict much of the data that has been generated using cells lacking expression of either HOIP or HOIL-1.

The main issue with using overexpression systems to study LUBAC is that it almost certainly disrupts the tight regulation of LUBAC that occurs in physiological systems, critical to appropriate LUBAC function, with “inappropriate regulation of Met1-Ub giving rise to severe and potentially fatal pathologies”<sup>503</sup>. This tight regulation is achieved by stable complex formation of LUBAC with de-ubiquitinases (DUBs) OTULIN and CYLD, which cleave M1-Ub chains to tightly regulate the activity of LUBAC<sup>543,544</sup>. Loss of OTULIN results in accumulation of M1-linked ubiquitin chains, which is thought to interfere with LUBAC function by causing autoubiquitination<sup>545</sup>, highlighting the detrimental effects of hyperactive LUBAC. Additionally, overexpression of a catalytically active protein complex like LUBAC is likely to result in above-physiological levels of ubiquitin chain generation, which may lead to binding of ubiquitin chains to proteins that would not normally be targeted, potentially giving rise to a differing phenotype. Previous occurrence of this has been seen with HOIL-1 overexpression, which was shown to promote proteasome-mediated degradation of IRF3<sup>542</sup>, conflicting with both biochemical analyses showing IRF3 is not a substrate for HOIL-1 and studies showing HOIL-1-deficiency in fibroblasts does not affect IRF3 stability<sup>213</sup>. Occurrence of either or both aforementioned processes may account for the differing phenotypes seen between overexpression and studies and those that use knock-out or knock-down techniques.

The importance of understanding how HOIP regulates signalling processes, and the biological implications of this are highlighted by the effect of mutations of HOIP, both in humans and in mice. Full HOIP  $-/-$  mice die during embryonic development, due to sensitisation to aberrant TNFR1-mediated cell death activation<sup>516,519</sup>, as do mice expressing catalytically inactive HOIP<sup>518,546</sup>, and in mice with an endothelial deletion of HOIP<sup>516</sup>. However, mice with other cell-type specific deletions of HOIP are possible, as has been done in B cells and alveolar epithelium<sup>519,534</sup>, likely due to the importance of the endothelium in maintenance of the vascular architecture during embryogenesis<sup>516</sup>. In humans, mutations in HOIP result in immune dysregulation with complex clinical characteristics<sup>547,548</sup>, sharing phenotypes seen in mice with either partial HOIL-1  $-/-$  or full SHARPIN  $-/-$  mice<sup>338,504,508,511,549,550</sup>. These characteristics include immunodeficiency, likely due to impaired IFN, NF- $\kappa$ B and MAPK activation<sup>500,501</sup>, defective development of T and B cells<sup>519,551,552</sup>, and loss of dendritic cell homeostasis<sup>553</sup>, which leads to increased susceptibility to infection caused by an impaired antibody response<sup>547</sup>. Paradoxically, HOIP mutation also causes autoinflammation, thought to be driven by aberrant cell death activation or hyperactivation of monocytes causing excessive pro-inflammatory cytokine production<sup>548</sup>. The two known clinical cases differ slightly in their manifestation, likely because only one of the mutations impairs the expression of HOIP, and therefore prevents formation of a stable LUBAC complex.

### 5.10.2 A suggested two-step mechanism for the regulation of RIG-I signalling by LUBAC and M1-ubiquitin chains

The mechanism by which LUBAC regulates RIG-I signalling has not yet been conclusively described, with differing mechanisms and conflicting outcomes suggested. However, through using multiple different methods to analyse the outputs of RIG-I signalling across a range of time points, we propose a dynamic model for RIG-I regulation by HOIP and M1 ubiquitin chains.

We have shown that HOIP is required for efficient transcription of IFN-I, IFN-III, ISGs and chemokines, as well as NF- $\kappa$ B-dependent genes *NFKBIA* and *TNFA*, from which we can infer that HOIP regulates the RIG-I-signalling pathway at a point required for both IRF3 and NF- $\kappa$ B activation. We have also shown that that RIG-I, MAVS and NEMO, but not TBK1, IKK $\epsilon$ , TANK/NAP1/SINTBAD, RIP1 or Optineurin, were required for both IRF3 and NF- $\kappa$ B activation during SeV infection. Also fitting with this, we showed that LUBAC components HOIP and SHARPIN interact with known RIG-I signalling proteins NEMO and TBK1. In addition to this, we showed that the catalytic activity of HOIP is only partially required for its role in RIG-I signalling, with no defect in IRF3 and NF- $\kappa$ B activation and chemokine secretion at early time points in cells expressing a catalytically inactive mutant of

HOIP, but lower levels of transcription of both IFN-I and NF- $\kappa$ B-dependent genes and chemokine secretion at later time points.

This requirement for the ligase activity of HOIP at later time points and the demonstrated interaction between LUBAC and RIG-I signalling proteins has allowed us to propose a model for HOIP-mediated regulation of RIG-I signalling. We suggest that HOIP, and possibly the other LUBAC proteins HOIL-1 and SHARPIN, are required for proper formation of the RIG-I signalling complex, probably acting as scaffold proteins. LUBAC then conjugates M1-linked ubiquitin chains to proteins in the signalling complex to amplify the signalling outputs, either by enhancing recruitment of other signalling proteins or stabilisation the active signalling complex to extend signalling. This is analogous to the suggested mechanism for TNF signalling regulation, where the enzymatic activity of HOIP is required for the enhanced and sustained recruitment of NEMO to the signalling complex, and the resultant downstream signalling<sup>501</sup>. This could be tested by using a fluorescently tagged M1-ubiquitin-binding domain, such as GFP-UBAN (ubiquitin-binding in ABIN and NEMO), which would enable us to monitor the timing of the generation of M1-linked ubiquitin chains<sup>554</sup>.

Until this study, the requirement of the ligase activity of HOIP for its regulation of RIG-I signalling was unclear. A ubiquitin-chain independent mechanism of downregulation of RIG-I signalling by LUBAC was proposed by Inn et al., as overexpression of RING mutants of both HOIL-1 and HOIP with no catalytic activity did not prevent the ability of the proteins to suppress SeV or RIG-I-induced IFN-I activation<sup>213</sup>. But conversely, the ligase activity of either TRAF2 or HOIP was shown to be required for IRF3 activation by RIG-I<sup>135</sup>. Our data does not agree directly with either of these studies, but together they do support our suggestion of a dual role for HOIP as a scaffold protein and producer of M1-ubiquitin chains.

We cannot yet confirm the target of M1-linked ubiquitin chains in the RIG-I signalling complex, however the interaction of HOIP with NEMO and TBK1 provide possible targets to be further explored. Alongside TRIM25, NEMO has previously been proposed as a target for M1-Ub chains in the RIG-I complex<sup>213,505</sup>. However, the studies proposing these proteins as targets of M1-linked ubiquitination suggest that this is detrimental to RIG-I-driven immune signalling, which is inconsistent with our data. An additional study disputes this further, showing that only ubiquitin binding by NEMO and not ubiquitination of NEMO, was essential for MAVS signalling<sup>135</sup>.

The targets of M1-linked ubiquitination are better characterised in other signalling pathways. In TNFR1 signalling, NEMO both binds to and is ubiquitinated by M1-Ub chains, both of which are required efficient IKK $\beta$  phosphorylation and downstream NF- $\kappa$ B activation<sup>338,501,528</sup>. RIP1 is also a

target for the conjugation of M1-linked ubiquitin chains in TNFR signalling, preventing formation of complex II and limiting the subsequent programmed cell death activation<sup>500-502</sup>. Alternatively, Emmerich et al have suggested that M1-Ub chains are conjugated directly onto K63-linked chains, forming M1/K63-hybrid ubiquitin chains during IL-1, TLR1, 2 and 3, TNFR1 and NOD1 signalling<sup>518,555</sup>, allowing the recruitment of multiple protein complexes at the same location to facilitate downstream signalling. To speculate around the likelihood of these known targets of M1-linked ubiquitination to play the same role during RIG-I signalling, we considered the requirement for NEMO and RIP1 in RIG-I signalling. In our model NEMO, but not RIP1, is absolutely required for activation of both IRF3 and NF- $\kappa$ B by RIG-I, processes also both regulated by HOIP. It is also known that both NEMO and HOIP bind to K63-linked ubiquitin chains and each other<sup>135,505,518</sup>. Therefore, we propose that the most likely targets of M1-Ub chains in the RIG-I signalling complex are NEMO and the K63-linked ubiquitin chains generated by TRAFs, responsible for recruitment of NEMO.

Our data on the role of M1-Ub chains in RIG-I signalling adds to the wealth of literature highlighting the importance of ubiquitin chains and E3 ligases in antiviral RIG-I signalling<sup>46,556,557</sup>, as well as the bank of knowledge for how M1-Ub ubiquitin chains regulate immune signalling pathways.

### 5.10.3 HOIP does not act to restrict virus replication in our system

In addition to regulating immune signalling outcomes, LUBAC has previously been shown to restrict virus infection. Our data with RNA viruses IAV PR8 and ZIKV PE243 showed that HOIP had no effect on either viral protein production or viral replication, however the use of a multi-step growth curve may have yielded a different result. This contradicts the only previous study of virus restriction by HOIP, which showed that loss of HOIP in the alveolar epithelium of mice resulted in higher viral titres during IAV infection<sup>506</sup>, but *in vivo* studies like this are done in the context of a whole organism with a complete immune system, so this is not directly comparable to our cell-based assays.

HOIL-1 and SHARPIN have also been previously shown to affect virus replication, with expression of HOIL-1 beneficial for the replication of VSV in both MEF and HEK293 cells under certain conditions, but not for MNoV replication in BMDC<sup>213,504,509</sup>. The presence of SHARPIN also appeared to enhance VSV replication in MEF cells but had no effect on the IAV viral load in *cpdm* mice was unaffected<sup>432,505</sup>. Although significant, these phenotypes are strikingly mild compared to the impact of RIG-I on RNA virus replication, with viral yield during VSV infection 100-fold higher in cells lacking RIG-I<sup>437</sup>, which is surprising, considering how important HOIP is for RIG-I driven activation of IFN and pro-inflammatory antiviral signalling. Having said this, we did not detect this strikingly enhanced ZIKV replication in RIG-I -/- cells during preliminary growth curve experiments with ZIKV, so this may

well be a condition-specific phenomenon. To better understand the full impact of HOIP on virus replication, the virus replication needs to be more carefully analysed using single- and multi-step growth curves at both high and low MOI.

#### 5.10.4 Involvement of LUBAC in RIG-I-driven cell death

A predominant feature of LUBACs regulation of other signalling pathways is that it controls a molecular switch between immune signalling and activation of programmed cell death pathways. We have showed that in our system, stimulation of RIG-I by synthetic RNAs and SeV did not drive cell death, irrespective of the presence of HOIP. The only cell death we observed was at late time points following ZIKV infection, but only at times where we have shown that immune signalling was no longer dependent on RIG-I, indicating that RIG-I does not drive this cell death.

Previously, HOIP has been shown to protect against RIG-I-driven cell death, with loss of HOIP from alveolar epithelial cells in mice resulting in enhanced lung injury during infection with IAV WSN<sup>534</sup>. This supports what has been shown during TLR3 activation, where loss of HOIP expression in HaCaT and HeLa cells sensitised them to Poly(I:C)-induced apoptosis, characterised by increased caspase-8 and -3 dependent cell death<sup>432</sup>. This was also shown *in vivo*, where an inducible HOIP knockout in primary murine keratinocytes (PMK) resulted in a lower viability after Poly(I:C) stimulation<sup>432</sup>. All of these findings are in contrast to work by Chattopadhyay et al., which shows that LUBAC drives M1-linked ubiquitination of IRF3, resulting in its interaction with Bax and activating IRF3- and RIG-I-dependent, TNF-independent cell death termed RIPA<sup>530,558–560</sup>. Notably, these studies describe a function of LUBAC that is very different to what occurs in other signalling pathways, where the presence of both LUBAC and/or M1-Ub chains prevents the receptor signalling complex from driving cell death<sup>432,502,523,561</sup>.

HOIL-1 and SHARPIN have also been implicated regulating RIG-I-driven cell death. Mutation of SHARPIN in *cpdm* MEF and mice resulted in higher levels of cell death and increased caspase 3 cleavage during infection with VSV, also seen during stimulation of TLR3 with Poly(I:C)<sup>432,505</sup>. Contrastingly, mice expressing a truncated version of HOIL-1 showed decreased lung injury during IAV WSN infection, suggesting full-length HOIL-1 enhanced cell death in this system<sup>534</sup>. However, although as true HOIL-1 *-/-* mice are not viable<sup>335,507</sup>, all data generated using these mice must be carefully considered.

Finally, in addition to RIPA, another model of SeV-induced RIG-I-dependent cell death has also been proposed. In L929 cells, infection with SeV resulted induction of TNF-independent RIG-I-dependent necroptosis, at time points as early as 10 hours post infection<sup>529</sup>. We did not observe this, likely

because A549 cells do not express RIP3, making them necroptosis-incompetent. However, preliminary assays using A549 cells stably overexpressing RIP3 showed that SeV infection still did not result in any visible cell death, even in the presence of caspase inhibitor Z-VAD.

Given that direct RIG-I-induced cell death was not observed in our cells, any future investigations of LUBAC's possible regulation of RIG-I-induced death would have to be carried out in different cell systems.

## 5.11 Conclusion

By examining RIG-I signalling outcomes in WT and HOIP-deficient A549 cells, we have been able to demonstrate the requirement of HOIP for the efficient activation of signalling pathway components, transcription of IFN-I and antiviral genes, and secretion of chemokines in response to activation of RIG-I by both synthetic RNAs and RNA viruses. Using a ligase-dead mutant of HOIP, we showed that the catalytic activity of HOIP is only partially responsible for its function in RIG-I signalling, and that this appears to be more pronounced at later time points. Demonstration of the interaction of LUBAC components HOIP and SHARPIN with NEMO and TBK1 during SeV infection supports the incorporation of LUBAC into the RIG-I signalling complex. Together, this enables us to propose a mechanism by which HOIP/LUBAC is required for efficient formation of the RIG-I signalling complex, and the subsequent production and conjugation of M1 ubiquitin chains in the signalling complex acts to amplify and prolong signalling, likely through enhanced recruitment of downstream signalling proteins.

# Chapter Six: The role of accessory proteins HOIL-1 and SHARPIN in RIG-I signalling

---

## 6.1 Introduction

Previous studies exploring the role of LUBAC in RIG-I signalling, and in many other signalling pathways, have examined the role of a single LUBAC component and attributed the phenotype seen to the function LUBAC as a complex, or to M1-linked ubiquitin chains. However, recent studies have shown that aside from contributing to the generation of M1-Ub chains by stabilising HOIP, HOIL-1 and SHARPIN also contribute independently to signalling outcomes, by regulating or directing the function of LUBAC<sup>562-566</sup>, as well as independently regulating signalling<sup>567,568</sup>. Because of this, we wanted to explore the individual contribution of all three LUBAC components to RIG-I signalling.

Therefore, having shown that HOIP is required for the efficient activation of IRF3 and NF- $\kappa$ B-dependent responses downstream of RIG-I, we next examined the effect of loss of HOIL-1 and SHARPIN expression on the immune response to synthetic RNAs 3p-hpRNA and Poly(I:C) and RNA viruses SeV and IAV R+K. As before, the outputs of RIG-I activation: signalling protein phosphorylation; immune gene transcription; and chemokine secretion, were analysed by Western blotting, qPCR and ELISA respectively. From this, we have demonstrated that HOIL-1 is required for RIG-I driven immune responses to both synthetic RNAs and RNA viruses, but that the role of SHARPIN is unclear.

## 6.2 HOIL-1 is required for a RIG-I-driven immune response to synthetic RNAs and RNA viruses

HOIL-1, like HOIP, is a member of the RING-in-between-RING family of E3 ligases. However, it was initially shown to have very limited activity in vitro and is incapable synthesising of M1-linked ubiquitin chains<sup>521</sup>. However, despite limited catalytic activity, HOIL-1 is required for the efficient generation of M1-Ub chains by HOIP, binding to release HOIP from the auto-inhibited conformation it forms on its own<sup>515,521</sup>. Additionally, more recent studies have identified additional catalytic-dependent roles for HOIL-1 in LUBAC signalling<sup>562,564,566,569</sup>. HOIL-1 also has LUBAC-independent functions, predominantly involving its ability to regulate protein degradation through conjugation of

K48 ubiquitin chains to proteins, linking HOIL-1 to regulation of antiviral signalling, cancer, cell death pathways and iron metabolism<sup>567</sup>.

Previous reports of the impact of HOIL-1 on RIG-I signalling are conflicting, reporting both positive and negative regulation<sup>135,213,504,505,534</sup>. To study the role of HOIL-1 in the RIG-I-driven immune response, RIG-I was stimulated in WT and HOIL-1-deficient MEF cells. Generation HOIL-1-deficient A549 cells using CRISPR/Cas9 technology was attempted, but this was unsuccessful within the time frame of this project. Instead MEF TNF -/- HOIL-1 +/- and TNF -/- HOIL-1 -/- cells were stimulated with synthetic RNAs and RNA viruses and the immune response measured by qPCR and Western blotting.

### 6.2.1 Characterisation of the immune response in MEF TNF -/- HOIL-1 +/- and HOIL-1 -/- cells

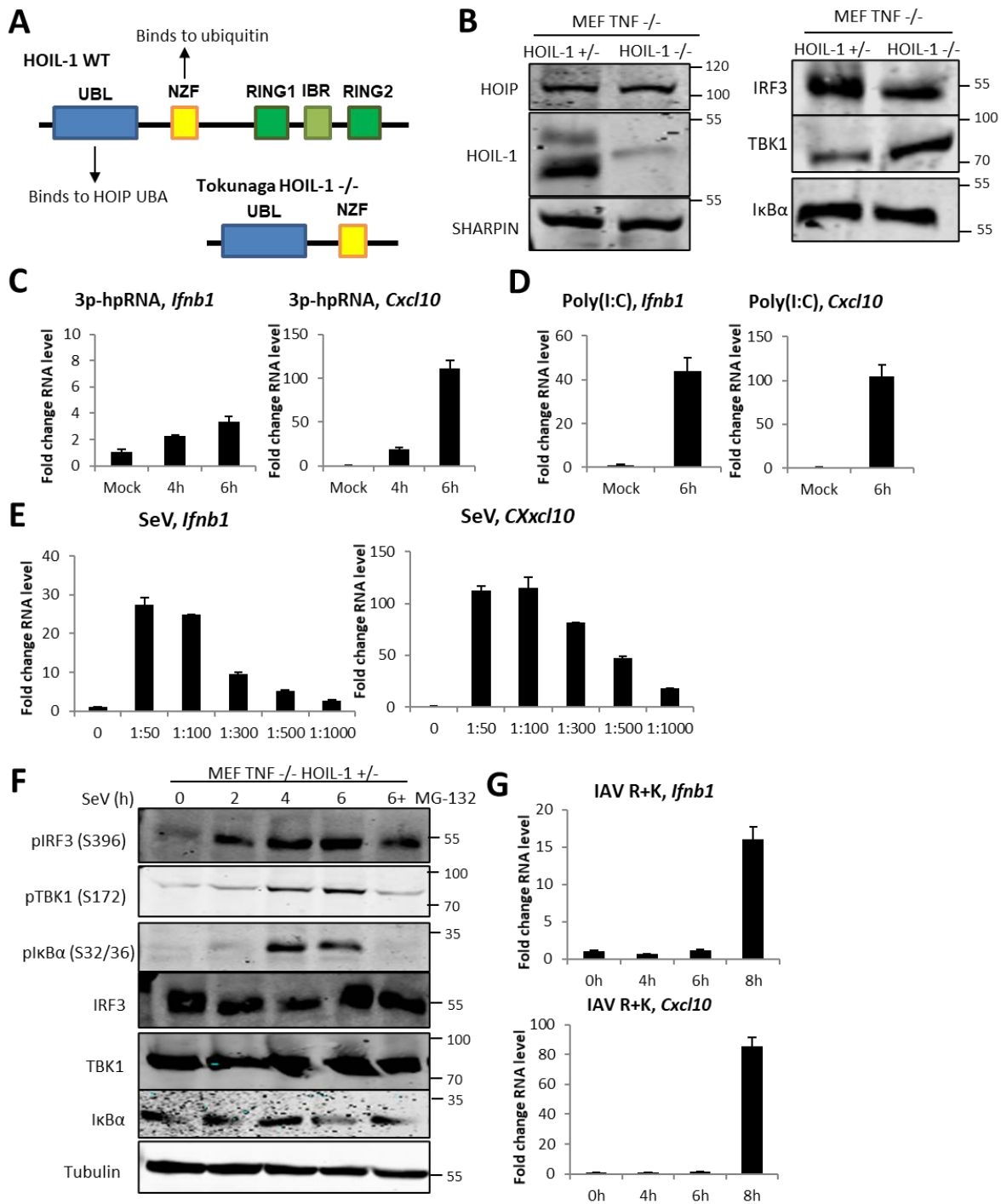
MEF TNF -/- HOIL-1 +/- and MEF TNF -/- HOIL-1 -/- cells were generated by immortalisation of mouse embryonic fibroblasts (MEF) cells from a true HOIL-1 -/- mouse<sup>335</sup>. Generation of just HOIL-1 -/- MEF cells is not possible as complete deletion of HOIL-1 in mice results in embryonic lethality, with embryos dying at day ten (E10) due to epithelial cell death in the yolk sack epithelium<sup>335,570</sup>. The additional deletion of TNF in these mice allows survival of embryos until day E16.5, enabling the generation of MEF cells. Because of this, the control “WT” MEF cells used in these experiments are a homozygous deletion for TNF and heterozygous for HOIL-1 (MEF TNF -/- HOIL-1 +/-) and the HOIL-1 deficient cells are a homozygous deletion for both TNF and HOIL-1 (MEF TNF -/- HOIL-1 -/-). Apparent HOIL-1 -/- mice and MEF cells generated by Tokunaga et al<sup>507</sup> have been used in previous HOIL-1 studies, however they retain expression of an N-terminal truncation of HOIL-1, retaining its ubiquitin and HOIP binding domains, shown in Figure 6.2.1A.

Protein expression of LUBAC components and RIG-I signalling proteins was examined by Western blotting in MEF TNF -/- HOIL-1 +/- and HOIL-1 -/- cells (Figure 6.3.1B), confirming loss of HOIL-1 expression in MEF TNF -/- HOIL-1 -/- cells. Expression of HOIP and SHARPIN appeared unaffected by loss of HOIL-1, as was expression of RIG-I signalling components IRF3, TBK1 and I $\kappa$ B $\alpha$ .

As our previous studies were done in A549 cells, before examining the contribution of HOIL-1, stimulation of RIG-I in MEF cells was tested. qPCR after stimulation of MEF TNF -/- HOIL +/- cells with 3p-hpRNA (Figure 6.2.1C) and Poly(I:C) (Figure 6.2.1D) showed similar levels of *Cxcl10* transcription with both RNAs, but only Poly(I:C) transfection induced *Ifnb1* transcription, as seen in A549 cells. MEF TNF -/- HOIL-1 +/- cells were also infected with varying dilutions of SeV (Figure 6.2.1E), resulting in transcription of both *Ifnb1* and *Cxcl10*, which increased significantly more at higher

concentrations, up to 1:100. Therefore, a 1:100 dilution was used for all future SeV infection studies. Western blotting during SeV infection at 1:100 dilution also detected phosphorylation of IRF3, TBK1 and I $\kappa$ B $\alpha$  (Figure 6.2.1F). Basal activation of IRF3 and TBK1 was detected in unstimulated cells, but this increased significantly with infection, with levels peaking at 6 hours post-infection. Finally, qPCR analysis of IAV R+K infection of MEF TNF<sup>-/-</sup> HOIL-1<sup>+/-</sup> cells showed transcription of both *Ifnb1* and *Cxcl10*, but not until 8 hours post-infection (Figure 6.2.1G). This is delayed compared to A549 cells, where significant levels of transcription were detected only 6 hours post infection with IAV R+K, likely due to the differing kinetics of virus infection in different cell types.

These data show that stimulation with 3p-hpRNA, Poly(I:C), SeV and IAV R+K induces an immune response in MEF cells, allowing us to use these cells to investigate the impact of HOIL-1 on RIG-I signalling. As we did not generate RIG-I-deficient MEF cells to test the specificity of our stimulation methods, we cannot claim to know that they are RIG-I-specific in this cell line, especially Poly(I:C) and IAV R+K, as they have been shown to activate MDA5 and TLR3 in MEF cells previously<sup>95</sup>.



### 6.2.1 Characterising the MEF TNF -/- HOIL-1 +/- cell line

A) Schematic of expressed portion of in previously published “Tokunaga HOIL-1 -/-” mice (UBL = ubiquitin-like, NZF = nuclear protein localisation 4 (Npl4) zinc finger, ZnF = zinc finger, UBA = ubiquitin associated, RING = really interesting new gene and IBR = in-between-ring. B) Western blot analysis of MEF TNF -/- HOIL-1 +/- and TNF -/- HOIL-1 -/- cells. qPCR to measure transcription of indicated genes in MEF TNF -/- HOIL-1 +/- cells after stimulation with C) 1 μg 3p-hpRNA (n=2, data representative of >3 independent assays), D) 1 μg Poly(I:C) (n=2, data representative of >3 independent assays), E) infection with SeV for 6 hours at varying dilutions (n=2, data from one independent assay) and G) infection with IAV R+K at MOI 5 (n=2, data representative of >3 independent assays). F) Western blot analysis of MEF TNF -/- HOIL-1 +/- cells infected with SeV at 1:100 dilution with and without 10 μM MG-132 (data representative of >3 independent assays).

## 6.2.2 The synthetic RNA-driven immune response is dependent on HOIL-1

Following this confirmation that MEF cells are suitable as a model cell line to study the role of HOIL-1 in RNA sensing, MEF TNF<sup>-/-</sup> HOIL-1<sup>+/-</sup> and HOIL-1<sup>-/-</sup> cells were transfected with 3p-hpRNA and Poly(I:C) and transcription of immune genes was measured by qPCR. Stimulation with 3p-hpRNA resulted in transcription of *Cxcl10*, *Isg15*, *Isg56* (the murine homolog of human *ISG54*) and *Il6* (Figure 6.2.2.A), but not *Ifnb1*, *Ifnl1* or *Nfkbia* (not shown). HOIL-1-deficient cells showed significantly reduced transcription of all genes except *Isg15*, whose transcription was only significantly reduced 4 hours after stimulation. Transfection with Poly(I:C) yielded similar results (Figure 6.2.2B), with transcription of *Ifnb1*, *Cxcl10*, *Isg15*, *Isg56* and *Il6* all robustly induced in HOIL-1<sup>+/-</sup> cells and expressed to a significantly lower level in HOIL-1<sup>-/-</sup> cells. This data shows that like HOIP, HOIL-1 is required for the RIG-I-driven transcription of immune genes in response to synthetic RNAs.

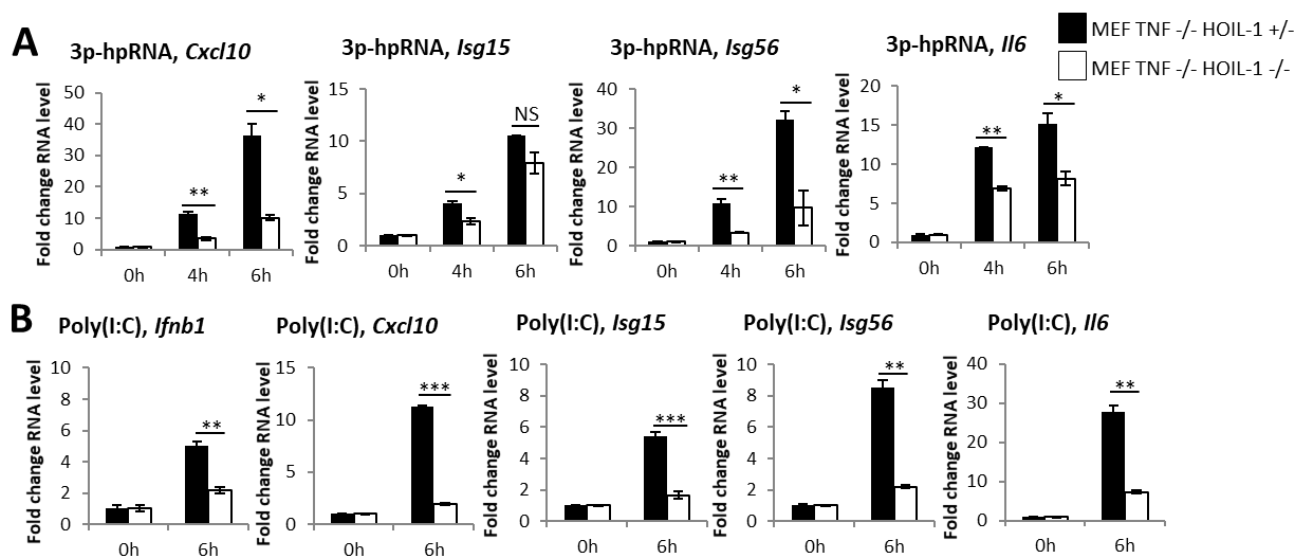


**Figure 6.2.2: Synthetic RNA-driven expression of immune genes is dependent on HOIL-1**

qPCR to measure transcription of indicated genes in MEF TNF<sup>-/-</sup> HOIL-1<sup>+/-</sup> and TNF<sup>-/-</sup> HOIL-1<sup>-/-</sup> cells stimulated with A) 1 μg 3p-hpRNA (n=2, data representative of 3 independent assays) and B) 1 μg Poly(I:C) (n=2, data representative of 3 independent assays).

## 6.2.3 The antiviral transcriptional response to SeV infection is dependent on HOIL-1

To see if HOIL-1 plays a similar role in RIG-I signalling in response to RNA virus infection, the response of HOIL-1<sup>+/-</sup> and HOIL-1<sup>-/-</sup> cells to infection SeV and IAV R+K was also measured by qPCR analysis (Figure 6.2.3A and B).

SeV infection of HOIL-1<sup>+/-</sup> cells resulted in a very similar transcriptional profile to A549 cells, except for *Ifnl2/3*, which is not transcribed in MEFs whereas its human homolog *IFNL1* was in A549s.

Transcription of all genes was significantly reduced in HOIL-1  $-/-$  cells at 4 hours post-infection, with *Ifnb1*, *Cxcl10*, *Isg56* and *Nfkb1a* also significantly reduced at 6 hours. As seen in A549 cells, infection of MEF HOIL  $+/-$  and HOIL  $-/-$  cells with IAV R+K resulted in variable levels of both *Ifnb1* and *Cxcl10* transcription between experimental replicates (Figure 6.2.3B). This was apparently due to large variations in the response in HOIL-1  $+/-$  cells between experiments, as transcription appeared consistent in HOIL-1  $-/-$  cells. As also seen in A549 cells, this appeared to correlate with transcription of the NS1 protein being uneven between the two cell lines, preventing us from describing the role of HOIL-1 during IAV infection.

Our data shows that loss of HOIL-1 results in reduced immune gene transcription in response to both synthetic RNAs and RNA viruses, meaning that even though the transcriptional phenotype seen in HOIL-1  $-/-$  cells is less stark than in HOIP  $-/-$  cells, HOIL-1 is required for efficient RIG-I-driven transcription.

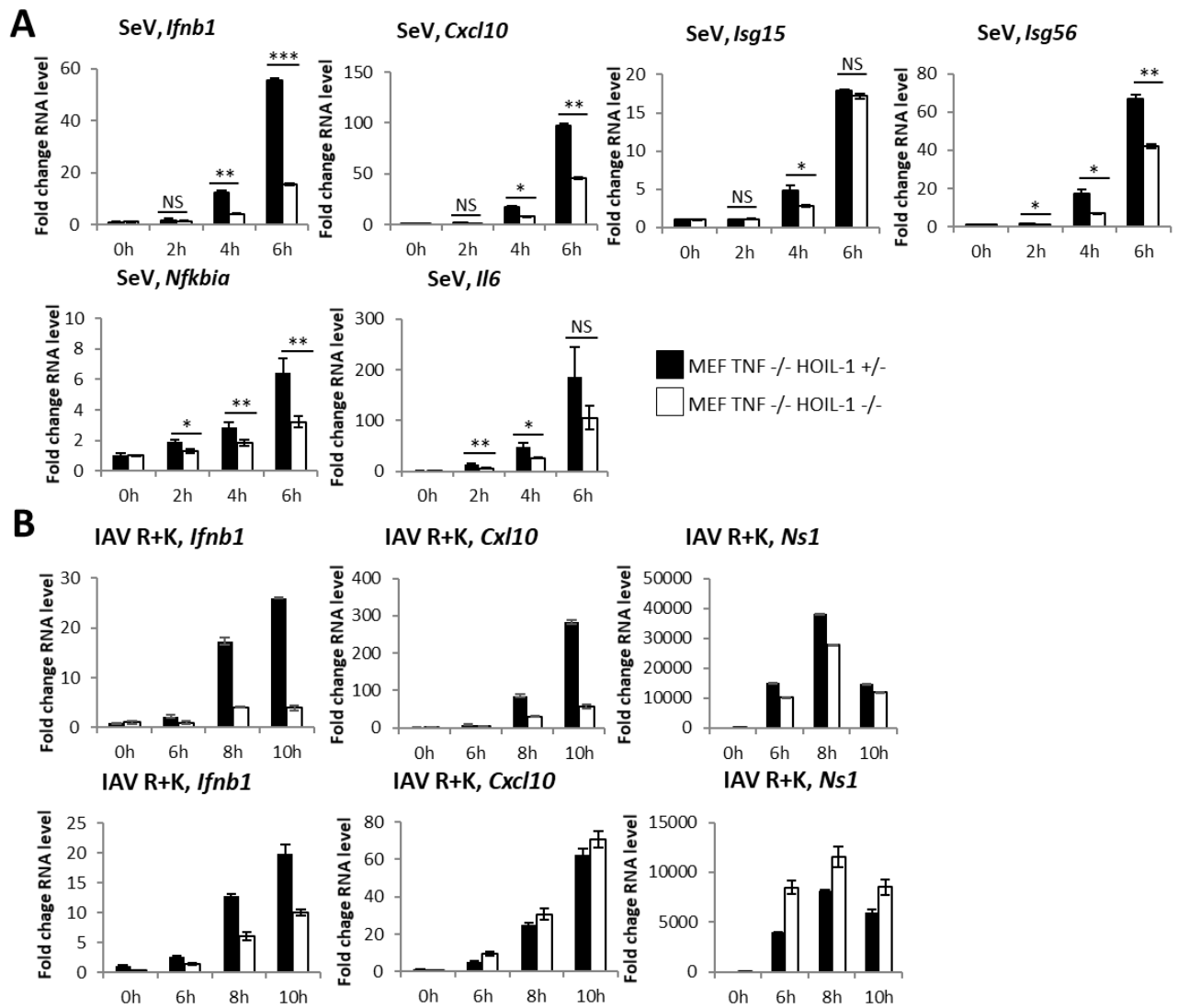


**Figure 6.2.3: HOIL-1 is required for RNA virus-driven immune gene expression**

qPCR to measure transcription of indicated genes in MEF TNF<sup>-/-</sup> HOIL-1<sup>+/-</sup> and HOIL-1<sup>-/-</sup> cells infected with A) SeV at 1:100 dilution (n=2, data representative of >3 independent assays) and B) IAV R+K at MOI 5 (n=2, data is representative of differing experimental results experienced).

### 6.2.4 HOIL-1 is required for activation of RIG-I signalling proteins during SeV infection

The role of HOIL-1 on signalling protein activation was then studied by Western blotting, measuring phosphorylation during SeV infection of MEF TNF<sup>-/-</sup> HOIL-1<sup>+/-</sup> and HOIL-1<sup>-/-</sup> cells (Figure 6.2.4). In cells lacking HOIL-1 expression, lower levels of phospho-IRF3, TBK1 and IκBα were detected, indicating that HOIL-1 is required for efficient RIG-I signalling protein phosphorylation.

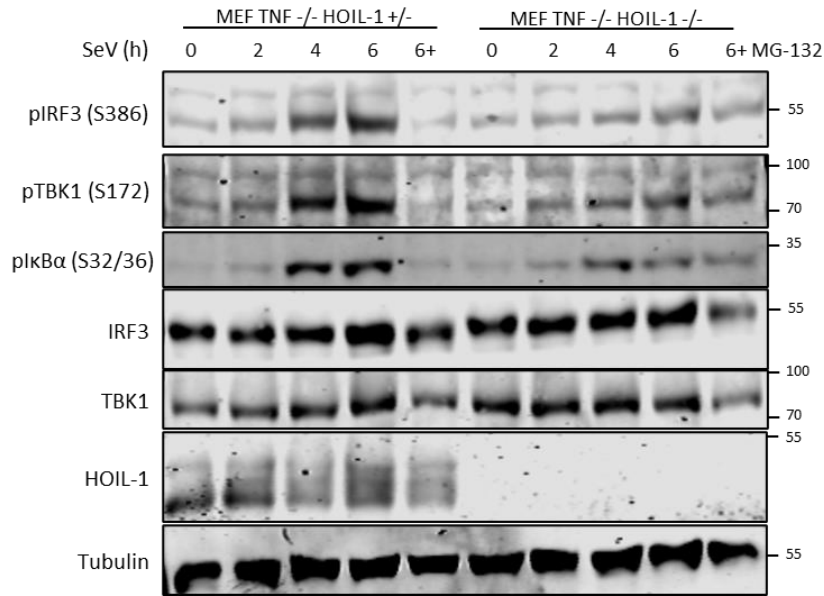


**Figure 6.2.4: HOIL-1 is required for SeV-driven activation of signalling pathway components**  
Western blot analysis of MEF TNF <sup>-/-</sup> HOIL-1 <sup>+/-</sup> and <sup>-/-</sup> cells infected with SeV at 1:100 dilution with (+) or without the presence of 10 μM MG-132 (data representative of >3 independent assays).

### 6.3 SHARPIN is not required for a RIG-I driven immune response to synthetic RNAs or RNA virus infection

SHARPIN is the third and most recently discovered component of LUBAC<sup>508,511</sup>, where it binds to and stabilises HOIP in its active confirmation, enabling efficient generation of M1-ubiquitin chains<sup>335,570</sup>. Before it was linked to LUBAC, SHARPIN was known to function in excitatory synapses in the brain, as well as in regulation of inflammation and immune development<sup>571,572</sup>. Interestingly, SHARPIN is the only component of LUBAC for which knockout mice are viable, named *cpdm* mice after their chronic proliferative dermatitis phenotype, caused by sensitisation of SHARPIN-deficient cells to TNF-driven apoptosis<sup>573</sup>.

#### 6.3.1 Generation of A549 SHARPIN <sup>-/-</sup> cells

To study the role of SHARPIN in RIG-I signalling, SHARPIN-deficient A549 cells were generated using CRISPR/Cas9 technology. Figure 6.3.1A shows the location targeted by the sgRNA in exon 4 of SHARPIN, in relation to the start codon. Loss of SHARPIN expression was confirmed by Western blotting (Figure 6.3.1B), with expression of HOIP and HOIL-1 appearing unaffected by loss of SHARPIN.

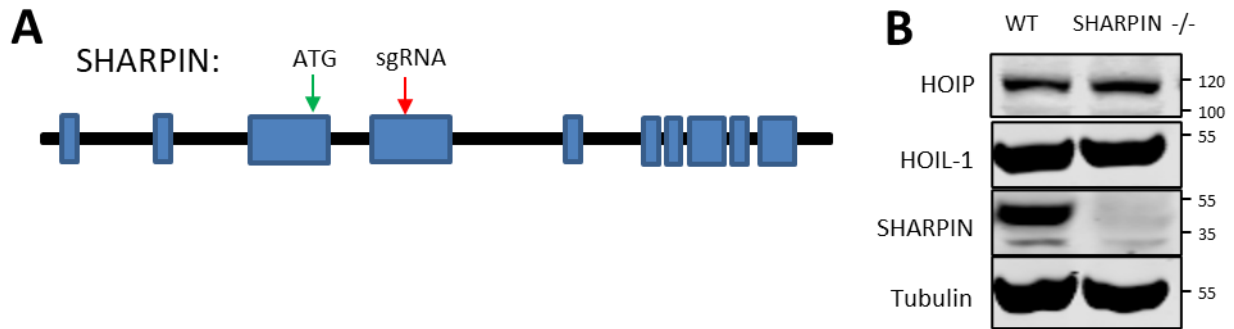


**Figure 6.3.1: Characterisation of SHARPIN  $-/-$  A549 cells**

A) Schematic of position of start ATG and small guide RNA used for CRISPR KO of SHARPIN in A549 cells, blue boxes represent exons and black line represents introns. B) Western blot analysis of LUBAC components in A549 WT and SHARPIN  $-/-$  cells.

### 6.3.2 Mixed requirement of SHARPIN for a synthetic RNA-driven immune response in A549 cells

To determine the requirement of SHARPIN for a synthetic RNA-driven immune response, A549 WT and SHARPIN  $-/-$  cells were transfected with 3p-hpRNA and Poly(I:C) and transcription of genes known to be induced in WT cells was measured by qPCR (Figure 6.3.2A and B). With both synthetic RNAs, loss of SHARPIN expression did not detrimentally affect transcription of either *IFNB1* or *CXCL10* but did result in significantly reduced transcription of both *ISG15* and *ISG54*. This shows that the effect of SHARPIN on RNA-induced immune transcription is mixed, with a clear effect on ISGs, but not the IFN $\beta$  response.

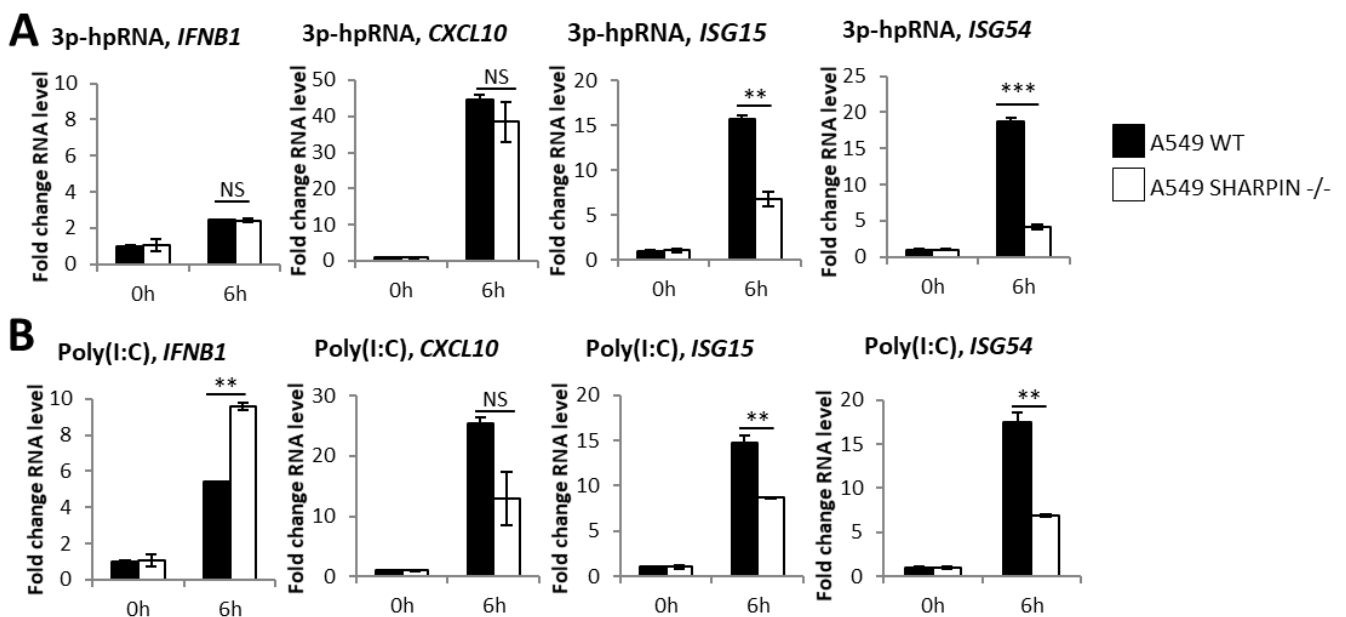


**Figure 6.3.2: SHARPIN is not required for synthetic RNA-driven immune gene transcription in A549 cells**  
qPCR to measure transcription of indicated genes in A549 WT and SHARPIN <sup>-/-</sup> cells stimulated with A) 1 µg 3p-hpRNA (n=2, data representative of 2 independent assays) and B) 1 µg Poly(I:C) (n=2, data representative of 2 independent assays).

### 6.3.3 SHARPIN is not required for the SeV-driven immune response in A549 cells

Next, the effect of SHARPIN on an RNA virus-driven immune response was examined by measuring transcription, signalling protein phosphorylation and chemokine secretion in A549 WT and SHARPIN <sup>-/-</sup> cells infected with SeV. SHARPIN-deficient cells transcribed significantly higher levels of all tested genes in response to SeV infection, compared to WT (Figure 6.3.3A). Somewhat conversely, Western blotting analyses showed that loss of SHARPIN expression appeared to have no effect on phosphorylation of TBK1 or IκBα (Figure 6.3.3B), with SHARPIN <sup>-/-</sup> cells actually having slightly lower levels of phospho-IRF3 than WT, especially at 2 hours post-infection. Having said that, this reduction is nowhere near as marked as in cells lacking HOIP or HOIL-1 and was not visible in every experimental repeat. ELISA analysis during SeV infection showed higher levels of CXCL10 secretion in SHARPIN <sup>-/-</sup> cells, both at 6- and 24-hours post-infection (Figure 6.3.3C), aligning with qPCR data.

These data show that SHARPIN is not essential for the RIG-I-driven immune response to RNA virus infection, in fact data from the two most sensitive techniques, qPCR and ELISA, suggest that SHARPIN may actually negatively regulate RIG-I signalling, as has been indicated by some previous studies.

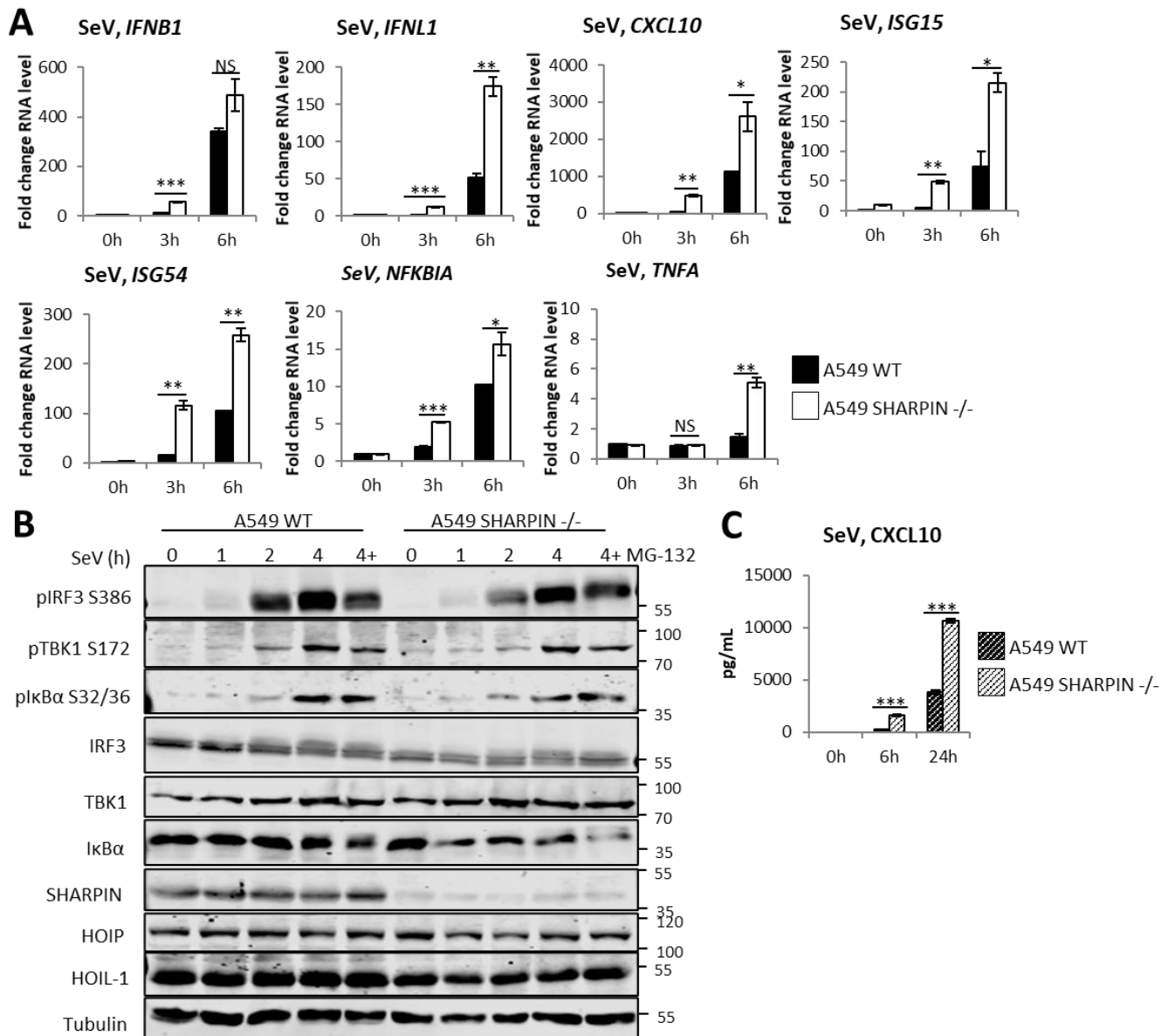


**Figure 6.3.3: SHARPIN is not required for the SeV-driven response in A549 cells**

SeV infection of A549 WT and SHARPIN  $-/-$  cells at 1:300 dilution. A) qPCR to measure transcription of indicated genes in A549 WT and SHARPIN  $-/-$  cells infected with SeV at 1:300 dilution ( $n=2$ , data representative of 2 independent assays), B) Western blotting analysis of signalling protein phosphorylation with (+) and without the presence of 10  $\mu$ M MG-132 (data representative of 3 independent assays) and C) ELISA analysis of CXCL10 secretion ( $n=2$ , data representative of 2 independent assays).

### 6.3.4. SHARPIN is not required for a RIG-I-driven immune response in MEF cells

As the lack of requirement for SHARPIN in RIG-I-dependent antiviral signalling differed from what was seen for both HOIP and HOIL-1, we wanted to confirm this with an additional model cell line.

Therefore, MEFs extracted from WT and *cpdm* mice were used to further study the requirement of SHARPIN for RIG-I-driven immune signalling<sup>508,571,572</sup>.

After Western blotting analysis confirmed loss of SHARPIN expression in *cpdm* MEFs (Figure 6.3.4A), transcription of immune genes was analysed by qPCR in WT and *cpdm* cells stimulated with 3p-hpRNA, Poly(I:C) and SeV. 3p-hpRNA transfection resulted in transcription of *Ifnb1*, *Cxcl10*, *Isg15* and *Isg56*, all of which appeared to be unaffected in *cpdm* cells (Figure 6.3.4B). On the other hand, during Poly(I:C) stimulation, transcription of *Cxcl10*, *Isg15* and *Isg56* all was reduced *cpdm* cells (Figure 6.3.4C), with only *Ifnb1* not detrimentally affected. This was not as marked during SeV infection, where transcription of both *Ifnb1* and *Cxcl10* was consistently reduced in SHARPIN *-/-* cells through the time course, but not transcription of *Isg15*, *Isg56*, *Nfkb1a* or *Il6* (Figure 6.3.4D).

As was described for A549 WT and SHARPIN *-/-* cells, the data generated in MEF WT and *cpdm* cells was not conclusive, with outcomes varying for different genes, assays and stimulation methods. Despite this, the data from both cell types allows us to conclude that SHARPIN is not required for RIG-I-driven IFN activation. Finally, as the phenotype in SHARPIN-deficient cells is different to that seen in HOIL-1-deficient cells, we can conclude that the phenotype in HOIL-1 *-/-* cells is not solely down to loss of HOIP activity caused by reversion to its auto-inhibited confirmation in the absence of either HOIL-1 or SHARPIN to stabilise it.

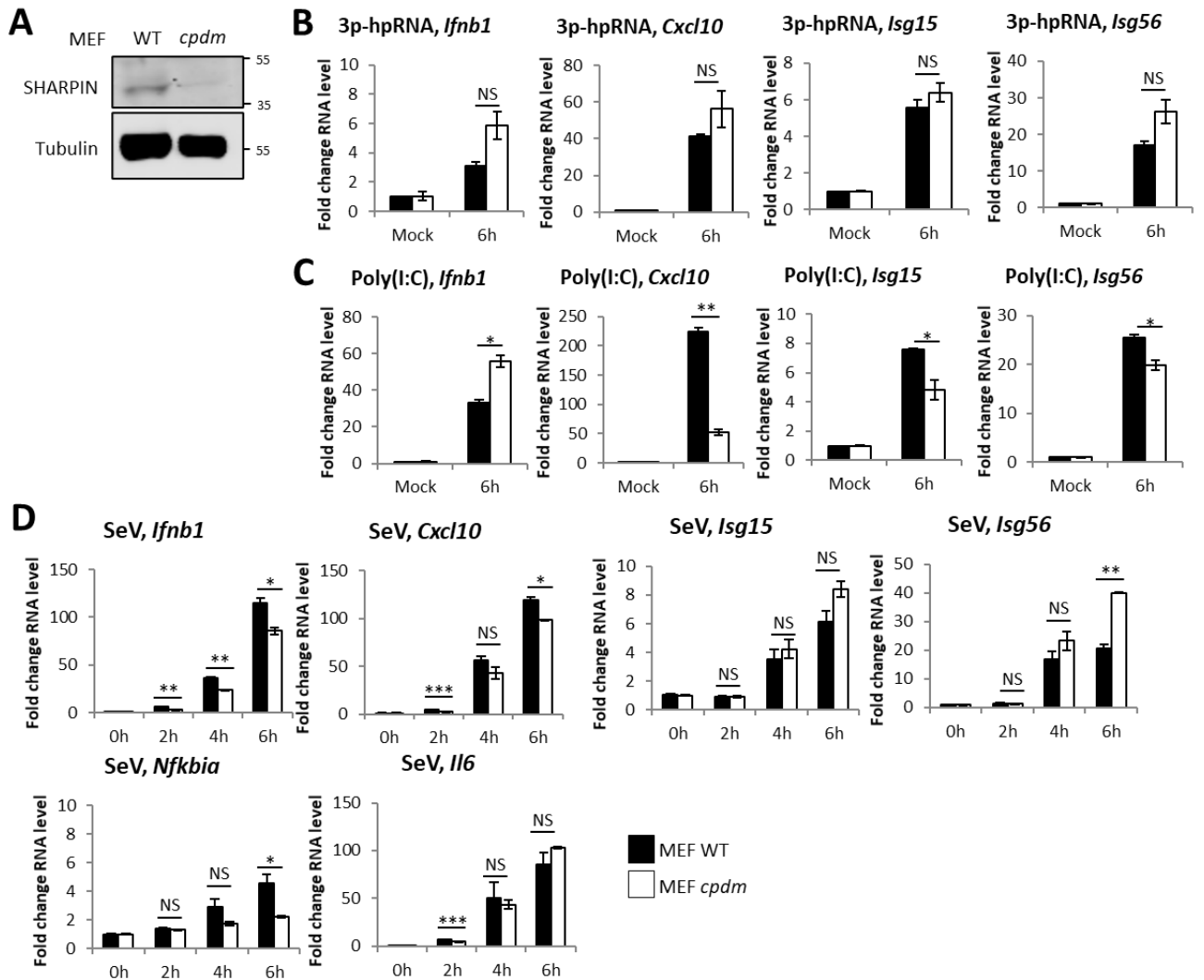


**Figure 6.3.4: SHARPIN is not required for RIG-I driven immune gene transcription in MEF cells**

A) Western blotting analysis of MEF WT and *cpdm* cells. qPCR to measure transcription of indicated genes in MEF WT and *cpdm* cells stimulated with B) 1  $\mu$ g 3p-hpRNA (n=2, data representative of 2 independent assays), C) 1  $\mu$ g Poly(I:C) (n=2, data representative of 2 independent assays) and D) SeV infection at 1:300 dilution (n=2, data representative of 2 independent assays).

## 6.4 Discussion

Through the work in this chapter, we analysed how the LUBAC accessory components HOIL-1 and SHARPIN regulate RIG-I signalling. Using A549 and MEF cells lines lacking expression of either HOIL-1 or SHARPIN, we have shown differing contributions to RIG-I signalling outcomes. This exploration of the independent functions of HOIL-1 and SHARPIN resolves some of the conflicting literature regarding the role of LUBAC in RIG-I signalling and provides a more detailed analysis of the function of LUBAC in regulation of immune signalling pathways, both as individual components and as a complex.

### 6.4.1 HOIL-1, like HOIP, is required for RIG-I-driven immune responses

Our data shows that HOIL-1 is required for activation of both IRF3 and NF- $\kappa$ B and the resultant downstream signalling by RIG-I, as was seen for HOIP. These observations support much of what we know about the role of HOIL-1 in other signalling pathways, where it has been shown to play an essential role in NF- $\kappa$ B activation during stimulation of cells with cytokines, PRR ligands, following genotoxic stress and in MAPK signalling in response to CD-40 and TNF $\alpha$ <sup>338,501,508,511,528,574–576</sup>.

However, our data disputes much of what has been previously published about the role of HOIL-1 in RIG-I signalling, possibly because very few previous studies have used a clean knockout system to study HOIL-1. Previously, studies utilising knockdown of HOIL-1 in multiple cell types including A549 and MEFs have shown that loss of HOIL-1 results in increased IRF3 activation and IFN-I induction in response to infection with SeV and VSV<sup>135,213,505,542</sup>. Conversely, another study indicated that knockdown of HOIL-1 in A549 cells reduced IFN-I and IL-6 secretion during IAV infection<sup>534</sup>, which is more in line with our data.

Many of the previous studies examining the role of HOIL-1 in RIG-I signalling also utilised cells from a mouse previously suggested to lack HOIL-1 expression<sup>507</sup>. Using cells from this mouse, 'loss' of HOIL-1 expression has resulted in various outcomes during RNA virus infection, with both increased and unaffected IFN-I and IFN-III activation detected in response to SeV and VSV infection<sup>213,504</sup>. Having said this, during activation of MDA5 by MNoV and TMEV, these 'HOIL-1 knockout' cells had reduced IRF3, IFN-I and IFN-III activation<sup>504</sup>, despite both MDA5 and RIG-I converging at MAVS to signal via a common pathway<sup>46</sup>. Cells from this mouse, however, are not completely HOIL-1 null as they still express a small amount (approximately 10%) of a 30 kDa truncated version of HOIL-1. This truncated HOIL-1 is missing its catalytic RBR E3 ligase domain, a region known not to be critical for m1-linked ubiquitination of substrates<sup>562</sup>. The truncated protein does, however, still contain the ubiquitin like (UBL) domain responsible for binding to HOIP in the LUBAC complex<sup>510</sup>, shown to be sufficient to support M1-Ub chain synthesis by HOIP<sup>510</sup>, and the NZF domain, which is required for binding to polyubiquitin chains and is essential for its role in NF- $\kappa$ B activation downstream of TNF and IL-1B<sup>337,528,577</sup>. The biological importance of the expression of these domains of HOIL-1 is highlighted by the fact that Tokunaga HOIL-1  $-/-$  mice and knock-in mice expressing the catalytically inactive HOIL-1 RBR mutant are viable<sup>564</sup>, whereas complete HOIL-1  $-/-$  mice die in utero<sup>335,528</sup>.

The cells used in this study lack expression of any part of the HOIL-1 protein, meaning that both of the dual functions of HOIL-1, stabilisation of HOIP and as an E3 ligase, are prevented. Thus, this study shows the true effect of HOIL-1 on RIG-I signalling.

## 6.4.2 SHARPIN is not required for gene transcription following RIG-I activation

Using two SHARPIN deficient cell lines we have shown that, in contrast to HOIP and HOIL-1, the third LUBAC component SHARPIN is not essential for RIG-I-driven immune responses. Generally, loss of SHARPIN had no effect on RIG-I signalling outcomes, with some SHARPIN-deficient cells even displaying increased immune signalling outputs following RIG-I activation. As with HOIL-1  $-/-$  cells, this phenotype was not caused by loss of HOIP or HOIL-1 expression as has been previously observed<sup>338,547</sup>.

Our data supports some of what has already been described about the role of SHARPIN in RIG-I signalling in MEF cells, where disruption of SHARPIN expression had no effect on IRF3 activation or I $\kappa$ B $\alpha$  phosphorylation and resulted in a modest increase in IFN-I production in response to SeV and VSV infection<sup>135,505</sup>. However, in these studies NF- $\kappa$ B activation and IFN-I production was reduced in *cpdm* MEFs during RNA virus infection. In TLR3 signalling, knockdown of SHARPIN or use of cells from *cpdm* mice also resulted in a mixed phenotype, with reduced NF- $\kappa$ B activation and chemokine secretion but unaffected IRF3 activation response to extracellular Poly(I:C)<sup>432</sup>.

This opposes studies of the role of SHARPIN in other immune signalling pathways, which have been much more conclusive, showing that SHARPIN is required for activation of NF- $\kappa$ B and JNK/ERK signalling pathways in response to stimulation with TNF $\alpha$ , IL-1 $\beta$ , CD-40 and LPS<sup>338,508,511</sup>. Because SHARPIN does not have a RBR ligase domain, unlike HOIP and HOIL-1, its role in these pathways is solely attributed to its function within LUBAC. SHARPINs function in LUBAC instead depends on its protein-binding ability, binding to and stabilising HOIP in its active conformation<sup>338,528,578</sup> and binding target proteins such as NEMO to facilitate conjugation of M1-linked ubiquitin chains<sup>330,331</sup>. The interaction between SHARPIN and NEMO has also been shown to be necessary for regulation of RIG-I signalling<sup>505</sup>. It is currently unclear why SHARPIN is definitively required for NF- $\kappa$ B activation by many immune receptors including RNA sensor TLR3 but has a non-essential function in RIG-I-driven IFN-I activation. This may be due to differing mechanisms of activating NF- $\kappa$ B between the pathways, requiring differing adaptor proteins, only some of which can be influenced by SHARPIN. Alternatively, this may be due to LUBAC-independent functions of SHARPIN in other pathways, as it is known to bind caspase-1 in a LUBAC-independent fashion<sup>579</sup>, as well as many proteins involved in regulation of NF- $\kappa$ B signalling<sup>580</sup>.

### 6.4.3 In addition to their function in LUBAC, HOIP, HOIL-1 and SHARPIN all have independent functions in signalling pathways

Our data shows that HOIL-1 function similarly to HOIP in RIG-I signalling, with the phenotype observed in complete HOIL-knockout MEF cells phenocopying what we saw in HOIP-deficient A549 cells: reduced activation of IFN-I and NF- $\kappa$ B-dependent responses. This data supports our model that LUBAC positively regulates RIG-I signalling in different cell types and in both humans and mice.

Initially, we entirely attributed the phenotype seen in HOIL-1-deficient cells to its ability to stabilise HOIP in its active conformation, supported by the fact that the phenotype in HOIL-1  $-/-$  cells was more moderate than in cells lacking HOIP, with higher levels of immune gene transcription detected. This was partially expected, as HOIP contains the catalytic domain of LUBAC responsible for the generation of M1-ubiquitin chains<sup>515</sup>. Furthermore, both HOIL and SHARPIN alone are able to stabilise HOIP sufficiently to induce NF- $\kappa$ B activation<sup>338,508,511,581</sup>, with knockout of HOIL-1 previously shown to severely impair HOIP expression both in MEFs and A549 cells<sup>213,528,534</sup>. We did not, however, detect altered HOIP expression in HOIL-1  $-/-$  cells, so we can attribute the phenotype in HOIL-1-deficient cells to the function of HOIL-1, not indirect loss of HOIP.

Although initially reported to have limited activity, recent studies demonstrating the ubiquitin ligase activity of the HOIL-1 RBR domain<sup>521,562,582,583</sup>, have lead us to consider that the phenotype seen in HOIL-1  $-/-$  cells may also be caused by loss of HOIL-1 ligase activity. HOIL's E3 ligase activity is required for the priming lysine modification then enables ubiquitin chain addition to NEMO<sup>562</sup>, as well as for the formation of unusual oxyester bonds between ubiquitin and serine and threonine residues on substrate proteins, important for controlling the outcome of immune receptor signalling<sup>564,566</sup>. This unusual E3 ligase activity of HOIL-1 occurs in a co-ordinated relay mechanism with HOIP to promote the generation of heterotypic K63/M1-ubiquitin chains in both TNF and TLR signalling<sup>566,584</sup>. Analysis of HOIL-1 E3 ligase mutant (C458S) mice, determined that this atypical chain formation can result in opposing signalling outcomes. This has been demonstrated during IL-18 and TLR-driven myddosome activation in cytotoxic T cells and bone marrow-derived macrophages (BMDMs), where HOIL-1's E3 ligase activity and the resulting ester-linked ubiquitin chains restrict IL-18 signalling but are required for TLR-driven efficient IL-12 and IL-6 secretion<sup>584</sup>. IL-18 restriction occurs because the presence of both normal isopeptide-linked ubiquitin chains and ester-linked chains limits the size of the ubiquitin chain, reducing the recruitment of downstream signalling proteins like TRAF6. Conversely, ester-linked ubiquitin chains in TLR signalling enables 'priming' events, driving ubiquitination of IRAK2 that allows its interaction with TRAF6 and drives downstream cytokine secretion<sup>584,585</sup>. In addition to assisting in M1-ubiquitin chain formation, HOIL-1 can

negatively regulate LUBAC activity. HOIL-1's RBR domain catalyses the conjugation of mono-ubiquitin onto LUBAC subunits, on to which HOIP then adds M1-chains, attenuating the function of LUBAC in TNF signalling<sup>563</sup>. The importance of the ligase function of HOIL-1 is further highlighted by the fact that the E2 conjugating enzyme that binds HOIL, UBE2L3, is recruited to the TNF-RSC alongside LUBAC<sup>501,586</sup> and findings showing that presence of full length HOIL-1 is required for the greatest ubiquitination activity of LUBAC, even though the UBA domain alone is sufficient to relieve HOIP auto-inhibition<sup>587</sup>.

These previously described roles of the HOIL-1 RBR domain, whose expression is lost in Tokunaga HOIL -/- mice and cells, in negative regulation of LUBAC may explain the increased immune signalling seen in these cells. Expression of the UBL and NZF domains of HOIL-1, which are still expressed in Tokunaga HOIL -/- cells, are sufficient to stabilise HOIP enabling efficient function of LUBAC, but the lack of HOIL-1 RBR domain means that the negative regulation of LUBAC by HOIL-1 mono-ubiquitination no longer occurs. This may also be the case for HOIL-1-knockdown, where cells express enough HOIL-1 to stabilise HOIP, but not sufficient to elicit its E3 ligase function to regulate LUBAC activity.

Having said this, it must be acknowledged that studies using Tokunaga HOIL -/- mice or cells to examine the role of LUBAC in other signalling pathways have not seen the same phenotype that we did when studying RIG-I signalling, where HOIL-1 appears to negatively regulate signalling, although enhanced or delayed TNF-induced JNK activation has been reported in these cells<sup>508,528,576,588</sup>.

Generally, in other signalling pathways, studies using these cells found that HOIL-1 was required for NF- $\kappa$ B activation. This difference could possibly be explained by differing primary outputs between TNF-RSC and RIG-I signalling, where TNFR only activates NF- $\kappa$ B activation, whereas the predominant output of RIG-I activation is IRF3-dependent IFN-induction. Thus, the mechanism of regulation of these signalling complexes by LUBAC may differ, possibly meaning a different requirement for the ligase activity of HOIL-1.

Alternatively, the different outcomes of RIG-I and TNF signalling in 'Tokunaga' HOIL-1 -/- cells may also be explained by the described role for HOIL-1's K48-linked E3 ligase activity as a negative regulator of many immune signalling pathways including TNF-R and IL-1R signalling<sup>589</sup>, PKC activation<sup>590-593</sup> and anti-viral IRF3 activation<sup>213,542</sup>. In this instance, loss of RBR domain expression would not only result in loss of LUBAC activity but loss of negative regulation of these pathways, resulting in a positive phenotype. However, the function of HOIL-1 as a K48-ubiquitin ligase is disputed, as many of these studies relied on overexpression of HOIL-1 or HOIL-1 mutants.

Overexpression of a catalytically active E3 ligase, as previously described for HOIP, may result in aberrant ubiquitination of proteins that would not generally be a target of ubiquitination in physiological settings. The contribution of HOIL-1's E3 ligase activity to its function in signalling pathways could be assessed more accurately through the use of an E3 ligase-inactive HOIL-1[C458/460S] mutant, which was previously used to demonstrate the role of HOIL-1 in modulating HOIP's activity<sup>521,564</sup>.

Our data suggests that unlike HOIL-1, SHARPIN does not play a role in RIG-I signalling in our system, either in its requirement for stabilising HOIP for efficient LUBAC function, or for any independent functions. This is supported by data surrounding their biological significance because SHARPIN-deficient mice, unlike mice lacking expression of either HOIP or HOIL-1, are viable, displaying an inflammatory phenotype, predominantly in the skin<sup>594</sup>. Additionally, whilst evidence of disease-causing mutations in HOIP and HOIL-1 have been found in humans, no disease has been attributed to mutations in SHARPIN, suggesting that this may not be pathogenic in humans.

Considering this, we suggest that the reason for differing requirements for HOIL-1 and SHARPIN in RIG-I signalling is not related to their shared function of stabilising the active LUBAC complex. Only one of HOIL-1 or SHARPIN is required to stabilise HOIP in its active conformation<sup>338,508</sup>, meaning in theory that in the absence of either protein, the other can compensate for this. Instead, we propose that their differing requirement is caused by the role of their alternative functions in RIG-I signalling, with the phenotype we see in HOIL-1-deficient cells caused by its other M1-ubiquitin chain related functions<sup>564,566</sup> and the absence of a phenotype in SHARPIN-deficient cells suggesting that it does not have a specific role in RIG-I signalling besides stabilising HOIP. To test this, RIG-I signalling outcomes must be examined using a HOIL-1/SHARPIN double-knockout cell line rescued with stable expression of a ligase-inactive HOIL-1 mutant. One fact that may counter this hypothesis that LUBAC-independent functions of HOIL-1 and SHARPIN are responsible for the differing phenotypes, is that the presence of all three LUBAC components results in the most efficient formation of M1-ubiquitin chains by LUBAC<sup>338</sup>. However, we have shown that M1-ubiquitin chains are only partially required for the function of LUBAC in RIG-I signalling, and are not required for the initial activation of IRF3 and NF-κB, meaning potentially that SHARPIN would not be required for the initial activation of IRF3 and NF-κB by RIG-I. This may also explain why the requirement for SHARPIN differs between RIG-I signalling and other signalling pathways, as almost all immune signalling pathways except TCR signalling, B cell signalling, and now RIG-I activation have been shown to need the E3 ligase activity of LUBAC for efficient immune activation<sup>519,524</sup>.

Despite not being required for RIG-I signalling in A549 cells, the focus of most previous studies into SHARPIN may give us an insight into its primary function in immune signalling, namely regulating the activation of cell death pathways. SHARPIN-deficient cells are hypersensitive to TNF-driven cell death<sup>338,511</sup>, the activation of which in epidermal keratinocytes results in the chronic proliferative dermatitis phenotype seen in *cpdm* mice<sup>573</sup>. This is prevented by LUBAC-enabled activation of NF- $\kappa$ B, which protects the cells from apoptosis by activating transcription of anti-apoptotic genes such as Bcl2<sup>595-597</sup>, with SHARPIN seeming to play a predominant role in regulating this. SHARPIN also appears to protect cells from cell death activated by TLR-dependent RNA sensing pathways, with SHARPIN-deficient HaCaT cells and *cpdm* PMK cells sensitised to Poly(I:C)-induced cell death<sup>432</sup>. This is further supported by IAV-infected *cpdm* mice showing increased cell death in the lungs, independent of viral load<sup>432</sup> and *cpdm* MEF cells being sensitised to RIG-I-driven cell death during VSV infection<sup>505</sup>.

We did not specifically study the role of SHARPIN in RIG-I-driven cell death in our system. However, after 24 hours of SeV infection, only very limited CPE was visible in SHARPIN-deficient A549 and MEF cells, suggesting loss of SHARPIN did not sensitise the cells to SeV-driven death. The lack of cell death in our system may be caused by the fact we did not infect SHARPIN-deficient cells with an active replicating/productive virus. However, Poly(I:C), which has been used to induce TLR3-driven cell death<sup>432</sup>, did not induce visible cell death in our SHARPIN  $-/-$  cells, although this was only assessed at early time points.

Despite not observing a cell death phenotype with SHARPIN in our system, previous data showing that SHARPIN is predominantly responsible for regulating cell death in other signalling pathways, coupled with our results showing that SHARPIN does not contribute to RIG-I-driven immune activation, allows us to propose this as an alternative function for SHARPIN in RIG-I signalling. We suggest a mechanism by which HOIP and HOIL act to drive immune activation by functioning as a scaffold and subsequently conjugate M1-ubiquitin chains to the RIG-I complex, and SHARPIN exists in the complex to block the activation of cell death pathways. SHARPIN may also play a role in determining the target of M1-ubiquitination in the signalling complex, as has previously been shown with NEMO in TLR signalling<sup>330,331</sup>, but this was not essential for effective function of LUBAC in the RIG-I signalling complex in our system. The lack of requirement for SHARPIN for directing M1-linked ubiquitin chains may be because there are multiple targets of M1-ubiquitination in the signalling complex, or multiple mechanisms of conjugating ubiquitin onto the same target, or because M1 chains are conjugated onto other ubiquitin chains already present in the signalling complex.

## 6.5 Conclusion

The data presented in this thesis shows that HOIP and HOIL-1 are required for optimal activation of both IRF3 and NF- $\kappa$ B by RIG-I, but that SHARPIN is not required for this process. We propose a two-step model by which HOIP and HOIL-1 regulate RIG-I signalling in which LUBAC acts as scaffold to allow proper formation of the RIG-I signalling complex and then conjugates M1-Ub within the complex to enhance and stabilise recruitment of downstream signalling proteins, illustrated by schematics in Figure 6.5.1 and Figure 6.5.2 respectively. By comparing the phenotype we saw in HOIP- and HOIL-1-deficient cells and HOIP-C885S-expressing cells with the phenotype seen in cells lacking known RIG-I signalling components, we can adapt our earlier proposed RIG-I signalling model to include LUBAC. We suggest that LUBAC is recruited to the RIG-I signalling complex by binding K63-ubiquitin chains, upon which it recruits/activates TBK1 and conjugates M1 chains to NEMO, enhancing its recruitment and boosting downstream signalling.

We propose this as a mechanism because the phenotype seen in both HOIP- and HOIL-1-deficient cells is most similar to NEMO  $-/-$  cells, as they all show reduced activation of both IRF3 and NF- $\kappa$ B and the resultant immune gene transcription and chemokine secretion. This suggests that LUBAC is involved in either recruitment of NEMO to the RIG-I signalling complex, or in NEMO's function within the complex. The only difference is that TBK1 phosphorylation is lost in HOIP and HOIL-1  $-/-$  cells but is not affected by loss of NEMO. This suggests that in addition to modulating NEMO function, LUBAC is required for efficient activation and/or recruitment of TBK1. All of this is reinforced by our data showing that LUBAC interacts with both NEMO and TBK1 during RIG-I stimulation. M1-ubiquitin chains do not appear to be required for the role of LUBAC in regulating either TBK1 or IRF3 activation, or the phosphorylation and degradation of I $\kappa$ B $\alpha$  to activate NF- $\kappa$ B, so this is only dependent on the presence of HOIP and HOIL at the RIG-I complex and not M1-ubiquitin chain formation. M1 chains are, however, required to enhance recruitment of signalling proteins and boost downstream responses. We suggest that this may be caused by the formation of M1/K63-linked hybrid ubiquitin chains, that function to amplify IRF3 activation in the RIG-I signalling complex, likely modulating it around the level of NEMO recruitment and activation.

The mechanism by which this regulation occurs also relies on our knowledge of LUBAC at the TNF-RSC. In TNF signalling, both NEMO and LUBAC are initially recruited by binding to ubiquitin chains generated by cIAPs<sup>501,598,599</sup>. LUBAC then conjugates M1-linked ubiquitin chains to NEMO<sup>334,338,501</sup>, which enhances its recruitment and retention because NEMO has a much higher affinity for M1-ubiquitin chains than K63/K11-linked chains<sup>599-603</sup>. The recruitment of TBK1 and IKK $\epsilon$  to the TNF-RSC is also mediated largely by M1-ubiquitin chains, as well as TANK, NAP1 and SINTBAD<sup>333</sup>. Similarly,

TRAF proteins have been shown to produce K63-ubiquitin chains that recruit NEMO to the RIG-I signalling complex. Therefore, we propose that K63-ubiquitin chains generated by TRAFs recruit LUBAC and NEMO to the RIG-I signalling complex, and that the presence of both LUBAC and NEMO here enables recruitment and activation of TBK1 and IRF3, as well as NF- $\kappa$ B. We cannot rule out the additional contribution of oxy-ester-linked ubiquitin chains catalysed by HOIL-1 in the RIG-I signalling complex, although IRAK2, a protein not involved in RIG-I signalling, is the only known target of this chain type<sup>584</sup>.

### Step 1: Complex formation

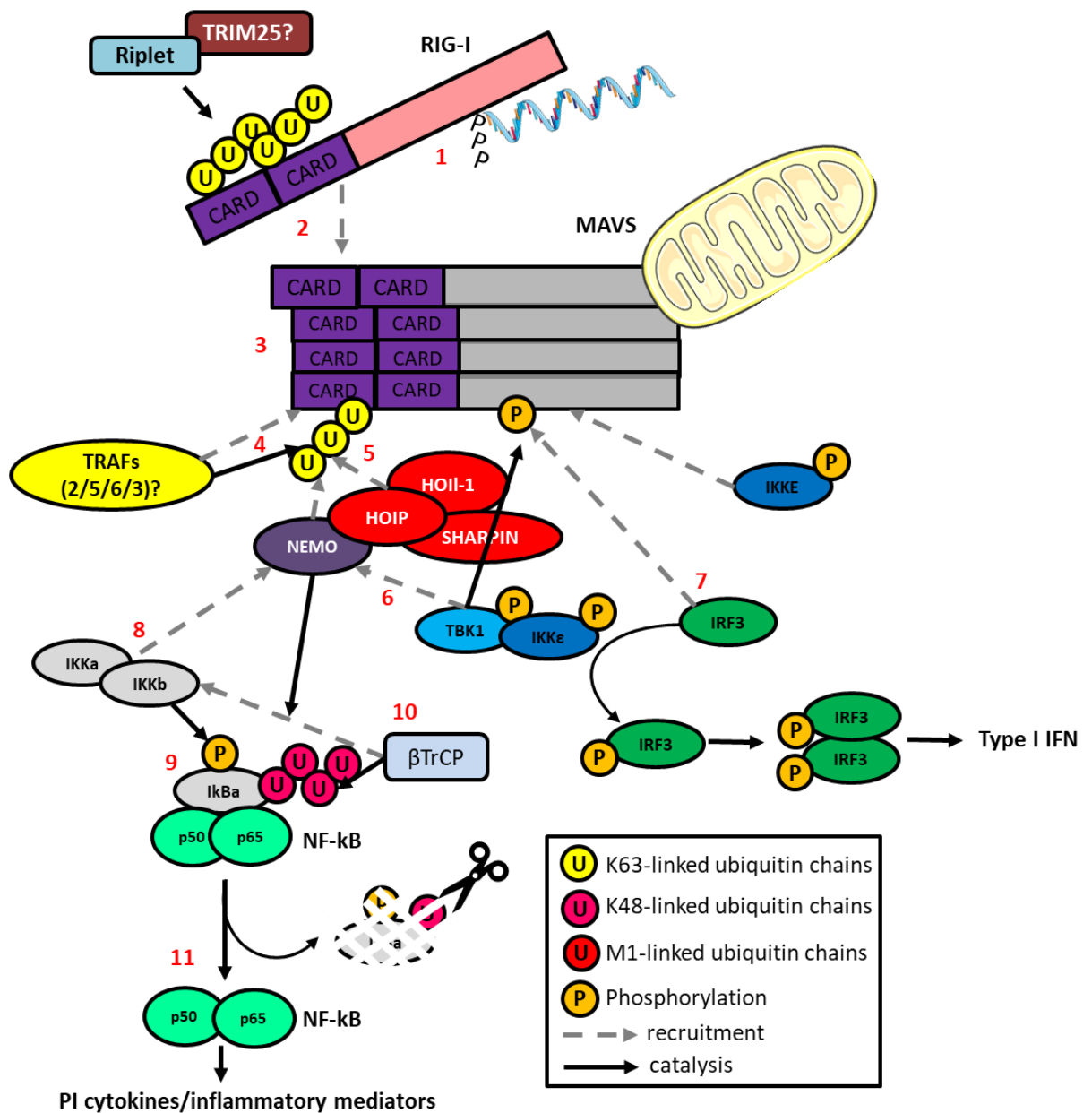


**Figure 6.5.1: Schematic of the proposed mechanism of LUBACs involvement in RIG-I signalling complex formation**

Complex initiation

1. RIG-I binds to RNA with 5'ppp and regions of double-stranded secondary structure
2. This alongside ubiquitination of RIG-I CARD domains by Riplet and TRIM25 activates RIG-I CARD, which is recruited to MAVS at the mitochondrial outer membrane
3. Activation of MAVS by RIG-I (and a wealth of other modifications) causes oligomerization of MAVS via the CARD domain
4. TRAF proteins are recruited to MAVS, where they add K63-linked ubiquitin chains to the CARD domain of MAVS
5. NEMO and LUBAC are recruited by binding K63 ubiquitin chains

IRF3 activation

6. TBK1 and IKK $\epsilon$  are recruited to the signalling complex where they phosphorylate MAVS
7. IRF3 is recruited to the phosphorylated MAVS, and once in proximity with activated TBK1, is phosphorylated, inducing dimerization, translocation to the nucleus and activation of an IFN-I response

NF- $\kappa$ B activation

8. IKK $\alpha$  and  $\beta$  are recruited to the signalling complex,
9. IKK $\beta$  phosphorylates I $\kappa$ B $\alpha$  to initiate its degradation
10. NEMO facilitates the recruitment of the ubiquitin and proteasomal degradation machinery to IKK $\beta$ , where it ubiquitinates I $\kappa$ B $\alpha$ , inducing its degradation by the 26S proteasome
11. NF- $\kappa$ B subunits are released into the nucleus to activate transcription of pro-inflammatory responses

## Step 2: M1 chains enhance signalling complex outputs

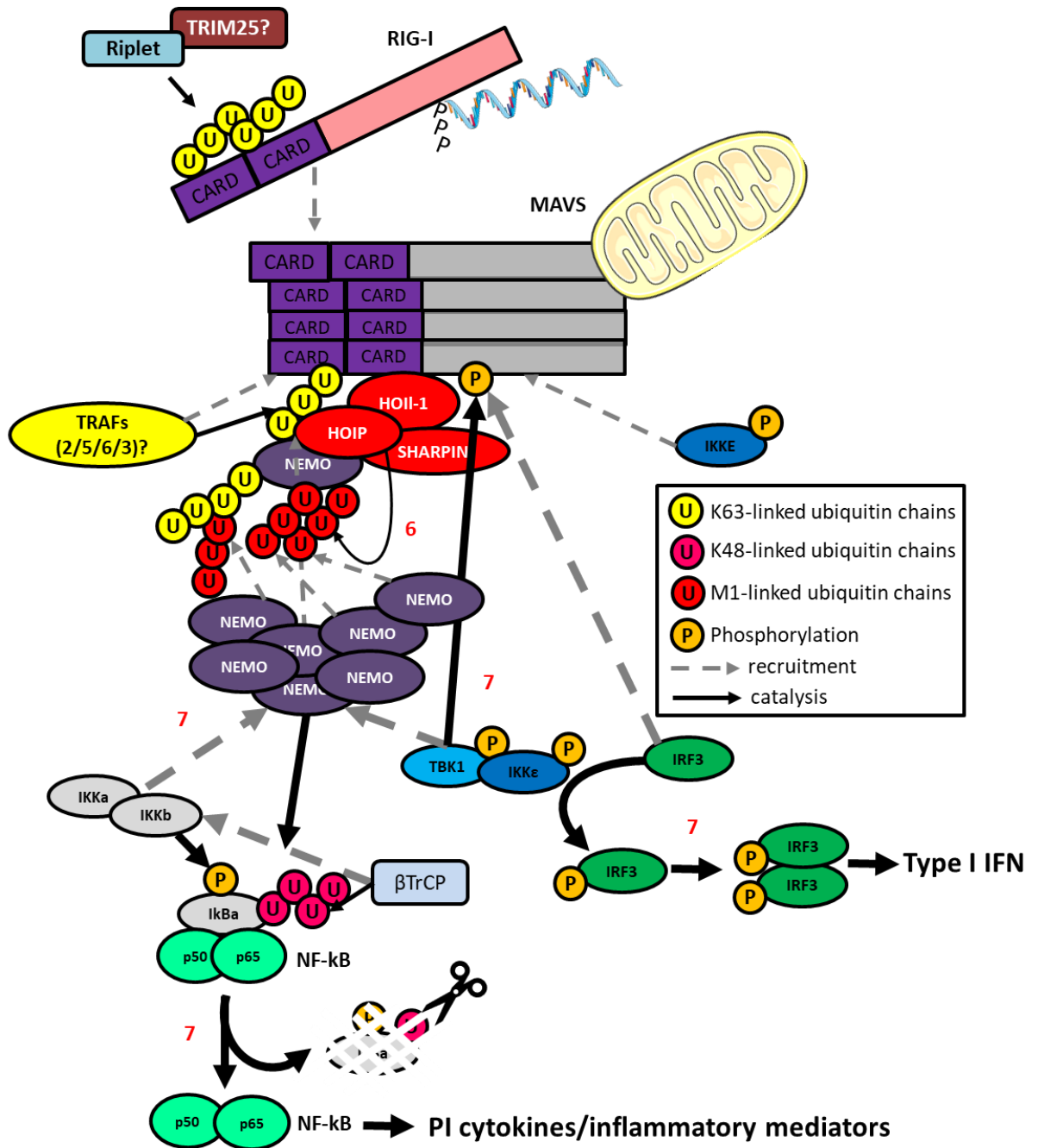


**Figure 6.5.2: Schematic of the proposed mechanism of LUBACs involvement in RIG-I signalling complex enhancement**

Complex initiation (as before steps 1-5)

Complex enhancement

6. LUBAC conjugates M1-linked ubiquitin chains to NEMO and K63-linked ubiquitin chains, generating K63/M1-linked chains and enhancing the recruitment of NEMO
7. IRF3 and NF-κB activation continues via the same mechanism, but are enhanced due to stronger recruitment of NEMO and TBK1/IKKε

The data generated in this body of work has allowed us to suggest a mechanism by which LUBAC, M1-ubiquitin chains and the individual components HOIP, HOIL-1 and SHARPIN regulate RIG-I signalling. Additionally, our demonstration of the differing roles of the individual LUBAC components in RIG-I signalling goes some way to explain the highly conflicting literature surrounding regulation of RIG-I by LUBAC, as previously the individual function of all three components has been attributed to LUBAC as a complex.

# Bibliography

---

1. Janeway, C. A. Approaching the Asymptote? Evolution and Revolution in Immunology. *Cold Spring Harbor Symposia on Quantitative Biology* **54**, 1–13 (1989).
2. Matzinger, P. Tolerance, Danger, and the Extended Family. *Annual Review of Immunology* **12**, 991–1045 (1994).
3. Tuffs, S. W., Haeryfar, S. M. M. & McCormick, J. K. Manipulation of Innate and Adaptive Immunity by Staphylococcal Superantigens. *Pathogens* **7**, (2018).
4. Chaplin, D. D. Overview of the Immune Response. *The Journal of allergy and clinical immunology* **125**, S3 (2010).
5. Romo, M. R., Pérez-Martínez, D. & Ferrer, C. C. Innate immunity in vertebrates: an overview. *Immunology* **148**, 125–139 (2016).
6. Matsui, T. & Amagai, M. Dissecting the formation, structure and barrier function of the stratum corneum. *International Immunology* **27**, 269–280 (2015).
7. McGhee, J. R. & Fujihashi, K. Inside the Mucosal Immune System. *PLOS Biology* **10**, e1001397 (2012).
8. Gallucci, S. An Overview of the Innate Immune Response to Infectious and Noninfectious Stressors. *The Innate Immune Response to Non-infectious Stressors: Human and Animal Models* 1–24 (2016) doi:10.1016/B978-0-12-801968-9.00001-5.
9. Hartl, D. *et al.* Innate Immunity of the Lung: From Basic Mechanisms to Translational Medicine. *Journal of Innate Immunity* **10**, 487–501 (2018).
10. Akira, S. & Takeda, K. Toll-like receptor signalling. *Nature reviews. Immunology* **4**, 499–511 (2004).
11. Akira, S., Uematsu, S. & Takeuchi, O. Pathogen Recognition and Innate Immunity. *Cell* **124**, 783–801 (2006).
12. van der Meer, J., Joosten, L., Riksen, N. & Netea, M. Trained immunity: A smart way to enhance innate immune defence. *Molecular immunology* **68**, 40–44 (2015).
13. Gasteiger, G. *et al.* Cellular Innate Immunity: An Old Game with New Players. *Journal of Innate Immunity* **9**, 111–125 (2017).
14. Zhang, C., Yang, M. & Ericsson, A. C. Function of Macrophages in Disease: Current Understanding on Molecular Mechanisms. *Frontiers in Immunology* **0**, 635 (2021).
15. Murray, P. J. & Wynn, T. A. Protective and pathogenic functions of macrophage subsets. *Nature Reviews Immunology* 2011 11:11 **11**, 723–737 (2011).

16. Häger, M., JCowland, L. & Borregaard, N. Neutrophil granules in health and disease. *Journal of internal medicine* **268**, 25–34 (2010).
17. Vorobjeva, N. v. & Chernyak, B. v. NETosis: Molecular Mechanisms, Role in Physiology and Pathology. *Biochemistry. Biokhimiia* **85**, 1178 (2020).
18. Veglia, F., Sanseviero, E. & Gabrilovich, D. I. Myeloid-derived suppressor cells in the era of increasing myeloid cell diversity. *Nature Reviews Immunology* **2021 21:8 21**, 485–498 (2021).
19. Panda, S. K. & Colonna, M. Innate Lymphoid Cells in Mucosal Immunity. *Frontiers in Immunology* **0**, 861 (2019).
20. Steinman, R. & Hemmi, H. Dendritic cells: translating innate to adaptive immunity. *Current topics in microbiology and immunology* **311**, 17–58 (2006).
21. Vivier, E., Tomasello, E., Baratin, M., Walzer, T. & Ugolini, S. Functions of natural killer cells. *Nature Immunology* **2008 9:5 9**, 503–510 (2008).
22. Buchmann, K. Evolution of Innate Immunity: Clues from Invertebrates via Fish to Mammals. *Frontiers in Immunology* **0**, 459 (2014).
23. Cooper, M. D. & Herrin, B. R. How did our complex immune system evolve? *Nature Reviews Immunology* **2010 10:1 10**, 2–3 (2010).
24. Rosenzweig, S. D. Primary Immunodeficiency Affecting the Innate Immune System. *Encyclopedia of Life Sciences* (2011) doi:10.1002/9780470015902.A0001240.PUB2.
25. Chinen, J. & Shearer, W. T. Secondary immunodeficiencies, including HIV infection. *The Journal of allergy and clinical immunology* **125**, 195–203 (2010).
26. Christen, U. Pathogen infection and autoimmune disease. *Clin Exp Immunol.* **195**, 10–14 (2019).
27. Blach-Olszewska, Z. & Leszek, J. Mechanisms of over-activated innate immune system regulation in autoimmune and neurodegenerative disorders. *Neuropsychiatric Disease and Treatment* **3**, 365 (2007).
28. Karin, M., Lawrence, T. & Nizet, V. Innate Immunity Gone Awry: Linking Microbial Infections to Chronic Inflammation and Cancer. *Cell* **124**, 823–835 (2006).
29. Kahaly, G. & Hansen, M. Type 1 diabetes associated autoimmunity. *Autoimmunity reviews* **15**, 644–648 (2016).
30. Weyand, C. & Goronzy, J. The immunology of rheumatoid arthritis. *Nature immunology* **22**, 10–18 (2021).
31. Dendrou, C., Fugger, L. & Friese, M. Immunopathology of multiple sclerosis. *Nature reviews. Immunology* **15**, 545–558 (2015).

32. Lee-Kirsch, M. A. The Type I Interferonopathies. *Annual Reviews in Medicine* **68**, 297–315 (2017).
33. Kato, H. & Fujita, T. RIG-I-like receptors and autoimmune diseases. *Current Opinion in Immunology* **37**, 40–45 (2015).
34. Kato, H., Oh, S.-W. & Fujita, T. RIG-I-Like Receptors and Type I Interferonopathies. *Journal of Interferon & Cytokine Research* **37**, 207 (2017).
35. Hidaka, F. *et al.* A missense mutation of the Toll-like receptor 3 gene in a patient with influenza-associated encephalopathy. *Clinical Immunology* **119**, 188–194 (2006).
36. Esposito, S. *et al.* Toll-like receptor 3 gene polymorphisms and severity of pandemic A/H1N1/2009 influenza in otherwise healthy children. *Virology Journal* *2012* **9**:1 **9**, 1–8 (2012).
37. Alexander, C. & Rietschel, E. Th. Bacterial lipopolysaccharides and innate immunity: *Journal of Endotoxin research* **7**, 167–202 (2011).
38. Kawasaki, T. & Kawai, T. Toll-Like Receptor Signaling Pathways. *Frontiers in Immunology* **0**, 461 (2014).
39. El-Zayat, S. R., Sibaii, H. & Mannaa, F. A. Toll-like receptors activation, signaling, and targeting: an overview. *Bulletin of the National Research Centre* *2019* **43**:1 **43**, 1–12 (2019).
40. Bermejo-Jambrina, M. *et al.* C-Type Lectin Receptors in Antiviral Immunity and Viral Escape. *Frontiers in Immunology* **0**, 590 (2018).
41. Geijtenbeek, T. B. H. & Gringhuis, S. I. Signalling through C-type lectin receptors: shaping immune responses. *Nature Reviews Immunology* *2009* **9**:7 **9**, 465–479 (2009).
42. Kim, Y. K., Shin, J.-S. & Nahm, M. H. NOD-Like Receptors in Infection, Immunity, and Diseases. *Yonsei Medical Journal* **57**, 5 (2016).
43. Okude, H., Ori, D. & Kawai, T. Signaling Through Nucleic Acid Sensors and Their Roles in Inflammatory Diseases. *Frontiers in Immunology* **0**, 3657 (2021).
44. Alexopoulou, L., Holt, A. C., Medzhitov, R. & Flavell, R. A. Recognition of double-stranded RNA and activation of NF- $\kappa$ B by Toll-like receptor 3. *Nature* **413**, 732–738 (2001).
45. Heil, F. *et al.* Species-specific recognition of single-stranded RNA via toll-like receptor 7 and 8. *Science (New York, N.Y.)* **303**, 1526–1529 (2004).
46. Rehwinkel, J. & Gack, M. U. RIG-I-like receptors: their regulation and roles in RNA sensing. *Nature Reviews Immunology* 1–15 (2020) doi:10.1038/s41577-020-0288-3.
47. Hemmi, H. *et al.* A Toll-like receptor recognizes bacterial DNA. *Nature* **408**, 740–745 (2000).
48. Unterholzner, L. *et al.* IFI16 is an innate immune sensor for intracellular DNA. *Nature Immunology* *2010* **11**:11 **11**, 997–1004 (2010).

49. Chiu, Y.-H., MacMillan, J. B. & Chen, Z. J. RNA Polymerase III Detects Cytosolic DNA and Induces Type I Interferons through the RIG-I Pathway. *Cell* **138**, 576–591 (2009).
50. Takaoka, A. *et al.* DAI (DLM-1/ZBP1) is a cytosolic DNA sensor and an activator of innate immune response. *Nature* **448**, 501–505 (2007).
51. Lugrin, J. & Martinon, F. The AIM2 inflammasome: Sensor of pathogens and cellular perturbations. *Immunological Reviews* **281**, 99–114 (2018).
52. Sun, L., Wu, J., Du, F., Chen, X. & Chen, Z. J. Cyclic GMP-AMP Synthase Is a Cytosolic DNA Sensor That Activates the Type I Interferon Pathway. *Science* **339**, 786–791 (2013).
53. Ferguson, B. J., Mansur, D. S., Peters, N. E., Ren, H. & Smith, G. L. DNA-PK is a DNA sensor for IRF-3-dependent innate immunity. 1–17 (2012) doi:10.7554/eLife.00047.
54. Broz, P. & Dixit, V. M. Inflammasomes: mechanism of assembly, regulation and signalling. *Nature Reviews Immunology* **16**, 407–420 (2016).
55. Lamkanfi, M. & Dixit, V. M. Mechanisms and Functions of Inflammasomes. *Cell* **157**, 1013–1022 (2014).
56. Travassos, L. *et al.* Nod1 and Nod2 direct autophagy by recruiting ATG16L1 to the plasma membrane at the site of bacterial entry. *Nature immunology* **11**, 55–62 (2010).
57. Xiao, T. S. The nucleic acid-sensing inflammasomes. *Immunological reviews* **265**, 103 (2015).
58. Tatematsu, M., Funami, K., Seya, T. & Matsumoto, M. Extracellular RNA Sensing by Pattern Recognition Receptors. *Journal of Innate Immunity* **10**, 398–406 (2018).
59. Lee, H.-C., Chaturanga, K. & Lee, J.-S. Intracellular sensing of viral genomes and viral evasion. *Experimental & Molecular Medicine* **51**, 1–13 (2019).
60. Lester, S. N. & Li, K. Toll-Like Receptors in Antiviral Innate Immunity. *Journal of Molecular Biology* **426**, 1246 (2014).
61. Nour, A. M. & Modis, Y. Endosomal vesicles as vehicles for viral genomes. *Trends in cell biology* **24**, 449 (2014).
62. Delgado, M. A., Elmaoued, R. A., Davis, A. S., Kyei, G. & Deretic, V. Toll-like receptors control autophagy. *The EMBO Journal* **27**, 1110–1121 (2008).
63. Lee, H. K., Lund, J. M., Ramanathan, B., Mizushima, N. & Iwasaki, A. Autophagy-Dependent Viral Recognition by Plasmacytoid Dendritic Cells. *Science* **315**, 1398–1401 (2007).
64. Tatematsu, M., Nishikawa, F., Seya, T. & Matsumoto, M. Toll-like receptor 3 recognizes incomplete stem structures in single-stranded viral RNA. *Nature communications* **4**, (2013).
65. Karikó, K., Ni, H., Capodici, J., Lamphier, M. & Weissman, D. mRNA is an endogenous ligand for Toll-like receptor 3. *The Journal of biological chemistry* **279**, 12542–12550 (2004).

66. Cavassani, K. *et al.* TLR3 is an endogenous sensor of tissue necrosis during acute inflammatory events. *The Journal of experimental medicine* **205**, 2609–2621 (2008).
67. Petes, C., Odoardi, N. & Gee, K. The Toll for Trafficking: Toll-Like Receptor 7 Delivery to the Endosome. *Frontiers in Immunology* **0**, 1075 (2017).
68. Manavalan, B., Basith, S. & Choi, S. Similar Structures but Different Roles – An Updated Perspective on TLR Structures. *Frontiers in Physiology* **0**, 41 (2011).
69. Fitzgerald, K. A. *et al.* IKKE and TBK1 are essential components of the IRF3 signalling pathway. *Nature Immunology* **4**, 491–496 (2003).
70. Meylan, E. *et al.* RIP1 is an essential mediator of Toll-like receptor 3–induced NF- $\kappa$ B activation. *Nature Immunology* **2004 5:5 5**, 503–507 (2004).
71. Estornes, Y. *et al.* dsRNA induces apoptosis through an atypical death complex associating TLR3 to caspase-8. *Cell death and differentiation* **19**, 1482–1494 (2012).
72. Feoktistova, M. *et al.* cIAPs block Ripoptosome formation, a RIP1/caspase-8 containing intracellular cell death complex differentially regulated by cFLIP isoforms. *Molecular cell* **43**, 449–463 (2011).
73. Wu, B. & Hur, S. How RIG-I like receptors activate MAVS. *Current Opinion in Virology* vol. 12 91–98 (2015).
74. Rodriguez, K. R., Bruns, A. M. & Horvath, C. M. MDA5 and LGP2: Accomplices and Antagonists of Antiviral Signal Transduction. *Journal of Virology* **88**, 8194–8200 (2014).
75. Quicke, K., Kim, K., Horvath, C. & Suthar, M. RNA Helicase LGP2 Negatively Regulates RIG-I Signaling by Preventing TRIM25-Mediated Caspase Activation and Recruitment Domain Ubiquitination. *Journal of interferon & cytokine research : the official journal of the International Society for Interferon and Cytokine Research* **39**, 669–683 (2019).
76. Komuro, A. & Horvath, C. M. RNA- and Virus-Independent Inhibition of Antiviral Signaling by RNA Helicase LGP2. *Journal of Virology* **80**, 12332–12342 (2006).
77. Bamming, D. & Horvath, C. Regulation of signal transduction by enzymatically inactive antiviral RNA helicase proteins MDA5, RIG-I, and LGP2. *The Journal of biological chemistry* **284**, 9700–9712 (2009).
78. Kato, H. *et al.* Differential roles of MDA5 and RIG-I helicases in the recognition of RNA viruses. *Nature* **441**, 101–105 (2006).
79. Satoh, T. *et al.* LGP2 is a positive regulator of RIG-I– and MDA5-mediated antiviral responses. *Proceedings of the National Academy of Sciences* **107**, 1512–1517 (2010).
80. Uchikawa, E. *et al.* Structural Analysis of dsRNA Binding to Anti-viral Pattern Recognition Receptors LGP2 and MDA5. *Molecular Cell* **62**, 586 (2016).

81. Bruns, A. M. *et al.* ATP Hydrolysis Enhances RNA Recognition and Antiviral Signal Transduction by the Innate Immune Sensor, Laboratory of Genetics and Physiology 2 (LGP2) \*. *Journal of Biological Chemistry* **288**, 938–946 (2013).
82. Brisse, M. & Ly, H. Comparative Structure and Function Analysis of the RIG-I-Like Receptors: RIG-I and MDA5. *Frontiers in Immunology* **0**, 1586 (2019).
83. Hornung, V. *et al.* 5'-Triphosphate RNA is the ligand for RIG-I. *Science* **314**, 994–997 (2006).
84. Pichlmair, A. *et al.* RIG-I-mediated antiviral responses to single-stranded RNA bearing 5'-phosphates. *Science* **314**, 997–1001 (2006).
85. Lu, C. *et al.* The Structural Basis of 5' Triphosphate Double-Stranded RNA Recognition by RIG-I C-Terminal Domain. *Structure* **18**, 1032–1043 (2010).
86. Rehwinkel, J. *et al.* RIG-I Detects Viral Genomic RNA during Negative-Strand RNA Virus Infection. *Cell* **140**, 397–408 (2010).
87. Cui, S. *et al.* The C-terminal regulatory domain is the RNA 5'-triphosphate sensor of RIG-I. *Molecular cell* **29**, 169–179 (2008).
88. Goubau, D., Deddouche, S. & Reis e Sousa, C. Cytosolic Sensing of Viruses. *Immunity* vol. 38 855–869 (2013).
89. Schlee, M. *et al.* Recognition of 5' triphosphate by RIG-I helicase requires short blunt double-stranded RNA as contained in panhandle of negative-strand virus. *Immunity* **31**, 25–34 (2009).
90. Schmidt, A. *et al.* 5'-triphosphate RNA requires base-paired structures to activate antiviral signaling via RIG-I. *Proceedings of the National Academy of Sciences of the United States of America* **106**, 12067–72 (2009).
91. Linehan, M. M. *et al.* A minimal RNA ligand for potent RIG-I activation in living mice. *Science Advances* **4**, (2018).
92. Malathi, K. *et al.* RNase L releases a small RNA from HCV RNA that refolds into a potent PAMP. *RNA* **16**, 2108–2119 (2010).
93. Barik, S. What Really Rigs Up RIG-I? *Journal of Innate Immunity* **8**, 429–436 (2016).
94. Wu, B. *et al.* Structural Basis for dsRNA Recognition, Filament Formation, and Antiviral Signal Activation by MDA5. *Cell* **152**, 276–289 (2013).
95. Kato, H. *et al.* Length-dependent recognition of double-stranded ribonucleic acids by retinoic acid-inducible gene-I and melanoma differentiation-associated gene 5. *Journal of Experimental Medicine* **205**, 1601–1610 (2008).
96. Zheng, J. *et al.* HDX-MS reveals dysregulated checkpoints that compromise discrimination against self RNA during RIG-I mediated autoimmunity. *Nature communications* **9**, (2018).

97. Baum, A., Sachidanandam, R. & García-Sastre, A. Preference of RIG-I for short viral RNA molecules in infected cells revealed by next-generation sequencing. *Proceedings of the National Academy of Sciences of the United States of America* **107**, 16303–16308 (2010).
98. Rehwinkel, J. *et al.* RIG-I Detects Viral Genomic RNA during Negative-Strand RNA Virus Infection. *Cell* **140**, 397–408 (2010).
99. Liu, G., Park, H.-S., Pyo, H.-M., Liu, Q. & Zhou, Y. Influenza A Virus Panhandle Structure Is Directly Involved in RIG-I Activation and Interferon Induction. *Journal of Virology* **89**, 6067–6079 (2015).
100. Schuberth-Wagner, C. *et al.* A Conserved Histidine in the RNA Sensor RIG-I Controls Immune Tolerance to N1-2'O-Methylated Self RNA. *Immunity* **43**, 41–51 (2015).
101. Ren, X., Linehan, M. M., Iwasaki, A. & Pyle, A. M. RIG-I Selectively Discriminates against 5'-Monophosphate RNA. *Cell Reports* **26**, 2019-2027.e4 (2019).
102. Kato, H. *et al.* Differential roles of MDA5 and RIG-I helicases in the recognition of RNA viruses. *Nature* **441**, 101–105 (2006).
103. Gitlin, L. *et al.* Essential role of mda-5 in type I IFN responses to polyriboinosinic:polyribocytidylic acid and encephalomyocarditis picornavirus. *Proceedings of the National Academy of Sciences* **103**, 8459–8464 (2006).
104. Dias Junior, A. G., Sampaio, N. G. & Rehwinkel, J. A Balancing Act: MDA5 in Antiviral Immunity and Autoinflammation. (2019) doi:10.1016/j.tim.2018.08.007.
105. Cui, S. *et al.* The C-Terminal Regulatory Domain Is the RNA 5'-Triphosphate Sensor of RIG-I. *Molecular Cell* **29**, 169–179 (2008).
106. Jiang, F. *et al.* Structural basis of RNA recognition and activation by innate immune receptor RIG-I. *Nature* **479**, 423–427 (2011).
107. Pichlmair, A. *et al.* Activation of MDA5 requires higher-order RNA structures generated during virus infection. *Journal of virology* **83**, 10761–9 (2009).
108. Kolakofsky, D., Kowalinski, E. & Cusack, S. A structure-based model of RIG-I activation. *RNA* **18**, 2118 (2012).
109. Lian, H. *et al.* The Zinc-Finger Protein ZCCHC3 Binds RNA and Facilitates Viral RNA Sensing and Activation of the RIG-I-like Receptors. *Immunity* **49**, 438-448.e5 (2018).
110. Kowalinski, E. *et al.* Structural Basis for the Activation of Innate Immune Pattern-Recognition Receptor RIG-I by Viral RNA. *Cell* **147**, 423–435 (2011).
111. Patel, J. R. *et al.* ATPase-driven oligomerization of RIG-I on RNA allows optimal activation of type-I interferon. *EMBO reports* **14**, 780–787 (2013).

112. Myong, S. *et al.* Cytosolic Viral Sensor RIG-I Is a 5'-Triphosphate-Dependent Translocase on Double-Stranded RNA. *Science* **323**, 1070–1074 (2009).
113. Peisley, A., Wu, B., Yao, H., Walz, T. & Hur, S. RIG-I Forms Signaling-Competent Filaments in an ATP-Dependent, Ubiquitin-Independent Manner. *Molecular Cell* **51**, 573–583 (2013).
114. Civril, F. *et al.* The RIG-I ATPase domain structure reveals insights into ATP-dependent antiviral signalling. *EMBO reports* **12**, 1127–1134 (2011).
115. Lässig, C. *et al.* ATP hydrolysis by the viral RNA sensor RIG-I prevents unintentional recognition of self-RNA. *eLife* **4**, (2015).
116. Devarkar, S. C., Schweibenz, B., Wang, C., Marcotrigiano, J. & Patel, S. S. RIG-I Uses an ATPase-Powered Translocation-Throttling Mechanism for Kinetic Proofreading of RNAs and Oligomerization. *Molecular Cell* **72**, 355-368.e4 (2018).
117. Peisley, A., Wu, B., Xu, H., Chen, Z. & Hur, S. Structural basis for ubiquitin-mediated antiviral signal activation by RIG-I. *Nature* **509**, 110–114 (2014).
118. Wu, B. *et al.* Molecular Imprinting as a Signal-Activation Mechanism of the Viral RNA Sensor RIG-I. *Molecular Cell* **55**, 511–523 (2014).
119. Jiang, X. *et al.* Ubiquitin-Induced Oligomerization of the RNA Sensors RIG-I and MDA5 Activates Antiviral Innate Immune Response. *Immunity* **36**, 959–973 (2012).
120. Liu, H. *et al.* The mitochondrial targeting chaperone 14-3-3 $\epsilon$  regulates a RIG-I translocon that mediates membrane association and innate antiviral immunity. *Cell host & microbe* **11**, 528–537 (2012).
121. Zeng, W. *et al.* Reconstitution of the RIG-I Pathway Reveals a Signaling Role of Unanchored Polyubiquitin Chains in Innate Immunity. *Cell* **141**, 315–330 (2010).
122. Xian, H. *et al.* Stratified ubiquitination of RIG-I creates robust immune response and induces selective gene expression. *Science Advances* **3**, 1701764 (2017).
123. Sun, X. *et al.* A Hierarchical Mechanism of RIG-I Ubiquitination Provides Sensitivity, Robustness and Synergy in Antiviral Immune Responses. *Scientific Reports* **6**, (2016).
124. Gack, M. U. *et al.* TRIM25 RING-finger E3 ubiquitin ligase is essential for RIG-I-mediated antiviral activity. *Nature* **446**, 916–920 (2007).
125. C, C. *et al.* MAVS ubiquitination by the E3 ligase TRIM25 and degradation by the proteasome is involved in type I interferon production after activation of the antiviral RIG-I-like receptors. *BMC biology* **10**, (2012).
126. Wies, E. *et al.* Dephosphorylation of the RNA Sensors RIG-I and MDA5 by the Phosphatase PP1 Is Essential for Innate Immune Signaling. *Immunity* **38**, 437–449 (2013).

127. Cadena, C. *et al.* Ubiquitin-Dependent and -Independent Roles of E3 Ligase RIPLET in Innate Immunity. *Cell* **177**, 1187-1200.e16 (2019).
128. Gao, D. *et al.* REUL Is a Novel E3 Ubiquitin Ligase and Stimulator of Retinoic-Acid-Inducible Gene-1. *PLoS ONE* **4**, 5760 (2009).
129. Oshiumi, H. *et al.* The Ubiquitin Ligase Riplet Is Essential for RIG-I-Dependent Innate Immune Responses to RNA Virus Infection. *Cell Host & Microbe* **8**, 496–509 (2010).
130. Oshiumi, H., Matsumoto, M., Hatakeyama, S. & Seya, T. Riplet/RNF135, a RING Finger Protein, Ubiquitinates RIG-I to Promote Interferon- $\beta$  Induction during the Early Phase of Viral Infection \*. *Journal of Biological Chemistry* **284**, 807–817 (2009).
131. Kuniyoshi, K. *et al.* Pivotal role of RNA-binding E3 ubiquitin ligase MEX3C in RIG-I-mediated antiviral innate immunity. *Proceedings of the National Academy of Sciences* **111**, 5646–5651 (2014).
132. Yan, J., Li, Q., Mao, A.-P., Hu, M.-M. & Shu, H.-B. TRIM4 modulates type I interferon induction and cellular antiviral response by targeting RIG-I for K63-linked ubiquitination. *Journal of Molecular Cell Biology* **6**, 154–163 (2014).
133. Shi, Y. *et al.* Ube2D3 and Ube2N are essential for RIG-I-mediated MAVS aggregation in antiviral innate immunity. *Nature Communications* **2017 8:1** **8**, 1–14 (2017).
134. Hou, F. *et al.* MAVS Forms Functional Prion-like Aggregates to Activate and Propagate Antiviral Innate Immune Response. *Cell* **146**, 448–461 (2011).
135. Liu, S. *et al.* MAVS recruits multiple ubiquitin E3 ligases to activate antiviral signaling cascades. *eLife* (2013) doi:10.7554/eLife.00785.001.
136. Saha, S. K. *et al.* Regulation of antiviral responses by a direct and specific interaction between TRAF3 and Cardif. *EMBO Journal* **25**, 3257–3263 (2006).
137. Tang, E. D. & Wang, C.-Y. TRAF5 Is a Downstream Target of MAVS in Antiviral Innate Immune Signaling. *PLOS ONE* **5**, e9172 (2010).
138. Paz, S. *et al.* A functional C-terminal TRAF3-binding site in MAVS participates in positive and negative regulation of the IFN antiviral response. *Cell Research* **21**, 895–910 (2011).
139. Shi, Z. *et al.* Structural Insights into Mitochondrial Antiviral Signaling Protein (MAVS)-Tumor Necrosis Factor Receptor-associated Factor 6 (TRAF6) Signaling \*. *Journal of Biological Chemistry* **290**, 26811–26820 (2015).
140. Saha, S. K. *et al.* Regulation of antiviral responses by a direct and specific interaction between TRAF3 and Cardif. *The EMBO Journal* **25**, 3257–3263 (2006).
141. Xu, L.-G. *et al.* VISA Is an Adapter Protein Required for Virus-Triggered IFN- $\beta$  Signaling. *Molecular Cell* **19**, 727–740 (2005).

142. Seth, R. B., Sun, L., Ea, C. K. & Chen, Z. J. Identification and characterization of MAVS, a mitochondrial antiviral signaling protein that activates NF- $\kappa$ B and IRF3. *Cell* **122**, 669–682 (2005).
143. Fang, R. *et al.* MAVS activates TBK1 and IKK $\epsilon$  through TRAFs in NEMO dependent and independent manner. *PLoS Pathogens* **13**, 1–22 (2017).
144. Yang, X. D. & Sun, S. C. Targeting signaling factors for degradation, an emerging mechanism for TRAF functions. *Immunological Reviews* **266**, 56–71 (2015).
145. Pineda, G., Ea, C. K. & Chen, Z. J. Ubiquitination and TRAF signaling. *Advances in Experimental Medicine and Biology* vol. 597 80–92 (2007).
146. Yum, S., Li, M., Fang, Y. & Chen, Z. J. TBK1 recruitment to STING activates both IRF3 and NF- $\kappa$ B that mediate immune defense against tumors and viral infections. *Proceedings of the National Academy of Sciences* **118**, 2021 (2021).
147. Zeng, W., Xu, M., Liu, S., Sun, L. & Chen, Z. J. Key Role of Ubc5 and Lysine-63 Polyubiquitination in Viral Activation of IRF3. *Molecular Cell* **36**, 315–325 (2009).
148. Xia, Z. *et al.* Direct activation of protein kinases by unanchored polyubiquitin chains. *Nature* **461**, 114–119 (2009).
149. Zhao, T. *et al.* The NEMO adaptor bridges the nuclear factor- $\kappa$ B and interferon regulatory factor signaling pathways. *Nature Immunology* **8**, 592–600 (2007).
150. Sun, S.-C., Chang, J.-H. & Jin, J. Regulation of nuclear factor- $\kappa$ B in autoimmunity. *Trends in Immunology* **34**, 282–289 (2013).
151. Guo, B. & Cheng, G. Modulation of the interferon antiviral response by the TBK1/IKK $\alpha$  adaptor protein TANK. *Journal of Biological Chemistry* **282**, 11817–11826 (2007).
152. Sasai, M. *et al.* NAK-Associated Protein 1 Participates in Both the TLR3 and the Cytoplasmic Pathways in Type I IFN Induction. *The Journal of Immunology* **177**, 8676–8683 (2006).
153. Ryzhakov, G. & Randow, F. SINTBAD, a novel component of innate antiviral immunity, shares a TBK1-binding domain with NAP1 and TANK. *EMBO Journal* **26**, 3180–3190 (2007).
154. Chariot, A. *et al.* Association of the Adaptor TANK with the I $\kappa$ B Kinase (IKK) Regulator NEMO Connects IKK Complexes with IKK $\epsilon$  and TBK1 Kinases. *Journal of Biological Chemistry* **277**, 37029–37036 (2002).
155. Morton, S., Hesson, L., Peggie, M. & Cohen, P. Enhanced binding of TBK1 by an optineurin mutant that causes a familial form of primary open angle glaucoma. *FEBS Letters* **582**, 997–1002 (2008).
156. Gleason, C. E., Ordureau, A., Gourlay, R., Arthur, J. S. C. & Cohen, P. Polyubiquitin binding to optineurin is required for optimal activation of TANK-binding kinase 1 and production of interferon  $\beta$ . *Journal of Biological Chemistry* **286**, 35663–35674 (2011).

157. O'Loughlin, T. *et al.* OPTN recruitment to a Golgi-proximal compartment regulates immune signalling and cytokine secretion. *Journal of cell science* **133**, (2020).
158. Outlioua, A., Pourcelot, M. & Arnoult, D. The role of optineurin in antiviral type I interferon production. *Frontiers in Immunology* vol. 9 853 (2018).
159. Paz, S. *et al.* Ubiquitin-Regulated Recruitment of I $\kappa$ B Kinase  $\epsilon$  to the MAVS Interferon Signaling Adapter. *Molecular and Cellular Biology* **29**, 3401–3412 (2009).
160. Kishore, N. *et al.* IKK-i and TBK-1 are Enzymatically Distinct from the Homologous Enzyme IKK-2: COMPARATIVE ANALYSIS OF RECOMBINANT HUMAN IKK-i, TBK-1, AND IKK-2 \*. *Journal of Biological Chemistry* **277**, 13840–13847 (2002).
161. Ma, X. *et al.* Molecular basis of Tank-binding kinase 1 activation by transautophosphorylation. *Proceedings of the National Academy of Sciences of the United States of America* **109**, 9378–9383 (2012).
162. Pourcelot, M. *et al.* The Golgi apparatus acts as a platform for TBK1 activation after viral RNA sensing. *BMC Biology* **14**, 69 (2016).
163. Slowicka, K. & van Loo, G. Optineurin functions for optimal immunity. *Frontiers in Immunology* vol. 9 769 (2018).
164. Meena, N. P. *et al.* The TBK1-binding domain of optineurin promotes type I interferon responses. *FEBS Letters* **590**, 1498–1508 (2016).
165. Li, S., Wang, L., Berman, M., Kong, Y.-Y. & Dorf, M. E. Mapping a Dynamic Innate Immunity Protein Interaction Network Regulating Type I Interferon Production. *Immunity* **35**, 426–440 (2011).
166. Tu, D. *et al.* Structure and ubiquitination-dependent activation of TANK-binding kinase 1. *Cell reports* **3**, 747–758 (2013).
167. Hemmi, H. *et al.* The roles of two I $\kappa$ B kinase-related kinases in lipopolysaccharide and double stranded RNA signaling and viral infection. *Journal of Experimental Medicine* **199**, 1641–1650 (2004).
168. Mcwhirter, S. M. *et al.* IFN-regulatory factor 3-dependent gene expression is defective in *Tbk1*-deficient mouse embryonic fibroblasts. (2003).
169. Perry, A. K., Chow, E. K., Goodnough, J. B., Yeh, W. C. & Cheng, G. Differential requirement for TANK-binding kinase-1 in type I interferon responses to toll-like receptor activation and viral infection. *Journal of Experimental Medicine* **199**, 1651–1658 (2004).
170. Verhelst, K., Verstrepen, L., Carpentier, I. & Beyaert, R. I $\kappa$ B kinase  $\epsilon$  (IKK $\epsilon$ ): A therapeutic target in inflammation and cancer. *Biochemical Pharmacology* vol. 85 873–880 (2013).
171. Clément, J. F., Meloche, S. & Servant, M. J. The IKK-related kinases: From innate immunity to oncogenesis. *Cell Research* vol. 18 889–899 (2008).

172. Shimada, T. *et al.* IKK-i, a novel lipopolysaccharide-inducible kinase that is related to IκB kinases. *International Immunology* **11**, 1357–1362 (1999).
173. TenOever, B. R. *et al.* Multiple functions of the IKK-related kinase IKKε in interferon-mediated antiviral immunity. *Science* **315**, 1274–1278 (2007).
174. Jefferies, C. A. Regulating IRFs in IFN Driven Disease. *Frontiers in Immunology* **0**, 325 (2019).
175. Tamura, T., Yanai, H., Savitsky, D. & Taniguchi, T. The IRF Family Transcription Factors in Immunity and Oncogenesis. <http://dx.doi.org/10.1146/annurev.immunol.26.021607.090400> **26**, 535–584 (2008).
176. Au, W.-C., Moore, P. A., LaFleur, D. W., Tombal, B. & Pitha, P. M. Characterization of the Interferon Regulatory Factor-7 and Its Potential Role in the Transcription Activation of Interferon A Genes \*. *Journal of Biological Chemistry* **273**, 29210–29217 (1998).
177. Marié, I., Durbin, J. E. & Levy, D. E. Differential viral induction of distinct interferon-α genes by positive feedback through interferon regulatory factor-7. *The EMBO Journal* **17**, 6660–6669 (1998).
178. Smith, S. *et al.* Enhanced interferon regulatory factor 3 binding to the interleukin-23p19 promoter correlates with enhanced interleukin-23 expression in systemic lupus erythematosus. *Arthritis & Rheumatism* **64**, 1601–1609 (2012).
179. Koshiba, R. *et al.* Regulation of cooperative function of the Il12b enhancer and promoter by the interferon regulatory factors 3 and 5. *Biochemical and Biophysical Research Communications* **430**, 95–100 (2013).
180. Brownell, J. *et al.* Direct, Interferon-Independent Activation of the CXCL10 Promoter by NF- B and Interferon Regulatory Factor 3 during Hepatitis C Virus Infection. *Journal of Virology* **88**, 1582–1590 (2014).
181. Lin, R., Mamane, Y. & Hiscott, J. Structural and Functional Analysis of Interferon Regulatory Factor 3: Localization of the Transactivation and Autoinhibitory Domains. *Molecular and Cellular Biology* **19**, 2465–2474 (1999).
182. Goriely, S. *et al.* Interferon regulatory factor 3 is involved in Toll-like receptor 4 (TLR4)- and TLR3-induced IL-12p35 gene activation. *Blood* **107**, 1078–1084 (2006).
183. Sakaguchi, S. *et al.* Essential role of IRF-3 in lipopolysaccharide-induced interferon-β gene expression and endotoxin shock. *Biochemical and Biophysical Research Communications* **306**, 860–866 (2003).
184. Hardy, M., Owczarek, C., Jermiin, L., Ejdebäck, M. & Hertzog, P. Characterization of the type I interferon locus and identification of novel genes. *Genomics* **84**, 331–345 (2004).
185. Ivashkiv, L. B. & Donlin, L. T. Regulation of type I interferon responses. *Nature reviews. Immunology* **14**, 36 (2014).

186. Rusinova, I. *et al.* INTERFEROME v2.0: an updated database of annotated interferon-regulated genes. *Nucleic Acids Research* **41**, D1040 (2013).
187. Schoggins, J. W. *et al.* A diverse array of gene products are effectors of the type I interferon antiviral response. *Nature* **472**, 481 (2011).
188. Kotenko, S. v. *et al.* IFN- $\lambda$ s mediate antiviral protection through a distinct class II cytokine receptor complex. *Nature Immunology* **2002 4:1 4**, 69–77 (2002).
189. Stanifer, M. L., Pervolaraki, K. & Boulant, S. Differential Regulation of Type I and Type III Interferon Signaling. *International Journal of Molecular Sciences* **20**, (2019).
190. Grandvaux, N. *et al.* Transcriptional Profiling of Interferon Regulatory Factor 3 Target Genes: Direct Involvement in the Regulation of Interferon-Stimulated Genes. *Journal of Virology* **76**, 5532–5539 (2002).
191. Iwasaki, A. A virological view of innate immune recognition. *Annual review of microbiology* **66**, 177–196 (2012).
192. Schneider, W., Chevillotte, M. & Rice, C. Interferon-stimulated genes: a complex web of host defenses. *Annual review of immunology* **32**, 513–545 (2014).
193. Crosse, K. M., Monson, E. A., Beard, M. R. & Helbig, K. J. Interferon-Stimulated Genes as Enhancers of Antiviral Innate Immune Signaling. *Journal of Innate Immunity* **10**, 85 (2018).
194. Shi, H. *et al.* Positive regulation of interferon regulatory factor 3 activation by Herc5 via ISG15 modification. *Molecular and cellular biology* **30**, 2424–2436 (2010).
195. Feng, Q. *et al.* UBE1L Causes Lung Cancer Growth Suppression by Targeting Cyclin D1. *Molecular cancer therapeutics* **7**, 3780 (2008).
196. Kaur, S. *et al.* Dual Regulatory Roles of the Phosphatidylinositol 3-Kinase In Interferon Signaling. *Journal of immunology (Baltimore, Md. : 1950)* **181**, 7316 (2008).
197. Uddin, S. *et al.* Activation of the phosphatidylinositol 3-kinase serine kinase by IFN-alpha. *The Journal of Immunology* **158**, (1997).
198. Keegan, L. P., Leroy, A., Sproul, D. & O'Connell, M. A. Adenosine deaminases acting on RNA (ADARs): RNA-editing enzymes. *Genome Biology* **5**, 209 (2004).
199. Uddin, S. *et al.* Activation of the p38 mitogen-activated protein kinase by type I interferons. *The Journal of biological chemistry* **274**, 30127–30131 (1999).
200. Zhou, Z. *et al.* Type III interferon (IFN) induces a type I IFN-like response in a restricted subset of cells through signaling pathways involving both the Jak-STAT pathway and the mitogen-activated protein kinases. *Journal of virology* **81**, 7749–7758 (2007).

201. Zorzitto, J., Galligan, C., Ueng, J. & Fish, E. Characterization of the antiviral effects of interferon-alpha against a SARS-like coronavirus infection in vitro. *Cell research* **16**, 220–229 (2006).
202. Li, Y. *et al.* Role of p38alpha Map kinase in Type I interferon signaling. *The Journal of biological chemistry* **279**, 970–979 (2004).
203. Mikkelsen, S. S. *et al.* RIG-I-mediated Activation of p38 MAPK Is Essential for Viral Induction of Interferon and Activation of Dendritic Cells: DEPENDENCE ON TRAF2 AND TAK1<sup>1\*</sup><sup>3</sup>. *The Journal of Biological Chemistry* **284**, 10774 (2009).
204. Panaretakis, T. *et al.* Interferon alpha induces nucleus-independent apoptosis by activating extracellular signal-regulated kinase 1/2 and c-Jun NH2-terminal kinase downstream of phosphatidylinositol 3-kinase and mammalian target of rapamycin. *Molecular biology of the cell* **19**, 41–50 (2008).
205. Joshi, S. *et al.* Type I interferon (IFN)-dependent activation of Mnk1 and its role in the generation of growth inhibitory responses. *Proceedings of the National Academy of Sciences* **106**, 12097–12102 (2009).
206. Zhao, K.-W. *et al.* Interferon- $\alpha$ -induced Expression of Phospholipid Scramblase 1 through STAT1 Requires the Sequential Activation of Protein Kinase C $\delta$  and JNK \*. *Journal of Biological Chemistry* **280**, 42707–42714 (2005).
207. Jopling, C., i, M., Lancaster, A., Lemon, S. & Sarnow, P. Modulation of hepatitis C virus RNA abundance by a liver-specific MicroRNA. *Science (New York, N.Y.)* **309**, 1577–1581 (2005).
208. Rinn, J. L. & Chang, H. Y. Genome regulation by long noncoding RNAs. *Annual review of biochemistry* **81**, 145–166 (2012).
209. Schneider, W. M., Chevillotte, M. D. & Rice, C. M. Interferon-Stimulated Genes: A Complex Web of Host Defenses. *Annual review of immunology* **32**, 513 (2014).
210. Wang, N., Liang, H. & Zen, K. Molecular mechanisms that influence the macrophage m1-m2 polarization balance. *Frontiers in immunology* **5**, (2014).
211. Chang, M., Lee, A., Fitzpatrick, L., Zhang, M. & Sun, S. NF-kappa B1 p105 regulates T cell homeostasis and prevents chronic inflammation. *Journal of immunology (Baltimore, Md. : 1950)* **182**, 3131–3138 (2009).
212. Oh, H. & Ghosh, S. NF- $\kappa$ B: roles and regulation in different CD4(+) T-cell subsets. *Immunological reviews* **252**, 41–51 (2013).
213. Inn, K. S. *et al.* Linear Ubiquitin Assembly Complex Negatively Regulates RIG-I- and TRIM25-Mediated Type I Interferon Induction. *Molecular Cell* (2011) doi:10.1016/j.molcel.2010.12.029.

214. Arimoto, K. *et al.* Negative regulation of the RIG-I signaling by the ubiquitin ligase RNF125. *Proceedings of the National Academy of Sciences* **104**, 7500–7505 (2007).
215. Wang, W. *et al.* RNF122 suppresses antiviral type I interferon production by targeting RIG-I CARDS to mediate RIG-I degradation. *Proceedings of the National Academy of Sciences* **113**, 9581–9586 (2016).
216. Maharaj, N. P., Wies, E., Stoll, A. & Gack, M. U. Conventional Protein Kinase C- (PKC- ) and PKC- Negatively Regulate RIG-I Antiviral Signal Transduction. *Journal of Virology* **86**, 1358–1371 (2012).
217. Sun, Z., Ren, H., Liu, Y., Teeling, J. L. & Gu, J. Phosphorylation of RIG-I by Casein Kinase II Inhibits Its Antiviral Response. *Journal of Virology* **85**, 1036–1047 (2011).
218. Gack, M. U., Nistal-Villán, E., Inn, K.-S., García-Sastre, A. & Jung, J. U. Phosphorylation-Mediated Negative Regulation of RIG-I Antiviral Activity. *Journal of Virology* **84**, 3220–3229 (2010).
219. Nistal-Villán, E. *et al.* Negative Role of RIG-I Serine 8 Phosphorylation in the Regulation of Interferon- $\beta$  Production \*. *Journal of Biological Chemistry* **285**, 20252–20261 (2010).
220. Luthra, P. *et al.* Mutual Antagonism between the Ebola Virus VP35 Protein and the RIG-I Activator PACT Determines Infection Outcome. *Cell Host & Microbe* **14**, 74–84 (2013).
221. Kok, K.-H. *et al.* The Double-Stranded RNA-Binding Protein PACT Functions as a Cellular Activator of RIG-I to Facilitate Innate Antiviral Response. *Cell Host & Microbe* **9**, 299–309 (2011).
222. Sowmya, P., Knoll, M., Gale, M. & Yueh-Ming, L. DHX15 Is a Coreceptor for RLR Signaling That Promotes Antiviral Defense Against RNA Virus Infection. <https://home.liebertpub.com/jir> **39**, 331–346 (2019).
223. Liu, B. *et al.* The ubiquitin E3 ligase TRIM31 promotes aggregation and activation of the signaling adaptor MAVS through Lys63-linked polyubiquitination. *Nature immunology* **18**, 214–224 (2017).
224. Song, N. *et al.* MAVS O-GlcNAcylation Is Essential for Host Antiviral Immunity against Lethal RNA Viruses. *Cell Reports* **28**, 2386-2396.e5 (2019).
225. Dai, T. *et al.* FAF1 Regulates Antiviral Immunity by Inhibiting MAVS but Is Antagonized by Phosphorylation upon Viral Infection. *Cell Host & Microbe* **24**, 776-790.e5 (2018).
226. Xue, B. *et al.* TRIM21 Promotes Innate Immune Response to RNA Viral Infection through Lys27-Linked Polyubiquitination of MAVS. *Journal of Virology* **92**, (2018).
227. Jin, S. *et al.* Tetherin Suppresses Type I Interferon Signaling by Targeting MAVS for NDP52-Mediated Selective Autophagic Degradation in Human Cells. *Molecular Cell* **68**, 308-322.e4 (2017).

228. Castanier, C. *et al.* MAVS ubiquitination by the E3 ligase TRIM25 and degradation by the proteasome is involved in type I interferon production after activation of the antiviral RIG-I-like receptors. *BMC Biology* 2012 10:1 **10**, 1–13 (2012).
229. You, F. *et al.* PCBP2 mediates degradation of the adaptor MAVS via the HECT ubiquitin ligase AIP4. *Nature Immunology* 2009 10:12 **10**, 1300–1308 (2009).
230. Zhou, X., You, F., Chen, H. & Jiang, Z. Poly(C)-binding protein 1 (PCBP1) mediates housekeeping degradation of mitochondrial antiviral signaling (MAVS). *Cell Research* 2012 22:4 **22**, 717–727 (2011).
231. Choi, Y. B., Shembade, N., Parvatiyar, K., Balachandran, S. & Harhaj, E. W. TAX1BP1 Restrains Virus-Induced Apoptosis by Facilitating Itch-Mediated Degradation of the Mitochondrial Adaptor MAVS. *Molecular and Cellular Biology* **37**, 422–438 (2017).
232. Wang, Y., Tong, X. & Ye, X. Ndfip1 Negatively Regulates RIG-I-Dependent Immune Signaling by Enhancing E3 Ligase Smurf1-Mediated MAVS Degradation. *The Journal of Immunology* **189**, 5304–5313 (2012).
233. Pan, Y. *et al.* Smurf2 Negatively Modulates RIG-I-Dependent Antiviral Response by Targeting VISA/MAVS for Ubiquitination and Degradation. *The Journal of Immunology* **192**, 4758–4764 (2014).
234. Zhang, L. *et al.* Induction of OTUD1 by RNA viruses potently inhibits innate immune responses by promoting degradation of the MAVS/TRAF3/TRAF6 signalosome. *PLOS Pathogens* **14**, e1007067 (2018).
235. Yoo, Y.-S. *et al.* The mitochondrial ubiquitin ligase MARCH5 resolves MAVS aggregates during antiviral signalling. *Nature Communications* 2015 6:1 **6**, 1–14 (2015).
236. Zhong, B. *et al.* The E3 Ubiquitin Ligase RNF5 Targets Virus-Induced Signaling Adaptor for Ubiquitination and Degradation. *The Journal of Immunology* **184**, 6249–6255 (2010).
237. Liu, W. *et al.* Cyclophilin A-regulated ubiquitination is critical for RIG-I-mediated antiviral immune responses. *eLife* **6**, (2017).
238. Liu, S. *et al.* Phosphorylation of innate immune adaptor proteins MAVS, STING, and TRIF induces IRF3 activation. *Science* **347**, (2015).
239. Xiang, W. *et al.* PPM1A silences cytosolic RNA sensing and antiviral defense through direct dephosphorylation of MAVS and TBK1. *Science Advances* **2**, e1501889 (2016).
240. Nomoto, A., Detjen, B., Pozzatti, R. & Wimmer, E. The location of the polio genome protein in viral RNAs and its implication for RNA synthesis. *Nature* 1977 268:5617 **268**, 208–213 (1977).
241. Schuberth-Wagner, C. *et al.* A Conserved Histidine in the RNA Sensor RIG-I Controls Immune Tolerance to N1-2'-O-Methylated Self RNA. *Immunity* **43**, 41–51 (2015).

242. Bitko, V., Musiyenko, A., Bayfield, M. A., Maraia, R. J. & Barik, S. Cellular La Protein Shields Nonsegmented Negative-Strand RNA Viral Leader RNA from RIG-I and Enhances Virus Growth by Diverse Mechanisms. *Journal of Virology* **82**, 7977 (2008).
243. Cárdenas, W. *et al.* Ebola virus VP35 protein binds double-stranded RNA and inhibits alpha/beta interferon production induced by RIG-I signaling. *Journal of virology* **80**, 5168–5178 (2006).
244. Gack, M. U. *et al.* Influenza A Virus NS1 Targets the Ubiquitin Ligase TRIM25 to Evade Recognition by the Host Viral RNA Sensor RIG-I. *Cell Host and Microbe* **5**, 439–449 (2009).
245. Ban, J. *et al.* Human Respiratory Syncytial Virus NS 1 Targets TRIM25 to Suppress RIG-I Ubiquitination and Subsequent RIG-I-Mediated Antiviral Signaling. *Viruses* **10**, (2018).
246. Gupta, S. *et al.* Herpesvirus deconjugases inhibit the IFN response by promoting TRIM25 autoubiquitination and functional inactivation of the RIG-I signalosome. *PLOS Pathogens* **14**, e1006852 (2018).
247. Chiang, C. *et al.* The Human Papillomavirus E6 Oncoprotein Targets USP15 and TRIM25 To Suppress RIG-I-Mediated Innate Immune Signaling. *Journal of virology* **92**, (2018).
248. Manokaran, G. *et al.* Dengue subgenomic RNA binds TRIM25 to inhibit interferon expression for epidemiological fitness. *Science* **350**, 217–221 (2015).
249. Rajsbaum, R. *et al.* Species-Specific Inhibition of RIG-I Ubiquitination and IFN Induction by the Influenza A Virus NS1 Protein. *PLOS Pathogens* **8**, e1003059 (2012).
250. Vazquez, C., Tan, C. Y. & Horner, S. M. Hepatitis C Virus Infection Is Inhibited by a Noncanonical Antiviral Signaling Pathway Targeted by NS3-NS4A. *Journal of Virology* **93**, (2019).
251. Wang, D. *et al.* The Leader Proteinase of Foot-and-Mouth Disease Virus Negatively Regulates the Type I Interferon Pathway by Acting as a Viral Deubiquitinase. *Journal of Virology* **85**, 3758–3766 (2011).
252. Ma, J. *et al.* Zika Virus Non-structural Protein 4A Blocks the RLR-MAVS Signaling. *Frontiers in Microbiology* **0**, 1350 (2018).
253. Ling, Z., Tran, K. C. & Teng, M. N. Human Respiratory Syncytial Virus Nonstructural Protein NS2 Antagonizes the Activation of Beta Interferon Transcription by Interacting with RIG-I. *Journal of Virology* **83**, 3734–3742 (2009).
254. Boyapalle, S. *et al.* Respiratory Syncytial Virus NS1 Protein Colocalizes with Mitochondrial Antiviral Signaling Protein MAVS following Infection. *PLOS ONE* **7**, e29386 (2012).
255. Santiago, F. W. *et al.* Hijacking of RIG-I Signaling Proteins into Virus-Induced Cytoplasmic Structures Correlates with the Inhibition of Type I Interferon Responses. *Journal of Virology* **88**, 4572–4585 (2014).

256. Li, X.-D., Sun, L., Seth, R. B., Pineda, G. & Chen, Z. J. Hepatitis C virus protease NS3/4A cleaves mitochondrial antiviral signaling protein off the mitochondria to evade innate immunity. *Proceedings of the National Academy of Sciences* **102**, 17717–17722 (2005).
257. Qian, S. *et al.* Seneca Valley Virus Suppresses Host Type I Interferon Production by Targeting Adaptor Proteins MAVS, TRIF, and TANK for Cleavage. *Journal of Virology* **91**, (2017).
258. Pang, L. *et al.* The suppression of innate immune response by human rhinovirus C. *Biochemical and Biophysical Research Communications* **490**, 22–28 (2017).
259. Mukherjee, A. *et al.* The Coxsackievirus B 3Cpro Protease Cleaves MAVS and TRIF to Attenuate Host Type I Interferon and Apoptotic Signaling. *PLOS Pathogens* **7**, e1001311 (2011).
260. Feng, H. *et al.* Hepatovirus 3ABC proteases and evolution of mitochondrial antiviral signaling protein (MAVS). *Journal of Hepatology* **71**, 25–34 (2019).
261. Qin, Y. *et al.* NLRX1 Mediates MAVS Degradation To Attenuate the Hepatitis C Virus-Induced Innate Immune Response through PCBP2. *Journal of Virology* **91**, (2017).
262. Ding, S. *et al.* Rotavirus VP3 targets MAVS for degradation to inhibit type III interferon expression in intestinal epithelial cells. *eLife* **7**, (2018).
263. Shi, C.-S. *et al.* SARS-Coronavirus Open Reading Frame-9b Suppresses Innate Immunity by Targeting Mitochondria and the MAVS/TRAF3/TRAF6 Signalosome. *The Journal of Immunology* **193**, 3080–3089 (2014).
264. Wei, C. *et al.* The Hepatitis B Virus X Protein Disrupts Innate Immunity by Downregulating Mitochondrial Antiviral Signaling Protein. *The Journal of Immunology* **185**, 1158–1168 (2010).
265. Chen, Y. *et al.* Functional motifs responsible for human metapneumovirus M2-2-mediated innate immune evasion. *Virology* **499**, 361–368 (2016).
266. Qian, W. *et al.* The C-Terminal Effector Domain of Non-Structural Protein 1 of Influenza A Virus Blocks IFN- $\beta$  Production by Targeting TNF Receptor-Associated Factor 3. *Frontiers in Immunology* **0**, 779 (2017).
267. Uchida, S., Horie, R., Sato, H., Kai, C. & Yoneda, M. Possible role of the Nipah virus V protein in the regulation of the interferon beta induction by interacting with UBX domain-containing protein1. *Scientific Reports* **2018 8:1** **8**, 1–13 (2018).
268. Refolo, G. *et al.* Negative Regulation of Mitochondrial Antiviral Signaling Protein-Mediated Antiviral Signaling by the Mitochondrial Protein LRPPRC During Hepatitis C Virus Infection. *Hepatology* **69**, 34–50 (2019).
269. Fu, Y.-Z. *et al.* SARS-CoV-2 membrane glycoprotein M antagonizes the MAVS-mediated innate antiviral response. *Cellular & Molecular Immunology* **2020 18:3** **18**, 613–620 (2020).

270. Visser, L. *et al.* Dissecting distinct proteolytic activities of FMDV Lpro implicates cleavage and degradation of RLR signaling proteins, not its deISGylase/DUB activity, in type I interferon suppression. *PLoS pathogens* **16**, (2020).
271. Sankaran, N. & Weiss, R. A. Viruses: Impact on Science and Society. *Encyclopedia of Virology* 671 (2021) doi:10.1016/B978-0-12-814515-9.00075-8.
272. Ryu, W.-S. Virus Life Cycle. *Molecular Virology of Human Pathogenic Viruses* 31 (2017) doi:10.1016/B978-0-12-800838-6.00003-5.
273. Baltimore, D. Expression of animal virus genomes. *Bacteriological Reviews* **35**, 235 (1971).
274. Johnson, N. & Mueller, J. Updating the Accounts: Global Mortality of the 1918-1920 “Spanish” Influenza Pandemic. *Bulletin of the History of Medicine* **76**, 105–115 (2002).
275. Gayle, H. D. & Hill, G. L. Global Impact of Human Immunodeficiency Virus and AIDS. *Clinical Microbiology Reviews* **14**, 327 (2001).
276. Nicola, M. *et al.* The socio-economic implications of the coronavirus pandemic (COVID-19): A review. *International Journal of Surgery (London, England)* **78**, 185 (2020).
277. Yeyati, E. & Filippini, F. Pandemic Divergence: The social and economic costs of Covid-19. *VOX EU CEPR Policy Portal* (2021).
278. Whary, M. T., Baumgarth, N., Fox, J. G. & Barthold, S. W. Biology and Diseases of Mice. *Laboratory Animal Medicine: Third Edition* 43–149 (2015) doi:10.1016/B978-0-12-409527-4.00003-1.
279. Livingston, R. S. & Riley, L. K. Diagnostic Testing of Mouse and Rat Colonies for Infectious Agents. *Lab Animal* vol. 32 44–51 (2003).
280. Pritchett-Corning, K. R., Cosentino, J. & Clifford, C. B. Contemporary prevalence of infectious agents in laboratory mice and rats. *Laboratory Animals* **43**, 165–173 (2009).
281. Kolakofsky, D. Isolation and characterization of Sendai virus DI-RNAs. *Cell* **8**, 547–555 (1976).
282. Baum, A., Sachidanandam, R. & García-sastre, A. Preference of RIG-I for short viral RNA molecules in infected cells revealed by next-generation sequencing. **107**, 16303–16308 (2010).
283. Strahle, L., Garcin, D. & Kolakofsky, D. Sendai virus defective-interfering genomes and the activation of interferon-beta. *Virology* **351**, 101–111 (2006).
284. Childs, K. *et al.* mda-5, but not RIG-I, is a common target for paramyxovirus V proteins. *Virology* **359**, 190–200 (2007).
285. Strähle, L. *et al.* Activation of the Beta Interferon Promoter by Unnatural Sendai Virus Infection Requires RIG-I and Is Inhibited by Viral C Proteins. *Journal of Virology* **81**, 12227–12237 (2007).

286. Strähle, L., Garcin, D., le Mercier, P., Schlaak, J. F. & Kolakofsky, D. Sendai Virus Targets Inflammatory Responses, as Well as the Interferon-Induced Antiviral State, in a Multifaceted Manner. *Journal of Virology* **77**, 7903–7913 (2003).
287. Kato, K., Nakanishis, M., Kaneda, Y., Uchidat, T. & Okada, Y. Expression of hepatitis B virus surface antigen in adult rat liver. Co-introduction of DNA and nuclear protein by a simplified liposome method. *THE JOURNAL OF BIOLOGICAL CHEMISTRY* **266**, 3361–3364 (1991).
288. Johnston, M. The characteristics required for a Sendai virus preparation to induce high levels of interferon in human lymphoblastoid cells. *The Journal of general virology* **56**, 175–184 (1981).
289. Nakanishi, M. & Otsu, M. Development of Sendai Virus Vectors and their Potential Applications in Gene Therapy and Regenerative Medicine. *Current Gene Therapy* **12**, 410–416 (2012).
290. Martínez-Gil, L. *et al.* A Sendai Virus-Derived RNA Agonist of RIG-I as a Virus Vaccine Adjuvant. *Journal of Virology* **87**, 1290–1300 (2013).
291. Javanian, M. *et al.* A brief review of influenza virus infection. *Journal of Medical Virology* **93**, 4638–4646 (2021).
292. Paules, C. & Subbarao, K. Influenza. *The Lancet* **390**, 697–708 (2017).
293. Yoo, S. J., Kwon, T. & Lyoo, Y. S. Challenges of influenza A viruses in humans and animals and current animal vaccines as an effective control measure. *Clinical and Experimental Vaccine Research* **7**, 1–15 (2018).
294. CDC. Clinical Signs and Symptoms of Influenza. *Center for Disease Control and Prevention (US)* <https://www.cdc.gov/flu/professionals/acip/clinical.htm> (2020).
295. Iwasaki, A. & Pillai, P. S. Innate immunity to influenza virus infection. *Nature Reviews Immunology* vol. 14 315–328 (2014).
296. Palese, P. Influenza: Old and new threats. *Nature Medicine* vol. 10 S82–S87 (2004).
297. World Health Organisation. Influenza (Seasonal). [https://www.who.int/news-room/fact-sheets/detail/influenza-\(seasonal\)](https://www.who.int/news-room/fact-sheets/detail/influenza-(seasonal)) (2018).
298. Moghadami, M. A Narrative Review of Influenza: A Seasonal and Pandemic Disease. *Iranian Journal of Medical Sciences* **42**, 2 (2017).
299. Iwasaki, A. & Pillai, P. S. Innate immunity to influenza virus infection. *Nature reviews. Immunology* **14**, 315 (2014).
300. Liu, G. *et al.* Nuclear-resident RIG-I senses viral replication inducing antiviral immunity. *Nature Communications* **2018 9:1** **9**, 1–14 (2018).

301. Tapia, K. *et al.* Defective Viral Genomes Arising In Vivo Provide Critical Danger Signals for the Triggering of Lung Antiviral Immunity. *PLoS Pathogens* **9**, (2013).
302. te Velthuis, A. *et al.* Mini viral RNAs act as innate immune agonists during influenza virus infection. *Nature microbiology* **3**, 1234–1242 (2018).
303. Vlugt, C. de, Sikora, D. & Pelchat, M. Insight into Influenza: A Virus Cap-Snatching. *Viruses* **2018**, Vol. 10, Page 641 **10**, 641 (2018).
304. Hale, B., Albrecht, R. & García-Sastre, A. Innate immune evasion strategies of influenza viruses. *Future microbiology* **62623**, 1–29 (2010).
305. Kazmi, S. S., Ali, W., Bibi, N. & Nouroz, F. A review on Zika virus outbreak, epidemiology, transmission and infection dynamics. *Journal of Biological Research-Thessaloniki* **2020** *27*:1 **27**, 1–11 (2020).
306. Calvet, G. *et al.* Detection and sequencing of Zika virus from amniotic fluid of fetuses with microcephaly in Brazil: a case study. *The Lancet Infectious Diseases* **16**, 653–660 (2016).
307. Brasil, P. *et al.* Zika virus infection in pregnant women in rio de janeiro. *New England Journal of Medicine* **375**, 2321–2334 (2016).
308. Frontera, J. A. & Da Silva, I. R. F. Zika getting on your nerves? the association with the Guillain-Barré syndrome. *New England Journal of Medicine* vol. 375 1581–1582 (2016).
309. de Sousa, J. R., Azevedo, R. do S. da S., Quaresma, J. A. S. & Vasconcelos, P. F. da C. The innate immune response in Zika virus infection. *Reviews in Medical Virology* **31**, e2166 (2021).
310. Chazal, M. *et al.* RIG-I Recognizes the 5' Region of Dengue and Zika Virus Genomes. *Cell Reports* **24**, 320–328 (2018).
311. Zheng, Y. *et al.* Zika virus elicits inflammation to evade antiviral response by cleaving cGAS via NS 1-caspase-1 axis . *The EMBO Journal* **37**, (2018).
312. Bowen, J. R. *et al.* Zika Virus Antagonizes Type I Interferon Responses during Infection of Human Dendritic Cells. *PLoS Pathogens* **13**, (2017).
313. Hamel, R. *et al.* Biology of Zika Virus Infection in Human Skin Cells. *Journal of Virology* **89**, 8880–8896 (2015).
314. Riedl, W. *et al.* Zika Virus NS3 Mimics a Cellular 14-3-3-Binding Motif to Antagonize RIG-I- and MDA5-Mediated Innate Immunity. *Cell Host & Microbe* **26**, 493-503.e6 (2019).
315. Ngueyen, T. T. N., Kim, S.-J. & Myoung, J. Y. L. and J. Zika Virus Proteins NS2A and NS4A Are Major Antagonists that Reduce IFN- $\beta$  Promoter Activity Induced by the MDA5/RIG-I Signaling Pathway. *J. Microbiol. Biotechnol.* **29**, 1665–1674 (2019).
316. Xia, H. *et al.* An evolutionary NS1 mutation enhances Zika virus evasion of host interferon induction. *Nature Communications* **2018** *9*:1 **9**, 1–13 (2018).

317. Lin, S. *et al.* Zika virus NS5 protein antagonizes type I interferon production via blocking TBK1 activation. *Virology* **527**, 180–187 (2019).
318. Ding, Q. *et al.* Species-specific disruption of STING-dependent antiviral cellular defenses by the Zika virus NS2B3 protease. *Proceedings of the National Academy of Sciences of the United States of America* **115**, E6310–E6318 (2018).
319. Serman, T. M. & Gack, M. U. Evasion of Innate and Intrinsic Antiviral Pathways by the Zika Virus. *Viruses* **11**, (2019).
320. Komander, D. & Rape, M. The Ubiquitin Code. *Annu. Rev. Biochem* **81**, 203–229 (2012).
321. Rittinger, K. & Ikeda, F. Linear ubiquitin chains: Enzymes, mechanisms and biology. *Open Biology* vol. 7 (2017).
322. Komander, D. The emerging complexity of protein ubiquitination. *Biochemical Society transactions* **37**, 937–953 (2009).
323. Buetow, L. & Huang, D. T. Structural insights into the catalysis and regulation of E3 ubiquitin ligases. *Nature reviews. Molecular cell biology* **17**, 626 (2016).
324. Abcam. Ubiquitin proteins and their diverse functions in the cellular machinery. <https://www.abcam.com/index.html?pageconfig=resource&rid=13555>.
325. Kliza, K. & Husnjak, K. Resolving the Complexity of Ubiquitin Networks. *Frontiers in Molecular Biosciences* **0**, 21 (2020).
326. Swatek, K. N. & Komander, D. Ubiquitin modifications. *Cell Research 2016 26:4* **26**, 399–422 (2016).
327. Bremm, A. & Komander, A. Emerging roles for Lys11-linked polyubiquitin in cellular regulation. *Trends in biochemical sciences* **36**, (2011).
328. Cunningham, C. N. *et al.* USP30 and parkin homeostatically regulate atypical ubiquitin chains on mitochondria. *Nature Cell Biology 2014 17:2* **17**, 160–169 (2015).
329. Yuan, W. C. *et al.* K33-Linked Polyubiquitination of Coronin 7 by Cul3-KLHL20 Ubiquitin E3 Ligase Regulates Protein Trafficking. *Molecular Cell* **54**, 586–600 (2014).
330. Zak, D. E. *et al.* Systems analysis identifies an essential role for SHANK-associated RH domain-interacting protein (SHARPIN) in macrophage Toll-like receptor 2 (TLR2) responses. *Proceedings of the National Academy of Sciences* **108**, 11536–11541 (2011).
331. Bal, E. *et al.* Lack of interaction between NEMO and SHARPIN impairs linear ubiquitination and NF- $\kappa$ B activation and leads to incontinentia pigmenti. *Journal of Allergy and Clinical Immunology* **140**, 1671-1682.e2 (2017).
332. Chen, Y. *et al.* The hepatitis C virus protein NS3 suppresses TNF- $\alpha$  – stimulated activation of NF- $\kappa$ B by targeting LUBAC. *Science Signalling* **8**, ra118 (2015).

333. Lafont, E. *et al.* TBK1 and IKK $\epsilon$  prevent TNF-induced cell death by RIPK1 phosphorylation. *Nature Cell Biology* **20**, 1389–1399 (2018).
334. Draber, P. *et al.* LUBAC-Recruited CYLD and A20 Regulate Gene Activation and Cell Death by Exerting Opposing Effects on Linear Ubiquitin in Signaling Complexes. *Cell Reports* **13**, 2258–2272 (2015).
335. Peltzer, N. *et al.* LUBAC is essential for embryogenesis by preventing cell death and enabling haematopoiesis. *Nature* **1** (2018) doi:10.1038/s41586-018-0064-8.
336. Ran, F. A. *et al.* Genome engineering using the CRISPR-Cas9 system. *Nature Protocols* **8**, 2281–2308 (2013).
337. Haas, T. L. *et al.* Recruitment of the Linear Ubiquitin Chain Assembly Complex Stabilizes the TNF-R1 Signaling Complex and Is Required for TNF-Mediated Gene Induction. *Molecular Cell* (2009) doi:10.1016/j.molcel.2009.10.013.
338. Gerlach, B. *et al.* Linear ubiquitination prevents inflammation and regulates immune signalling. *Nature* **471**, 591–6 (2011).
339. Shigemoto, T. *et al.* Identification of Loss of Function Mutations in Human Genes Encoding RIG-I and MDA5: IMPLICATIONS FOR RESISTANCE TO TYPE I DIABETES \*. *Journal of Biological Chemistry* **284**, 13348–13354 (2009).
340. Pothlichet, J. *et al.* Study of Human RIG-I Polymorphisms Identifies Two Variants with an Opposite Impact on the Antiviral Immune Response. *PLOS ONE* **4**, e7582 (2009).
341. Ranoa, D. R. E. *et al.* STING promotes homeostasis via regulation of cell proliferation and chromosomal stability. *Cancer Research* **79**, 1465–1479 (2019).
342. Biola-Clier, M. *et al.* Comparison of the DNA damage response in BEAS-2B and A549 cells exposed to titanium dioxide nanoparticles. *Mutagenesis* **32**, 161–172 (2017).
343. Massa, D., Baran, M., Bengoechea, J. A. & Bowie, A. G. PYHIN1 regulates pro-inflammatory cytokine induction rather than innate immune DNA sensing in airway epithelial cells. *Journal of Biological Chemistry* **295**, jbc.RA119.011400 (2020).
344. Goulet, M. L. *et al.* Systems Analysis of a RIG-I Agonist Inducing Broad Spectrum Inhibition of Virus Infectivity. *PLoS Pathogens* **9**, (2013).
345. Wu, W. *et al.* RIG-I and TLR3 are both required for maximum interferon induction by influenza virus in human lung alveolar epithelial cells. *Virology* **482**, 181–188 (2015).
346. Alexopoulou, L., Holt, A. C., Medzhitov, R. & Flavell, R. A. Recognition of double-stranded RNA and activation of NF- $\kappa$ B by Toll-like receptor 3. *Nature* **413**, 732–738 (2001).
347. Matsumoto, M., Kikkawa, S., Kohase, M., Miyake, K. & Seya, T. Establishment of a monoclonal antibody against human Toll-like receptor 3 that blocks double-stranded RNA-mediated signaling. *Biochemical and Biophysical Research Communications* **293**, 1364–1369 (2002).

348. Kawai, T. & Akira, S. Toll-like receptor and RIG-1-like receptor signaling. *Annals of the New York Academy of Sciences* vol. 1143 1–20 (2008).
349. Dauletbaev, N., Cammisano, M., Herscovitch, K. & Lands, L. C. Stimulation of the RIG-I/MAVS Pathway by Polyinosinic:Polycytidylic Acid Upregulates IFN- $\beta$  in Airway Epithelial Cells with Minimal Costimulation of IL-8. *The Journal of Immunology* **195**, 2829–2841 (2015).
350. Hausmann, S., Marq, J.-B., Tapparel, C., Kolakofsky, D. & Garcin, D. RIG-I and dsRNA-Induced IFN $\beta$  Activation. *PLoS ONE* **3**, e3965 (2008).
351. Childs, K. S., Randall, R. E. & Goodbourn, S. LGP2 Plays a Critical Role in Sensitizing mda-5 to Activation by Double-Stranded RNA. *PLoS ONE* **8**, e64202 (2013).
352. Sugimoto, N., Mitoma, H., Kim, T., Hanabuchi, S. & Liu, Y. J. Helicase proteins DHX29 and RIG-I cosense cytosolic nucleic acids in the human airway system. *Proceedings of the National Academy of Sciences of the United States of America* **111**, 7747–7752 (2014).
353. Kohlway, A., Luo, D., Rawling, D. C., Ding, S. C. & Pyle, A. M. Defining the functional determinants for RNA surveillance by RIG-I. *EMBO reports* **14**, 772–779 (2013).
354. Gebhardt, A., Laudenbach, B. T. & Pichlmair, A. Discrimination of self and non-self ribonucleic acids. *Journal of Interferon and Cytokine Research* vol. 37 184–197 (2017).
355. Yoneyama, M. & Fujita, T. Function of RIG-I-like receptors in antiviral innate immunity. *The Journal of biological chemistry* **282**, 15315–8 (2007).
356. Taima, K. *et al.* Expression of IP-10/CXCL10 Is Upregulated by Double-Stranded RNA in BEAS-2B Bronchial Epithelial Cells. *Respiration* **73**, 360–364 (2006).
357. Brownell, J. *et al.* Direct, Interferon-Independent Activation of the CXCL10 Promoter by NF $\kappa$ B and Interferon Regulatory Factor 3 during Hepatitis C. *Journal of Virology* **88**, 1582–1590 (2014).
358. Doğanay, S. *et al.* Single-cell analysis of early antiviral gene expression reveals a determinant of stochastic IFNB1 expression. *Integrative Biology (United Kingdom)* **9**, 857–867 (2017).
359. Hu, J. *et al.* Role of cell-to-cell variability in activating a positive feedback antiviral response in human dendritic cells. *PLoS ONE* **6**, (2011).
360. Maniatis, T. *et al.* Structure and function of the interferon- $\beta$  enhanceosome. in *Cold Spring Harbor Symposia on Quantitative Biology* vol. 63 609–620 (Cold Spring Harbor Laboratory Press, 1998).
361. Munshi, N. *et al.* The IFN- $\beta$  enhancer: A paradigm for understanding activation and repression of inducible gene expression. in *Cold Spring Harbor Symposia on Quantitative Biology* vol. 64 149–159 (Cold Spring Harb Symp Quant Biol, 1999).
362. Talon, J. *et al.* Activation of Interferon Regulatory Factor 3 Is Inhibited by the Influenza A Virus NS1 Protein. *Journal of Virology* **74**, 7989–7996 (2000).

363. Wang, X. *et al.* Influenza A Virus NS1 Protein Prevents Activation of NF-kappa B and Induction of Alpha/Beta Interferon. *Journal of Virology* **74**, 11566–11573 (2000).
364. Rajsbaum, R. *et al.* Species-Specific Inhibition of RIG-I Ubiquitination and IFN Induction by the Influenza A Virus NS1 Protein. *PLoS Pathogens* **8**, (2012).
365. Donelan, N. R., Basler, C. F. & García-Sastre, A. A recombinant influenza A virus expressing an RNA-binding-defective NS1 protein induces high levels of beta interferon and is attenuated in mice. *Journal of virology* **77**, 13257–66 (2003).
366. Hughes, B. W., Addanki, K. C., Sriskanda, A. N., McLean, E. & Bagasra, O. Infectivity of Immature Neurons to Zika Virus: A Link to Congenital Zika Syndrome. *EBioMedicine* **10**, 65–70 (2016).
367. Brault, J.-B. *et al.* Comparative Analysis Between Flaviviruses Reveals Specific Neural Stem Cell Tropism for Zika Virus in the Mouse Developing Neocortex. *EBioMedicine* **10**, 71–76 (2016).
368. Chazal, M. *et al.* RIG-I Recognizes the 5' Region of Dengue and Zika Virus Genomes. *Cell Reports* **24**, 320–328 (2018).
369. Hertzog, J. *et al.* Infection with a Brazilian isolate of Zika virus generates RIG-I stimulatory RNA and the viral NS5 protein blocks type I IFN induction and signaling. *European Journal of Immunology* **48**, 1120–1136 (2018).
370. Hu, Y. *et al.* Zika virus antagonizes interferon response in patients and disrupts RIG-I-MAVS interaction through its CARD-TM domains. *Cell and Bioscience* **9**, 46 (2019).
371. Strottmann, D. M. *et al.* Genetic and biological characterization of zika virus isolates from different Brazilian regions. *Memorias do Instituto Oswaldo Cruz* **114**, (2019).
372. Bos, S. *et al.* The structural proteins of epidemic and historical strains of Zika virus differ in their ability to initiate viral infection in human host cells. (2018)  
doi:10.1016/j.virol.2017.12.003.
373. Honda, K., Takaoka, A. & Taniguchi, T. Type I Inteferon Gene Induction by the Interferon Regulatory Factor Family of Transcription Factors. *Immunity* vol. 25 349–360 (2006).
374. Wesselhoeft, R. A. *et al.* RNA Circularization Diminishes Immunogenicity and Can Extend Translation Duration In Vivo. *Molecular Cell* **74**, 508-520.e4 (2019).
375. Nice, T. J. *et al.* Interferon- $\lambda$  cures persistent murine norovirus infection in the absence of adaptive immunity. *Science* **347**, 269–273 (2015).
376. Hemann, E. A., Gale, M. & Savan, R. Interferon lambda genetics and biology in regulation of viral control. *Frontiers in Immunology* **8**, 1707 (2017).

377. Pott, J. *et al.* IFN- $\lambda$  determines the intestinal epithelial antiviral host defense. *Proceedings of the National Academy of Sciences of the United States of America* **108**, 7944–9 (2011).
378. Zhang, H. X. *et al.* RIG-I regulates NF- $\kappa$ B activity through binding to Nf- $\kappa$ b1 3'-UTR mRNA. *Proceedings of the National Academy of Sciences of the United States of America* **110**, 6459–6464 (2013).
379. Xu, H. *et al.* MicroRNA-122 supports robust innate immunity in hepatocytes by targeting the RTKs/STAT3 signaling pathway. *eLife* **8**, (2019).
380. Henkel, T. *et al.* Rapid proteolysis of I $\kappa$ B- $\alpha$  is necessary for activation of transcription factor NF- $\kappa$ B. *Nature* **365**, 182–185 (1993).
381. Chen, Z. *et al.* Signal-induced site-specific phosphorylation targets I $\kappa$ B $\alpha$  to the ubiquitin-proteasome pathway. *Genes and Development* **9**, 1586–1597 (1995).
382. Yaron, A. *et al.* Inhibition of NF- $\kappa$ B cellular function via specific targeting of the I $\kappa$ B-ubiquitin ligase. *EMBO Journal* **16**, 6486–6494 (1997).
383. Lopez, C. B., Yount, J. S., Hermesh, T. & Moran, T. M. Sendai Virus Infection Induces Efficient Adaptive Immunity Independently of Type I Interferons. *Journal of Virology* **80**, 4538–4545 (2006).
384. Erlandsson, L. *et al.* Interferon- $\beta$  is required for interferon- $\alpha$  production in mouse fibroblasts. *Current Biology* **8**, 223–226 (1998).
385. Lima, M. C. *et al.* The Transcriptional and Protein Profile From Human Infected Neuroprogenitor Cells Is Strongly Correlated to Zika Virus Microcephaly Cytokines Phenotype Evidencing a Persistent Inflammation in the CNS. *Frontiers in Immunology* **10**, 1928 (2019).
386. Loo, Y.-M. *et al.* Distinct RIG-I and MDA5 signaling by RNA viruses in innate immunity. *Journal of virology* **82**, 335–45 (2008).
387. Liu, H. M. *et al.* Regulation of Retinoic Acid Inducible Gene-I (RIG-I) Activation by the Histone Deacetylase 6. *EBioMedicine* **9**, 195–206 (2016).
388. Dunphy, G. *et al.* Non-canonical Activation of the DNA Sensing Adaptor STING by ATM and IFI16 Mediates NF- $\kappa$ B Signaling after Nuclear DNA Damage. *Molecular Cell* **71**, 745-760.e5 (2018).
389. Diner, E. J. *et al.* The Innate Immune DNA Sensor cGAS Produces a Noncanonical Cyclic Dinucleotide that Activates Human STING. *Cell Reports* **3**, 1355–1361 (2013).
390. Georgana, I., Sumner, R. P., Towers, G. J. & Maluquer de Motes, C. Virulent Poxviruses Inhibit DNA Sensing by Preventing STING Activation. *Journal of Virology* **92**, (2018).
391. Klarquist, J. *et al.* STING-Mediated DNA Sensing Promotes Antitumor and Autoimmune Responses to Dying Cells. *The Journal of Immunology* **193**, 6124–6134 (2014).

392. Woo, S. R. *et al.* STING-dependent cytosolic DNA sensing mediates innate immune recognition of immunogenic tumors. *Immunity* **41**, 830–842 (2014).
393. Ahn, J., Konno, H. & Barber, G. N. Diverse roles of STING-dependent signaling on the development of cancer. *Oncogene* **34**, 5302–5308 (2015).
394. Schilling, M. *et al.* RIG-I Plays a Dominant Role in the Induction of Transcriptional Changes in Zika Virus-Infected Cells, which Protect from Virus-Induced Cell Death. *Cells* **2020**, Vol. 9, Page 1476 **9**, 1476 (2020).
395. Broggi, A. *et al.* Type III interferons disrupt the lung epithelial barrier upon viral recognition. *BioArchive (preprint)* (2020) doi:10.1101/2020.05.05.077867.
396. Forbester, J. L. *et al.* IRF5 promotes influenza-induced inflammatory responses in human iPSC-derived 1 myeloid cells and murine models 2 3 Running title: IRF5 promotes influenza-induced inflammatory responses 4 5 Affiliations Downloaded from. *J. Virol* (2020) doi:10.1128/JVI.00121-20.
397. Schreiner, P. *et al.* Human Herpesvirus-6 Reactivation, Mitochondrial Fragmentation, and the Coordination of Antiviral and Metabolic Phenotypes in Myalgic Encephalomyelitis/Chronic Fatigue Syndrome. *ImmunoHorizons* **4**, 201–215 (2020).
398. Kumar, A., Zhang, J. & Yu, F. S. X. Toll-like receptor 3 agonist poly(I:C)-induced antiviral response in human corneal epithelial cells. *Immunology* **117**, 11–21 (2006).
399. Farina, G. A. *et al.* Poly(I:C) drives type I IFN- and TGF $\beta$ -mediated inflammation and dermal fibrosis simulating altered gene expression in systemic sclerosis. *Journal of Investigative Dermatology* **130**, 2583–2593 (2010).
400. Huang, C. C. *et al.* A pathway analysis of poly(I:C)-induced global gene expression change in human peripheral blood mononuclear cells. *Physiological Genomics* **26**, 125–133 (2006).
401. Doyle, S. E. *et al.* IRF3 Mediates a TLR3/TLR4-Specific Antiviral Gene Program. *Immunity* **17**, 251–263 (2002).
402. Tamassia, N. *et al.* Activation of an Immunoregulatory and Antiviral Gene Expression Program in Poly(I:C)-Transfected Human Neutrophils. *The Journal of Immunology* **181**, 6563–6573 (2008).
403. Geiss, G. *et al.* A Comprehensive View of Regulation of Gene Expression by Double-stranded RNA-mediated Cell Signaling. *Journal of Biological Chemistry* **276**, 30178–30182 (2001).
404. Alexopoulou, L., Holt, A. C., Medzhitov, R. & Flavell, R. A. Recognition of double-stranded RNA and activation of NF- $\kappa$ B by Toll-like receptor 3. *Nature* **413**, 732–738 (2001).
405. Guillot, L. *et al.* Involvement of Toll-like receptor 3 in the immune response of lung epithelial cells to double-stranded RNA and influenza A virus. *Journal of Biological Chemistry* **280**, 5571–5580 (2005).

406. Stowell, N. C. *et al.* Long-term activation of TLR3 by Poly(I:C) induces inflammation and impairs lung function in mice. *Respiratory Research* **10**, 43 (2009).
407. Mandhana, R. & Horvath, C. M. Sendai Virus Infection Induces Expression of Novel RNAs in Human Cells. *Scientific Reports* **8**, 1–12 (2018).
408. Strähle, L., Garcin, D., Le Mercier, P., Schlaak, J. F. & Kolakofsky, D. Sendai Virus Targets Inflammatory Responses, as Well as the Interferon-Induced Antiviral State, in a Multifaceted Manner. *Journal of Virology* **77**, 7903–7913 (2003).
409. Yount, J. S., Gitlin, L., Moran, T. M. & López, C. B. MDA5 participates in the detection of paramyxovirus infection and is essential for the early activation of dendritic cells in response to Sendai Virus defective interfering particles. *Journal of immunology (Baltimore, Md. : 1950)* **180**, 4910–8 (2008).
410. Chen, S. *et al.* SAMHD1 suppresses innate immune responses to viral infections and inflammatory stimuli by inhibiting the NF- $\kappa$ B and interferon pathways. *Proceedings of the National Academy of Sciences of the United States of America* **115**, E3798–E3807 (2018).
411. Soares, F. *et al.* NLRX1 does not inhibit MAVS-dependent antiviral signalling. *Innate Immunity* **19**, 438–448 (2013).
412. Hu, M. M., Liao, C. Y., Yang, Q., Xie, X. Q. & Shu, H. B. Innate immunity to RNA virus is regulated by temporal and reversible sumoylation of RIG-I and MDA5. *Journal of Experimental Medicine* **214**, 973–989 (2017).
413. Ramos, I. *et al.* Innate Immune Response to Influenza Virus at Single-Cell Resolution in Human Epithelial Cells Revealed Paracrine Induction of Interferon Lambda 1. *Journal of Virology* **93**, (2019).
414. Zhou, F. *et al.* Influenza A virus inhibits influenza virus replication by inducing IL-37. *Journal of Clinical Laboratory Analysis* **33**, e22638 (2019).
415. Wang, J. *et al.* Innate immune response to influenza A virus in differentiated human alveolar type II cells. *American Journal of Respiratory Cell and Molecular Biology* **45**, 582–591 (2011).
416. Söderholm, S. *et al.* Immuno-modulating properties of saliphenylhalamide, SNS-032, obatoclox, and gemcitabine. *Antiviral Research* **126**, 69–80 (2016).
417. Mana R. Ehlers & Rebecca M. Todd. Genesis and Maintenance of Attentional Biases: The Role of the Locus Coeruleus-Noradrenaline System. *Neural Plasticity* **1**, 2–3 (2017).
418. Sheng, Z. *et al.* Next-generation sequencing analysis of cellular response to influenza B virus infection. *Viruses* **12**, (2020).
419. Hatada, E. & Fukuda, R. Binding of influenza a virus NS1 protein to dsRNA in vitro. *Journal of General Virology* **73**, 3325–3329 (1992).

420. Wang, W. *et al.* RNA binding by the novel helical domain of the influenza virus NS1 protein requires its dimer structure and a small number of specific basic amino acids . RNA binding by the novel helical domain of the influenza virus NS1 protein requires its dimer struct. *Rna* **5**, 195–205 (1999).
421. Lee, S. & Baldrige, M. T. Interferon-lambda: A potent regulator of intestinal viral infections. *Frontiers in Immunology* vol. 8 749 (2017).
422. Thomson, S. *et al.* The role of transposable elements in the regulation of IFN-lambda1 gene expression. *Proceedings of the National Academy of Sciences of the United States of America* **106**, 11564–11569 (2009).
423. Hamel, R. *et al.* African and Asian Zika virus strains differentially induce early antiviral responses in primary human astrocytes. (2017) doi:10.1016/j.meegid.2017.01.015.
424. Devarkar, S. C., Schweibenz, B., Wang, C., Marcotrigiano, J. & Patel, S. S. RIG-I Uses an ATPase-Powered Translocation-Throttling Mechanism for Kinetic Proofreading of RNAs and Oligomerization. *Molecular Cell* **72**, 355-368.e4 (2018).
425. Berke, I. C. & Modis, Y. MDA5 cooperatively forms dimers and ATP-sensitive filaments upon binding double-stranded RNA. *The EMBO Journal* **31**, 1714–1726 (2012).
426. InvivoGen. Poly(I:C) HMW | High molecular weight, synthetic dsRNA. <https://www.invivogen.com/polyic-hmw>.
427. Yoshino, H., Iwabuchi, M., Kazama, Y., Furukawa, M. & Kashiwakura, I. Effects of retinoic acid-inducible gene-i-like receptors activations and ionizing radiation cotreatment on cytotoxicity against human non-small cell lung cancer in vitro. *Oncology Letters* **15**, 4697–4705 (2018).
428. Li, Y. *et al.* Protein Kinase Regulated by dsRNA Downregulates the Interferon Production in Dengue Virus- and dsRNA-Stimulated Human Lung Epithelial Cells. *PLoS ONE* **8**, e55108 (2013).
429. Kotla, S., Peng, T., Bumgarner, R. E. & Gustin, K. E. Attenuation of the type I interferon response in cells infected with human rhinovirus. *Virology* **374**, 399–410 (2008).
430. Benitez, A. A. *et al.* In Vivo RNAi Screening Identifies MDA5 as a Significant Contributor to the Cellular Defense against Influenza A Virus. *Cell Reports* **11**, 1714–1726 (2015).
431. Zharkov, M. I., Zenkova, M. A., Vlassov, V. v. & Chernolovskaya, E. L. Molecular Mechanism of the Antiproliferative Activity of Short Immunostimulating dsRNA. *Frontiers in Oncology* **9**, (2019).
432. Zinngrebe, J. *et al.* LUBAC deficiency perturbs TLR3 signaling to cause immunodeficiency and autoinflammation. *The Journal of Experimental Medicine* **213**, 2671 LP – 2689 (2016).
433. Invivogen. MAVS-Knockout NF-kB & IFN Reporter A549 lung carcinoma. <https://www.invivogen.com/a549-dual-ko-mavs>.

434. Sun, Q. *et al.* The Specific and Essential Role of MAVS in Antiviral Innate Immune Responses. *Immunity* **24**, 633–642 (2006).
435. Kumar, H. *et al.* Essential role of IPS-1 in innate immune responses against RNA viruses. *Journal of Experimental Medicine* **203**, 1795–1803 (2006).
436. Tissari, J., Sirén, J., Meri, S., Julkunen, I. & Matikainen, S. IFN- $\alpha$  Enhances TLR3-Mediated Antiviral Cytokine Expression in Human Endothelial and Epithelial Cells by Up-Regulating TLR3 Expression. *The Journal of Immunology* **174**, 4289–4294 (2005).
437. Kato, H. *et al.* Cell type-specific involvement of RIG-I in antiviral response. *Immunity* **23**, 19–28 (2005).
438. Guillot, L. *et al.* Involvement of Toll-like receptor 3 in the immune response of lung epithelial cells to double-stranded RNA and influenza A virus. *Journal of Biological Chemistry* **280**, 5571–5580 (2005).
439. Goffic, R. Le *et al.* Detrimental Contribution of the Toll-Like Receptor (TLR)3 to Influenza A Virus-Induced Acute Pneumonia. *PLoS Pathogens* **2**, e53 (2006).
440. le Goffic, R. *et al.* Cutting Edge: Influenza A Virus Activates TLR3-Dependent Inflammatory and RIG-I-Dependent Antiviral Responses in Human Lung Epithelial Cells. *The Journal of Immunology* **178**, 3368–3372 (2007).
441. Wu, W. *et al.* IRF7 is required for the second phase interferon induction during influenza virus infection in human lung epithelia. *Viruses* **12**, 377 (2020).
442. Chen, X. *et al.* Host immune response to influenza A virus infection. *Frontiers in Immunology* **9**, 1–13 (2018).
443. Chang, T. H., Liao, C. L. & Lin, Y. L. Flavivirus induces interferon-beta gene expression through a pathway involving RIG-I-dependent IRF-3 and PI3K-dependent NF- $\kappa$ B activation. *Microbes and Infection* **8**, 157–171 (2006).
444. Loo, Y.-M. *et al.* Distinct RIG-I and MDA5 Signaling by RNA Viruses in Innate Immunity. *Journal of Virology* **82**, 335–345 (2008).
445. Bustos-Arriaga, J. *et al.* Activation of the Innate Immune Response against DENV in Normal Non-Transformed Human Fibroblasts. *PLoS Neglected Tropical Diseases* **5**, e1420 (2011).
446. Lundberg, R. *et al.* Zika virus non-structural protein NS5 inhibits the RIG-I pathway and interferon lambda 1 promoter activation by targeting IKK epsilon. *Viruses* **11**, (2019).
447. Sprokholt, J. K. *et al.* RIG-I-like receptor activation by dengue virus drives follicular T helper cell formation and antibody production. *PLoS Pathogens* **13**, 1–19 (2017).
448. Saha, S. K. *et al.* Regulation of antiviral responses by a direct and specific interaction between TRAF3 and Cardif. *EMBO Journal* **25**, 3257–3263 (2006).

449. Kondo, H., Miyoshi, K., Sakiyama, S., Tangoku, A. & Noma, T. Differential Regulation of Gene Expression of Alveolar Epithelial Cell Markers in Human Lung Adenocarcinoma-Derived A549 Clones. *Stem Cells International* **2015**, (2015).
450. Jiang, Z. *et al.* Poly(dI-dC)-induced Toll-like Receptor 3 (TLR3)-mediated Activation of NF $\kappa$ B and MAP Kinase Is through an Interleukin-1 Receptor-associated Kinase (IRAK)-independent Pathway Employing the Signaling Components TLR3-TRAF6-TAK1-TAB2-PKR. *Journal of Biological Chemistry* **278**, 16713–16719 (2003).
451. Kawai, T. & Akira, S. The role of pattern-recognition receptors in innate immunity: Update on toll-like receptors. *Nature Immunology* vol. 11 373–384 (2010).
452. Kishore, N. *et al.* IKK-i and TBK-1 are enzymatically distinct from the homologous enzyme IKK-2. Comparative analysis of recombinant human IKK-i, TBK-1, and IKK-2. *Journal of Biological Chemistry* **277**, 13840–13847 (2002).
453. Pomerantz, J. L. & Baltimore, D. NF- $\kappa$ B activation by a signaling complex containing TRAF2, TANK and TBK1, a novel IKK-related kinase. *The EMBO Journal* **18**, 6694–6704 (1999).
454. Tojima, Y. *et al.* NAK is an I $\kappa$ B kinase-activating kinase. *Nature* **404**, 778–782 (2000).
455. Peters, R. T., Liao, S. M. & Maniatis, T. IKK $\epsilon$  is part of a novel PMA-inducible I $\kappa$ B kinase complex. *Molecular Cell* **5**, 513–522 (2000).
456. Taft, J. *et al.* Human TBK1 deficiency leads to autoinflammation driven by TNF-induced cell death. *Cell* (2021) doi:10.1016/J.CELL.2021.07.026.
457. Wang, N., Ahmed, S. & Haqqi, T. M. Genomic structure and functional characterization of the promoter region of human I $\kappa$ B kinase-related kinase IKKi/IKK $\epsilon$  gene. *Gene* **353**, 118–133 (2005).
458. Guo, J. *et al.* IKBKE is induced by STAT3 and tobacco carcinogen and determines chemosensitivity in non-small cell lung cancer. *Oncogene* **32**, 151–159 (2013).
459. Fitzgerald, K. A. *et al.* IKK $\epsilon$  and TBK1 are essential components of the IRF3 signaling pathway. *Nature Immunology* **4**, 491–496 (2003).
460. McWhirter, S. M. *et al.* IFN-regulatory factor 3-dependent gene expression is defective in Tbk1-deficient mouse embryonic fibroblasts. *Proceedings of the National Academy of Sciences of the United States of America* **101**, 233–238 (2004).
461. Fujita, F. *et al.* Identification of NAP1, a Regulatory Subunit of I $\kappa$ B Kinase-Related Kinases That Potentiates NF- $\kappa$ B Signaling. *Molecular and Cellular Biology* **23**, 7780–7793 (2003).
462. Ryzhakov, G. & Randow, F. SINTBAD, a novel component of innate antiviral immunity, shares a TBK1-binding domain with NAP1 and TANK. *EMBO Journal* **26**, 3180–3190 (2007).
463. Sasai, M. *et al.* NAK-Associated Protein 1 Participates in Both the TLR3 and the Cytoplasmic Pathways in Type I IFN Induction. *The Journal of Immunology* **177**, 8676–8683 (2006).

464. Guo, B. & Cheng, G. Modulation of the interferon antiviral response by the TBK1/IKKi adaptor protein TANK. *Journal of Biological Chemistry* **282**, 11817–11826 (2007).
465. Sasai, M. *et al.* Cutting Edge: NF- $\kappa$ B-Activating Kinase-Associated Protein 1 Participates in TLR3/Toll-IL-1 Homology Domain-Containing Adapter Molecule-1-Mediated IFN Regulatory Factor 3 Activation. *The Journal of Immunology* **174**, 27–30 (2005).
466. Chau, T. L. *et al.* Are the IKKs and IKK-related kinases TBK1 and IKK- $\epsilon$  similarly activated? *Trends in Biochemical Sciences* vol. 33 171–180 (2008).
467. Michallet, M. C. *et al.* TRADD Protein Is an Essential Component of the RIG-like Helicase Antiviral Pathway. *Immunity* **28**, 651–661 (2008).
468. Nakhaei, P., Genin, P., Civas, A. & Hiscott, J. RIG-I-like receptors: Sensing and responding to RNA virus infection. *Seminars in Immunology* vol. 21 215–222 (2009).
469. Roth, S. & Ruland, J. Caspase-8: Clipping off RIG-I signaling. *Immunity* vol. 34 283–285 (2011).
470. Rajput, A. *et al.* RIG-I RNA helicase activation of irf3 transcription factor is negatively regulated by caspase-8-mediated cleavage of the RIP1 protein. *Immunity* **34**, 340–351 (2011).
471. Zhu, G., Wu, C. J., Zhao, Y. & Ashwell, J. D. Optineurin Negatively Regulates TNF $\alpha$ -Induced NF- $\kappa$ B Activation by Competing with NEMO for Ubiquitinated RIP. *Current Biology* **17**, 1438–1443 (2007).
472. Tanishima, M. *et al.* Identification of optineurin as an interleukin-1 receptor-associated kinase 1-binding protein and its role in regulation of MyD88-dependent signalling. *Journal of Biological Chemistry* **292**, 17250–17257 (2017).
473. Nakazawa, S. *et al.* Linear ubiquitination is involved in the pathogenesis of optineurin-associated amyotrophic lateral sclerosis. *Nature Communications* **7**, 1–14 (2016).
474. Sudhakar, C., Nagabhushana, A., Jain, N. & Swarup, G. NF- $\kappa$ B mediates tumor necrosis factor  $\alpha$ -induced expression of optineurin, a negative regulator of NF- $\kappa$ B. *PLoS ONE* **4**, 5114 (2009).
475. Bakshi, S., Taylor, J., Strickson, S., McCartney, T. & Cohen, P. Identification of TBK1 complexes required for the phosphorylation of IRF3 and the production of interferon  $\beta$ . *Biochemical Journal* **474**, 1163–1174 (2017).
476. Munitic, I. *et al.* Optineurin Insufficiency Impairs IRF3 but Not NF- $\kappa$ B Activation in Immune Cells. *The Journal of Immunology* **191**, 6231–6240 (2013).
477. Mankouri, J. *et al.* Optineurin negatively regulates the induction of IFN $\beta$  in response to RNA virus infection. *PLoS Pathogens* **6**, 1000778 (2010).
478. Yang, Y., Xu, J., Ge, S. & Lai, L. CRISPR/Cas: Advances, Limitations, and Applications for Precision Cancer Research. *Frontiers in Medicine* **0**, 115 (2021).

479. Vazquez, C. & Horner, S. M. MAVS Coordination of Antiviral Innate Immunity. *Journal of Virology* **89**, 6974–6977 (2015).
480. Clark, K. *et al.* Novel cross-talk within the IKK family controls innate immunity. *Biochemical Journal* **434**, 93–104 (2011).
481. Chen, Z. J. Ubiquitin Signaling in the NF- $\kappa$ B Pathway. *Nature cell biology* **7**, 758 (2005).
482. Tsuchiya, Y. *et al.* Nuclear IKK $\beta$  Is an Adaptor Protein for I $\kappa$ B $\alpha$  Ubiquitination and Degradation in UV-Induced NF- $\kappa$ B Activation. *Molecular cell* **39**, 570–582 (2010).
483. Lin, R., Mamane, Y. & Hiscott, J. Structural and Functional Analysis of Interferon Regulatory Factor 3: Localization of the Transactivation and Autoinhibitory Domains. *Molecular and Cellular Biology* **19**, 2465–2474 (1999).
484. Sharma, S. *et al.* Triggering the interferon antiviral response through an IKK-related pathway. *Science* **300**, 1148–1151 (2003).
485. Pomerantz, J. L. NF-kappa B activation by a signaling complex containing TRAF2, TANK and TBK1, a novel IKK-related kinase. *The EMBO Journal* **18**, 6694–6704 (1999).
486. Lin, R. *et al.* Dissociation of a MAVS/IPS-1/VISA/Cardif-IKK $\epsilon$  Molecular Complex from the Mitochondrial Outer Membrane by Hepatitis C Virus NS3-4A Proteolytic Cleavage †. *JOURNAL OF VIROLOGY* **80**, 6072–6083 (2006).
487. Hemmi, H. *et al.* The Roles of Two I B Kinase-related Kinases in Lipopolysaccharide and Double Stranded RNA Signaling and Viral Infection. *The Journal of Experimental Medicine J. Exp. Med.* **199**, 1641–1650 (2004).
488. Solis, M. *et al.* Involvement of TBK1 and IKK $\epsilon$  in lipopolysaccharide-induced activation of the interferon response in primary human macrophages. *European Journal of Immunology* **37**, 528–539 (2007).
489. Balka, K. R. *et al.* TBK1 and IKK $\epsilon$  Act Redundantly to Mediate STING-Induced NF- $\kappa$ B Responses in Myeloid Cells. *Cell Reports* **31**, 107492 (2020).
490. Helgason, E., Phung, Q. T. & Dueber, E. C. Recent insights into the complexity of Tank-binding kinase 1 signaling networks: The emerging role of cellular localization in the activation and substrate specificity of TBK1. *FEBS Letters* **587**, 1230–1237 (2013).
491. Outlioua, A., Pourcelot, M. & Arnoult, D. The role of optineurin in antiviral type I interferon production. *Frontiers in Immunology* vol. 9 853 (2018).
492. Balachandran, S., Thomas, E. & Barber, G. N. A FADD-dependent innate immune mechanism in mammalian cells. *Nature* **432**, 401–405 (2004).
493. Helgason, E., Phung, Q. T. & Dueber, E. C. Recent insights into the complexity of Tank-binding kinase 1 signaling networks: The emerging role of cellular localization in the activation and substrate specificity of TBK1. *FEBS Letters* **587**, 1230–1237 (2013).

494. Clark, K., Plater, L., Peggie, M. & Cohen, P. Use of the pharmacological inhibitor BX795 to study the regulation and physiological roles of TBK1 and I $\kappa$ B Kinase  $\epsilon$ : A distinct upstream kinase mediates ser-172 phosphorylation and activation. *Journal of Biological Chemistry* **284**, 14136–14146 (2009).
495. Wagner, S. A., Satpathy, S., Beli, P. & Choudhary, C. SPATA2 links CYLD to the TNF- $\alpha$  receptor signaling complex and modulates the receptor signaling outcomes. *The EMBO Journal* **35**, 1868–1884 (2016).
496. Zhang, C. *et al.* Structural basis of STING binding with and phosphorylation by TBK1. *Nature* **567**, 394–398 (2019).
497. Thurston, T. L. M., Ryzhakov, G., Bloor, S., von Muhlinen, N. & Randow, F. The TBK1 adaptor and autophagy receptor NDP52 restricts the proliferation of ubiquitin-coated bacteria. *Nature immunology* **10**, 1215–1222 (2009).
498. Wild, P. *et al.* Phosphorylation of the autophagy receptor optineurin restricts Salmonella growth. *Science (New York, N.Y.)* **333**, 228–233 (2011).
499. Wang, L., Li, S. & Dorf, M. E. NEMO binds ubiquitinated TANK-binding kinase 1 (TBK1) to regulate innate immune responses to RNA viruses. *PloS one* **7**, (2012).
500. Iwai, K. & Tokunaga, F. Linear polyubiquitination: a new regulator of NF- $\kappa$ B activation. *EMBO Reports* **10**, 706–713 (2009).
501. Haas, T. L. *et al.* Recruitment of the Linear Ubiquitin Chain Assembly Complex Stabilizes the TNF-R1 Signaling Complex and Is Required for TNF-Mediated Gene Induction. *Molecular Cell* **36**, 831–844 (2009).
502. Peltzer, N., Darding, M. & Walczak, H. Holding RIPK1 on the Ubiquitin Leash in TNFR1 Signaling. *Trends in Cell Biology* **26**, 445–461 (2016).
503. Fiil, B. K. & Gyrd-Hansen, M. The Met1-linked ubiquitin machinery in inflammation and infection. *Cell Death and Differentiation* vol. 28 557–569 (2021).
504. MacDuff, D. A. *et al.* HOIL1 Is Essential for the Induction of Type I and III Interferons by MDA5 and Regulates Persistent Murine Norovirus Infection. *Journal of Virology* **92**, (2018).
505. Belgnaoui, S. M. *et al.* Linear Ubiquitination of NEMO Negatively Regulates the Interferon Antiviral Response through Disruption of the MAVS-TRAF3 Complex. *Cell Host & Microbe* **12**, 211–222 (2012).
506. Brazee, P. L., Dada, L. A. & Sznajder, J. I. *Linear ubiquitin assembly complex regulates lung epithelial driven responses during influenza infection Graphical abstract Find the latest version* : (2019).
507. Tokunaga, F. *et al.* Involvement of linear polyubiquitylation of NEMO in NF- $\kappa$ B activation. *Nature Cell Biology* **11**, 123–132 (2009).

508. Tokunaga, F. *et al.* SHARPIN is a component of the NF- $\kappa$ B-activating linear ubiquitin chain assembly complex. *Nature* **471**, 633–636 (2011).
509. Zhang, M. *et al.* Negative feedback regulation of cellular antiviral signaling by RBCK1-mediated degradation of IRF3. *Cell Research* **18**, 1096–1104 (2008).
510. Kirisako, T. *et al.* A ubiquitin ligase complex assembles linear polyubiquitin chains. *EMBO Journal* **25**, 4877–4887 (2006).
511. Ikeda, F. *et al.* SHARPIN forms a linear ubiquitin ligase complex regulating NF- $\kappa$ B activity and apoptosis. *Nature* **471**, 637–641 (2011).
512. Wilusz, C. J., Wormington, M. & Peltz, S. W. The cap-to-tail guide to mRNA turnover. *Nature Reviews Molecular Cell Biology* vol. 2 237–246 (2001).
513. Akiyama, B. M. *et al.* Zika virus produces noncoding RNAs using a multi-pseudoknot structure that confounds a cellular exonuclease. *Science* **354**, 1148–1152 (2016).
514. Fennell, L. M. *et al.* Site-specific ubiquitination of the E3 ligase HOIP regulates cell death and immune signaling. *bioRxiv* 742544 (2019) doi:10.1101/742544.
515. Smit, J. J. *et al.* The E3 ligase HOIP specifies linear ubiquitin chain assembly through its RING-IBR-RING domain and the unique LDD extension. *EMBO Journal* **31**, 3833–3844 (2012).
516. Peltzer, N. *et al.* HOIP deficiency causes embryonic lethality by aberrant TNFR1-mediated endothelial cell death. *Cell Reports* **9**, 153–165 (2014).
517. Bowman, J. *et al.* Posttranslational modification of HOIP blocks toll-like receptor 4-mediated linear-ubiquitin-chain formation. *mBio* **6**, (2015).
518. Emmerich, C. H. *et al.* Activation of the canonical IKK complex by K63/M1-linked hybrid ubiquitin chains. *Proceedings of the National Academy of Sciences of the United States of America* **110**, (2013).
519. Sasaki, Y. *et al.* Defective immune responses in mice lacking LUBAC-mediated linear ubiquitination in B cells. *EMBO Journal* **32**, 2463–2476 (2013).
520. Dubois, S. M. *et al.* A catalytic-independent role for the LUBAC in NF- $\kappa$ B activation upon antigen receptor engagement and in lymphoma cells. *Blood* **123**, 2199–203 (2014).
521. Stieglitz, B., Morris-Davies, A. C., Koliopoulos, M. G., Christodoulou, E. & Rittinger, K. LUBAC synthesizes linear ubiquitin chains via a thioester intermediate. *EMBO Reports* **13**, 840–846 (2012).
522. Degterev, A. *et al.* Identification of RIP1 kinase as a specific cellular target of necrostatins. *Nature Chemical Biology* **4**, 313–321 (2008).
523. de Almagro, M. C. *et al.* Coordinated ubiquitination and phosphorylation of RIP1 regulates necroptotic cell death. *Cell Death and Differentiation* **24**, 26–37 (2017).

524. Dubois, S. M. *et al.* A catalytic-independent role for the LUBAC in NF- $\kappa$ B activation upon antigen receptor engagement and in lymphoma cells. *Blood* **123**, 2199–2203 (2014).
525. Kelliher, M. A. *et al.* The death domain kinase RIP mediates the TNF-induced NF- $\kappa$ B signal. *Immunity* **8**, 297–303 (1998).
526. Lee, T. H. *et al.* The Death Domain Kinase RIP1 Is Essential for Tumor Necrosis Factor Alpha Signaling to p38 Mitogen-Activated Protein Kinase. *Molecular and Cellular Biology* **23**, 8377–8385 (2003).
527. Haas, T. L. *et al.* Recruitment of the Linear Ubiquitin Chain Assembly Complex Stabilizes the TNF-R1 Signaling Complex and Is Required for TNF-Mediated Gene Induction. *Molecular Cell* **36**, 831–844 (2009).
528. Tokunaga, F. *et al.* Involvement of linear polyubiquitylation of NEMO in NF -  $\kappa$  B activation. *Nature Cell Biology* **11**, 123–132 (2009).
529. Schock, S. N. *et al.* Induction of necroptotic cell death by viral activation of the RIG-I or STING pathway. (2017) doi:10.1038/cdd.2016.153.
530. Chattopadhyay, S., Kuzmanovic, T., Zhang, Y., Wetzel, J. L. & Sen, G. C. Ubiquitination of the Transcription Factor IRF-3 Activates RIP1, the Apoptotic Pathway that Protects Mice from Viral Pathogenesis. *Immunity* **44**, 1151–1161 (2016).
531. Belmokhtar, C. A., Hillion, J. & Ségal-Bendirdjian, E. Staurosporine induces apoptosis through both caspase-dependent and caspase-independent mechanisms. *Oncogene* **20**, 3354–3362 (2001).
532. Feng, G. & Kaplowitz, N. Mechanism of staurosporine-induced apoptosis in murine hepatocytes. *American journal of physiology. Gastrointestinal and liver physiology* **282**, G825–G834 (2002).
533. van Opdenbosch, N. & Lamkanfi, M. Caspases in Cell Death, Inflammation, and Disease. *Immunity* vol. 50 1352–1364 (2019).
534. Brazee, P. L. *et al.* Linear ubiquitin assembly complex regulates lung epithelial-driven responses during influenza infection. *The Journal of Clinical Investigation* **130**, 1301 (2020).
535. Khan, M., Syed, G. H., Kim, S. J. & Siddiqui, A. Hepatitis B Virus-Induced Parkin-Dependent Recruitment of Linear Ubiquitin Assembly Complex (LUBAC) to Mitochondria and Attenuation of Innate Immunity. *PLoS Pathogens* **12**, (2016).
536. Oikawa, D. *et al.* Molecular bases for HOIPINs-mediated inhibition of LUBAC and innate immune responses. *Communications Biology* 2020 3:1 **3**, 1–17 (2020).
537. Bertrand, M. *et al.* cIAP1 and cIAP2 facilitate cancer cell survival by functioning as E3 ligases that promote RIP1 ubiquitination. *Molecular cell* **30**, 689–700 (2008).

538. Damgaard, R. B. *et al.* The Ubiquitin Ligase XIAP Recruits LUBAC for NOD2 Signaling in Inflammation and Innate Immunity. *Molecular Cell* **46**, 746–758 (2012).
539. Yang, S. *et al.* Pellino3 ubiquitinates RIP2 and mediates Nod2-induced signaling and protective effects in colitis. *Nature immunology* **14**, 927–936 (2013).
540. Cohen, P. & Strickson, S. The role of hybrid ubiquitin chains in the MyD88 and other innate immune signalling pathways. *Cell Death and Differentiation* vol. 24 (2017).
541. Hrdinka, M. & Gyrd-Hansen, M. The Met1-Linked Ubiquitin Machinery: Emerging Themes of (De)regulation. *Molecular Cell* **68**, 265–280 (2017).
542. Zhang, M. *et al.* Negative feedback regulation of cellular antiviral signaling by RBCK1-mediated degradation of IRF3. *Cell Research* **18**, 1096–1104 (2008).
543. Elliott, P. R. *et al.* SPATA2 Links CYLD to LUBAC, Activates CYLD, and Controls LUBAC Signaling. *Molecular Cell* **63**, 990–1005 (2016).
544. Elliott, P. R. *et al.* Molecular basis and regulation of OTULIN-LUBAC interaction. *Molecular Cell* (2014) doi:10.1016/j.molcel.2014.03.018.
545. Fiil, B. K. *et al.* OTULIN restricts Met1-linked ubiquitination to control innate immune signaling. *Molecular cell* **50**, 818 (2013).
546. Shimizu, S. *et al.* Differential Involvement of the Npl4 Zinc Finger Domains of SHARPIN and HOIL-1L in Linear Ubiquitin Chain Assembly Complex-Mediated Cell Death Protection. *Molecular and Cellular Biology* **36**, 1569–1583 (2016).
547. Boisson, B. *et al.* Human HOIP and LUBAC deficiency underlies autoinflammation, immunodeficiency, amylopectinosis, and lymphangiectasia. *The Journal of experimental medicine* **212**, 939–51 (2015).
548. Oda, H. *et al.* Second Case of HOIP Deficiency Expands Clinical Features and Defines Inflammatory Transcriptome Regulated by LUBAC. *Frontiers in Immunology* **10**, 479 (2019).
549. HogenEsch, H., Janke, S., Boggess, D. & Sundberg, J. P. Absence of Peyer's Patches and Abnormal Lymphoid Architecture in Chronic Proliferative Dermatitis (cpdm/cpdm) Mice. *The Journal of Immunology* **162**, 3890–3896 (1999).
550. Seymour, R., Sundberg, J. P. & HogenEsch, H. Abnormal lymphoid organ development in immunodeficient mutant mice. *Veterinary Pathology* vol. 43 401–423 (2006).
551. Teh, C. E. *et al.* Linear ubiquitin chain assembly complex coordinates late thymic T-cell differentiation and regulatory T-cell homeostasis. *Nature Communications* 2016 7:1 **7**, 1–15 (2016).
552. Sasaki, Y. & Iwai, K. Crucial Role of Linear Ubiquitin Chain Assembly Complex-Mediated Inhibition of Programmed Cell Death in TLR4-Mediated B Cell Responses and B1b Cell Development. *Journal of immunology (Baltimore, Md. : 1950)* **200**, 3438–3449 (2018).

553. Xin Wu, L., Tang, Y., Zhang, S. & Zhao, X. Autoinflammation Induced – HOIP Deficiency MyD88-Dependent Signaling Is Required for. (2021) doi:10.4049/jimmunol.2100173.
554. van Wijk, S. J. L. *et al.* Fluorescence-Based Sensors to Monitor Localization and Functions of Linear and K63-Linked Ubiquitin Chains in Cells. *Molecular Cell* **47**, 797–809 (2012).
555. Emmerich, C. *et al.* Lys63/Met1-hybrid ubiquitin chains are commonly formed during the activation of innate immune signalling. *Biochemical and biophysical research communications* **474**, 452–461 (2016).
556. Maelfait, J. & Beyaert, R. Emerging Role of Ubiquitination in Antiviral RIG-I Signaling. *Microbiology and Molecular Biology Reviews : MMBR* **76**, 33 (2012).
557. Okamoto, M., Kouwaki, T., Fukushima, Y. & Oshiumi, H. Regulation of RIG-I Activation by K63-Linked Polyubiquitination. *Frontiers in Immunology* **8**, (2017).
558. Chattopadhyay, S. *et al.* Role of interferon regulatory factor 3-mediated apoptosis in the establishment and maintenance of persistent infection by Sendai virus. *Journal of Virology* **87**, 16–24 (2013).
559. Chattopadhyay, S. *et al.* Viral apoptosis is induced by IRF-3-mediated activation of Bax. *The EMBO Journal* **29**, 1762–1773 (2010).
560. Chattopadhyay, S., Yamashita, M., Zhang, Y. & Sen, G. C. The IRF-3/Bax-mediated apoptotic pathway, activated by viral cytoplasmic RNA and DNA, inhibits virus replication. *Journal of virology* **85**, 3708–16 (2011).
561. Rickard, J. A. *et al.* TNFR1-dependent cell death drives inflammation in Sharpin-deficient mice. *eLife* **3**, (2014).
562. Smit, J. J. *et al.* Target specificity of the E3 ligase LUBAC for ubiquitin and NEMO relies on different minimal requirements. *Journal of Biological Chemistry* **288**, 31728–31737 (2013).
563. Fuseya, Y. *et al.* The HOIL-1L ligase modulates immune signalling and cell death via monoubiquitination of LUBAC. *Nature Cell Biology* **22**, 663–673 (2020).
564. Kelsall, I. R., Zhang, J., Knebel, A., Arthur, S. J. C. & Cohen, P. The E3 ligase HOIL-1 catalyses ester bond formation between ubiquitin and components of the Myddosome in mammalian cells. *Proceedings of the National Academy of Sciences of the United States of America* **116**, 13293–13298 (2019).
565. Petrova, T., Zhang, J., Nanda, S. K., Figueras-Vadillo, C. & Cohen, P. HOIL-1-catalysed ester-linked ubiquitylation restricts IL-18 signaling in cytotoxic T cells but promotes TLR signalling in macrophages. *The FEBS Journal* (2021) doi:10.1111/FEBS.15896.
566. Rodriguez Carvajal, A. *et al.* The linear ubiquitin chain assembly complex (LUBAC) generates heterotypic ubiquitin chains. *eLife* **10**, (2021).

567. Elton, L., Carpentier, I., Verhelst, K., Staal, J. & Beyaert, R. The multifaceted role of the E3 ubiquitin ligase HOIL-1: beyond linear ubiquitination. *Immunological Reviews* **266**, 208–221 (2015).
568. Krishnan, D., Menon, R. N. & Gopala, S. SHARPIN: Role in Finding NEMO and in Amyloid-Beta Clearance and Degradation (ABCD) Pathway in Alzheimer’s Disease? *Cellular and Molecular Neurobiology* **2021** 1–15 (2021) doi:10.1007/S10571-020-01023-W.
569. Fuseya, Y. *et al.* The HOIL-1L ligase modulates immune signalling and cell death via monoubiquitination of LUBAC. *Nature Cell Biology* **22**, 663–673 (2020).
570. Fujita, H. *et al.* Cooperative Domain Formation by Homologous Motifs in HOIL-1L and SHARPIN Plays A Crucial Role in LUBAC Stabilization. *Cell Reports* **23**, 1192–1204 (2018).
571. Lim, S. *et al.* Sharpin, a novel postsynaptic density protein that directly interacts with the shank family of proteins. *Molecular and Cellular Neuroscience* **17**, 385–397 (2001).
572. Seymour, R. E. *et al.* Spontaneous mutations in the mouse Sharpin gene result in multiorgan inflammation, immune system dysregulation and dermatitis. *Genes and Immunity* **8**, 416–421 (2007).
573. Kumari, S. *et al.* Sharpin prevents skin inflammation by inhibiting TNFR1-induced keratinocyte apoptosis. *eLife* **3**, (2014).
574. Zak, D. E. *et al.* Systems analysis identifies an essential role for SHANK-associated RH domain-interacting protein (SHARPIN) in macrophage Toll-like receptor 2 (TLR2) responses. *Proceedings of the National Academy of Sciences* **108**, 11536–11541 (2011).
575. J, N., Y, S., K, I. & ZH, W. LUBAC regulates NF- $\kappa$ B activation upon genotoxic stress by promoting linear ubiquitination of NEMO. *The EMBO journal* **30**, 3741–3753 (2011).
576. Hostager, B., Kashiwada, M., Colgan, J. & Rothman, P. HOIL-1L interacting protein (HOIP) is essential for CD40 signaling. *PloS one* **6**, (2011).
577. Sato, Y. *et al.* Specific recognition of linear ubiquitin chains by the Npl4 zinc finger (NZF) domain of the HOIL-1L subunit of the linear ubiquitin chain assembly complex. *Proceedings of the National Academy of Sciences of the United States of America* **108**, 20520–20525 (2011).
578. Liu, J. *et al.* Structural Insights into SHARPIN-Mediated Activation of HOIP for the Linear Ubiquitin Chain Assembly. *Cell Reports* **21**, 27–36 (2017).
579. Nastase, M. *et al.* An Essential Role for SHARPIN in the Regulation of Caspase 1 Activity in Sepsis. *The American journal of pathology* **186**, 1206–1220 (2016).
580. Khan, M. H. *et al.* The Sharpin interactome reveals a role for Sharpin in lamellipodium formation via the Arp2/3 complex. *Journal of Cell Science* **130**, 3094–3107 (2017).
581. Yagi, H. *et al.* A non-canonical UBA-UBL interaction forms the linear-ubiquitin-chain assembly complex. *EMBO reports* **13**, 462–468 (2012).

582. Tatematsu, K., Yoshimoto, N., Okajima, T., Tanizawa, K. & Kuroda, S. Identification of ubiquitin ligase activity of RBCK1 and its inhibition by splice variant RBCK2 and protein kinase C $\beta$ . *Journal of Biological Chemistry* **283**, 11575–11585 (2008).
583. Pao, K. *et al.* Activity-based E3 ligase profiling uncovers an E3 ligase with esterification activity. *Nature* **556**, 381–385 (2018).
584. Petrova, T., Zhang, J., Nanda, S. K., Figueras-Vadillo, C. & Cohen, P. HOIL-1-catalysed ester-linked ubiquitylation restricts IL-18 signaling in cytotoxic T cells but promotes TLR signalling in macrophages. *The FEBS Journal* (2021) doi:10.1111/FEBS.15896.
585. Pruneda, J. N. & Damgaard, R. B. Ester-linked ubiquitination by HOIL-1 controls immune signalling by shaping the linear ubiquitin landscape. *The FEBS Journal* febs.16118 (2021) doi:10.1111/FEBS.16118.
586. Fu, B., Li, S., Wang, L., Berman, M. & Dorf, M. The ubiquitin conjugating enzyme UBE2L3 regulates TNF $\alpha$ -induced linear ubiquitination. *Cell research* **24**, 376–379 (2014).
587. Stieglitz, B. *et al.* Structural basis for ligase-specific conjugation of linear ubiquitin chains by HOIP. *Nature* **503**, 422–426 (2013).
588. MacDuff, D. A. *et al.* Phenotypic complementation of genetic immunodeficiency by chronic herpesvirus infection. *eLife* **4**, 4494 (2015).
589. Tian, Y. *et al.* RBCK1 negatively regulates tumor necrosis factor- and interleukin-1-triggered NF-kappaB activation by targeting TAB2/3 for degradation. *The Journal of biological chemistry* **282**, 16776–82 (2007).
590. Gustafsson, N., Zhao, C., Gustafsson, J. & Dahlman-Wright, K. RBCK1 drives breast cancer cell proliferation by promoting transcription of estrogen receptor alpha and cyclin B1. *Cancer research* **70**, 1265–1274 (2010).
591. Vallentin, A. & Mochly-Rosen, D. RBCK1, a protein kinase Cbeta (PKCbeta)-interacting protein, regulates PKCbeta-dependent function. *The Journal of biological chemistry* **282**, 1650–1657 (2007).
592. Queisser, M. *et al.* HOIL-1L functions as the PKC $\zeta$  ubiquitin ligase to promote lung tumor growth. *American journal of respiratory and critical care medicine* **190**, 688–698 (2014).
593. Nakamura, M., Tokunaga, F., Sakata, S. & Iwai, K. Mutual regulation of conventional protein kinase C and a ubiquitin ligase complex. *Biochemical and biophysical research communications* **351**, 340–347 (2006).
594. Hogenesch, H. *et al.* A Spontaneous Mutation Characterized by Chronic Proliferative Dermatitis in C57BL Mice. *American Journal of Pathology* vol. 143 (1993).

595. Zhang, Y. *et al.* Activation of nuclear factor  $\kappa$ B pathway and downstream targets survivin and livin by SHARPIN contributes to the progression and metastasis of prostate cancer. *Cancer* **120**, 3208–3218 (2014).
596. Dutta, J., Fan, Y., Gupta, N., Fan, G. & Gélinas, C. Current insights into the regulation of programmed cell death by NF- $\kappa$ B. *Oncogene* *2006* **25**:51 **25**, 6800–6816 (2006).
597. Fan, Y., Dutta, J., Gupta, N., Fan, G. & Gélinas, C. Regulation of Programmed Cell Death by NF- $\kappa$ B and its Role in Tumorigenesis and Therapy. *Advances in Experimental Medicine and Biology* **615**, 223–250 (2008).
598. Gyrd-Hansen, M. & Meier, P. IAPs: from caspase inhibitors to modulators of NF- $\kappa$ B, inflammation and cancer. *Nature Reviews Cancer* *2010* **10**:8 **10**, 561–574 (2010).
599. Dynek, J. N. *et al.* c-IAP1 and Ubch5 promote K11-linked polyubiquitination of RIP1 in TNF signalling. *The EMBO Journal* **29**, 4198–4209 (2010).
600. Rahighi, S. *et al.* Specific Recognition of Linear Ubiquitin Chains by NEMO Is Important for NF- $\kappa$ B Activation. *Cell* **136**, 1098–1109 (2009).
601. Wu, C.-J., Conze, D. B., Li, T., Srinivasula, S. M. & Ashwell, J. D. Sensing of Lys 63-linked polyubiquitination by NEMO is a key event in NF- $\kappa$ B activation. *Nature Cell Biology* *2006* **8**:4 **8**, 398–406 (2006).
602. Laplantine, E. *et al.* NEMO specifically recognizes K63-linked poly-ubiquitin chains through a new bipartite ubiquitin-binding domain. *The EMBO Journal* **28**, 2885–2895 (2009).
603. Hadian, K. *et al.* NF- $\kappa$ B Essential Modulator (NEMO) Interaction with Linear and Lys-63 Ubiquitin Chains Contributes to NF- $\kappa$ B Activation \*. *Journal of Biological Chemistry* **286**, 26107–26117 (2011).